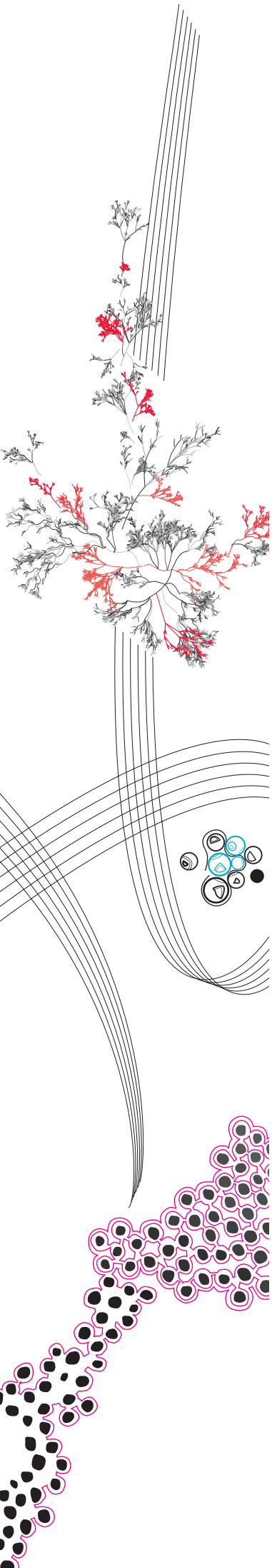

PDENG THESIS

Development of a 2-DoF Ankle Exoskeleton

Ir. M.E. Grootens

September 17, 2019

University of Twente
Faculty of Engineering Technology
Department of Biomechanical Engineering

Graduation Committee:
Prof.dr.ir. H. VAN DER KOOIJ
Ir. E.E.G. HEKMAN
Prof.dr.ir. D.M. BROUWER, PDEng
Dr.ir. T.H.J. VANEKER

Document ID:
BW-PDEng-008

University of Twente
Faculty of Engineering Technology
Department of Biomechanical Engineering

This research is funded by NWO/TTW, project no. 14429.

UNIVERSITY OF TWENTE.

NWO Applied and Engineering Sciences

Development of a 2-DoF Ankle Exoskeleton

PDEng Thesis

by

Martijn Edwin Grootens

Born on May 20, 1990, in Arnhem, The Netherlands

September 17, 2019

University of Twente
Faculty of Engineering Technology
Department of Biomechanical Engineering

Abstract

This PDEng thesis describes the development of a 2-degree-of-freedom (2-DoF) ankle exoskeleton. The work is carried out within the HeRoS Project and it is funded by NWO/TTW under grant number 14429 (Chapter 1).

The human ankle has two degrees-of-freedom (DoFs): plantar flexion–dorsiflexion and inversion–eversion. A literature review showed that current ankle exoskeletons only provide a single DoF to their wearer; plantar flexion–dorsiflexion. However, even during walking in a straight line, significant inversion–eversion motion is made by the ankle. As the existing exoskeletons constrain inversion–eversion, there is a mismatch between the DoFs of the exoskeleton and those of the ankle joint of its wearer. This is the motivation for the research presented in this report: the development of a 2-DoF ankle exoskeleton (Chapter 2).

Two design tracks are followed. First, the *inverted Muscle Skeleton* (iMS) approach is taken (Chapter 5). The HeRoS Project is set up based on this approach: only a soft flexible structure is to be used around the ankle so that natural ankle movement remains inherently unconstrained. Unfortunately, evaluation of prototypes and analysis of their behavior led to the conclusion that the design method cannot be used for the design of an ankle exoskeleton.

The second method follows a more traditional design approach, making use of a rigid mechanical structure around the ankle (Chapter 6). Based on literature about the ankle joint, a simple model of its natural behavior is produced. This model is used to develop an exoskeleton joint that is worn around the ankle. The conceptual design is further developed into a working proof-of-principle prototype (Chapter 7).

Various tests were conducted with the final prototype (Chapter 8). The device can deliver up to 74 Nm of plantar flexion torque and it allows the ankle to move naturally. The behavior of the prototype was compared to that of two other ankle exoskeletons and test subjects preferred the new design over the other devices.

The next steps for the project are to improve the design, for example by reducing the overall mass and volume, and to use the prototype in experiments, for example during gait; the report gives recommendations for both (Chapter 9). This thesis ends with a reflection on the design methodology and by considering the societal relevance of the project (Chapter 10).

Contents

PART

Problem Definition

CHAPTER 1

Introduction

This thesis documents the development and evaluation of a prototype *2-degree-of-freedom ankle exoskeleton*. The aim of this report is to enable further development of the concept, by reporting all the important steps and findings in the design and evaluation process. The appendices provide additional background information, as well as essential information needed to continue the project.

Note that this report does not describe a *product development*, but rather a *research and development* process. The project is funded by an *Innovational Research Incentives Scheme* and its goal is not to design a product (according to a well-defined set of user needs and system requirements), but to develop innovative hardware. More information on the project and its scope is given in Section 1.2.1.

1.1 Background

Figure 1.1-1 shows a patient with a spinal cord injury (SCI) walking on a test track, moving from one onto the next stepping stone. This is a very challenging task for him, as he is paralyzed from the waist down and can neither feel nor move his own legs.

The patient is wearing a lower-extremity *exoskeleton*—a set of robotic legs, in parallel to his own—and it is this 'robotic suit' that enables him to walk. The device shown in the figure is developed by the Symbitron+ team [1] and it is a research prototype; only one device exists and hardware and software are continuously tested and improved. A variety of similar scientific and commercial research projects exists and exoskeletons are also starting to become available for private purchase.

Figure 1.1-1
A patient walking in the Symbitron+ WE2 lower-body exoskeleton. (Source: [1])

Exoskeletons are not only being built for the lower extremities (the hips, legs, and feet), but also for the upper extremities (the trunk, shoulders, arms, and hands). *Wearable robotics*, whether they are worn on the upper or lower body, range from highly complex and powerful robotic devices that span multiple limbs, to very simple devices that only fulfill a small task, such as helping stroke survivors lift their toes during walking.

Heavy, rigid, and powerful devices exist, such as the one shown in Figure 1.1-1, but there are very lightweight devices as well, made from fabric and worn inconspicuously under normal clothes.

Hardware is developed for a variety of applications. Exoskeletons are used to give *assistance* to those who will never be able to complete a task without help; an example is the exoskeleton in Figure 1.1-1. However, exoskeletons are also used for *rehabilitation*, as they can relieve physiotherapists by supporting patients during training. Another application is *augmentation* of human abilities, for instance by supporting factory workers with the handling of heavy equipment or by reducing the energy expenditure of soldiers so that they can go faster or farther. Finally, hardware is also developed for *human movement research*; either to investigate how people move or to investigate how they react to given assistance or disturbances.

No matter the function of the device or the targeted body part, all devices have two things in common: (1) they are difficult to design properly and (2) they are difficult to control so that they perform well. The human body is constantly changing shape (muscles contracting, soft tissue being moved or compressed) and none of the biological joints shows linear behavior like the simple hinges used by roboticists. Moreover, it is very difficult to know exactly what the wearer of a robotic device wants it to do (intention detection).

Poor hardware (which is slow, uncomfortable, or does not stay in place) can never perform beyond its own limited technical capabilities, no matter how good the control software. On the other hand, the hardware can be perfect, but when the software does not take advantage of the hardware's full potential, then the overall performance is still poor. Developing wearable robotics is challenging and requires an inherently interdisciplinary approach: mechanics, electronics, software, the body of the wearer *and* their mind should all be in sync.

The title of this thesis is "*Development of a 2-DoF Ankle Exoskeleton*", so the focus is on exoskeletons for the ankle. An example of an existing device is the Achilles Ankle Exoskeleton that is shown in Figure 1.1-2. Many similar designs can be found in literature and they all use rigid joints that provide a single axis of rotation to the ankle.

The human ankle joint however, has *two* degrees-of-freedom and neither of the two rotation axes is rigid or fixed. This means that the natural movement of the ankle is constrained when an exoskeleton with only a single degree-of-freedom is worn.

The aim of this research is to develop a wearable robotic device that allows the ankle to move freely in its natural degrees-of-freedom, while still being able to deliver torques to the ankle. No such device exists yet (see the literature review in Chapter 2), despite the fact that free movement in *all* degrees-of-freedom of the ankle is necessary even for simple tasks such as walking in a straight line.

Figure 1.1-2
Achilles Ankle Exoskeleton. (Source: [2])

1.2 Preface

This section provides a context for the design assignment and it explains the somewhat unconventional design method that was used.

1.2.1 The HeRoS Project and the iMS design approach

The work in this thesis is carried out as a PDEng assignment at the Department of Biomechanical Engineering of the University of Twente. The assignment is part of a larger project called *HeRoS*, which stands for "Herman's Robotic Suit"—Herman being the thesis supervisor for this PDEng assignment.

The HeRoS Project is funded by NWO/TTW through an *Innovational Research Incentives Scheme* (project number 14429); the goal of this grant is to enable innovative research. The aim of the five-year project is to develop novel hardware to assist paraplegics and allow them to walk again. Multiple people are active in the team, investigating various topics, such as actuator design, control algorithms, and wearable hardware design.

The original project goal was to develop a completely soft robotic suit, based on a design method called the *inverted Muscle Skeleton* (iMS) *approach*. Since this is a newly proposed method, it was decided to build the flexible robotic suit in a modular way: first the knee, then the ankle, and finally the hip. The results obtained for the knee are published in [3] and included as Appendix D in this report.

After construction of a prototype for the knee, the next HeRoS Project milestone is the design of a suit module for the ankle, based on the iMS approach. This is the start of this PDEng assignment and the efforts are described in Chapter 5. Unfortunately, the iMS approach was found infeasible for the design of an ankle module, and a new path is taken in Chapter 6: this new direction led to the successful development of a prototype, which is described in Chapter 7.

1.2.2 Design methodology and course of the project

During a 'normal design project', or at least according to the books, one starts by identifying stakeholders, their needs, and setting system requirements. Then, after a thorough investigation of the problem at hand, conceptual solutions are proposed and the best of these is picked based on analysis and evaluation outcomes. The chosen concept is then developed into a final prototype.

However, in the case of the HeRoS Project, funding was given for the development of a proposed concept. The project goal was 'to use the iMS approach to develop a flexible robotic suit' and not 'to develop a flexible robotic suit'. For this reason, the project described in this report is not 'a normal design project', as a prescribed concept is used to develop a prototype.

As explained in Section 1.2.1, after a significant investment of time and effort, the prescribed concept was found infeasible and another approach had to be taken. Fortunately, valuable experience was gained from the process, and Chapter 7 describes the successful design of a working prototype—although not based on the iMS approach.

Note that the prescription of the iMS approach also influenced the earlier problem investigation phases of the project. As it was already defined what would be built and the focus was on quickly developing hardware, there was no need for doing a thorough literature review or a stakeholder analysis: the goal was to first demonstrate the iMS working principle.

After concluding that the iMS approach was not feasible, a more traditional approach was used. This report, therefore, does include a literature review, a state of the art, and a concept development process.

None of this is necessarily a bad thing, but the reader should be informed before reading this thesis. Had the iMS approach been feasible, then good results would have been produced at a fast pace. Section 10.1 looks back at the design methodology that was used.

1.3 Project goal and motivation

The Achilles, shown in Figure 1.1-2, is an example of an ankle exoskeleton. It was explained in Section 1.1 that this device provides a single axis of rotation to the ankle; this axis is fixed and perpendicular to the sagittal plane. However, as the human ankle joint is composed of bones, ligaments, and muscles, it does not have a single fixed axis of rotation; the natural movement of the ankle is thus constrained by current ankle exoskeletons.

The goal of the PDEng assignment is to design an ankle exoskeleton that provides full freedom of movement to the ankle and is able to deliver significant ankle torque. (The meaning of significant ankle torque is defined in Section 3.5.3.) The focus is on demonstrating the feasibility and usefulness of making such a device.

The motivation for this project will become clear while reading the literature review in Chapter 2; the reasons are summarized in Section 2.5.

1.4 Outline of this thesis

Part I of this report defines the design problem. In this part, after this introduction, Chapter 2 continues with a literature review that explains the motivation for the project. Chapter 3 then discusses the stakeholders, their needs, and it considers use cases and system requirements for the HeRoS Project.

The design process is described in Part II. It starts with an introduction in Chapter 4, followed by two 'design tracks'. The first is the iMS approach, which is documented in Chapter 5, and the second follows a more traditional approach, which is described in Chapter 6. The design of the final proof-of-principle prototype is documented in Chapter 7.

Part III is the last of this report. It presents the results of the evaluation of the prototype in Chapter 8 and conclusions and recommendations are given in Chapter 9. A reflection on the project is given in Chapter 10: it looks back at the design methodology that was used and it discusses the societal impact and relevance of the project.

Supplementary materials and appendices are included starting from page 99.

CHAPTER 2

Literature Review

This chapter presents background information, which provides the motivation for the project. The behavior and anatomy of the ankle is discussed and an overview of existing ankle exoskeletons is given. The final section summarizes the motivation for the development of a 2-DoF ankle exoskeleton.

2.1 Definitions

This section defines the body planes, global coordinate system, and degrees-of-freedom that will be used throughout this report. Note that 'degree-of-freedom' will often be abbreviated to DoF and 'range-of-motion' to RoM. The terms 'exoskeleton', 'active orthosis', and simply 'orthosis' will be used interchangeably.

2.1.1 Body planes and global coordinate system

Figure 2.1-1 defines the *body planes* and the global coordinate system that will be used in this report: the *sagittal* plane corresponds to the xz-plane; the *frontal plane* corresponds to the yz-plane; the *transverse plane* corresponds to the xy-plane.

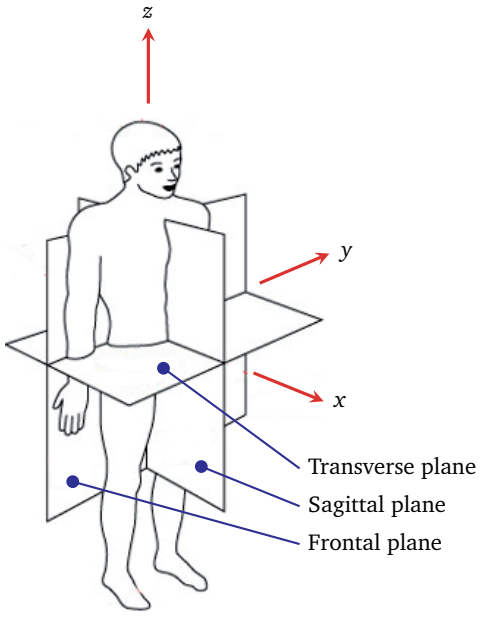

Figure 2.1-1
Body planes and global coordinate system.

2.1.2 The degrees-of-freedom of the lower extremities

The degrees-of-freedom of the lower extremities and their positive and negative directions are defined in Figures 2.1-2(a), (b), and (c). The ankle has two DoFs: plantar flexion–dorsiflexion and inversion–eversion; the dorsiflexion and inversion directions are assumed positive.

The shown pose is the 'zero configuration', in which all joint angles are zero. The configuration of the ankle in this zero configuration is often referred to as a 'straight ankle'. The plantar flexion–dorsiflexion and inversion–eversion motions of the ankle are shown in Figure 2.1-2(d) and (e).

When talking about either lower limb, the 'internal side' is the side between the legs (or the side of the big toe) and the 'external side' is the outer side of the leg (or the side of the little toe).

Ankle exoskeletons are devices that are worn on the lower leg and foot of a person. They should fit well and support the bones, joints, and muscles of the wearer. It therefore is useful to get a basic idea of the anatomy of the limbs on which the device is worn. An overview of the bones and joints in the lower leg and foot, and the muscles that establish the motions of the ankle and foot, is provided in Appendix A.1.

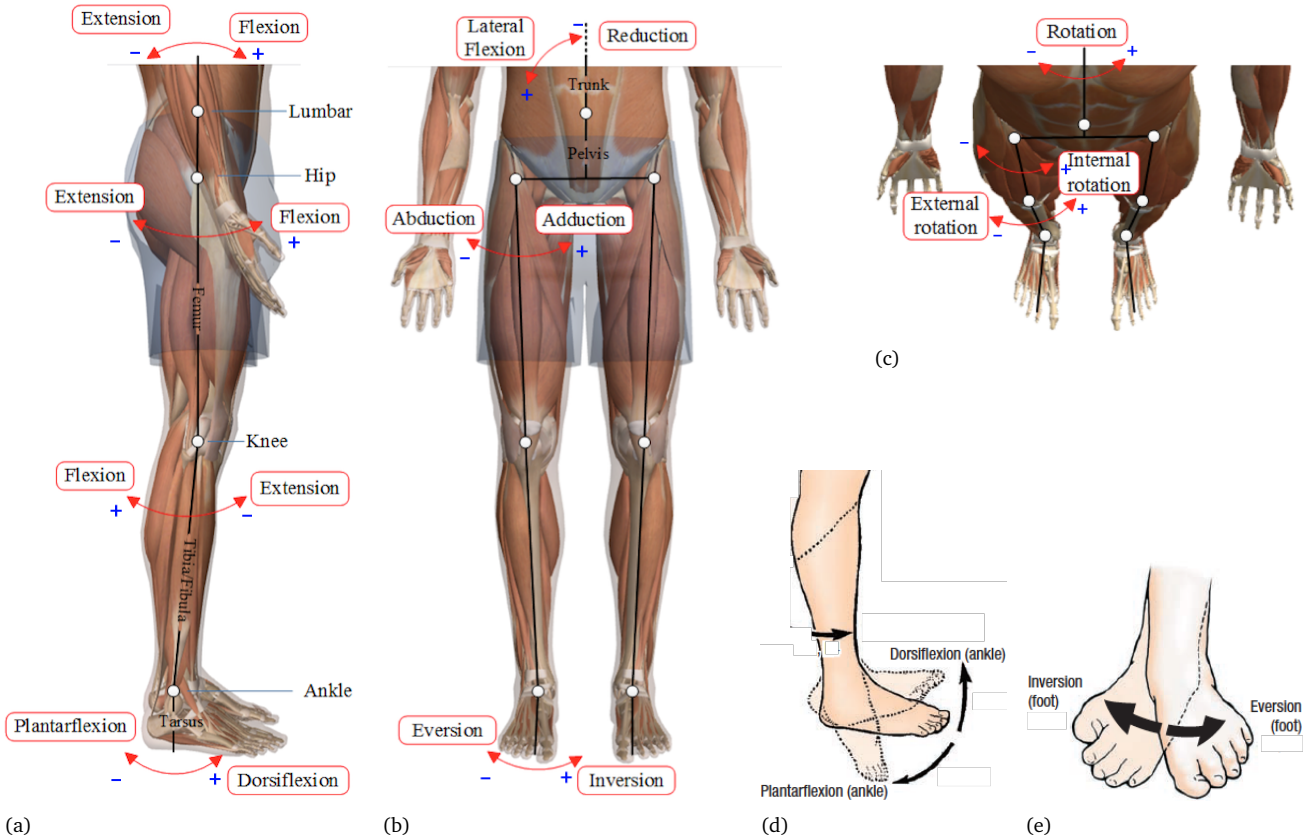

Figure 2.1-2

Definition of the degrees-of-freedom of the lower extremities (Source: [4, 5]): (a) lateral view (on the sagittal plane); (b) anterior view (on the frontal plane); (c) top view (on the transverse plane); (d) ankle plantar flexion–dorsiflexion; (e) ankle inversion–eversion.

2.2 The ankle and foot during walking

Ankle exoskeletons are used for a wide variety of applications, but they are often used for walking. It is therefore relevant to have a closer look at the behavior of the ankle and foot during gait.

2.2.1 The gait cycle

A graphical representation of the gait cycle is shown in Figure 2.2-1. The foot is in contact with the floor ('stance phase') for approximately 60% of the cycle; during the other 40% the leg is swinging through the air ('swing phase').

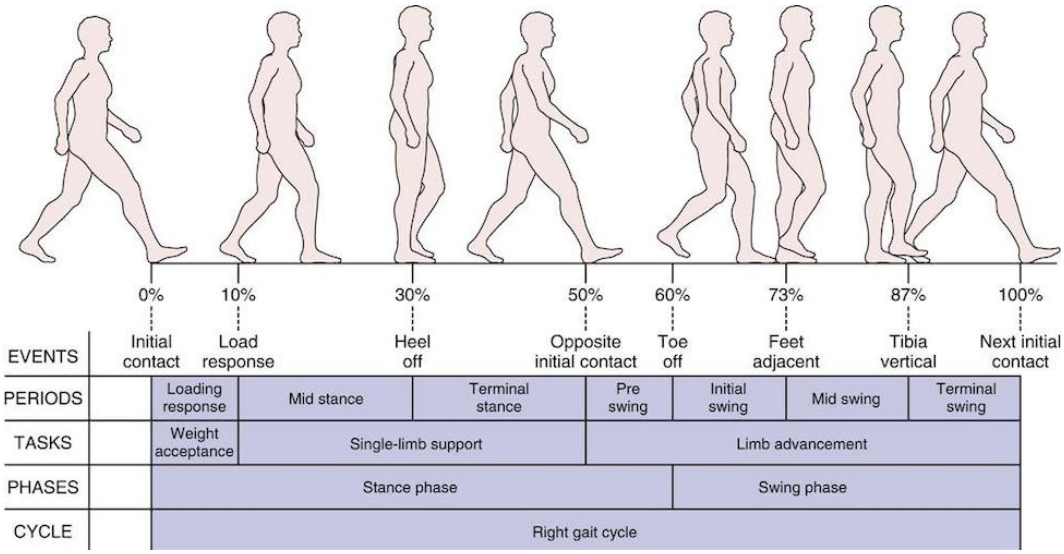

Figure 2.2-1
Events, periods, tasks, and phases in the gait cycle for the right leg.

Figure 2.2-2 defines the *step length* and *step width*, which are parameters that may influence the design of an ankle exoskeleton. The step width is normally within the range of $[5, 10]$ cm and the step length is approximately 72 cm, so that the *stride length* is approximately 144 cm [6].

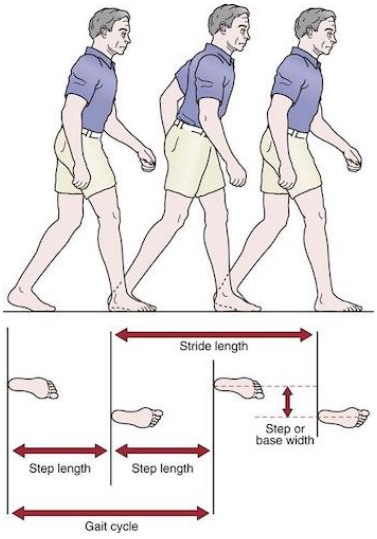

Figure 2.2-2
Step length, stride length, and step width.

2.2.2 Plantar flexion–dorsiflexion and inversion–eversion during walking

Figure 2.2-3 shows the angles of plantar flexion–dorsiflexion and inversion–eversion during normal walking. The figure is purely meant to illustrate the global behavior, as there is a wide variety in gait patterns between individuals and the angles also change with varying walking speed. There is a large variation between the data sets that are published by different authors as well.

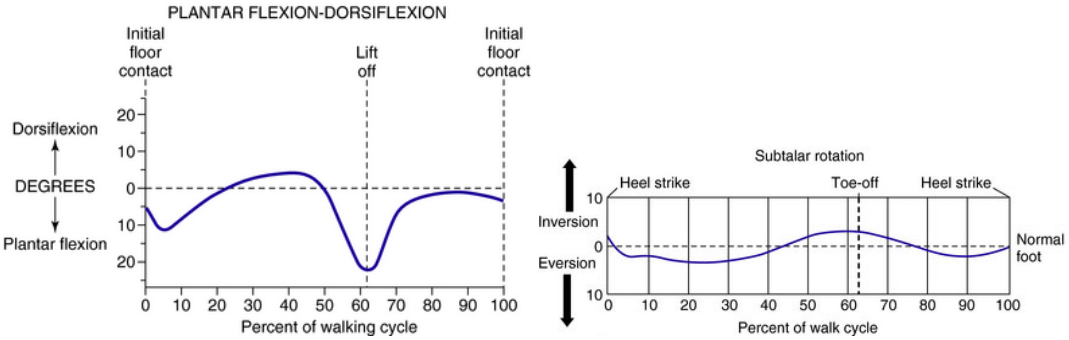

(a) (Source: [7]) (b) (Source: [7])

Figure 2.2-3
Motion of the ankle and foot during gait: (a) shows the plantar flexion–dorsiflexion angle and (b) shows the inversion–eversion angle.

2.2.3 Pronation–supination

The combined motion of the ankle and foot that is made during walking is called *pronation–supination* and it is shown in Figure 2.2-4. Pronation is the combination of eversion of the foot, dorsiflexion of the ankle, and adduction of the foot. Supination is the combination of inversion of the foot, plantar flexion of the ankle, and abduction of the forefoot.

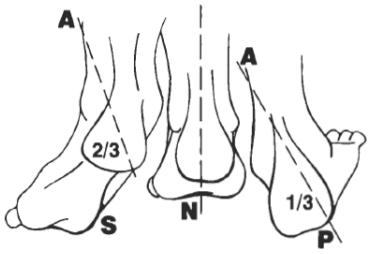

Figure 2.2-4
Pronation–supination of the right foot. The neutral position is indicated by 'N', supination by 'S' and pronation by 'P'. (Source: [8])

2.2.4 Conclusion

Even during walking in a straight line, the ankle does not behave like a rigid single-axis joint.

2.3 Biomechanics of the ankle and foot

Appendix A.1 discusses the bones, joints, and muscles in the lower leg and foot and Figure 2.1-2 shows the degrees-of-freedom of the ankle. Section 2.2 concludes that the ankle does not behave like a single-axis joint, so in this section we will investigate the behavior of the ankle joint and we discus *the orientation* of the axes of rotation of both degrees-of-freedom.

In 1969, a study on 46 cadaver legs was carried out to determine the exact locations of the axes of rotation of the *talocrural* (plantar flexion–dorsiflexion) and *talocalcaneal* (inversion–eversion) joints [9]. It was concluded that, for the purpose of brace design, both joints can be considered to only have a single axis of rotation.

However, a large variation in location and orientation was found between subjects, which needs to be taken into account when designing braces—or exoskeletons. The researchers furthermore found that it is feasible to determine the axis of the talocrural joint based on skeletal landmarks. Unfortunately, no method to determine the orientation of the talocalcaneal joint *in vivo* was found.

2.3.1 Orientation of the plantar flexion–dorsiflexion axis

The results for the orientation of the plantar flexion–dorsiflexion axis are shown in Figure 2.3-1. It can be seen that the axis is rotated both with respect to the axis of the leg and the longitudinal axis of the foot. The measured angles are indicated in the figures, where the range of values is shown by the shaded area and the mean value is denoted by $\bar{x}$.

For the angle with respect to the axis of the lower leg, the measured values are within the range of $[68, 88]°$, the mean value is $\mu = 80°$ and the standard deviation $\sigma = 4°$. For the angle with respect to the longitudinal axis of the foot, the range is $[69, 99]°$. The mean and standard deviation are $\mu = 84°$ and $\sigma = 7°$.

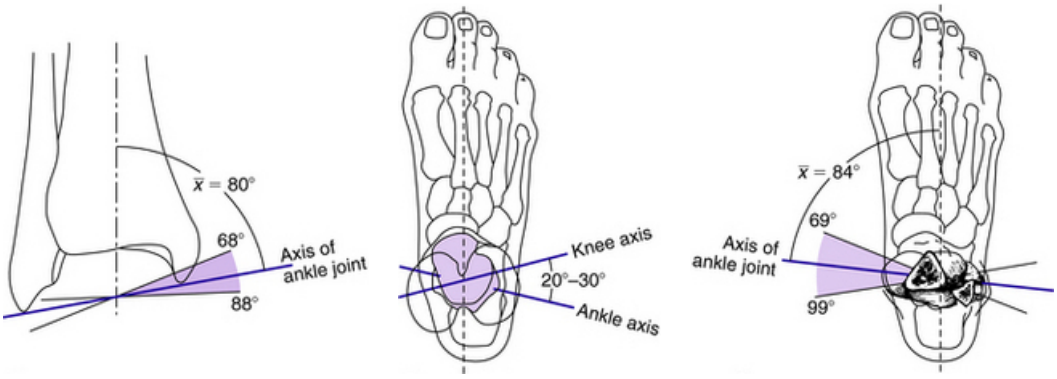

(a) (b) (c)

Figure 2.3-1

Orientation of the ankle plantar flexion–dorsiflexion axis [9]. Figure (a) shows that the axis is tilted with respect to the transverse plane; (b) shows the orientation with respect to the knee axis; and (c) shows the orientation with respect to the sagittal plane. (Source: [7])

2.3.2 Orientation of the inversion–eversion axis

Figure 2.3-2 shows the results for the orientation of the inversion–eversion axis; the mean and range of values are shown.

The angles with respect to the longitudinal axis of the foot are in the range $[4, 47]°$, the mean is $\mu = 23°$ and the standard deviation $\sigma = 11°$. For the angle with respect to transverse plane the range is $[20.5, 68.5]°$, and the mean and standard deviation are $\mu = 41°$ and $\sigma = 9°$.

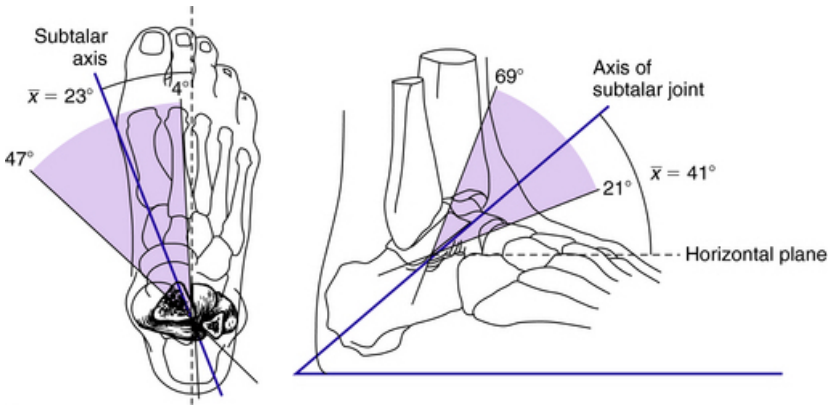

Figure 2.3-2
Orientation of the ankle inversion–eversion axis [9]: (a) with respect to the sagittal plane and (b) with respect to the transverse plane. (Source: [7])

The researchers also measured the angle and distance between the axes of the talocrural and talocalcaneal joints. The results for the measured angle and distance are shown in Figure 2.3-3. It is interesting to see that for all but one subject, the inversion–eversion axis lies below the plantar flexion–dorsiflexion axis. The axes do not cross.

When the axes are projected on the transverse plane, the angles are in the range of $[37, 77.5]°$, the mean is $\mu = 61°$ and the standard deviation is $\sigma = 8°$. The true angles are in the range of $[41, 75]°$, the mean is $\mu = 62°$ and the standard deviation is $\sigma = 7°$. Figure (c) shows the perpendicular distance between both axes. The values are in the range of $[-5, 12]$ mm, with the mean at $\mu = 5$ mm and a standard deviation of $\sigma = 3$ mm.

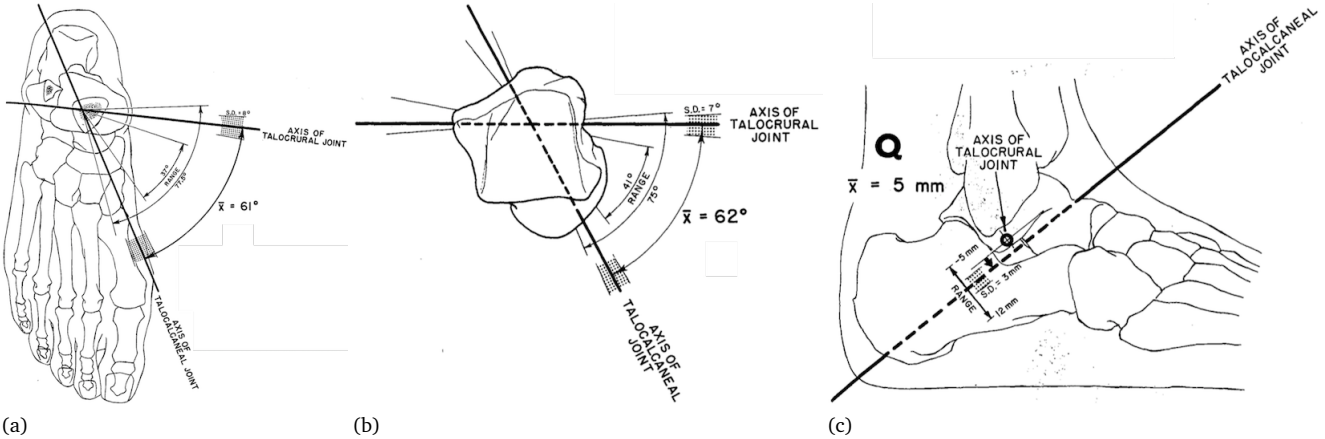

Figure 2.3-3
Angle and distance between the plantar flexion–dorsiflexion and inversion–eversion axis. Figure (a) shows the angle projected on the transverse plane and (b) shows the true angle. (Source: [9])

2.3.3 Orientation of the flexion–extension axis of the toes

The orientation of the flexion–extension axis of the toes with respect to the longitudinal axis of the foot is shown in Figure 2.3-4.

The measured angles are in the range of $[53.5, 72.5]^\circ$, the mean is $\mu = 62^\circ$ and the standard deviation is $\sigma = 6^\circ$.

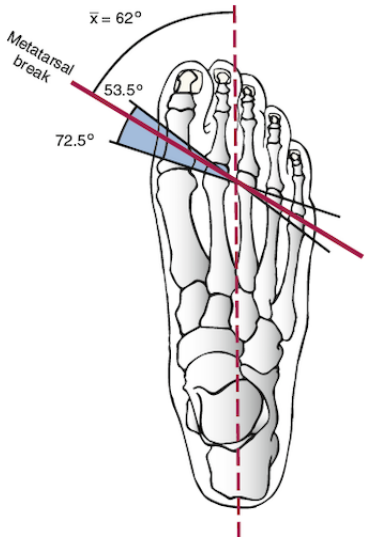

Figure 2.3-4
Orientation of the flexion–extension axis of the toes (the metatarsal break) with respect to the longitudinal axis of the foot [9]. (Source: [10])

2.3.4 Estimating the orientation of the plantar flexion–dorsiflexion axis

An estimate of the orientation of the plantar flexion–dorsiflexion axis can be made by using the index fingers as is shown in Figure 2.3-5. The axis goes through the ankle just below the tips of the *malleoli*, which are the bony landmarks on both sides of the ankle.

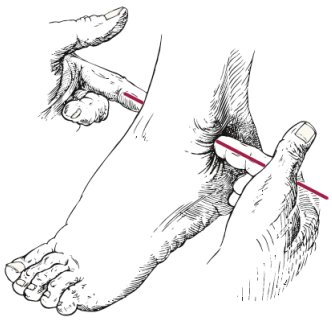

Figure 2.3-5
Estimating the orientation of the plantar flexion–dorsiflexion axis. (Source: [10])

2.4 Ankle exoskeletons

The ankle has *two* degrees-of-freedom and during gait, motion occurs in both degrees-of-freedom—even when simply walking in a straight line. This combined motion during walking is called pronation–supination.

Chapter 1 explains that this thesis is about the development of an exoskeleton for the ankle. Such devices already exist and Appendix A.2 provides an overview of ankle exoskeletons and their applications. A selection of devices is show in Figure 2.4-1. The reader is referred to the appendix for more details on the specific devices, but all of the devices in the figure have a mechanical hinge at the ankle joint. These hinges provide a *single* axis of rotation, perpendicular to the sagittal plane. This does not match with the degrees-of-freedom of the human ankle joint. Hence, these ankle exoskeletons constrain the natural movement of the ankle.

(a) (Source: [11]) (b) (Source: [12]) (c) (Source: [13]) (d) (Source: [14])

Figure 2.4-1

A selection of photographs of ankle exoskeletons discussed in Appendix A.2: (a) actuation with a pneumatic muscle (McKibben actuator); (b) series-elastic actuation using a spring in series with a spindle drive; (c) series-elastic actuation through a spring in series with a Bowden cable; (d) passive mechanism which locks and releases the ankle joint.

2.5 Motivation for this project

Generally, ankle exoskeletons consist of a rigid structure (or at least one that is not intended to be compliant), with a single joint (see Appendix A.2). This joint is perpendicular to the sagittal plane and it is meant to allow plantar flexion–dorsiflexion.

However, as is explained in Section 2.3, the plantar flexion–dorsiflexion axis of the human ankle is *not* perpendicular to the sagittal plane. Furthermore, the ankle has a *second* degree-of-freedom. Moreover, it was shown in Section 2.2 that even for the most simple walking task—walking in a straight line—combined motion takes place in *both* these degrees-of-freedom: pronation–supination. To complicate matters even further, a large variation between individuals was found for the orientation of both joint axes.

There is a *mismatch* between the degrees-of-freedom provided by the existing ankle exoskeletons and the degrees-of-freedom of the wearer's ankle. The final evaluation in Chapter 8 (more specifically in Section 8.3) indeed confirms that test subjects find the existing devices constraining and uncomfortable.

The absence of lightweight and powerful ankle exoskeletons that allow free movement of the ankle brings us to the motivation for this project. A 2-DoF ankle exoskeleton is a novel contribution to the state-of-the-art of wearable robotics. It has the potential to greatly improve wearer comfort and it opens up new possibilities for human movement research during complex tasks, such as walking on uneven terrain or with complex walking patterns.

CHAPTER 3

HeRoS System Requirements

The scope and goals of the HeRoS Project are described in Section 1.2.1 and the rather unconventional course of the project is explained in Section 1.2.2. For reasons explained in those sections, only a small set of system requirements is defined for the the ankle exoskeleton. However, in this chapter a global overview of the steps taken in a 'systems engineering' project is given.

It is assumed that the ankle exoskeleton is developed as a research platform for the Wearable Robotics Lab of the Department of Biomechanical Engineering at the University of Twente. Section 3.1 looks at the ankle exoskeleton as part of a larger 'system of systems'. Section 3.2 considers the relevant stakeholders and Section 3.3 their needs. Section 3.4 considers use cases and applications for the device and Section 3.5 considers the system requirements for the HeRoS Project.

3.1 System of Interest (SoI) and System of Systems (SoS)

The Wearable Robotics Lab of the Department of Biomechanical Engineering at the University of Twente is a laboratory that is used to research the (applications of the) hardware and software of wearable robotics.

The laboratory can be seen as a *System of Systems* (SoS), as it contains a variety of systems that can be used independently or together. One can think of various measurement systems, such as muscle activity (EMG) sensors, a motion capture system, force plates, or an oxygen consumption measurement system. The laboratory also contains equipment such as treadmills, fall-protection, et cetera, which can be controlled or from which data can be recorded.

The *System of Interest* (SoI) for the PDEng assignment is the ankle exoskeleton that is to be developed as a research platform for the Wearable Robotics Lab.

Figure 3.1-1 shows how the SoI fits within the SoS of the Wearable Robotics Lab. Note that depending on the specific experiment being carried out, the researcher decides which systems are used and how they interact. For instance, the ankle torque that is to be generated by the exoskeleton may be dictated by measurements of muscle activity using the EMG system. Or the treadmill speed may be set based on the measured oxygen consumption. The data acquisition and control computer is used to couple the various systems.

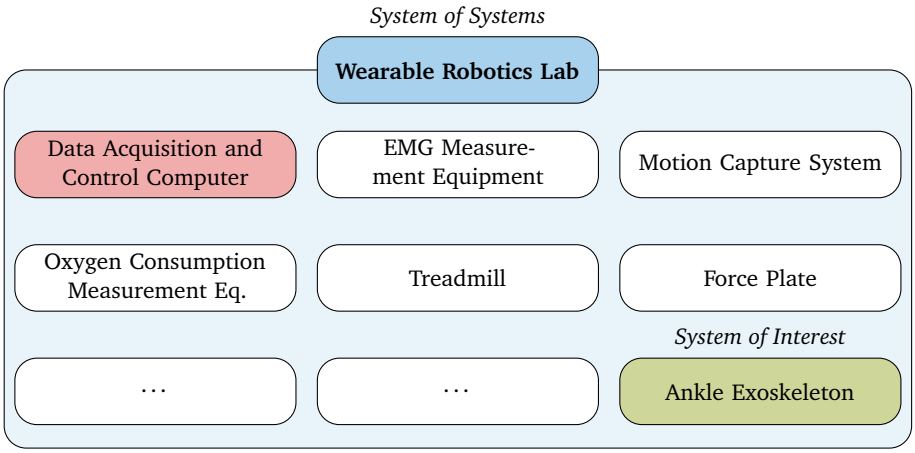

Figure 3.1-1
The Wearable Robotics Lab can be seen as a System of Systems (SoS). The System of Interest (SoI) is the ankle exoskeleton that is to be designed.

3.2 Stakeholders

This section describes the most important stakeholders for the development of the ankle exoskeleton. A unique ID is assigned to each stakeholder which is used throughout this report. All stakeholders are listed in Table 3.2-1.

Note that the ankle exoskeleton is considered a research platform intended for internal use and in-house development.

Table 3.2-1
List of stakeholders and their identifiers.

ID	Name
SH01-WRLB	Wearable Robotics Lab
SH02-DBME	Department of Biomechanical Engineering
SH03-UTWE	University of Twente
SH04-METC	Ethical review committee
SH05-RESR	Researchers
SH06-SUBJ	Test subjects
SH07-TECH	Technicians
SH08-NWOT	NWO/TTW
SH09-HERO	HeRoS Project team

3.2.1 Indirect stakeholders

Firstly, there is a number of stakeholders that is very important to take into consideration, but that is not directly using the exoskeleton.

SH01-WRLB: **Wearable Robotics Lab** The exoskeleton will be part of the inventory of the Wearable Robotics Lab.

SH02-DBME: **Department of Biomechanical Engineering** The Department of Biomechanical Engineering employs the researchers that will be conducting research using the exoskeleton.

SH03-UTWE: **University of Twente** The Department of Biomechanical Engineering is a research group at the University of Twente.

SH04-METC: **Ethical review committee** All experiments with human test subjects need to pass review by a (medical) ethical review committee. It is very important that this committee is convinced of the safety of the hardware that is used for these experiments.

3.2.2 Direct stakeholders

Secondly, there is a number of stakeholders that will be working directly with the exoskeleton.

SH05-RESR: **Researchers** The researchers are the people that will be using the ankle exoskeleton to do experiments with test subjects. Note that the exoskeleton can be used independently, but will often be used together with other equipment in the lab, such as a treadmill, motion capture system, or EMG measurement system (see Section 3.1).

SH06-SUBJ: **Test subjects** The test subjects will wear the exoskeleton, which will apply torques to their ankle. Note that there are two distinct types of test subjects:

- healthy individuals and
- patients with movement impairments.

SH07-TECH: **Technicians** The technicians of the lab will be responsible for maintenance, modification and upgrades of the exoskeleton during its lifetime. (It may be necessary to adjust components of the exoskeleton for specific experiments. One can think of the integration of IMUs, markers, or modifications for a specific test subject.) Note that there are

- mechanical engineering technicians,
- electrical engineering technicians, and
- software engineering technicians responsible for the system.

3.2.3 Other stakeholders

Finally, there are two other stakeholders with significant influence in the design project.

SH08-NWOT: **NWO/TTW** The PDEng project is part of the larger HeRoS Project, which is funded by an NWO/TTW Innovational Research Incentives Scheme grant (project number 14429). It is NWO's mission to facilitate scientific research with an impact for people and society.

SH09-HERO: **HeRoS Project team** The goal of the HeRoS Project is to develop novel hardware and software for wearable assistive devices. The team consists of members that are working on various projects; these other projects may have influence on the choices that are made in the design process of the ankle exoskeleton.

Note that the exoskeleton is developed for the Wearable Robotics Lab at the University of Twente and is, therefore, not a commercial product. The exoskeleton will not be brought to the market, so it is not necessary to consider suppliers, manufacturing companies, distribution centers, ..., as important stakeholders.

3.3 Identification of stakeholder needs

In this section we consider a selection of needs of the most important stakeholders that were discussed in Section 3.2.

3.3.1 Enterprise and business management levels

The exoskeleton is developed for the Wearable Robotics Lab, which is part of the Department of Biomechanical Engineering of the University of Twente. Figure 3.3-1 shows this 'enterprise structure'; we consider these three bodies to together form 'the enterprise'.

At the enterprise and business levels we can identify a number of needs or strategies.

- The Wearable Robotics Lab wants to have a wide variety of high-quality equipment that is well-integrated with the other equipment (examples were given in Figure 3.1-1). This is important to attract external students and researchers and to set up (international) collaborations. The laboratory can also be used by external parties, so it is important to have good and reliable equipment.

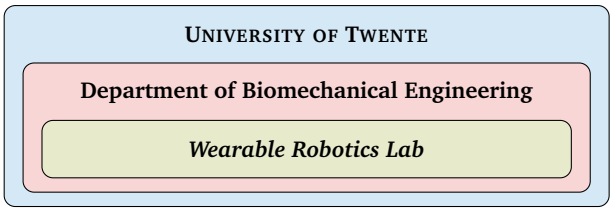

Figure 3.3-1
Enterprise structure.

- The Department of Biomechanical Engineering does cutting-edge research and needs to have access to high-quality and state-of-the-art equipment to be able to compete with research groups in the internationally-oriented fields of biomechatronics, biomechanics, and human movement science.
- The University of Twente's motto is "*High Tech, Human Touch*". This is very relevant for the project, as we're talking about wearable robotics that are used for experiments with both healthy people and patients.

3.3.2 Business operations level

At the business operations level we encounter the needs of the stakeholders. The stakeholders were introduced in Section 3.2. Three of the stakeholders form the 'business management' levels; their strategies and needs were discussed in Section 3.3.1. They are listed, together with the needs of the other stakeholders, in Table 3.3-1 (note that this list is not comprehensive, as is explained in Section 1.2.2). The remainder of this section discusses where these needs are coming from. In Section 3.5, we will consider the transformation of the stakeholder needs to requirements at the system level.

Ethical review committee

The research that will be done using the exoskeleton needs to be approved by a (medical) ethical review committee. Whether approval will be given depends on the experiment, but it also depends on whether the committee is convinced that the exoskeleton is safe. The committee is not a stakeholder in the sense that it has an interest in the exoskeleton or the research for which it is used, but they decide whether approval for use of the exoskeleton will be given.

Researchers

The researchers can use the exoskeleton for a wide variety of experiments. For all these experiments, the device needs to deliver joint torques, and the researcher decides what the desired joint torques are. They can be preprogrammed reference profiles, but more often the desired joint torques are dynamically computed based on measurements from either the exoskeleton itself or any of the other equipment in the Wearable Robotics Lab. This means that it is very important that the researchers can easily program the exoskeleton and integrate it with existing or new equipment. Specifically, the EMG measurement system, EtherCAT fieldbus and Matlab/Simulink, are mentioned during interviews with the researchers.

It is very important for the researchers that the exoskeleton is able to accurately track the desired torque reference. This need will impose requirements on technical specifications such as torques, powers, system bandwidths, et cetera. Because the requirements are dependent on the specific experiment that is done, a large number of use cases is defined; the technical requirements will be based on these use cases, so that the exoskeleton accommodates a large variety of experiments. The use cases are described in Section 3.4.

A variety of sensory data is needed from the exoskeleton so that it is useful in different research applications. The exact needs and wishes are collected by interviewing the researchers.

It is important for the researcher that the active ankle orthosis can quickly and easily be donned and doffed. Either independently by healthy test subjects, or by the researcher when experiments are carried out with patients.

Table 3.3-1

Stakeholder needs. The table lists the unique identifier for each need, a short description of the need, and the stakeholder(s) from which the need is originating.

ID	Name	Stakeholders
ND01-HTHT	Keep motto in mind: “High Tech, Human Touch”	SH03-UTWE
ND02-RSWR	Doing cutting-edge research into wearable robotic hardware and software	SH02-DBME
ND03-RSBM	Doing cutting-edge research into biomechanics and human movement	SH02-DBME
ND04-OFEQ	Offering high-quality equipment to researchers (“High-Tech”)	SH01-WRLB
ND05-OFWR	Offering high-quality wearable robotics to researchers (“High-Tech, Human Touch”)	SH01-WRLB
ND06-INTG	Compatibility/Integration with state-of-the art measurement equipment	SH01-WRLB, SH02-DBME
ND07-SAFE	Safety for all users, in particular the test subjects (“Human Touch”)	SH03-UTWE, SH02-DBME, SH01-WRLB
ND08-DRDC	Presence of a device report and up-to-date inspection reports	SH04-METC, SH05-RESR
ND09-RADC	Presence of risk analysis documentation	SH04-METC, SH05-RESR
ND10-IEMG	Integration with existing hardware and software: Delsys Wireless EMG	SH05-RESR
ND11-IBUS	Integration with existing hardware and software: EtherCAT fieldbus	SH05-RESR
ND12-IMAT	Integration with existing hardware and software: Matlab/Simulink	SH05-RESR
ND13-EPRG	Easy programming of high-level functionality	SH05-RESR
ND14-APUC	Suitability of the device for a wide range of use cases (Section 3.4)	SH05-RESR
ND15-SANG	Availability of sensory data: ankle joint angles	SH05-RESR
ND16-STRQ	Availability of sensory data: ankle joint torques	SH05-RESR
ND17-SHST	Availability of sensory data: heel strike detection	SH05-RESR
ND18-STOE	Availability of sensory data: toe-off detection	SH05-RESR
ND19-PIEV	Passive ankle inversion–eversion DoF	SH05-RESR
ND20-PDTC	Torque-controlled plantar flexion–dorsiflexion DoF	SH05-RESR
ND21-EDDO	Easy donning and doffing	SH05-RESR, SH06-SUBJ
ND22-QDDO	Quick donning and doffing	SH05-RESR, SH06-SUBJ
ND23-SWER	Safety for people wearing the device	SH06-SUBJ
ND24-SWRK	Safety for people working with the device	SH05-RESR
ND25-SMNT	Safety for people doing maintenance on the device	SH07-TECH
ND26-COMF	Comfort while wearing the device	SH06-SUBJ
ND27-FITR	Fit to a wide range of body shapes and sizes	SH05-RESR
ND28-NATM	No hinderance of natural ankle movement	SH05-RESR
ND29-MMEC	Easy replacement and modification of mechanical components	SH07-TECH
ND30-MELC	Easy replacement and modification of electrical components	SH07-TECH
ND31-MSFT	Easy replacement and modification of (low-level) software	SH07-TECH
ND32-IHMF	Ability to manufacture components in-house	SH07-TECH
ND33-LACT	Use of linear actuators developed within the project	SH09-HERO
ND34-NOVL	Novel design; contribution to the state-of-the-art	SH09-HERO

Good alignment of the joints of the exoskeleton with the ankle joint is important to allow for natural ankle movement, to prevent power losses, and ensure that everything works as expected. The device needs to be lightweight, so that wearing it has minimal influence on the natural movement of the wearer [15].

Test subjects

It is important for the test subjects that the exoskeleton makes a safe impression, as it is a powered wearable device. Donning and doffing should be as easy and quick as possible. It is important that the device is comfortable to wear. This results in several requirements, one of which is that the alignment of the joints needs to be good. The exoskeleton shall not hinder movement of the test subject.

Technicians

The exoskeleton is a research device. This means that it is very probable that components will need to be replaced, modified, or updated. It is important that mechanical and electrical components are easily accessible and can be easily replaced. It should be possible to easily update both low-level and high-level software. It would be very practical if components that are likely to be replaced can be manufactured in the (3D printing) workshops at the University of Twente. Quick modification and repair to minimize down-time, especially when the device is used during ongoing experiments, is in the interest of the researchers.

HeRoS Project team

Within the HeRoS Project, a new type of linear actuator is under development. It is preferable that these actuators be used in the ankle exoskeleton. This influences the design decisions.

3.4 HeRoS use cases

As explained, the ankle exoskeleton is intended as a research platform. This means that the tasks it has to perform can vary widely. Some experiments for which the device could be used are listed below.

- Providing assistive torques to the paretic leg of a stroke surviver during stair climbing.
- Fully taking over actuation of the ankle of a patient with a paralyzed lower leg and allowing him to stand up from a chair.
- Enforcing a prescribed movement pattern on the ankle of a sitting SCI patient, as a means of physical therapy.
- Providing disturbance torques to a healthy individual standing on a force plate, to investigate strategies that humans use to keep balance.
- Injecting power into the gait cycle of a healthy subject on a treadmill, to decrease the metabolic cost of walking.

There is a range of *use cases* during which the exoskeleton has to provide assistive (or disturbing) torques or motion profiles. These use cases need to be defined to be able to set system requirements.

The use cases are listed in Table 3.4-1 (with unique identifiers) and their descriptions are given in Appendix B.2. Note that the uses cases are defined with a full lower-body exoskeleton in mind, as is explained in Section 1.2.1. However, the same use cases are relevant for the ankle orthosis alone.

The use cases are defined based on relevant *activities of daily living* (ADL), interviews with both SCI patients and their therapists, and on the CYBATHLON exoskeleton race track [16]. The CYBATHLON is an exoskeleton race and a description of the race track is given in Appendix B.1. These use cases need to be considered during the design process.

Table 3.4-1
List of use case IDs and names.

Case ID	Name
UC01-TRAN	Transport
UC02-DONN	Donning
UC03-DOFF	Doffing
UC04-SIST	Sit-to-stand
UC05-STSI	Stand-to-sit
UC06-SITW	Sitting with exoskeleton
UC07-STND	Standing
UC08-MANP	Standing—Object manipulation
UC09-BEND	Standing—Bending
UC10-WALK	Walking
UC11-NARR	Walking—Narrow space
UC12-SLLM	Walking—Slalom
UC13-SLPU	Walking—Walking up slope
UC14-SLPD	Walking—Walking down slope
UC15-TERR	Walking—Walking rough terrain
UC16-TILT	Walking—Walking tilted ground
UC17-STRA	Walking—Stair ascent
UC18-STRD	Walking—Stair descent
UC19-CRRY	Walking—Carrying object

3.5 HeRoS exoskeleton system requirements

The system requirements for the ankle exoskeleton can be derived from the stakeholder needs (Section 3.3), wishes, safety and other regulations, and the use cases (Section 3.4). A structured method, like presented in the INCOSE guide [17], should be used to formally transform the stakeholder needs to this set of system requirements. Numerical values should be specified where possible.

3.5.1 Technical requirements on torque, velocity, and power

Section 3.4 lists a number of research applications of the ankle exoskeleton and the use cases that should be considered. The technical specifications differ greatly for the various use cases, but also for the different experiments.

For example, climbing a flight of stairs may require large joint torques and low joint velocities, whereas normal walking requires smaller torques, yet higher velocities. This is a problem for design, as the combination of actuator and transmission is typically chosen for a *specific* task.

The exoskeleton needs to deliver significantly more torque when it has to provide full assistance to a paraplegic individual, than when it only has to prevent drop-foot in a stroke-survivor. This means that the research for which the exoskeleton is used also greatly influences the required technical specifications.

The wide range of requirements makes actuator and transmission selection challenging. However, the various research applications also pose a problem. One can imagine that an exoskeleton that can fully support a paraplegic during all use cases becomes very heavy and bulky. Consequently, it can then no longer be used to reduce the metabolic cost of walking in a healthy individual because the added mass is too large [15].

A literature review was carried out to collect data on range-of-motion, joint powers, and other specifications, for the series of use cases. Assuming the exoskeleton has to provide full assistance, maximum values can be picked to set the requirements. This review is included in Appendix C.1 and the derived HeRoS exoskeleton requirements are listed in Appendix C.2.

3.5.2 Anthropometrics

Anthropometric data is collected in Appendix C as well, to help during the design process. Here another difficulty is introduced: there is a large variation in body mass and body shape between individuals of the same sex and an even larger difference when both sexes are considered. It is not possible to create a design that fits everybody—or every body.

3.5.3 Requirements for the proof-of-principle prototype

Section 1.2.1 explains that the original goal of the HeRoS project, for which the specifications in Appendix C are written, was the design of a full lower-body flexible robotic suit. Section 1.2.2 explains the origin of the research and development project that is described in this report.

The goal of this thesis is to investigate the feasibility of building a 2-DoF ankle exoskeleton. Actuator design is not part of the PDEng assignment, as another HeRoS team member is working on the development of a new type of actuator—the working principle behind these actuators is described in [18]. It was also explained that system specifications vary widely depending on the (research) use case.

The PDEng assignment focuses on creating a proof-of-principle prototype. For this reason, the system requirements are reduced to the set listed in Table 3.5-1. Only the most important stakeholder needs are considered and few technical requirements regarding actuator performance are set. It is required (RQ12-LACT) to use linear actuators, so that the exoskeleton can serve as a test platform for the new actuators that are developed within the project. Furthermore, a minimum torque requirement (RQ09-DTRQ and RQ10-PTRQ) is specified, as the prototype should demonstrate a working principle. The Achilles ankle exoskeleton can deliver up to 70 Nm, so half this maximum torque is chosen as 'significant torque' for demonstration purposes.

The specifications of the range-of-motion and the requirement that the ankle should be able to move naturally (RQ06-FREE), are the most important system requirements. The plantar flexion–dorsiflexion range-of-motion is chosen based on the specifications in Appendix 3.5 (RQ01-DROM and RQ02-PROM); the inversion–eversion RoM is chosen based on the ankle behavior during gait (RQ03-IROM and RQ04-EROM), as is described in Section 2.2.

The specifications of shoe size and body length are chosen based on the fact that, if these requirements are satisfied, at least 10 people from within the department can participate in an experiment as test subject.

Table 3.5-1
The condensed set of system requirements for the ankle exoskeleton.

ID	Name
RQ01-DROM	The maximum dorsiflexion angle shall be at least 30°.
RQ02-PROM	The maximum plantar flexion angle shall be at least 50°.
RQ03-IROM	The maximum inversion angle shall be at least 15°.
RQ04-EROM	The maximum eversion angle shall be at least 15°.
RQ06-FREE	The wearer shall be able to naturally move their ankle, only limited by the specified ends of the RoM.
RQ08-CTRL	The plantar flexion–dorsiflexion torque of the device shall be controlled on-line.
RQ09-DTRQ	The device shall be able to generate dorsiflexion torques of at least 35 Nm.
RQ10-PTRQ	The device shall be able to generate plantar flexion torques of at least 35 Nm.
RQ12-LACT	The device shall use linear actuators.
RQ14-WECR	It shall be impossible for the wearer to crush or catch their fingers in the system.
RQ15-WRCR	It shall be impossible for the researcher to crush or catch their fingers in the system.
RQ16-SHRP	The system shall have no sharp edges.
RQ18-SHOE	The prototype shoe size shall be EU 43.
RQ19-BDYL	The prototype shall fit people with body lengths in the range of $[170, 190]$ cm.

3.6 Conclusions

Section 3.5.3 defines the set of system requirements for the proof-of-principle prototype that is developed in this report. The prototype is intended to demonstrate the feasibility of designing a 2-DoF ankle exoskeleton. Thorough evaluation must show whether improvements in performance and comfort are achieved when comparing the prototype to current 1-DoF ankle exoskeletons—only then is it useful to start a product development process.

PART II

Design Process

CHAPTER 4

Synthesis of Design Solutions

Section 1.2.1 of this report provides information about the context of this PDEng assignment. It is explained that the research is carried out as part of the HeRoS Project and that within this project, other team members are working on—among other topics—design of a new type of linear actuator which is described in [18].

Funding for the HeRoS Project was provided for the development of the so-called *iMS approach*. This means that, although this chapter is titled 'Synthesis of Design Solutions', the 'Design Solution' is prescribed by the project. It was decided to use a *hands-on* approach: demonstrating working principles in practice and quickly developing working hardware. Chapter 5 describes the evaluation and analysis of prototypes based on this iMS approach and a short introduction to the method is given in Section 4.1.

Unfortunately, the iMS approach was found unsuitable for the design of a 2-DoF ankle exoskeleton and a more traditional approach had to be taken. This second analysis and evaluation process is described in Chapter 6 and a short introduction is given in this chapter as well (Section 4.2). Note that requirement `RQ12-LACT` still applies and that the new design should use linear actuators, to allow future integration of the newly developed HeRoS actuators. The design of the final proof-of-principle prototype is described in Chapter 7.

4.1 Soft robotic orthoses based on the iMS approach

In the human body, muscles exert *tension* forces which act on the bones, causing the bones to be loaded with *compression* forces. This is shown in Figure 4.1-1(a).

Various researchers have followed a *biomimetic* design approach, to create so-called *exosuits*. In

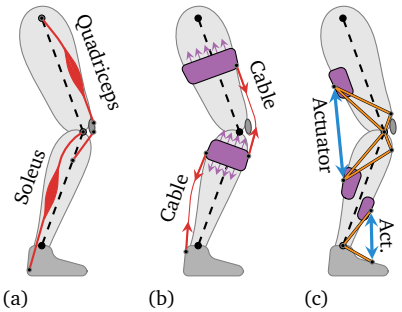

Figure 4.1-1
Knee extension and ankle plantar flexion using (a) the human musculoskeletal system, (b) a biomimetic exosuit, and (c) the iMS approach. (Source: [3])

these suits, *pulling* actuators, such as Bowden cables or McKibben artificial muscles, are used to exert tension forces on a flexible suit. An illustration of this concept for the knee and ankle is shown in Figure 4.1-1(b) and examples of actual designs are discussed in the state-of-the-art in Appendix A.2.5.

These biomimetic designs generally exert large shear forces on the body of the wearer. This is needed for the straps and cuffs, shown in purple in Figure 4.1-1(b), to stay in place. However, the maximum shear force that can be comfortably applied to the wearer is limited [19]. This means that the torques that can be generated remain limited in comparison to the torques generated by conventional exoskeletons.

For this reason, the *inverted Muscle Skeleton* (iMS) approach has been proposed as a novel method for the design of wearable robotics. Detailed information about the iMS approach can be found in Appendix D or [3]. However, the basic idea is to 'invert' biology, by using actuators that deliver *compression* forces (rather than the tension forces delivered by the biological muscles) and a structure consisting of flexible materials such as straps, that is loaded in *tension* (rather than in compression, as are the biological bones). The concept is shown in Figure 4.1-1(c) for the ankle and knee.

The design method was previously used to create a pneumatically actuated knee orthosis that was successful in providing knee extension torques that help reduce the muscle activity during one-legged knee bends. An overview of this device is shown in Figure 4.1-2 and details can be found in Appendix D.

Based on these results, it seems feasible to apply the same method to the design of an active ankle orthosis. One or two linear actuators—which are under development within the HeRoS Project—can be placed anterior to the ankle as is shown in Figure 4.1-1(c). A flexible network of straps can then be used to keep the actuator anchor points in place. The forces acting on the body can be distributed using for example a shell on the lower leg and via the shoe on the foot.

The use of a flexible structure to keep the actuators in place allows the ankle to move freely, as there are no mechanical joints that require alignment with the biological joints: this is the main objective of this PDEng project.

Analysis of iMS concepts and evaluation of various prototypes is discussed in Chapter 5.

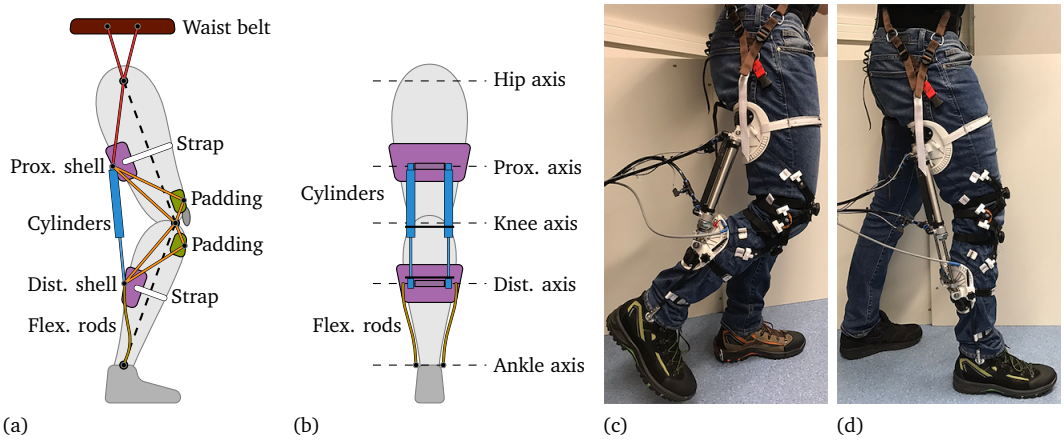

Figure 4.1-2

Knee orthosis prototype based on the iMS approach: (a) lateral view schematic, (b) posterior view schematic, (c) prototype in knee flexion (d) prototype with a slightly bent knee.

4.2 Rigid exoskeletons using traditional joints

The iMS approach aims at minimizing the use of rigid components in the orthosis design. However, it is also possible to construct a rigid exoskeleton that provides the required degrees-of-freedom to the ankle.

The same actuator layout as in the iMS approach (actuators anterior to the leg) will be used. This means that `RQ12-LACT`, which requires the use of linear actuators, is satisfied. However, we replace the network of flexible straps with rigid links. A mechanism, with multiple joints, needs to be designed so that the rigid exoskeleton allows the ankle to move freely.

The analysis and evaluation of concepts is presented in Chapter 6 and the design of the final proof-of-principle prototype can be found in Chapter 7.

CHAPTER 5

iMS Concepts

The *inverted Muscle Skeleton* (iMS) approach forms the basis of the HeRoS Project; it is the prescribed design method for the 2-DoF ankle exoskeleton. An introduction to the approach was given in Section 4.1 and more details can be found in Appendix D or [3].

5.1 The iMS approach for assistance to the ankle

Figure 5.1-1 shows the schematic drawing that was shown earlier in Figure 4.1-1(c). The idea is that linear actuators (which are being developed within the HeRoS Project) are placed anterior to the ankle. They fulfill the 'inverted' function of the human muscles: they *push* instead of *pull*—hence the name *inverted* Muscle Skeleton approach.

The actuators are hinged to shells that comfortably distribute the compression forces onto the body; one at the lower leg (purple) and one at the foot (the shoe). The essential element that interconnects all components is a network of *flexible* materials, such as fabric or webbing (orange). The function of this network is to prevent the actuator anchor points from sliding away from the ankle: upwards along the leg for the purple shell, and downwards and to the right for the attachment on the foot.

Finally, the connection point at the ankle needs to be kept in place for all of this to work. This can be realized by using straps that pass under the foot and behind the heel. In practice, fixing it to a shoe should have the same effect and it is a good way of comfortably distributing the forces over the sole and heel of the foot.

The iMS approach has three main advantages. Firstly, the absence of rigid components that interconnect the actuator anchor points and the absence of complex mechanical joints greatly reduce the mass of the device. This is an important advantage, because it is known that adding mass distally to the body alters gait and increases the metabolic cost of walking [15].

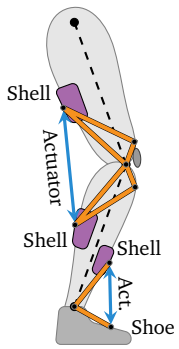

Figure 5.1-1
The iMS approach for the knee and ankle. (Source: [3])

Secondly, the absence of mechanical single-axis joints is assumed to take away the need for precise alignment of the exoskeleton with the body—misalignment between the human joints and those of an exoskeleton can cause discomfort and even injury [20].

Finally, because a flexible suit is used instead of one or more single-axis joints, it is expected that the ankle can move freely in both plantar flexion–dorsiflexion *and* inversion–eversion.

In conclusion, it should be possible to develop a device that is significantly more comfortable than a regular exoskeleton, while using high-force linear actuators still allows the delivery of high joint torques.

The remainder of this chapter will start with the evaluation of a number of early prototypes and then continue with the analysis of the iMS concept. We explained in Section 1.2 why this 'hands-on' approach is used and we reflect on it in Section 10.1.

5.2 Evaluation of prototypes

To demonstrate the iMS working principle, a large number of prototypes was built. The focus of these prototypes is on the successful generation of plantar flexion torques, while leaving (passive) inversion–eversion unconstrained. An early iteration, built by an exchange student as part of her BSc. graduation assignment, is shown in Figure 5.2-1. All other prototypes use a similar setup, so we use this example to discuss the main components.

(a) (b)

Figure 5.2-1
Ankle orthosis prototype by an exchange student: (a) anterior and (b) lateral view. (Source: [21])

Two parallel pneumatic cylinders are used for actuation. The pneumatic cylinders serve as a temporary solution; they will be replaced by the high-power and compact linear actuators that are under development within the HeRoS Project. Two cylinders are used to generate sufficient torque. Moreover, the use of two cylinders may allow active control of inversion–eversion, by independently controlling the cylinders. An advantage of pneumatic cylinders is that they are fully back-drivable, which allows us to evaluate prototypes in 'minimal impedance mode'.

A regular boot is used as an interface to the foot and the cylinders are connected to the *sole* of the shoe. When the cylinders push during ground contact, they push directly onto the floor. The shoe distributes the forces comfortably over the foot when the cylinders are pulling or when there is no ground contact. The shoe itself is part of the flexible structure that is needed to keep the connection point at the ankle in place (seen as the silver bolt in the lateral view).

A shell at the lower leg is used to distribute the forces over the anterior side of the leg.

Finally, a network of flexible materials connects the lower leg shell to the connection points on the shoe, at both sides of the ankle joint. This construction prevents the shell from sliding

(a) (b) (c)

Figure 5.2-2
Lateral view of a series of prototypes based on the iMS approach: (a) a prototype with a shell on the lower leg; (b) a prototype with a rigid ring around the leg; (c) a prototype with a bracket anteriorly around the leg. All prototypes use two parallel pneumatic cylinders.

upwards along the lower leg as the cylinders exert a pushing force.

Note that only compression forces act on the body and no shear forces, as they are borne by the flexible structures; this is inherent to the iMS approach.

Figure 5.2-2 shows three examples of additional prototypes. The remainder of this section discusses the most important observations, the challenges, and some of the design iterations.

5.2.1 Keeping the interface at the lower leg in place

The iMS approach assumes, as Figure 5.1-1 shows, that as long as the actuators exert a compression force, only a cable from the ankle to the anchor points at the lower leg should suffice to keep the components on the leg in place.

The idea is that relative motion between the shell and lower leg is prevented by an equilibrium of three forces: (1) the compressive actuator force; (2) the compressive normal force between the shell and the lower leg; and (3) the tension force in the cable to the ankle.

In practice however, we could not find a way to keep the shell in place using these three forces. When the wearer moves their foot in plantar flexion faster or farther than the actuator can follow, the contact between the shell and lower leg is lost. Problems also occur when donning the device, because initially there is no contact between the shell and lower leg: the normal force needed for the equilibrium is not yet present. It is concluded that an additional structure is required to prevent the shell from sliding down the leg.

Figure 5.2-2(a) shows a potential solution that strictly follows the iMS approach: only flexible structures loaded with tension forces are used. In this prototype, the lower leg shell is suspended from a cable network that attaches to a hip belt. This network passes through the knee joint to transport the tension forces via straps around the upper leg to the waist belt. This makes the design unnecessarily complex and it introduces many other new challenges, as all straps should be fitted to the body and need to stay in place.

Another solution is shown in Figure 5.2-2(b); here small flexible rods are used to support the lower leg shell by exerting small upwards (compression) forces. This of course is a slight deviation from the iMS approach, but it is more effective and less complex than the previous solution.

5.2.2 Shells as an interface to the lower leg

Figure 5.2-3 shows a *Pain Pressure Threshold* (PPT) map of the lower extremities [22]. The PPT indicates the amount of pressure that can be exerted onto the body, before causing pain.

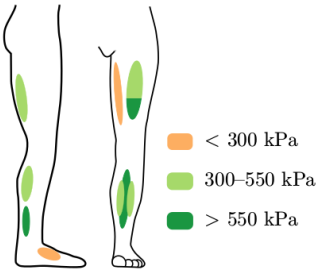

Figure 5.2-3
Pain Pressure Threshold (PPT) data for the lower leg. (Source: [23])

The figure suggests that the anterior side of the lower leg can withstand rather large compressive forces, provided that they are properly distributed. However, we could not find a way to comfortably distribute the forces by using shell-like structures.

A large number of shells was constructed (examples are shown in Figures 5.2-1 and 5.2-2(a)) and improved with various padding materials. All test subjects except one identified forces applied through these shells as uncomfortable or even painful.

One should note that the forces applied in these tests were significantly smaller than required for fully assisting the ankle of a paraplegic individual. As SCI patients can no longer feel their legs, the discomfort or pain is not registered, which results in a high risk of serious injury. Hence, shells are unfit for the distribution of forces onto the lower leg.

At the posterior side of the leg, large amounts of soft tissue enable the body to take the shape of a shell: application of forces to the back of both leg as in Figure 4.1-2 therefore is not a problem. However, at the anterior side of the leg, only a thin layer of skin separates the shin bone from the shell. It might be possible to create a custom shell, fitted to the shin of each test subject like in [24], but this is tedious, expensive, and impractical, and it does not guarantee comfort.

Thus, an interface is needed which conforms to the body instead of having the body conform to the interface.

5.2.3 A comfortable interface to the lower leg

A first iteration of a design that uses a conforming lower leg interface is shown in Figure 5.2-2(c). A rigid ring, onto which the actuators apply their compression forces, is placed around the lower leg. However, the ring does *not* come into contact with the leg. Instead, two padded straps are mounted within the ring: both pass from the internal to the external side of the leg, one anteriorly to the leg and the other posteriorly. These straps can be tightened using the dials on the front of the ring, to position the leg in the center of the ring.

This construction ensures that no rigid parts touch the leg; only the straps within the ring are in contact with the leg. As the straps conform to the body, it is possible to more comfortably apply a compression force to the leg.

Although this proof-of-principle is a significant improvement over the rigid shells, it is quite bulky and makes donning and doffing complicated as both the foot and lower leg need to pass through the ring.

A further design improvement is shown in Figure 5.2-4. Only half a ring is used and a Velcro strap behind the leg is used to adjust the device and keep everything in place. The test subject can first don the shoe and then pull the lower leg interface towards him, before closing the strap behind their leg.

5.2.4 Passive motion

The advantage of the use of pneumatic cylinders is that they are fully back-drivable when no tubing is connected. This means that it is straightforward to observe the passive or ‘minimal

(a) (b)

Figure 5.2-4
A comfortable interface for the distribution of normal forces anterior to the lower leg: (a) 3D view and (b) top view. A rigid bracket is used to hold a padded strap that interfaces with the body. The strap assumes the shape of the leg and no rigid components are pressing on the leg.

impedance' behavior of the orthoses—note that there is significant friction in the standard Festo cylinders used in the prototypes. This is particularly relevant, as one of the key goals of the project is to allow the ankle to move freely and naturally.

Figure 5.2-5 shows four of the extrema of the range-of-motion that can be achieved using one of the prototypes. We see in (a) and (b) that it indeed is possible to achieve both plantar flexion and dorsiflexion motion. It is promising to see that the prototype also allows the ankle to move in eversion and inversion, as is shown in (c) and (e) respectively.

Note that in this early prototype, ball-joints are used on the rod-ends at the shoe, but not at the shell. This means that radial forces are exerted on the cylinder rods during inversion–eversion, which is undesirable as they should only be loaded axially. This will become a problem when the cylinders are pressurized; in a design update the joints need to be modified.

(a) (b) (c) (d) (e)

Figure 5.2-5
Passive motion of the foot for one of the prototypes: (a) plantar flexion; (b) dorsiflexion; (c) eversion; (d) straight ankle; and (e) inversion.

5.2.5 Pressurizing the cylinders: generating ankle torques

The first observation after pressurizing the pneumatic cylinders and thereby generating a plantar flexion torque is that the rigid shells as used in the prototypes from Figures 5.2-1 and 5.2-2(a) are extremely uncomfortable. This was discussed in Section 5.2.2, design improvements to solve this were discussed in Section 5.2.3, and were implemented in the prototypes shown in Figure 5.2-2(b) and (c).

A more problematic observation is that the shell at the lower leg rotates around the lower leg as soon as only the slightest inversion–eversion motion is made. This results in the device being twisted either to the internal or the external side of the leg, thus rendering it incapable of generating any ankle torque or restoring its position.

Were the ankle to make a perfect plantar flexion–dorsiflexion motion about an axis that is parallel to both actuator axes, the shell might stay in place. However, the goal of the project is to enable inversion–eversion and the philosophy behind the iMS approach is specifically not to constrain natural movement of the body. Moreover, as was discussed in Section 2.2.3 and shown in Figure 2.2-4, the ankle always makes a *combined* plantar flexion–dorsiflexion and inversion–eversion motion—called pronation–supination—during walking.

Many attempts were made to prevent the shell from rotating around the leg. A large number of prototypes with a variety of strap configurations was constructed, but no solution was found to keep the shell in place using only flexible materials, which is a requirement of the iMS approach. A theoretical analysis of the rotation phenomenon can be found in Section 5.3.

5.2.6 Joint alignment and (loss of) cable tension

One of the ideas behind the iMS approach is that the absence of rigid joints takes away the need to precisely align the device with the joints of its wearer.

Unfortunately, this was already found to be false during the construction of the knee orthosis, which only has a single DoF. If we look at the knee orthosis in Figure 4.1-2(c) and (d), we see a cable connection point at the knee. It was found that good alignment with the knee joint is important to prevent the shells behind the leg from sliding up and down along the leg segments. However, for the knee orthosis the alignment is less critical, as the back of the leg consists of large amounts of soft tissue which can move with the shells without causing discomfort—provided that the motion is not too large.

For the ankle prototypes of Figure 5.2-2 however, it was found that correct alignment with the ankle joint is more important, as there is no soft tissue separating the shin bone from the skin (also see Section 5.2.2). This means that the interface on the lower leg will slide up and down over the skin at the shin when there is a misalignment between the connection point at the shoe and the ankle joint. This becomes particularly uncomfortable when large forces are exerted by the actuators.

Another problem occurs during inversion–eversion. Consider the situation in Figure 5.2-5(d), in which the ankle is straight. On both the internal and external side of the leg there is a cable going from the shell to a connection at the shoe, which should be aligned with the ankle joint. The cables have equal length and, as the cylinders are pressurized, are loaded with equal tension forces that prevent the shell from moving upwards. If there is zero inversion–eversion and if the connection points at the ankle are aligned correctly, making a plantar flexion–dorsiflexion motion as shown in Figure 5.2-5(a) and (b) should not cause any problem, as both cables remain loaded with the same tension force.

If we look at the everted situation shown in Figure 5.2-5(c), we can see that the distance from the shell to the ankle joint on the external side (right in the photo) has become shorter than the distance on the internal side (left in the photo). As cables are being used, this means that all the tension forces are carried by the internal cable (left), while the external cable (right) becomes slack. The opposite phenomenon can even more clearly be seen in Figure 5.2-5(e): the internal cable (left) has become slack and the external cable (right) carries all forces.

This is highly undesirable, as the lower leg shell is loaded asymmetrically. This causes, among other problems, a bending moment on the linear actuators which should only be loaded with pure axial forces. The bending moment may cause locking or even damage of the cylinders.

Although various cable configurations were considered and tested, no solution was found to prevent the asymmetrical loading of the shell during inversion–eversion.

5.3 Analysis of the iMS approach for assistance to the ankle

The evaluation of the iMS prototypes in Section 5.2 revealed a number of challenges. The most important one being that for all prototypes the lower leg interface rotates around the leg when the cylinders are pressurized. We will analyze this phenomenon to find a solution.

5.3.1 Modeling 2-DoF motion of the ankle

The biomechanics of the ankle are discussed in Section 2.3 and the orientation of the the plantar flexion–dorsiflexion and inversion–eversion axes are shown in Figures 2.3-1 and 2.3-2 on pages 11 and 12 respectively.

For analysis purposes, a simple model is proposed, in which the orientation of the foot with respect to the lower leg is a function of two angles. A detailed (mathematical) description of the model is given in Appendix E.1, but a short description will be given here.

For a given set of a dorsiflexion and inversion angle, $(\vartheta_{\text{df}}, \vartheta_{\text{iv}})$, and a dorsiflexion and an inversion axis of which the orientation is described by the unit vectors ω_{df} and ω_{iv}, the model behaves as follows.

1. We assume that the foot first makes a rotation by an angle ϑ_{df} about ω_{df}.
2. We assume that the orientation of ω_{iv} is not constant, but that it is rotated about ω_{df} over *half* the dorsiflexion angle, that is $\vartheta_{\text{df}}/2$. A new and *rotated* inversion–eversion axis $\hat{\omega}_{\text{iv}}$ is obtained.
3. Finally, the foot rotates by an angle ϑ_{iv} about $\hat{\omega}_{\text{iv}}$.

The new orientation of the foot thus is a combination of two subsequent rotations: first about ω_{df} and then about $\hat{\omega}_{\text{iv}}$, where the orientation of $\hat{\omega}_{\text{iv}}$ depends on ϑ_{df}. Note that the model assumes both axes to intersect in the ankle joint. A graphical overview of the behavior of the model is shown in Figure 5.3-1—the shown leg geometry is obtained from a 3D scan of the legs of a HeRoS Project team member.

5.3.2 Actuator configurations

Section 5.2.5 describes how the lower leg interfaces of the prototypes rotate around the lower leg as soon as the cylinders are pressurized. The phenomenon needs to be investigated and a solution needs to be found to prevent this.

All prototypes that were tested use two parallel pneumatic cylinders (see Figure 5.2-2). However, it might be that choosing a different actuator configuration is a solution to the issue. Therefore, the four different actuator concepts shown in Figure 5.3-2 are investigated. They are: Single (S), Double (D), V-shape (V) and A-shape (A). The (mathematical) description of the four configurations can be found in Appendix E.2.

5.3.3 Analysis of the rotation phenomenon

We have defined a simple 2-DoF model for the motion of the foot with respect to the lower leg as a function of a dorsiflexion and an inversion angle ϑ_{df} and ϑ_{iv} respectively. We have also defined four actuator configurations, (S), (D), (V), and (A). We need to understand why the lower leg interface rotates around the leg and whether it can be prevented.

The hypothesis is that the rotation phenomenon can be explained by the actuators generating a net torsion moment on the lower leg interface, acting around the axis of the lower leg, ω_{l}. The interface then rotates, as there is no counteracting moment. This hypothesis is tested and confirmed by the model in Appendix E.3.

Figure 5.3-3 shows a top view of the leg and the actuators of concept (D)—the grid layout corresponds to the one in Figure 5.3-1. The force action lines of the actuators are shown and so is the location of the leg axis ω_{l}, pointing upwards out of the figure. We assume that both actuators deliver equal force.

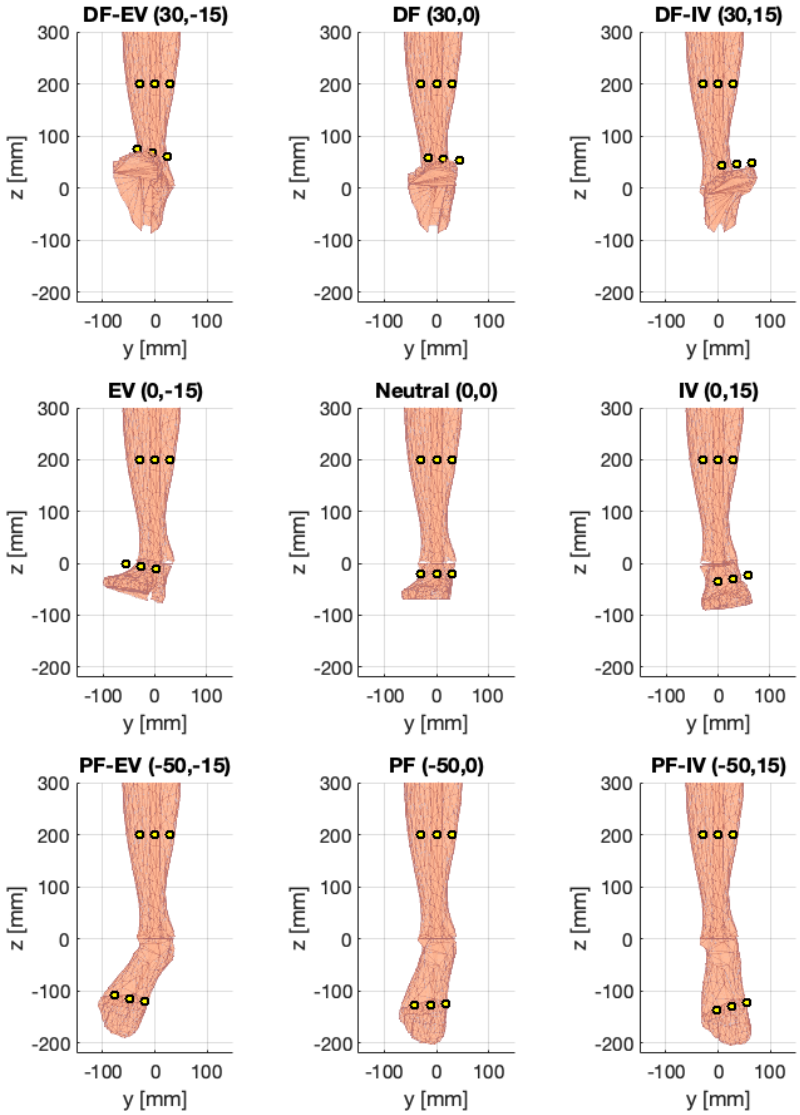

Figure 5.3-1
Motion of the foot in the ankle model. The zero configuration is shown in the center. From left to right: eversion to inversion. Bottom to top: plantar flexion to dorsiflexion. The following abbreviations are used in the titles. DF: dorsiflexion; PF: plantar flexion; IV: inversion; EV: eversion.

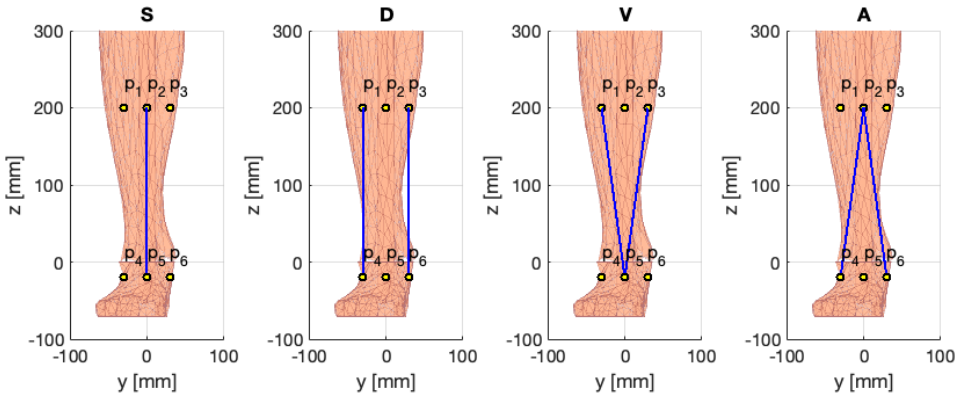

Figure 5.3-2
Frontal view of four actuator concepts; the position of the linear actuators are indicated by the blue lines. From left to right: Single actuator (S); Double actuator (D); V-shape (V); and A-shape (A).

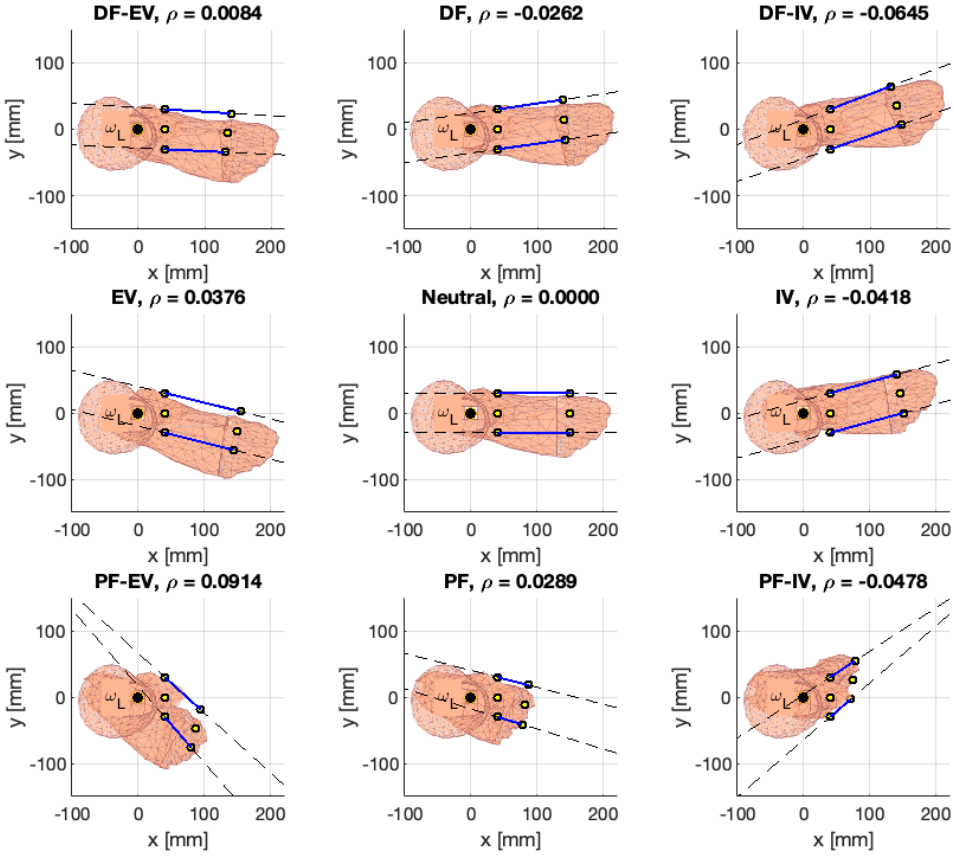

Figure 5.3-3
Top views showing the force action lines for the double actuator concept (D).

One can see that for the zero configuration in the center plot, the moments about ω_l due to both actuators cancel. However, there are net moments about the leg axis for the other configurations. A detailed analysis of the phenomenon is included in Appendix E.3, but it can be concluded that the same happens for all actuator configurations; the problem cannot be solved by choosing a different layout.

5.3.4 Cable tension

The configurations in Figure 5.3-1 are also used to investigate the changes in distance between the actuator anchor points and the connection points on either side of the ankle. These distances are not constant, so the problems with (loss of) cable tension that was described in Section 5.2.6 is indeed confirmed by the model—the problem cannot be solved by choosing a different actuator concept.

5.3.5 Final remarks

Some remarks regarding the modeling and analysis can be found in Appendix E.3.4, yet the main conclusion is that the iMS approach results in *inherently unstable* systems, as the flexible materials cannot be used to generate a moment to counteract the parasitic torques.

5.4 Conclusions

The iMS approach seemed a promising method for the design of a lightweight and comfortable ankle orthosis and was the foundation of the HeRoS Project. However, after a thorough investigation through both analysis and practical evaluation of prototypes, we concluded that it is not feasible to use the iMS approach to design an active ankle orthosis that allows both plantar flexion–dorsiflexion and inversion–eversion.

The main problem is caused by the desire to allow inversion–eversion. It follows from both theory and practice that using pushing linear actuators between the foot and lower leg results in an inherently unstable system, in which the interface on the lower leg rotates around the leg. It is not only undesirable to constrain inversion–eversion, but it is also impossible with the iMS approach.

Furthermore, the lower leg interface is loaded asymmetrically during inversion and eversion, as the cables on one side are loaded with all the forces, while the cables on the other side become slack. This causes bending moments in the lower leg interface and in the linear actuators, which are not designed to sustain bending moments: they might lock or even break.

One of the intended advantages of the iMS approach is that it was expected that alignment of the orthosis with the human ankle joint would not be critical. However, the opposite was found to be true, as the lower leg interface will slide up and down along the leg when the orthosis is not correctly aligned.

Finally, it was found infeasible to keep all system components in place with only the simple cable configuration shown in Figure 5.1-1. All the problems that were encountered require the addition of more and more straps or even rigid structures, thus yielding a design that is so complex that it defeats the purpose of following the iMS approach.

However, the knowledge and experience gained from investigating the iMS approach forms a solid basis for the development of more conventional exoskeleton concepts in Chapter 6.

CHAPTER 6

Conventional Concepts

This chapter discusses the analysis, evaluation, and design iterations of prototypes that rely on rigid mechanisms to provide the required degrees-of-freedom to the human ankle. Requirement RQ12-LACT (see Section 3.5.3) prescribes the use of linear actuators. For this reason, the same actuator configuration is used as in the iMS-based prototypes that are described in Chapter 5.

Two main types of solutions have been investigated: the first based on the Symbitron+ WE2 ankle module and the second derived from the orientation of the biological ankle axes. Note that this chapter focuses on the *passive* behavior of the prototyped mechanisms, because the load case on the mechanism is very high. The design of a final proof-of-principle prototype, built to withstand this load case, is described in Chapter 7.

6.1 Test platform for the first prototypes

Figure 6.1-1 shows a simple test platform that can be used to evaluate the behavior of various passive mechanisms at the ankle. It consists of (1) a cycling shoe with a rigid sole and attachment points on either side, and (2) a cuff worn around the lower leg with velcro strips on either side as attachment points. The prototyped mechanisms, in this case the rings indicated by (3), can easily be replaced, which allows for relatively quick evaluation of various designs.

The prototypes that are tested on this platform are made using rapid-prototyping techniques, such as 3D-printing and laser-cutting. These manufacturing steps can be carried out in-house, so that it is a relatively fast process.

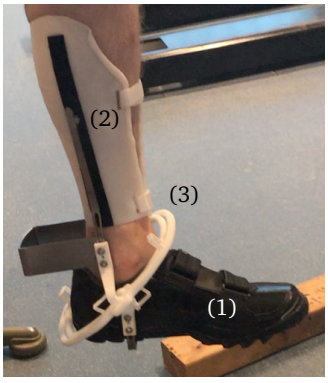

Figure 6.1-1
An interface to (1) the foot and (2) the lower leg to test joint mechanisms (3).

6.2 Analysis and evaluation of the mechanism of the WE2 ankle module

A full lower-body exoskeleton is under development within the Symbitron+ project [1]. The hardware development team of this project consists of people from both Delft University of Technology and the University of Twente. Figure 6.2-1(a) shows the Symbitron+ *WE2 exoskeleton*, worn by a patient (also shown larger in Figure 1.1-1 on page 3). It is a *modular* exoskeleton, which means that the various parts of the exoskeleton can be used independently: it is possible to use the ankle module as a standalone ankle exoskeleton.

A recent upgrade to the design of the ankle module of the WE2, is the addition of a second degree-of-freedom. This degree-of-freedom is passive and it is intended to allow the wearer to move their ankle in inversion–eversion. Figures 6.2-1(b) and (c) show CAD drawings of this new ankle module. Note that only the primary axis, which is perpendicular to the sagittal plane and intended for plantar flexion–dorsiflexion, is actuated. In this section, we investigate whether this same mechanism design can be used within the HeRoS Project.

(a) (b) (c)

Figure 6.2-1
The Symbitron+ WE2 lower-body exoskeleton: (a) worn by a patient; (b) and (c) the ankle module. (Source: [1])

6.2.1 Evaluation of a WE2-based passive mechanism

A passive mechanism was constructed based on the WE2 ankle module design and it is shown attached to the test platform in various positions in Figure 6.2-2. Note that the mechanism has the same layout as the device shown in Figures 6.2-1(b) and (c), but that it has no actuators and it is symmetric about the sagittal plane.

The ankle and foot can move freely and are not hindered by the presence of the mechanism.

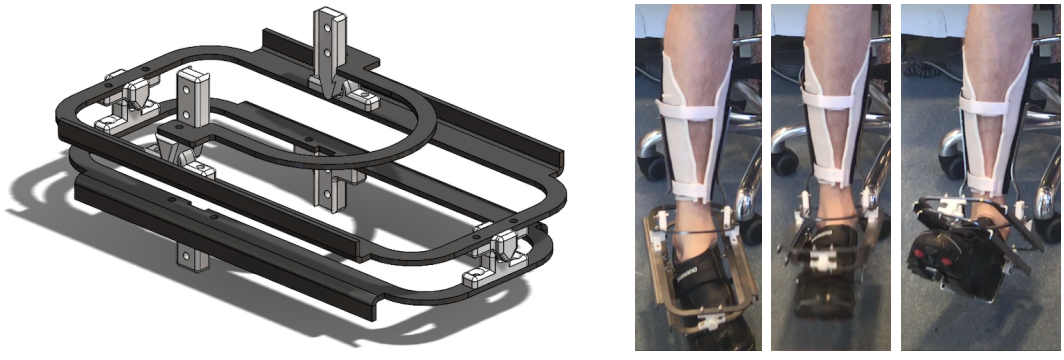

(a) (b) (c) (d)

Figure 6.2-2
Passive motion of a mechanism based on the WE2 ankle module: (a) CAD drawing; (b) plantar flexion-inversion (c) straight ankle; (d) dorsiflexion-eversion.

However, it seemed that the interface at the lower leg was rotating around the leg—similarly to the iMS concepts in Chapter 5, but without force being applied by actuators. For this reason, we investigated how the WE2 ankle module behaved for comparison.

6.2.2 Evaluation of the Symbitron+ WE2 ankle module (passive motion)

Figure 6.2-3 shows how the ankle module is worn as as standalone device, detached from the exoskeleton. The wearer sat on a bench and moved his foot in both inversion and eversion. Indeed the components attached to the lower leg rotate around the leg, comparable to our WE2-based prototype. A coupling was found between inversion and inwards rotation and eversion and outwards rotation.

(a) (b) (c)

Figure 6.2-3
Passive motion of the WE2 ankle module. Rotation of the device around the lower leg: (a) inversion results in inwards rotation; (b) straight ankle; (c) eversion results in outwards rotation.

The actuator components of the ankle module are rather heavy ($\sim$ 3.5 kg) and all the mass is placed on the external side of the leg. In the given configuration, in which the wearer is seated and has their lower leg stretched forward, gravity pulls on the actuator components so that they rotate outwards and thereby force the foot in eversion. The test subject reported that he had to 'lift' the mass of the actuator components to move from eversion in inversion. This behavior is analyzed in Section 6.2.3.

Figure 6.2-4 shows what happens when the ankle module is attached to the other components of the WE2 exoskeleton. The rotation of the module around the lower leg is constrained. As a results, the foot can no longer make a natural inversion–eversion motion. However, by tensioning the muscles, the foot can still rotate about the secondary axis of the device. The ankle is perfectly capable of making this motion, so it is not uncomfortable, but it is not a motion one can make actively when the foot is not touching the ground.

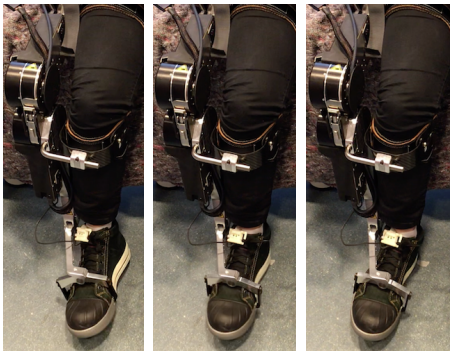

(a) (b) (c)

Figure 6.2-4
Symbitron+ WE2 ankle module attached to the full lower-body exoskeleton, passive motion: (a) inwards rotation; (b) neutral position; (c) outwards rotation.

6.2.3 Analysis

A simple model of the 2-DoF behavior of the human ankle joint has been described in Section 5.3.1 and more details are included in Appendix E.1. A grid of combined plantar flexion–dorsiflexion and inversion–eversion motion of this ankle model is shown in Figure 5.3-1 on page 38. Previously, this model was successfully used to explain the undesired rotation of the iMS prototypes. We can also use it to explain why the WE2 ankle module rotates around the lower leg during eversion and inversion motion.

Figure 6.2-5 shows a top view of the lower leg and foot for various combinations of dorsiflexion and inversion; the grid layout is the same as in Figure 5.3-1. Both axes of the device are drawn in the figure: the primary axis is indicated by the black line and the secondary by the blue. Dashed lines are used to more clearly indicate their orientation.

By construction, both axes are perpendicular to each other. As the secondary axis is attached to the foot, it moves with it. This results in a rotation of the primary axis—and thus of the whole exoskeleton—around the lower leg. The model thus confirms that the WE2 rotates around the lower leg, even when only a plantar flexion–dorsiflexion motion is made.

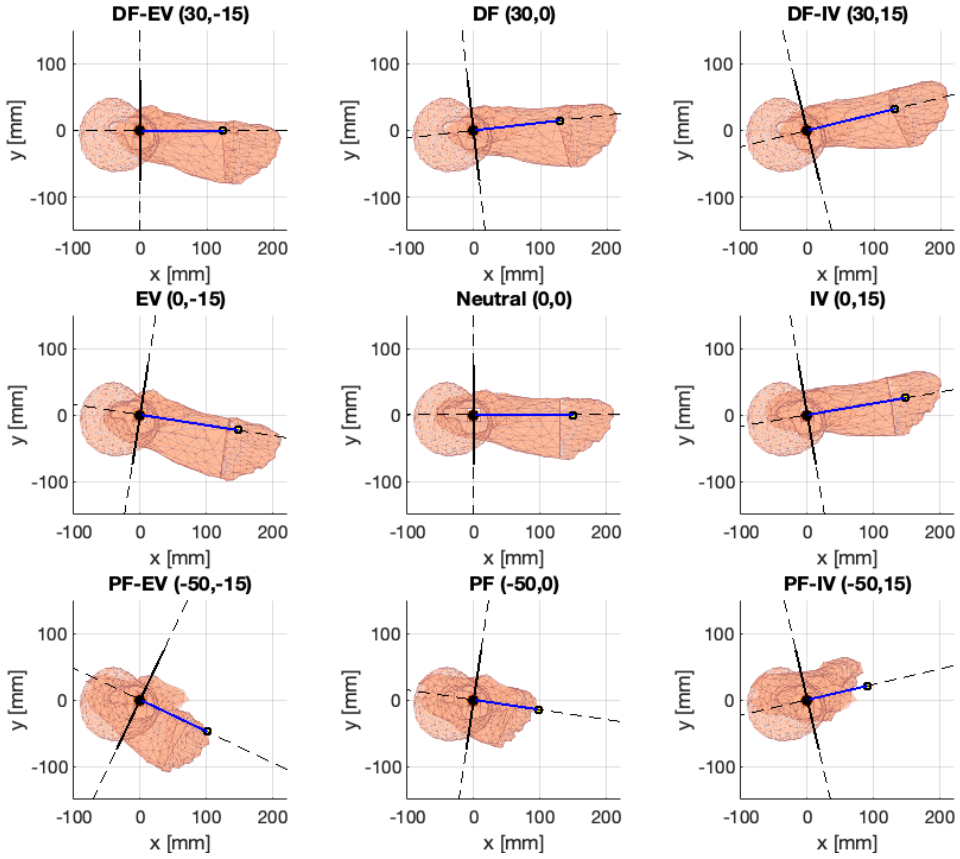

Figure 6.2-5
Top view of the lower leg and foot for various combinations of plantar flexion–dorsiflexion and inversion–eversion. The dashed lines indicate the directions of the axes of the WE2 ankle module.

6.2.4 Conclusion

It was found that the mechanism used in the WE2 ankle module results in a coupling between inversion–eversion and a rotation of the distal interface around the leg. This is undesirable in a stand-alone ankle exoskeleton, as the consequence is that also the plantar flexion–dorsiflexion axis of the device is rotating—meaning that the exact plantar flexion–dorsiflexion torque is undefined. Moreover, rotation of the components around the leg may cause chafing and discomfort.

Further evaluation of the WE2 ankle module, as part of a comparison with two other devices, is discussed in Section 8.3.

6.3 Development of a biomimetic ankle exoskeleton joint

The WE2 mechanism cannot be used in the exoskeleton, so a new concept needs to be developed. The ankle model that is described in Section 5.3.1 will serve as a basis for this new concept.

6.3.1 Mechanical implementation of the ankle model

The initial orientation (that is with a straight ankle) of the two ankle axes are described in Section 2.3. The model assumes that, for a given dorsiflexion and inversion angle ($\vartheta_{\text{df}}, \vartheta_{\text{iv}}$), the following happens. First, the foot rotates by an angle ϑ_{df} about the dorsiflexion axis. Then, as the inversion axis is not stationary, it rotates by an angle $\vartheta_{\text{df}}/2$ about the dorsiflexion axis. Finally, the foot rotates by an angle ϑ_{iv} about the rotated inversion axis.

This model can be implemented mechanically, by using a serial chain with three 1-DoF hinges. In the zero configuration, the 1st and 3rd hinge should be aligned with the dorsiflexion axis and the 2nd with the inversion axis. A schematic top view is shown in Figure 6.3-1(a), where the biological orientation of the axes are used. All three axes always intersect in the same point: the ankle joint. If a torsional spring is added to both axis 1 and axis 3, then axis 2 always stays centered at $\vartheta_{\text{df}}/2$ between the input and output of the mechanism. The mechanism input represents the lower leg and the output represents the foot (or vice versa).

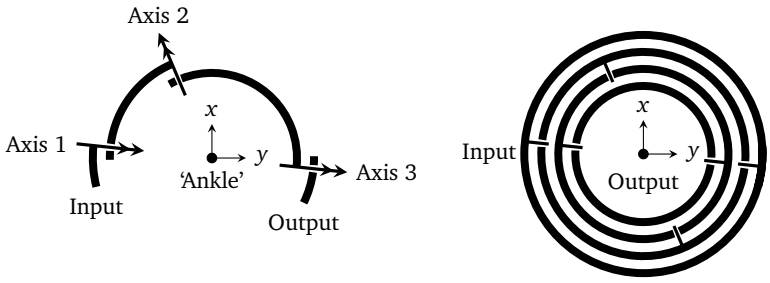

(a) (b)

Figure 6.3-1
Top view of a serial mechanism with three axes: (a) schematic serial chain; (b) rings with hinges on either side. Axis 1 and 3 are dorsiflexion axes and axis 2 is an inversion axis.

The mechanism can be built using a set of 'rings' so that for each of the three axes there is a 1-DoF hinge at either side of the ankle joint. This is schematically shown in Figure 6.3-1(b), where the outer ring is the mechanism input and the inner ring the input. A 3D CAD model is shown in Figure 6.3-2(a) and the 3D-printed mechanism is shown in (b). It is printed as a single part and it uses flexure springs between all rings, so that indeed the inversion axis rotates with $\vartheta_{\text{df}}/2$.

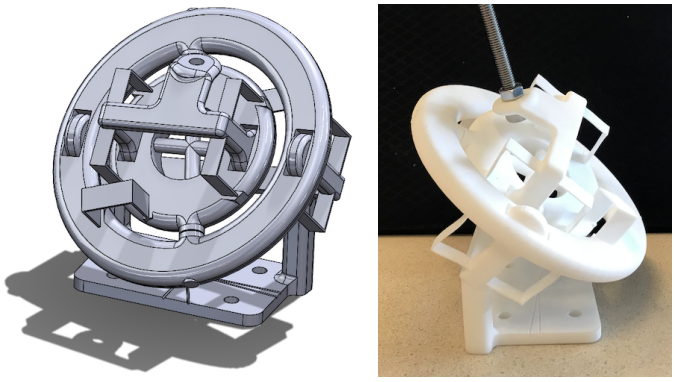

(a) (b)

Figure 6.3-2
Mechanical implementation of the theoretical ankle model for the right foot in a joint: (a) CAD model in a view on the right side of the back; (b) photograph in a view on the left side.

6.3.2 From mechanical ankle joint to exoskeleton joint

The joint model shown in Figure 6.3-2 was created with the intention of further developing it into an exoskeleton joint. Space can be created within the rings, so that it can contain the human ankle joint. The mounting plate at the table should be replaced by a shoe and the steel rod at the top should be replaced by an interface to the lower leg.

Figure 6.3-3 shows the result; the mechanism is connected to the test platform that was described in Section 6.1. One can see a set of two rings around the ankle. The smaller ring can rotate within the larger, around an inversion axis. The outer ring is connected to a dorsiflexion axis on the lower leg and the inner ring is connected to a dorsiflexion axis on the foot. Small flexures ensure the same equilibrium position and behavior as described earlier. The whole mechanism was 3D-printed as a single part, so that no assembly was required.

A number of test subjects was asked to wear the device and comment on the degrees-of-freedom and constraints. It was found that the mechanism provides complete freedom of movement to the ankle, although the range-of-motion is a bit too small. It is not necessary to (mathematically) analyze the behavior of this conceptual design, as it is the exact mechanical implementation of the model that would be used for this analysis.

Note that the axes of this first proof-of-principle are exactly aligned with the average axes of the human ankle, as shown in Figures 2.3-1 and 2.3-2 on pages 11 and 12. This makes the design quite complex, as all axes are tilted. Furthermore, the rings collide with the floor during plantar flexion, so the design is not yet suited for walking. The concept is promising, but further development is needed.

(a) (b) (c) (d)

Figure 6.3-3
Biomimetic concept with aligned axes, passive motion. Natural ankle movement: (a) CAD model; (e) inversion; (c) light plantar flexion; (d) eversion.

6.4 Development of a practical exoskeleton joint

Section 6.3 describes how the theoretical model of the behavior of the human ankle is implemented in a mechanical ankle joint. The concept is then developed further and a proof-of-principle exoskeleton joint is created.

The biomimetic design is completely aligned with the *average* human ankle axes, thus yielding a rather complex design with tilted axes. However, as was explained in Section 2.3, a large variation exists between individuals, so it might be possible to simplify the design by not sticking exactly to this 'biological alignment'.

The first step is to set the dorsiflexion axes of the mechanism perpendicular to the sagittal plane. This greatly simplifies the design and makes it easier to construct prototypes using standard materials such as (lasercut) plates and (rectangular) tubes.

The second step is to reconsider the orientation of the inversion axis within the rings. According to Figure 2.3-2, this axis is tilted 41° upwards with respect to the horizontal plane. This angle need not be reconsidered, as this orientation is variable anyway due to the construction of the

mechanism. However, the axis is also rotated 23° inwards with respect to the sagittal plane, with a large variation between individuals.

Two ways to further simplify the design are considered.

1. Setting the inversion axis of the mechanism perpendicular to both dorsiflexion axes.
2. Setting the inversion axis of the mechanism under 45° inwards with respect to the dorsiflexion axes.

The first option makes it possible to use the same mechanism for both the right and the left foot. The second option allows for removal of part of the rings, so that they no longer collide with the floor. A proof-of-principle of both possibilities was constructed and evaluated.

6.4.1 Joint mechanism with perpendicular axes

Implementation of the first simplification concept is shown in Figure 6.4-1. The mechanism was mounted to the test interface that was discussed in Section 6.1.

The design is simplified significantly and only uses geometrical shapes. The mechanism is 3D-printed in one part, but laser-cut steel plates are used to provide additional stiffness to the rings. Small flexures are used between the links for proper link alignment.

Test subjects still perceived complete freedom of movement of the ankle, although the range-of-motion in inversion–eversion is still limited due to the end stops of the mechanism.

A disadvantage of the design is that it still uses complete rings around the ankle and foot. The rings collide with the floor at large plantar flexion angles, so the concept is only suitable to demonstrate the working principle.

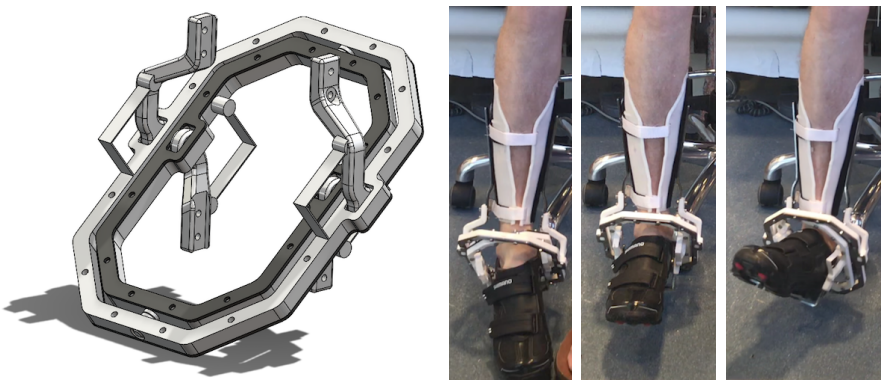

(a) (b) (c) (d)

Figure 6.4-1
Concept with perpendicular axes: (a) CAD drawing; (b) inversion; (c) straight ankle; (d) eversion.

6.4.2 Joint mechanism with a 45° internal angle

The second simplification concept is shown in Figure 6.4-2. The design update was also used to develop stiffer attachments to the shoe and lower leg, and to integrate attachment points for linear actuators.

The ring mechanism still makes use of 3D-printed components, but it is no longer printed as a single part. A glued and bolted sandwich construction of 3D printed components and laser-cut steel plates is used to provide more stiffness to the mechanism. The device also uses ball bearings at the four dorsiflexion joints and bushings for the inversion axis within the rings.

Another important design improvement is that the mechanism no longer uses closed rings. The internal part at the posterior side of the rings is removed, so that the rings no longer collide with the floor. This makes the prototype suitable for walking and other tasks. It also makes it easier to don the device, as one can pull on the back of the shoe.

Test subjects perceived complete freedom of movement of the ankle, only limited by the end stops of the mechanism.

(a) (b) (c) (d)

Figure 6.4-2
Concept with the inversion axis under 45°: (a) CAD drawing of the mechanism; (b) CAD drawing of the exoskeleton with actuators; (c) prototype in eversion; (d) prototype in inversion.

6.4.3 Evaluation and concept choice

Section 6.3.2 describes the design of a biomimetic exoskeleton joint mechanism that is completely aligned with the axes of the human ankle joint. The resulting design is too complex for practical implementation and two design simplifications were considered: Section 6.4.1 describes a design with perpendicular axes and Section 6.4.2 describes a design in which there is a 45° angle between the inversion axis and the dorsiflexion axes of the mechanism.

The passive behavior of all three concepts was thoroughly investigated, both during walking (in straight lines, in circles, while making cross-steps, ...) and with the foot freely moving in the air. Test subjects perceived no difference between the devices: all three prototypes provide complete freedom of movement to the ankle and no rotation of the lower leg interface is observed.

The choice was made to further develop the device with the perpendicular axes, because of its simpler design and the fact that the same mechanism can directly be used for both the left and the right foot.

6.5 Further development of the final concept

Before starting with the design of an actuated prototype, a final iteration is made on the design with the perpendicular axes. The goal of this extra iteration is to identify any design challenges and check for collisions of the mechanism with the ankle and foot of the wearer.

The result is shown in Figure 6.5-1. The updated components for the lower leg and shoe, that were presented in Section 6.4.2, are reused to obtain a stiffer structure. Combinations of 3D-printed parts and laser-cut plates are used. The most important design improvement is that the back half of the rings is removed. This leaves the back of the shoe completely free: donning becomes very easy, as one can put on the shoe like a regular shoe. More importantly, the design has become significantly less bulky and it can no longer collide with the floor.

Removing half of the rings does complicate the design. The inversion joint is only present at the front, so this joint is loaded with large bending moments when the rings are pulled apart or compressed. A hardened steel axle is press-fit into a steel clamping block which is integrated in the inner ring. An aluminum bearing housing with two internal roller bearings on either side is integrated in the external ring; the housing ensures that the bearings are not loaded with bending moments.

Thrust washers on either side of the bearing housing ensure smooth rotation during axial loading. A retaining ring is fixed in a groove at the end of the steel axle to prevent the bearing housing from sliding off the axle. This ensures that the two rings cannot move apart.

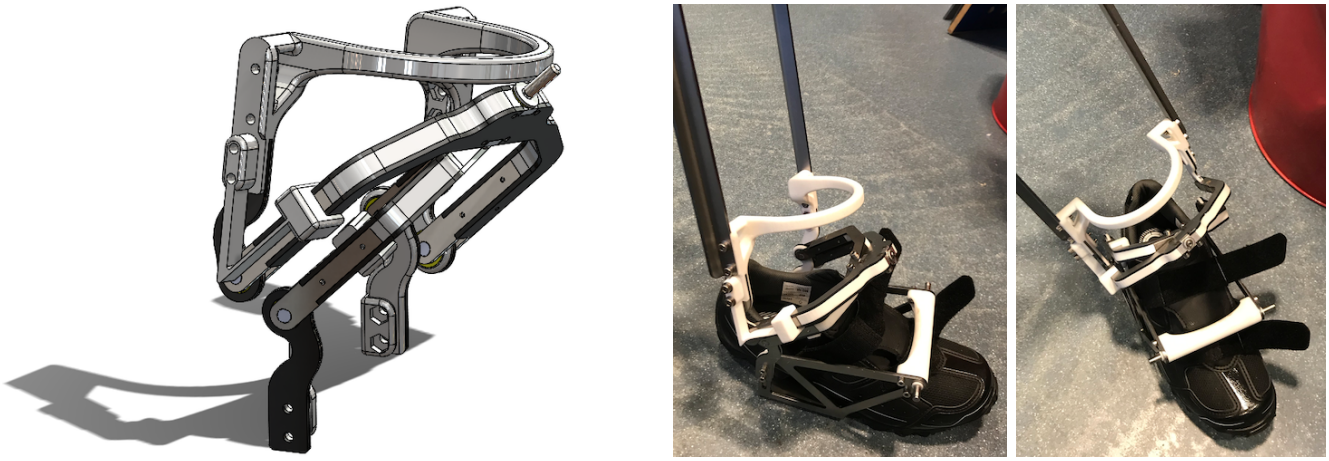

(a) (b) (c)

Figure 6.5-1
Concept with perpendicular axes: (a) CAD drawing; (b) in inversion; (c) in eversion.

Finally, roller bearings are used at the four dorsiflexion joints and 3D-printed leaf springs are used to define the equilibrium orientation of the rings.

6.5.1 Evaluation

A final evaluation was done before proceeding with the development of the actuated prototype. In the experiment, the prototype with perpendicular axes was compared to the prototype from Section 6.4.2 with the axes under 45°. Both prototypes have a similar level of detailing: they use the same shoe connection and lower leg interface; they both make use of proper bearings in all hinges; and a sandwich construction of 3D-printed material and laser-cut plates is used to provide stiffness to the mechanisms.

Three participants were recruited for the test. They each got to wear both prototypes simultaneously, as shown in Figure 6.5-2: the one on the right and the other on the left foot. The participants were instructed to execute the following tasks.

- Walking in straight lines;
- Walking in clockwise (CW) circles;
- Walking in counter-clockwise (CCW) circles;
- Making cross-steps;
- Moving the foot freely in the air, in all possible directions.

The goal was for them to comment on how the devices felt and whether they noticed any difference in behavior or the freedom of movement given by both devices.

The only difference identified by the participants was in range-of-motion: both devices have different end-stop locations. No difference in the degrees-of-freedom was found and both devices were found to provide complete freedom of movement to the ankle. No rotation around the leg was observed and none of the participants preferred one device over the other.

6.5.2 Analysis of mechanism behavior

The initial joint mechanism, as presented in Section 6.3, was based on a model of the ankle joint and it made use of axes that were aligned with the average orientation of the axes of the biological ankle joint.

This biomimetic concept, with a rather complex design due to the tilted axes, was taken as a basis for a much simpler design with perpendicular axes. Test subjects noticed no difference in the behavior of both mechanisms, even though the axes of the latter are not aligned with those of

(a) (b)

Figure 6.5-2
Movie frames of a test subject comparing the degrees-of-freedom and range-of-motion of the prototype with perpendicular axes (worn on the right foot, shown left in the photos) and the prototype with the axes under 45° (worn on the left foot, shown right in the photos): (a) left foot in plantar flexion-eversion; (b) right foot in plantar flexion-inversion.

the ankle. So, why does this simplified mechanism still provide complete freedom of movement to the ankle?

To answer this question, we use the ankle model that is described in Section 5.3.1. The definition of the coordinate systems Ψ_l at the lower leg and Ψ_f at the foot are shown in Figure 6.5-3.

The prototype has two plantar flexion–dorsiflexion axes. One is attached to the shoe and, because it moves with the foot, is always perpendicular to the xz-plane of Ψ_f on the foot. The other is attached to the lower leg interface and, as it moves with the leg, is always perpendicular to the xz-plane of Ψ_l on the lower leg.

By construction, the internal 'inversion' axis between both half rings is always perpendicular to both the first and the second plantar flexion–dorsiflexion axis. This means that the orientation of this axis can be found as the intersection of the xz-plane of the foot and the xz-plane of the lower leg. These intersections are shown in Figure 6.5-4 for various combinations of plantar flexion–dorsiflexion and inversion–eversion.

The first thing that catches the eye is that the intersection is not defined in the neutral position $(\vartheta_{df}, \vartheta_{iv}) = (0, 0)$. This is due to the fact that both planes are parallel. Were the foot to rotate exactly about the y axis, then both planes would stay parallel and the intersection remains undefined. This also means that the orientation of the ring mechanism is not defined by the orientation of the foot. However, it is kept in its equilibrium position by the flexures.

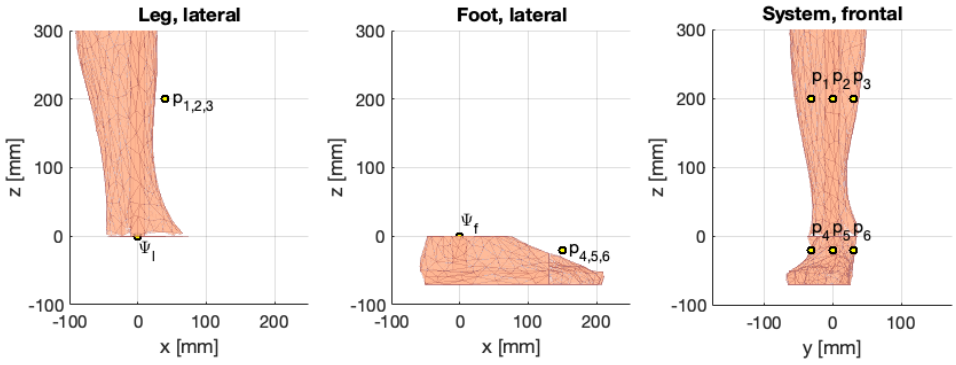

Figure 6.5-3
Definition of coordinate systems and points at the leg and foot. The left and middle figure provide a lateral view on the leg and foot respectively and the right figure shows a frontal view on both body parts in the reference configuration. (Copy from Figure E.1-2 on page 136.)

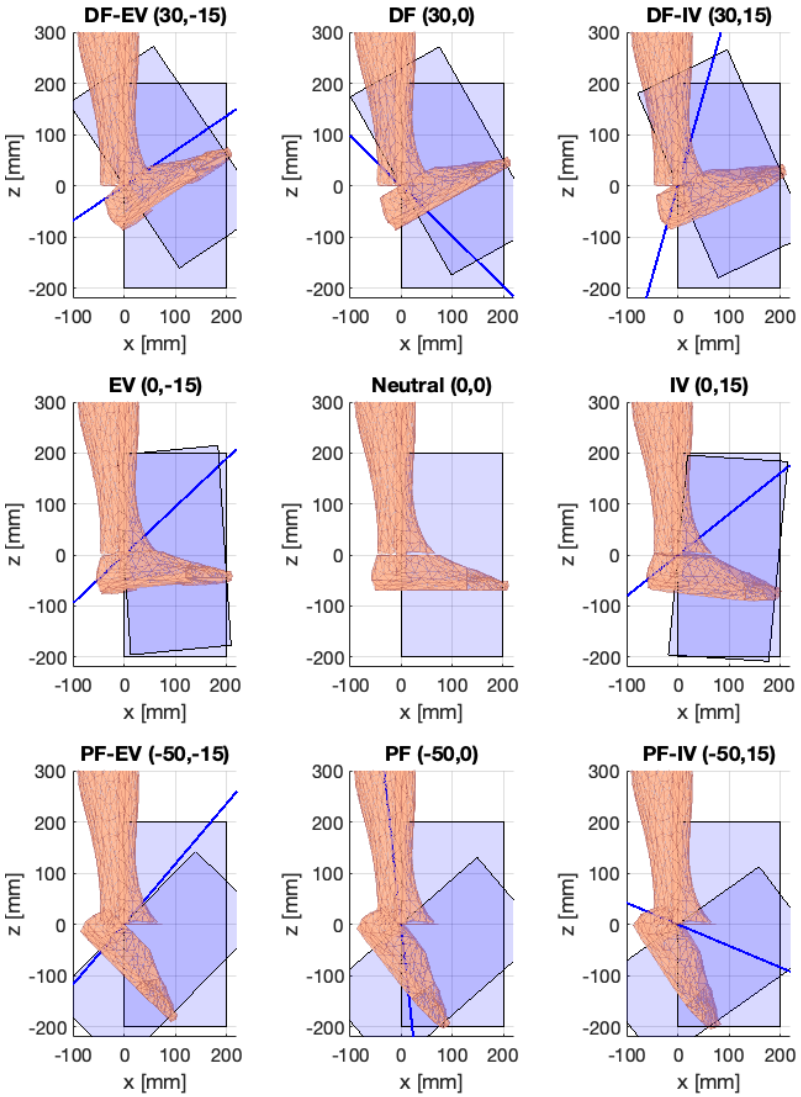

Figure 6.5-4
Intersections of the xz-plane of the lower leg with the xz-plane of the foot, shown for various combinations of plantar flexion–dorsiflexion and inversion–eversion.

The second thing that attracts attention, is that for the extrema of pure plantar flexion–dorsiflexion, the intersection points through the foot. This cannot happen in practice, so at these angles, one would expect the ring mechanism to collide with its end stops: either hitting the top of the foot, or the anterior side of the lower leg. However, this behavior was not observed in the actual prototypes.

The reason for the behavior predicted by the model can be explained as follows: the plantar flexion–dorsiflexion axis in the model is *almost* perpendicular to the xy-plane, yet it is slightly tilted. This means that the planes make a kind of screw motion when the foot rotates about this axis, and only a small dorsiflexion angle causes a large difference in the orientation of the intersection of the planes.

The joint mechanism actually is a *gimbal* mechanism and the $(\vartheta_{\mathrm{df}}, \vartheta_{\mathrm{iv}}) = (0, 0)$ situation, in which the orientation of the internal axis is undefined, is a singularity called *gimbal lock*. The large differences in orientation observed for small rotations are an effect of being close to the singularity.

It is indeed found possible to enforce this extreme behavior of the mechanism, however we were not able to reproduce this behavior when the prototype was worn on the leg. Though when the shoe is held fixed, and one uses their hands to force a particular twisting motion on the lower leg interface, it is possible to let the rings move very rapidly to either side, due to the singularity in the gimbal.

As mentioned earlier, in practice this behavior was not observed. Firstly, flexures are used to define the equilibrium position of the rings; it never happens that the orientation is undefined. Furthermore, the mathematical model is very rigid, whereas there is a significant amount of compliance in reality. No real 'ankle axis' exists, as the ankle joint is a composition of bones and ligaments, and there is compliance in the tissue of both the foot and lower leg. Finally, one cannot make a 'pure' plantar flexion–dorsiflexion motion, as this is not actually defined, and the motion will thus always be a combination of both plantar flexion–dorsiflexion and inversion–eversion. In the end, the combination of these factors ensures that no practical problems will occur.

The images in Figure 6.5-4 which show combinations of both plantar flexion–dorsiflexion and inversion–eversion, explain why the mechanism works so well. The foot can move freely, while the mechanism tilts smoothly up and down.

6.6 Conclusions

In this chapter, a concept is developed for the ankle joint mechanism for the ankle exoskeleton.

First, in Section 6.2, we investigated whether the mechanism of the WE2 ankle module can be used for a stand-alone ankle exoskeleton. This mechanism works satisfactorily in the full lower-body exoskeleton, but it was found unsuitable for use in a stand-alone ankle exoskeleton, as the resulting device would rotate around the lower leg.

Then, a *biomimetic* design approach was followed in Section 6.3. First, a simple model of the behavior of the ankle was made. Then, based on this model, a mechanism was designed that can be used as an exoskeleton joint.

The resulting exoskeleton mechanism worked well, but the mechanism was too complex due to all the tilted joint axes. Simplification steps were therefore made in Section 6.4 and a final design iteration was made (Section 6.5).

Based on the positive assessment of the test subjects, it is concluded the resulting mechanism is so promising that it will be developed further into a proof-of-principle prototype that will be actuated by linear actuators. The design of this final prototype is described in Chapter 7 and its evaluation in Chapter 8.

CHAPTER 7

Design of a Proof-of-Principle Prototype

Chapter 6 described the development of a mechanical ankle exoskeleton joint based on the orientation of the axes of the human ankle. This chapter describes the design of a final proof-of-principle prototype that can deliver up to 74 Nm of plantar flexion torque based on this concept.

7.1 Exoskeleton configuration and design focus

The global layout of the prototype is shown in Figure 7.1-1. Two linear actuators, which are parallel when the foot and leg remain in the xz-plane, will be placed anteriorly to the ankle. They exert either compression or tension forces between anchor points on the shoe and on the lower leg interface. A mechanism based on the concept that was developed in Chapter 6 will be placed at the ankle and rigid links are used to interconnect all components.

This particular layout is the same as for the iMS prototypes that are described in Chapter 5, so that the actuators that are developed in the HeRoS Project can still be used and `RQ12-LACT` is satisfied.

Due to the orientation of the actuators, high forces act upon the joint mechanism at the ankle: it is either loaded by compression or tension forces. The load case is very similar to that of the iMS approach (see Appendix D). The prototypes from Chapter 6 were not able to withstand these forces, so the main focus of this chapter is to design a mechanism that can withstand them.

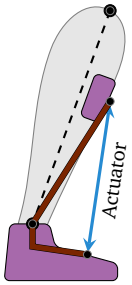

Figure 7.1-1
Layout of the prototype. Linear actuators are attached to anchor points on the shoe and the lower leg interface. A joint mechanism is placed at the ankle and rigid links are used to connect it to the actuator anchor points.

The goal is to create a proof-of-principle prototype that can deliver significant ankle torques, while still allowing the ankle to move in both plantar flexion–dorsiflexion and inversion–eversion. It is necessary to redesign both the connection to the shoe and the interface to the lower leg, so that they can withstand the large forces. However, the focus is on demonstrating the working principle of the joint mechanism, so the foot and leg interface will remain rather simple. An orthotist should be involved when the prototype is developed further.

7.2 Actuators and force control

Electro-hydraulic linear actuators are under development with the HeRoS Project, a first demonstration of the principle on which these actuators rely can be found in [18]. Unfortunately, the actuators are not yet ready to be used in the prototype, so a different solution is needed to demonstrate the working principle of the 2-DoF ankle exoskeleton.

7.2.1 Proof-of-principle actuators

Temporary linear actuators are needed for actuation of the prototype. A wide range of commercial-off-the-shelf linear actuators is available, yet they are heavy and non-back-drivable. Designing custom linear actuators is not desired, as the actuators are simply needed to demonstrate the working principle.

For this reason, the choice was made to use *frictionless* pneumatic cylinders. Regular cylinders were previously used in the iMS prototypes in Chapter 5. The chosen cylinders are from Airpel and they use a graphite piston moving through a cylinder with a glass lining. More details on the cylinders and the components needed to regulate the airflow can be found in Appendix F.1.

The advantage of these cylinders is that they are lightweight and have a good power-to-weight ratio. The force they can deliver is determined by the maximum allowable pressure and the cylinder diameter. Cylinders with a larger diameter can generate more force, but they also take up more space.

Cylinder diameter

A trade-off was made between actuator force (and thereby the maximum ankle torque) and actuator volume (and by that the size of the exoskeleton). Based on the available cylinder diameters, the choice was made to use cylinders with an internal diameter of 24 mm. The maximum absolute pressure for the Airpel cylinders is 8 bar, thus resulting in a maximum pushing force of 316 N per actuator. Using two of these actuators and building them into the prototype so that they have a 100 mm moment arm, would result in a 63 Nm plantar flexion torque, which is sufficient to demonstrate the working principle of the device, according to requirements `RQ09-DTRQ` and `RQ10-PTRQ`.

Actuator module design

Note that the length of the cylinders has not yet been determined. This is discussed in Section 7.3, *after* the design of the actuator module is determined, as it influences the range-of-motion of the exoskeleton.

To build the cylinders into the device, ball-joints are needed at both ends, as all internal angles change during combined dorsiflexion and inversion. Furthermore, a force sensor is needed to accurately control the force that is delivered by the cylinders.

Figure 7.2-1 shows the design of the actuator modules. Plastic rod-ends with a maximum pivot angle of 27° were selected, based on the maximum actuator force. A load cell is added to measure the force produced by the actuator. Aluminum parts are manufactured to interconnect all components and 3D-printed plastic covers are used to protect the actuator modules.

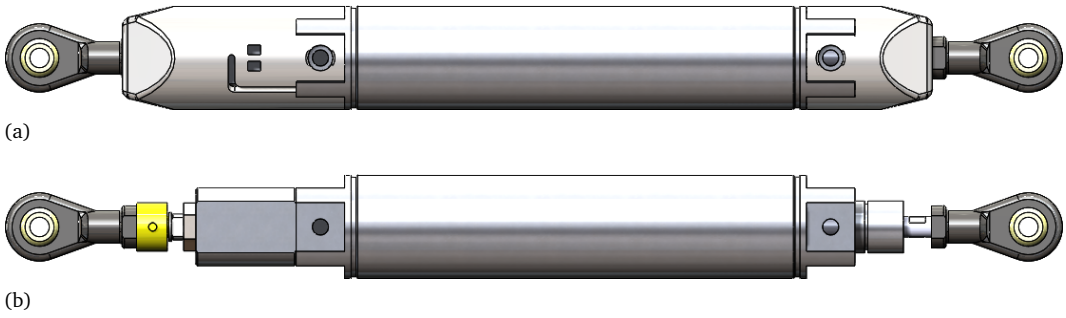

(a)

(b)

Figure 7.2-1
CAD drawing of the pneumatic actuator module: (a) with and (b) without protective covers.

7.2.2 Electronics and control

Bi-directional proportional control valves are used to regulate the flow of pressurized air to and from the cylinder chambers. Each cylinder has its own valve, which regulates the *direction* of the air flow—either to the extension or the retraction chamber—as well as the *size* of the air flow.

A nonlinear force control algorithm is used to control the valves; it combines both *sliding mode control*—using the fact that the mass flow of the air is proportional to the 1st time derivative of the cylinder force—and *proportional feedback control*.

A detailed description of the force control algorithm can be found in Appendix F and the electronic and pneumatic components needed to regulate the airflow are described in Appendix F.1.

7.3 Actuator stroke, anchor points, and range-of-motion

The actuator module design is shown in Figure 7.2-1 and a cylinder diameter of 24 mm was chosen. The cylinders are available in various piston strokes. The stroke determines, together with the location of the actuator anchor points, the final range-of-motion of the orthosis.

7.3.1 Actuator stroke selection

The range-of-motion required for plantar flexion–dorsiflexion is $\vartheta_{\text{df}} \in [-50, 30]°$, as is prescribed by `RQO2-PROM` and `RQO1-DROM` in Section 3.5.3. Note that this is a very large RoM and, based on the literature review in Appendix C.1, it is unlikely that the end stops will be hit during any of the use cases that are described in Appendix B. For this reason, and the desire to keep the actuator modules as short as possible, it is decided to exactly map the range-of-motion of the cylinders to this dorsiflexion range-of-motion. This is shown in a 2D view in Figure 7.3-1.

The ankle joint is denoted by J; the upper actuator anchor point is denoted by A; and the lower by B_i. Suppose the lower leg with anchor point A is held still and the foot moves in plantar flexion–dorsiflexion. The actuator anchor point on the foot then moves on a circle with radius r_B.

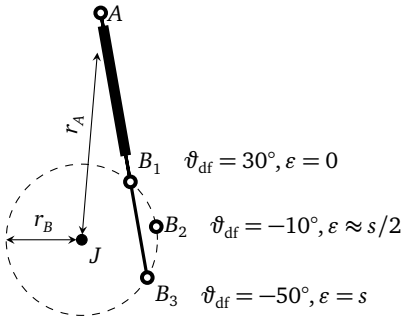

Figure 7.3-1
2D analysis to determine the cylinder stroke based on the required range-of-motion.

We require that an ankle angle $\vartheta_{df} = 30°$ corresponds with cylinder position $\varepsilon = 0$ (full retraction, indicated by B_1) and an ankle angle $\vartheta_{df} = -50°$ corresponds to a cylinder position $\varepsilon = s$, with s the cylinder stroke (full extension, indicated by B_3). Note that the action lines AB_1 and AB_3 are collinear. The center of the dorsiflexion RoM lies at $\vartheta_{df} = -10°$ and is indicated by B_2; it corresponds *approximately* to the center of the actuator RoM which lies at $\varepsilon = s/2$.

The upper anchor point A lies at a constant radius r_A from the ankle joint, fixed to the lower leg. The lower anchor point B_i lies at a constant radius r_B from the ankle joint, fixed on the foot. These two radii determine the range-of-motion, but the *orientation* of the actuator module can be chosen freely, without altering the RoM, or the delivered torque.

We chose to match the actuator RoM to the 2D dorsiflexion RoM. The values of r_A and r_B are then uniquely defined by the actuator stroke and the module design that is shown in Figure 7.2-1. As a result, the larger the stroke, the larger both radii become and the more torque can be delivered. However, the design also becomes bulkier and the anchor point A might end up above the knee. Decreasing the stroke will make the whole device more compact. Yet, the space into which the exoskeleton ankle joint needs to fit also becomes smaller and there is a risk of the cylinder rods colliding with the rings around the ankle.

After careful consideration of all possibilities, it was decided to use cylinders with a stroke of $s = 125$ mm. The resulting distance from the ankle to the upper anchor point then becomes $r_A = 400.5$ mm and the distance to the lower anchor point becomes $r_B = 97.2$ mm. The length r_A is quite large, causing the exoskeleton to become higher than desired, yet it stays below the knee joint. The height cannot be decreased further, because then r_B would also decrease. The radius r_B is quite small, but based on the prototypes from Chapter 6 it is deemed feasible to fit the joint mechanism within the remaining space.

7.3.2 Actuator anchor locations

As mentioned before, although r_A and r_B are determined, the orientation of the actuators can still be chosen freely. It can be seen in Figure 7.3-1 that the distance from the ankle joint J to the line AB_i is minimal at the extrema of the piston position. The cylinders are to be mounted anterior to the lower leg. To prevent the cylinders from colliding with the leg, their orientation is chosen so that they are parallel to the axis of the lower leg at maximum dorsiflexion and maximum plantar flexion.

7.3.3 From cylinder space to ankle joint space

The minimum length of the actuator module is $AB_1 = 331$ mm and with a stroke of 125 mm, its maximum length is $AB_3 = 456$ mm. Figure 7.3-2 shows that the relation between actuator length and dorsiflexion angle is almost linear when we assume no inversion and dorsiflexion about an axis perpendicular to the sagittal plane.

The moment arm of the actuators with respect to the ankle joint determines, together with the maximum force that can be generated, the ankle torque that is delivered. It can easily be seen in Figure 7.3-1 that this moment arm varies over the range-of-motion and is minimal at the extrema.

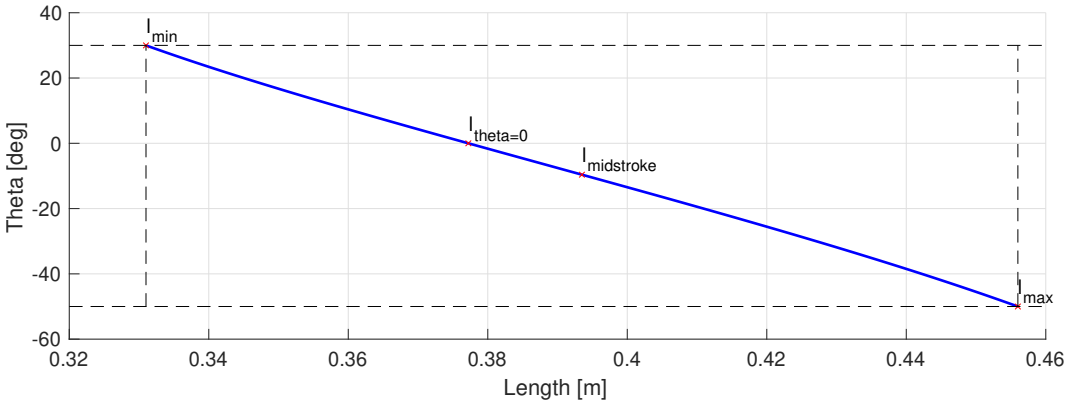

Figure 7.3-2
Relation between the actuator length AB_i and the resulting 2D dorsiflexion angle ϑ_{df} of the ankle.

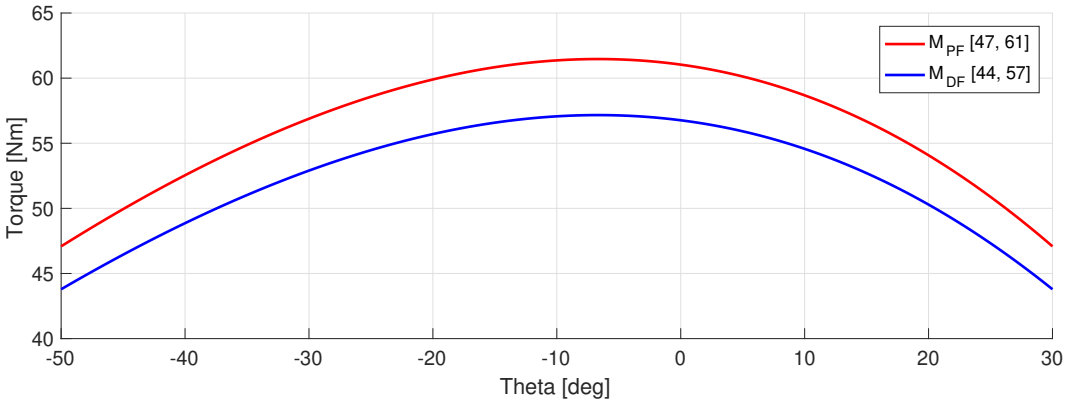

Figure 7.3-3
Relation between the ankle angle ϑ_{df} and the maximum plantar flexion torque and maximum dorsiflexion torque that can be delivered with a supply pressure of 8 bar.

We assume an available supply pressure of 8 bar. The maximum pushing force that can be delivered by two cylinders then is 632 N and the maximum pulling force is −593 N. The difference in pulling and pushing force is due to a difference in piston area for both chambers, see Appendix F. This also means that there is a difference in the maximum plantar flexion and dorsiflexion torque.

Figure 7.3-3 shows the maximum torque as a function of the ankle angle. Note that we assume dorsiflexion about an axis perpendicular to the sagittal plane and no inversion. The minimum torque that can be delivered over the whole RoM in either direction is 44 Nm, so that both requirements `RQ10-PTRQ` and `RQ09-DTRQ` are satisfied. The maximum plantar flexion torque that can be delivered is 61 Nm and the maximum dorsiflexion torque is 57 Nm. Generally, plantar flexion is more important when assisting gait—see the literature review in Appendix C.1.

7.3.4 Resulting freedom of movement for the ankle in 3D

We will look into the 3D range-of-motion that the chosen actuator layout gives to the ankle. After investigation, the width between both actuators (both at the leg and at the foot) was set to 100 mm. This leaves enough space between the cylinder rods for the ankle joint mechanism, without causing the exoskeleton to become too wide on either side of the foot.

The same ankle model that was previously used for the other analyses will be used to investigate the RoM of the prototype. The model is described in Section 5.3.1 and its behavior is shown in Figure 5.3-1 on page 38 for various combinations of dorsiflexion and inversion.

A discrete 2D grid is constructed for dorsiflexion angles $\vartheta_{df} \in [-50, 30]°$ and inversion angles $\vartheta_{iv} \in [-30, 30]°$. At all combinations $(\vartheta_{df}, \vartheta_{iv})$, the configuration of the lower leg and foot is computed using the model. Note that the actuator anchor points move with the foot and leg, so we can compute the configuration of both actuators for each of the leg configurations.

Figure 7.3-4 shows the resulting grid. The color of the markers denotes whether the given combination of ankle angles can be achieved with the actuators. Green indicates that the configuration is reachable. Red means that the cylinder on the *internal* side of the leg would need to become shorter than possible and blue denotes that it would need to be longer than possible. Magenta denotes that the cylinder on the *external* side of the leg would be extended further than possible. It does not happen within this grid that the external cylinder becomes too short.

Additionally, it is verified whether the pivot angle in the rod-ends remains smaller than their maximum 27°. This is the case for all configurations, so the rod ends do not limit the RoM.

The freedom of movement is limited at the extreme combinations of dorsiflexion-eversion and plantar flexion-inversion. This can be explained by considering the orientation of the human inversion axis—see Figure 2.3-2 on page 12. No significant improvements are achieved when varying the width between the actuators. Moreover, the ankle behavior is 'just a model' based on average data and it is not useful to set strict requirements on the RoM that should be achieved by this model. The current configuration is thus accepted for further development.

Black markers in Figure 7.3-4 are used to indicate which combinations of $(\vartheta_{df}, \vartheta_{iv})$ can be achieved by the Achilles Ankle Exoskeleton. Our mechanism has a substantially larger range-of-motion.

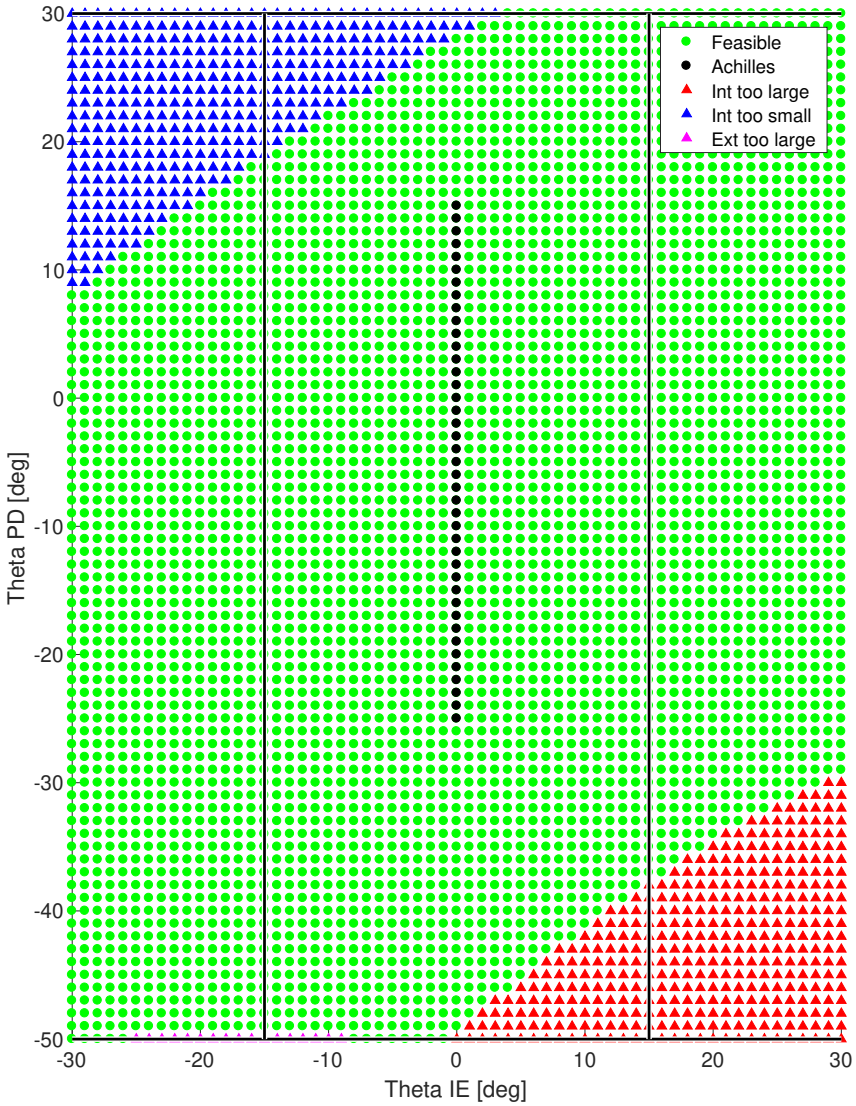

Figure 7.3-4

Discrete evaluation of workspace reachability with the chosen actuator configuration for combinations of dorsiflexion and inversion $(\vartheta_{\mathrm{df}}, \vartheta_{\mathrm{iv}})$. The required RoM is indicated by the black lines: $\vartheta_{\mathrm{df}} \in [-50, 30]^\circ$ and $\vartheta_{\mathrm{iv}} \in [-15, 15]^\circ$.

7.3.5 Mock-up to test the layout

Pneumatic cylinders were chosen for the actuation of the exoskeleton. Their diameter was chosen based on a trade-off between size and force and heir stroke was determined by the requirements on the plantar flexion–dorsiflexion range-of-motion. The orientation of the anchor points was chosen so that the cylinders do not come into contact with the leg.

With all actuator anchor points defined, a final mock-up was constructed to check the feasibility of the design. This mock-up is shown in Figure 7.3-5. 3D-printing and laser-cutting techniques are used to quickly manufacture the mock-up. It shows that the layout is feasible and does not collide with the leg: the joint mechanism can be designed.

(a) (b)

Figure 7.3-5
Mock-up to test the feasibility of the chosen actuator anchor points: (a) CAD drawing; (b) close-up photograph showing sufficient space between the ankle and cylinder rods for the joint mechanism and sufficient space within the rings for the ankle.

7.4 Joint mechanism design

The joint mechanism that will be used in the prototype is described in Section 6.5 and Figure 6.5-1 on page 49 shows its design. The mechanism in the final prototype will be loaded with significant forces, as can be understood from Figure 7.1-1.

7.4.1 2D load case

The load case will be considered in 2D: only the important directions—that is those in which mechanism failure is expected—will be considered. It is assumed that the ring mechanism is only loaded by a force F in the xz-plane, acting on the ball bearings on the dorsiflexion axes. This is shown in Figures 7.4-1(a) and (b).

The force F is an interaction force between the one ring and the interface to the foot and the other ring and the interface to the lower leg. The force depends on the ankle angle; the chosen locations for the actuator anchor points; the location of the force acting on the lower leg; and the maximum force generated by both actuators together, which is 632 N. The 'worst case' value for F is 650 N, so this is the value for which the mechanism will be designed.

The rings can rotate about the dorsiflexion axes, as is indicated by the 'Tilt' arrows. This means that the angle under which the force F acts on the mechanism changes. Figure 7.4-1(c) shows the interaction forces between the rings, for an arbitrary ring orientation. Not only the rings are subject to bending moments, but also the axle which lets the one ring rotate within to the other: this is a critical part in the design. For convenience we call this axle the *ring axle*.

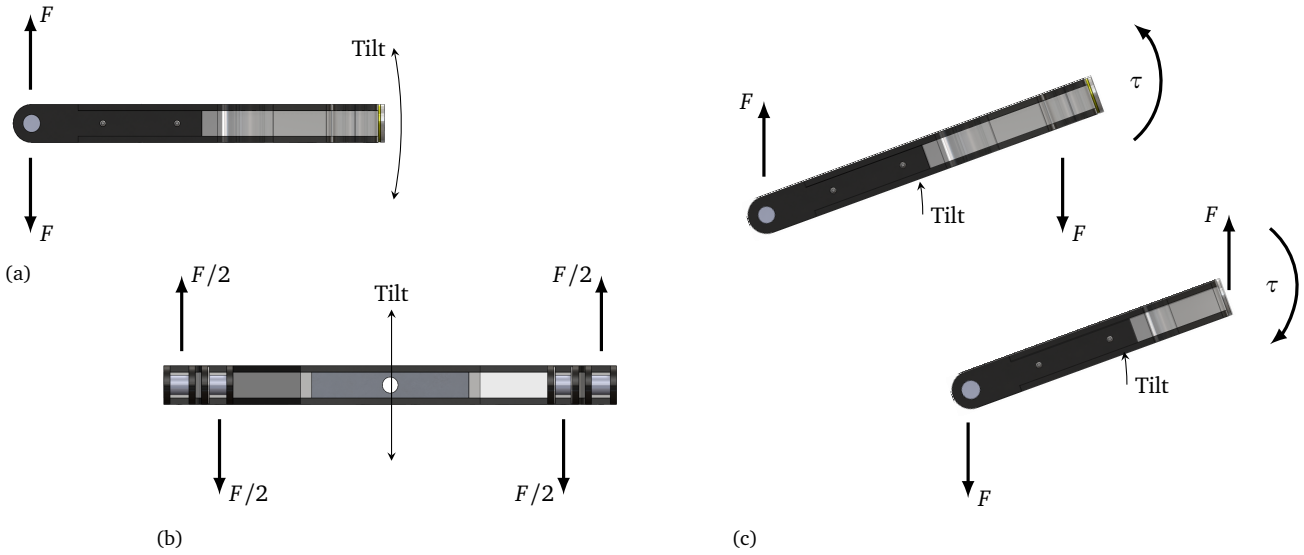

Figure 7.4-1
Load case: (a) lateral view and (b) posterior view on the radial forces acting on the dorsiflexion axes of the rings, the rings are pulled 'apart' as one ring is pulled upwards and the other downwards; (c) simple free body diagram illustrating the interaction between both rings.

There are two important situations.

Pure bending When the rings are parallel to the x-axis, the situation shown in Figure 7.4-1(a) and (b) is obtained. The rings are loaded with internal bending moments. A high bending stress occurs in the ring axle; however, it is not loaded by axial forces.

Pure axial loading When the ring mechanism is tilted counter-clockwise, so that it is aligned with the z-axis, the rings are loaded axially. If the force is directed so that the rings are pressed onto each other, no load is felt by the ring axle. However, the ring axle is purely loaded with an axial tension force when the rings are being pulled apart.

When the exoskeleton is in use, the loading of the mechanism will be a combination of both cases, as the orientation of the rings continually changes. The mechanism can withstand this changing load case if it can withstand both extreme cases.

7.4.2 Materials and manufacturing methods

The load case is quite demanding, in particular with respect to the loading of the ring axle and its bearings. A significant amount of time and effort was invested in considering material and manufacturing options that reduce the overall mass of the design. However, time constraints forced us to manufacture the prototype in-house and the following choices were made.

- Welded rectangular steel tubing with a $15 \times 15 \times 2$ mm cross section is used for the rings.
- A hardened steel axle is used for the ring axle, together with a clamping block and bearing housing made from steel.
- Regular ball bearings, needle bearings, and thrust washers are used.

Figure 7.4-2(a) shows the rings after welding and (b) shows the result after spray-painting and assembly.

Both the (external) size and the mass of the welded mechanism can be reduced by using more advanced materials and methods. Milling or 3D-printing of titanium, the use of carbon fiber reinforced plastics, and geometric optimization have been considered. However, the steel construction suffices to demonstrate the working principle.

The remainder of this section describes the most important considerations in the design of the ring mechanism.

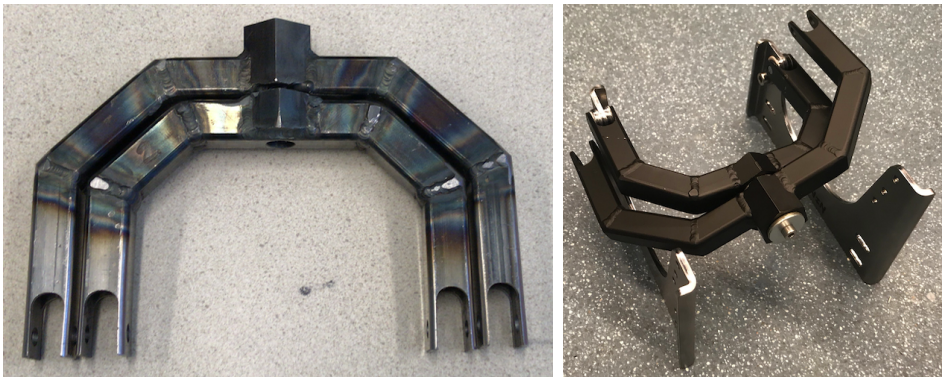

(a) (b)

Figure 7.4-2
The ring mechanism: (a) the welded rings before assembly; (b) the assembled mechanism after spray-painting.

7.4.3 Global ring dimensions, revision of actuator anchor locations, and RoM

The internal dimensions of the inner ring are dictated by the space needed for the ankle. Based on the evaluation of the previous prototypes, the inner width is set to 100 mm. The free distance needed anterior to the ankle is set to 65 mm. This is the distance from the dorsiflexion axis to the anterior inside of the inner ring.

The outer dimensions of the mechanism is determined by the size of the rectangular tubing and the need for space between both rings. The tubes have a $15 \times 15 \times 2$ mm cross section and the space needed between both rings is 2 mm. The minimum width of the whole mechanism thus is 164 mm and the minimum distance from the dorsiflexion axis to the anterior side of the mechanism is 97 mm.

The actuator stroke and anchor locations were determined in Section 7.3. We decided that the the anchor points at the foot should be placed at a distance $r_A = 97.2$ mm from the dorsiflexion axis. However, the outer dimensions of the ring mechanism becomes significantly larger than planned for: the tubular rings will collide with the cylinder rods. A design revision is needed.

After thorough investigation of the kinematics and the risk of collisions, it is determined that the dorsiflexion RoM of the ankle exoskeleton should be adjusted to $\vartheta_{\text{df}} \in [-45, 20]°$. The radii become $r_A = 405.5$ mm and $r_B = 116.3$. A disadvantage is that the plantar flexion–dorsiflexion RoM is decreased. However, the ankle torque that can be delivered is increased, as the actuator moment arm has become larger. The maximum plantar flexion torque is 74 Nm, compared to the 61 Nm of the previous layout.

7.4.4 Internal axle, bearing housing, and bearing selection

The same construction is used for the internal axis as in the prototype in Section 6.5. A hardened steel axle will be used, clamped on the one side and mounted in a bearing housing (with bearings at either side) on the other. There are two possibilities.

Clamping in the inner ring The axle is clamped in the inner ring and the bearing housing is mounted in the outer ring.

Clamping in the outer ring The axle is clamped in the outer ring and the bearing housing is mounted in the inner ring.

The choice is important for the bending load case that is described in Section 7.4.1. Both possibilities have been analyzed. The dimensions have been determined based on a variety of design considerations, such as the minimum space required for the ankle; the cross section of the tubes; and the space needed to mount the bearings.

Figure 7.4-3 shows the analytically computed stress distribution for both load cases, which was verified numerically by comparison to SPACAR [25]. Both the stress in the axle and the loading of the bearings was taken into consideration. Based on these considerations the axle diameter, bearing type, and length of the housing were determined.

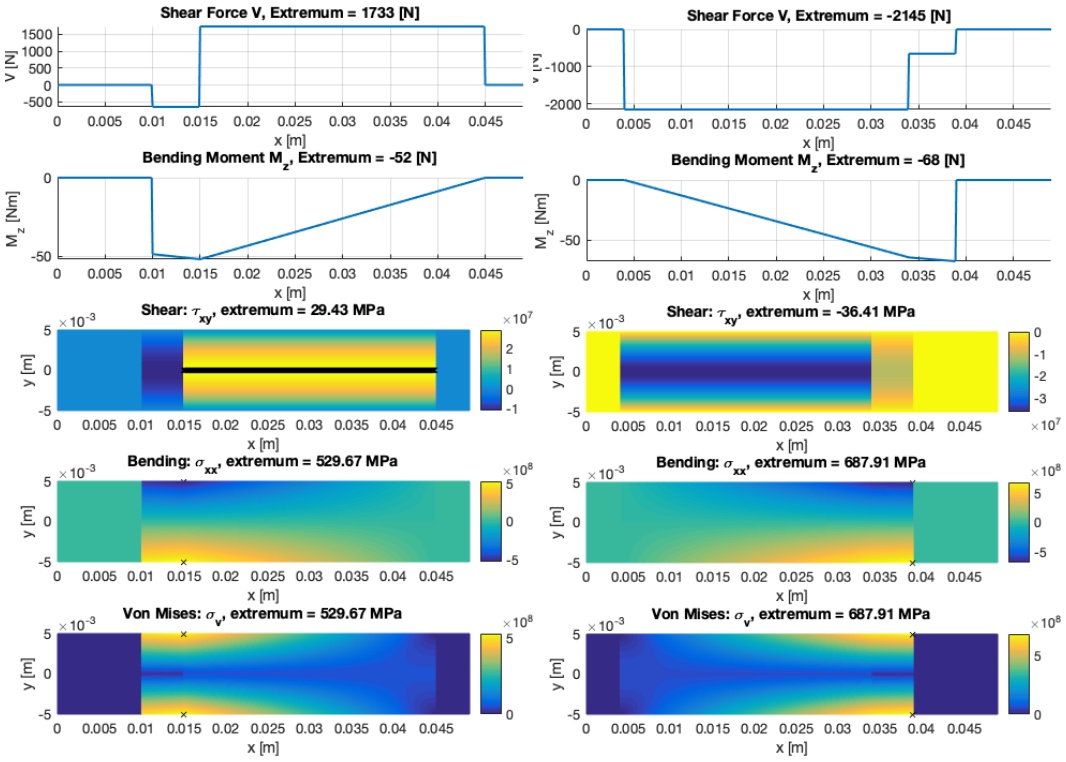

(a) (b)

Figure 7.4-3

Stress analysis for loading of the bearings: (a) clamped in the internal ring, bearing housing in the outer (b) clamped in the outer ring, bearing housing in the inner.

Clamping in the inner ring is preferable, because this allows for the bearing housing to stick out from the outer ring. This was also found to be the better choice regarding both axle and bearing loading.

Figure 7.4-2 already showed the implementation. A hardened steel axle with a diameter of 10 mm and total length of 49 mm is used. SKF needle bearings are press-fit into the housing. Thrust washers are placed on either side of the housing and a steel ring is bolted onto the external side of the axle; this construction ensures that the mechanism can withstand the axial load case, while always running smoothly.

7.4.5 Ring design and dorsiflexion bearing selection

The ring design is shown in Figure 7.4-2. A FEM analysis was carried out to verify that the assembled construction can withstand both load cases described in Section 7.4.1. The construction was found to be stronger then necessary: a smaller tube cross section would have sufficed, but 15 × 15 mm is the smallest available in the in-house workshop.

Hardened steel axles with a diameter of 6 mm and length of 15 mm are used for the four dorsiflexion hinges. Figure 7.4-2(a) shows how recesses are milled in the top of the rings. The axles are press-fit into the sides of the rings and bearings, which are selected for the load case, are mounted in the frames of the shoe and lower leg interface.

7.5 Design of other mechanical components

An overview of the prototype is shown in Figure 7.5-1. In this section some details of the design will be discussed. All components are manufactured in-house and the main production methods are 3D-printing using Selective Laser Sintering (SLS) and 2D laser-cutting of metal plates. In addition, plates are bent to provide structural stiffness.

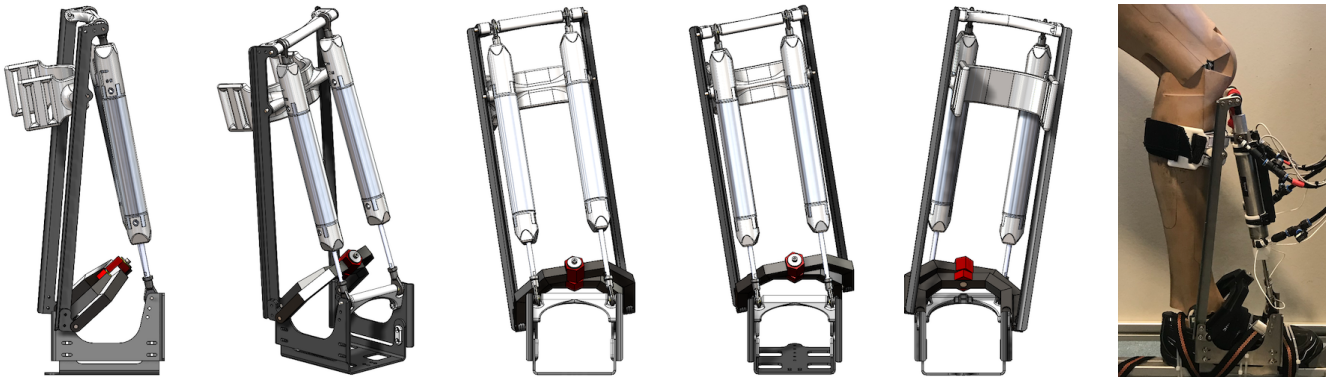

(a) (b) (c) (d) (e) (f)

Figure 7.5-1
The final prototype: (a)–(e) various views on the CAD model; (b) photograph of the actual device with all tubing and cables, mounted to a test bench.

7.5.1 Foot interface and exoskeleton frame

The shoe is the exoskeleton's interface to the foot. A comfortable Shimano mountainbiking shoe with Velcro closures is used. A rigid plate in the sole of the shoe makes it easy to mount it to the exoskeleton frame and the shoe has a rubber outsole for good traction.

The assembly that attaches to the shoe is shown in Figure 7.5-2(a). A bent plate is mounted to the bottom of the shoe. Two plates, one on either side of the shoe, are mounted onto the sole plate. The edges of the plates are bent to provide structural stiffness.

The outsole of the foot was modified by hand and the bottom plate was designed in such a way that as much rubber as possible is in contact with the floor. (The metal plate should be kept off the floor, as it has too little friction.) The result is shown in Figure 7.5-2(c)

A hardened steel axle is placed in a 3D-printed frame and mounted between the plates above the toes. This structure fulfills two functions. Firstly it serves as the anchor points for rod-ends of the actuators. Secondly, it provides stiffness to the exoskeleton structure that is mounted to the shoe.

A stack of three layers of steel plate provide enough thickness to use as the bearing housing for the dorsiflexion hinges. The internal ring of the joint mechanism is attached to the foot.

7.5.2 Lower-leg interface and exoskeleton frame

The actuator modules are rather long and the distance from the dorsiflexion axis to the top anchor points is $r_A = 405.5$ mm. As it is uncomfortable to apply pressure to the lower leg just below the knee, a construction was designed which applies the forces lower down the leg. The exoskeleton components for the lower leg are shown in Figure 7.5-3.

The frame on either side of the leg is made of steel, which is bent to provide stiffness. A similar construction as on the shoe is used for the actuator anchor points: a hardened steel axle within a

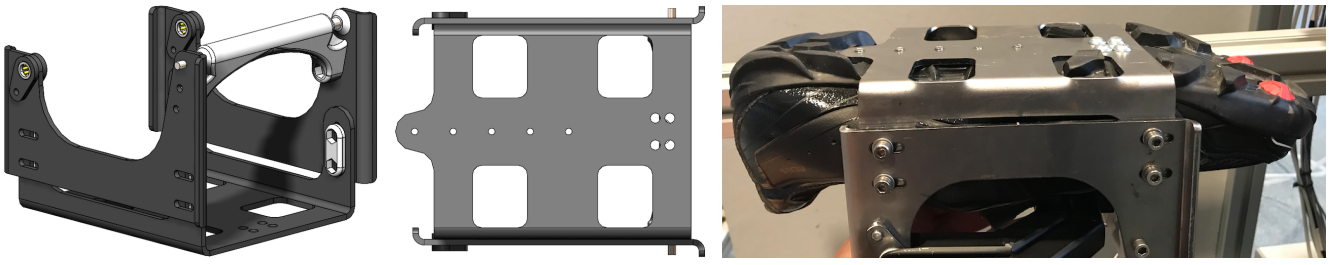

(a) (b) (c)

Figure 7.5-2
Foot exoskeleton frame: (a) CAD drawing of the subassembly with bearings; (b) bottom view of the CAD model with space for the rubber of the outsole; (c) photograph of the modified sole.

(a) (b)

Figure 7.5-3
Lower leg exoskeleton frame: (a) CAD drawing of the subassembly with bearings; (b) movie frame of walking in the prototype.

3D-printed structure is used to mount the actuators and provide stiffness to the exoskeleton.

A 3D-printed bracket is used to house straps that interface to the leg. This design is described in Section 5.2.3—note that the plastic is not in contact with the leg. The bracket provides additional stiffness to the lower-leg structure of the lower leg. Note that it can rotate around its mounting axis, so that it adapts to the leg of the wearer.

A stack of three plates is used as bearing housing for the dorsiflexion hinges. The lower-leg frame is connected to the outer ring of the joint mechanism.

7.6 Conclusions

This chapter described the design process of a proof-of-principle 2-DoF ankle exoskeleton. It is based on the mechanism that was developed in Chapter 6 and it is equipped with two independently controlled pneumatic actuator modules, which can provide torque in both the plantar flexion–dorsiflexion and inversion–eversion direction.

Project time constraints demanded rapid fabrication of the prototype, so that neither mass nor volume could be optimized. The use of steel tubes for the exoskeleton joint mechanism required a decrease of the dorsiflexion range-of-motion. However, this did result in an increase of the torque that can be delivered. The 2D dorsiflexion range-of-motion that is achieved is $\vartheta_{\mathrm{df}} \in [-45, 20]^\circ$ and the maximum 2D plantar flexion torque that can be delivered is 74 Nm.

The total mass of the prototype is 3.58 kg. This includes the mass of both actuator modules and the shoe, but not the external pneumatic valves and electronics that are used to regulate the airflow to and from the cylinders.

Testing and evaluation of the prototype is described in Chapter 8.

PART III

Evaluation

CHAPTER 8

Evaluation

The prototype that is described in Chapter 7 will be evaluated in this chapter. Section 8.1 describes a stress test in which the exoskeleton is loaded by the maximum actuator force. Motion control performance evaluation of the actuators is described in Section 8.2; this provides a nice demonstration of the DoFs of the device. The passive behavior of the device is compared to the behavior of both the Achilles Ankle Exoskeleton and the Symbitron+ WE2 ankle module. The experiment and its results are described in Section 8.3. Finally, the technical requirements are reviewed in Section 8.4. Conclusions and recommendations can be found in Chapter 9.

8.1 Stress test: maximum loading of the prototype

The ring mechanism of the prototype has been designed to withstand the load case that is described in Section 7.4.1. It is an important test—yet potentially destructive—to verify whether the manufactured mechanism can indeed withstand the maximum actuator force. More importantly, the device should not fail while it is being worn by a test subject.

Because it is dangerous (and uncomfortable) to perform this maximum force test with a human test subject, a test bench is used. The test bench is specifically designed to test the hardware developed in the HeRoS Project; see Appendix G for more information.

Figure 8.1-1 shows the prototype mounted to the test leg. The position of the hip joint of the leg is locked in-place and ideally the foot should be fixed to the frame. Unfortunately, there are no external fixation points on the shoe or prototype, so straps are used to fix the foot and shoe to the frame of the test setup; this fixation is not fully rigid.

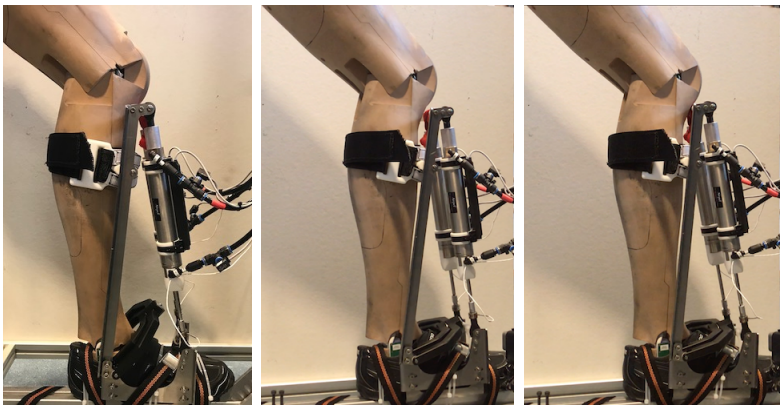

(a) (b) (c)

Figure 8.1-1
The prototype attached to the test leg: (a) photograph of the device while it is turned off; (b) movie frame of the device at maximum pushing force; (c) movie frame at maximum pulling force.

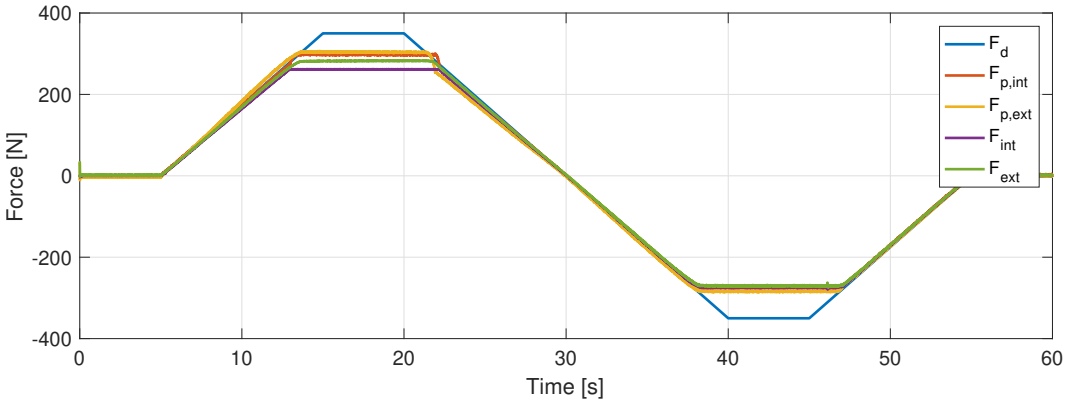

Figure 8.1-2
Maximum load test: actuator force as a function of time. The reference force $F_d \in [-350, 350]$ N is equal for both cylinders. The forces $F_{p,int}$ and $F_{p,ext}$ are the force in the internal and external cylinder respectively, computed based on the pressure measurements in the chambers. The force F_{int} and F_{ext} are the respective measurements from the force sensors.

The rings are loaded with a force that either pulls them apart, or compresses them (see Section 7.4.1). The orientation of the rings in the xz-plane determines whether the rings and the internal axle are loaded with bending moments or with axial forces. Bending is the worst case scenario; this is the load case for which the internal axle is designed. This worst case loading happens when the rings are approximately perpendicular to the force action lines of the actuators; this is the orientation in which we will carry out the stress test.

It can be seen in the photographs that the rings are not tilted exactly perpendicular to the cylinder rods. This is due to the shapes of the lower leg and foot of the test bench; the shoe; and the prototype. This is also precisely the reason that the prototype was developed: to allow the foot to take its natural position—in this case the 'natural' position of the foot of the test bench.

With the prototype fixed to the leg and the leg fixed in the frame, the reference force F_d for *both* actuators is first ramped up to 350 N. It is kept constant for five seconds and then ramped down to −350 N. The reference force then is slowly increased back to zero. This reference force pattern is repeated multiple times. The force reference and the actual forces in both cylinders are shown in Figure 8.1-2. The forces in the internal and external cylinder are shown both based on the pressure measurements and on the force sensor measurements. Figure 8.1-3 shows the measurements of the supply pressure and the pressures in the four cylinder chambers. The remainder of this section discusses the data that is presented in the figures.

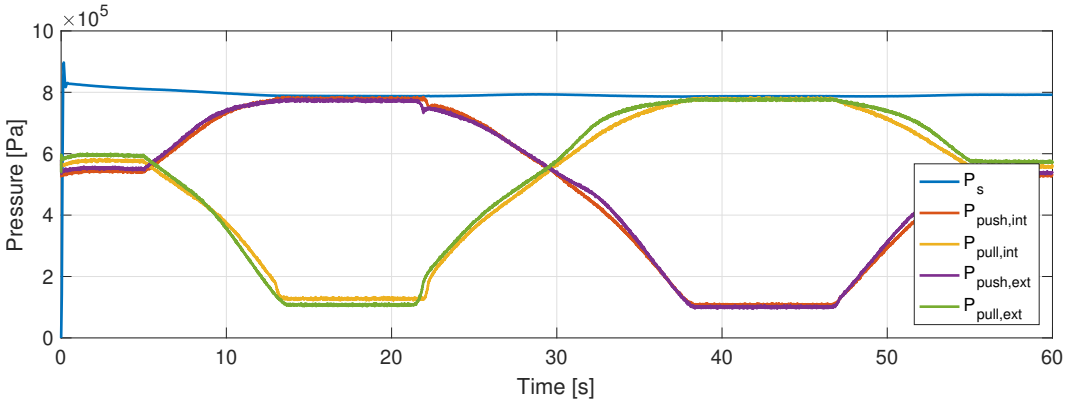

Figure 8.1-3
Maximum load test: pressure measurements as a function of time. The pressure '$P_{pull,int}$' in the retraction chamber of the internal cylinder does not completely drop to atmospheric pressure.

8.1.1 Force control and sensor calibration

The 'pneumatic force' F_p is the cylinder force as computed based on the chamber pressures. The cylinders are frictionless, so this force should be equal to the actual force that is delivered by the cylinders. However, for reasons explained in Appendix F, the pressure sensors are not suitable for use as force measurement in the control loop. Therefore, force sensors have been added to the cylinders; these force sensors are used to control the actuators.

The pneumatic force should be equal to the force sensor measurements. However, as can be seen in Figure 8.1-2, this is the case for neither the internal nor the external cylinder. What can be observed is that

$$\max F_{p,int} > \max F_{int}, \qquad \min F_{p,int} < \min F_{int},$$
$$\max F_{p,ext} > \max F_{ext}, \qquad \min F_{p,ext} < \min F_{ext}.$$

This can be explained by inaccurate calibration of the force sensors. No proper calibration setup was available, so the sensors were calibrated by simply hanging weights from them. Additionally, when mounting the sensors in the prototype and tightening the nuts, a preload is added to the sensors.

This force sensor measurement offset introduced by assembly is compensated for post-hoc by adding an equal but opposite offset to the sensor measurement in the software. However, no proper setup was available to calibrate the sensors after integration in the exoskeleton, so this offset was determined manually and is only an approximation.

Furthermore, the pressure sensors are commercial-off-the-shelf components, for which unfortunately no proper calibration data is available. For example, small differences between the sensors were observed.

However, in the end none of this is a real problem: the errors are relatively small compared to the maximum forces and are unlikely to be observed by a test subject wearing the device. To optimize performance, the force sensor offset should be tuned for each test subject at the beginning of an experiment.

8.1.2 Varying supply pressure and leakage

The supply pressure P_{sup} is measured continuously during the experiments. This measured value is then used in the force controller (see Appendix F for more details). We found that the supply pressure is not constant even though a constant pressure was commanded (see Figure 8.1-3). It fluctuates depending on the amount of air that is being used.

When maximum positive or negative force is required, the pressure on one side of the cylinders rises to the supply pressure P_{sup}, while the pressure on the opposite side drops to the atmospheric pressure P_{atm}. Significant leakage then occurs via the valve through the exhausts and a small drop in the available supply pressure is observed—the supply pressures rises again when the valve is closed and the compressor is able to completely refill the pressure tank.

Another interesting observation is that at maximum pushing force, the pressure in the retraction chamber of the internal cylinder does not fully drop to the atmospheric pressure. This explains why the maximum force delivered by the external actuator is larger than that of the internal actuator: $F_{ext} > F_{int}$ and $F_{p,ext} > F_{p,int}$.

Both valves received the same control signal in this case (maximum open to one side), so either the internal valve did not fully execute its task, or there is more leakage to the retraction chamber for another reason. In either case the phenomenon can be explained by a difference between the characteristics of both valves[1].

Furthermore, the maximum chamber pressure remains slightly below the maximum available supply pressure P_{sup}, even though the valve is completely opened to the supply. This is due to leakage via the valves through the exhausts; one can hear a lot of air escaping through the exhausts when the valves are fully open to either side.

[1] Earlier during the project, the manufacturer was contacted to obtain more information about the characteristics of the valves. They could not provide us with more detailed information, but we were told to expect differences between valves.

8.1.3 Maximum force in both cylinders

Another observation in the data in Figure 8.1-2 is that the actuators are not able to generate the desired force of 350 N and −350 N. This is expected, since the maximum force is 316 N per actuator at 8 bar. We set the reference force F_{d} to 350 N by choice to ensure that the cylinders would load the prototype at their maximum capabilities.

The difference between the pneumatic force and the measurements from the sensors was explained by the sensor calibration. The difference in the maximum force of both cylinders was explained by different valve characteristics.

For this experiment, the pneumatic force can be used to determine the maximum actuator force with which the prototype was loaded. In this case we have

$$\max F_{\mathrm{p,int}} = 301 \text{ N}, \qquad \min F_{\mathrm{p,int}} = -284 \text{ N},$$
$$\max F_{\mathrm{p,ext}} = 307 \text{ N}, \qquad \min F_{\mathrm{p,ext}} = -287.$$

The sum of the extrema thus are $\max F_{\mathrm{p}} = 608$ N and $\min F_{\mathrm{p}} = -571$ N. The first value is the maximum force that corresponds to delivery of a plantar flexion torque; it exerts a tension force on the mechanism of the prototype. The second is the maximum force that corresponds to delivery of a dorsiflexion torque; it exerts a compression force on the mechanism. These values are very close to the theoretical values computed in Section 7.4.1.

8.1.4 Cylinder motion

Two movie frames of the prototype at maximum pushing and at maximum pulling force of the actuators are shown in Figure 8.1-1(b) and (c) respectively. It can, although not very clearly, be seen that there is some displacement of both cylinders. Figure 8.1-4 shows the measurements from the position sensors of both cylinders.

The first thing that can be noticed, is that there is a difference between the position of both pistons. This is due to the prototype adapting to the shape of the foot and leg of the test setup and it is also the reason that the rings are tilted slightly upwards.

There is some extension as the cylinders start to push and some retraction when they start to pull. It can clearly be seen in the recorded movies that the ankle is making a small plantar flexion–dorsiflexion motion. This occurs due to the combined compliance of the test leg, the prototype, and the imperfect fixation of the foot to the frame.

The most important contribution to the motion is due to the imperfect fixation of the foot. The shoe is strapped to the frame using nylon bands which stretch under load. When the actuators push, the toes are pressed onto the frame and the heel moves up. When the actuators pull, the opposite happens and the toes move up, while the heel is pressed onto the frame.

During the experiment, the change in angle between the cylinder force action lines and the rings is very small. The change in direction under which the mechanism is loaded changes so little that we neglect it for this stress test.

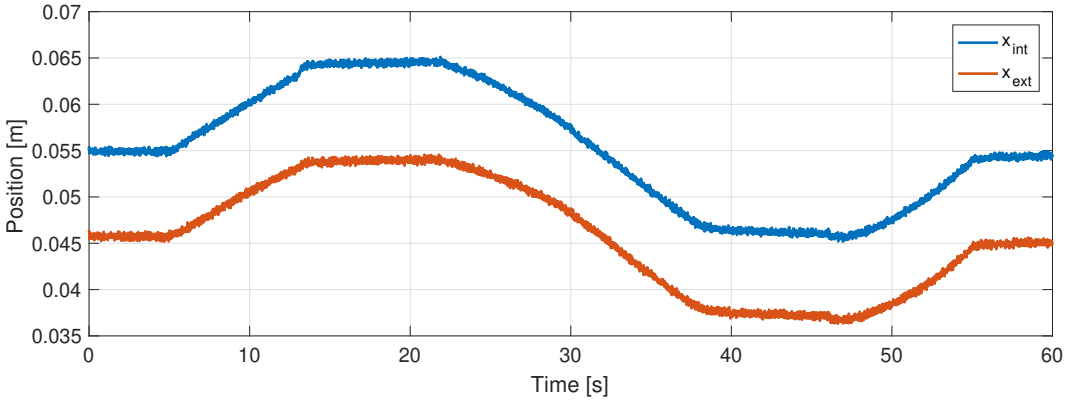

Figure 8.1-4
Maximum load test: cylinder positions as a function of time. At can be observed that, although the test leg is fixed, there still is some cylinder motion.

8.1.5 Conclusions

The test was repeated multiple times, without the prototype showing any sign of (permanent) deformation. The requirements imposed by the load case are met. Furthermore, the mechanism can safely be used without the risk of failure under high loads.

8.2 Motion control

A position controller is implemented to independently control the position of both pistons. The following simple proportional feedback control law is used:

$$F_{\mathrm{d},i} = k(x_{\mathrm{d},i} - x_i).$$

Here k is a virtual spring stiffness, x_i is the piston position of actuator i (either the internal or external cylinder) and $x_{\mathrm{d},i}$ is the desired position for this piston. The control law returns the reference force $F_{\mathrm{d},i}$ which in turn is realized by the low-level force controller that is described in Appendix F. (Note that no value for $\dot{F}_{\mathrm{d},i}$ is sent to the controller.) The value of k is tuned manually and a high gain can be chosen without destabilizing the system (values up to 5000 N/m were used with the controller running at 1000 Hz).

Note that the performance of this controller can be improved (1) by adding a damping component to remove oscillations and increase stability; (2) by adding integral action to remove a steady-state error; (3) by computing a reference signal $\dot{F}_{\mathrm{d},i}$; and (4) by overall better tuning of the control gains. However, exoskeletons are usually used in torque control mode, so it is not considered useful to further improve the performance of the position controller.

Yet, the position controller is useful for demonstration purposes, either by manually setting the position set points or by playing a preprogrammed motion profile. A simple profile is implemented that lets both actuators follow a sinusoidal wave. A small delay is set between both reference profiles, so that the device demonstrates combinations of plantar flexion–dorsiflexion and inversion–eversion.

Figure 8.2-1 shows the position measurements from both cylinders; the first plot shows the pistons following a 0.25 Hz sine wave and the second plot shows them following a 1 Hz profile. The range-of-motion of the reference signal is set to $[0.05, 0.120]$ m, so that the we stay clear from the cylinder end stops. The frame onto which the prototype is mounted is not rigid, which causes the small vibrations seen in the plots. Movies have been recorded at various speeds and Figure 8.2-2 shows a selection of movie frames.

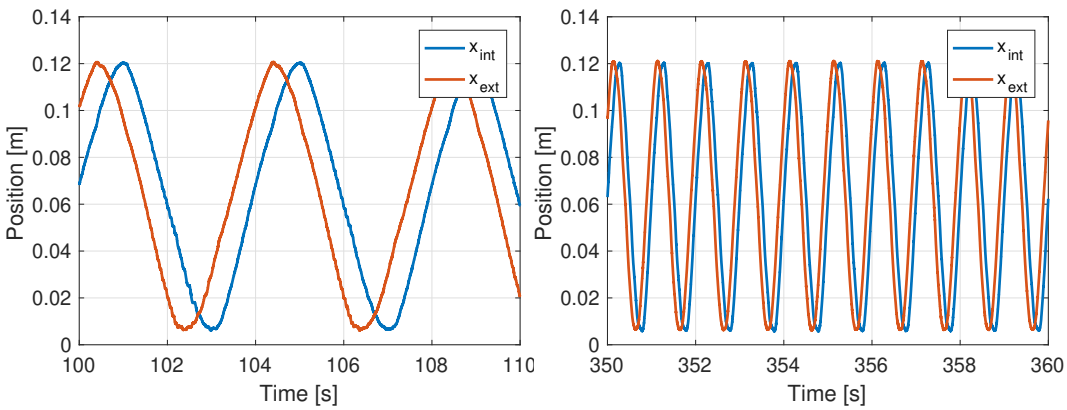

(a) (b)

Figure 8.2-1
Demonstration motion, piston position of both cylinders: (a) shows the motion at 0.25 Hz and (b) shows the motion at 1 Hz.

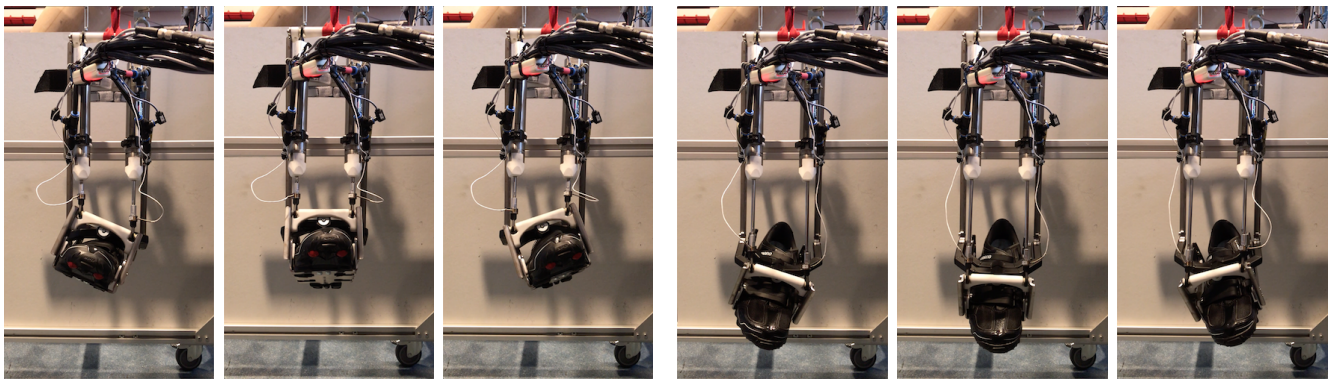

(a) (b) (c) (d) (e) (f)

Figure 8.2-2
The prototype mounted to a frame, while the position of both actuators is controlled independently. Note that the prototype is slightly tilted backwards. The shoe is moved into: (a) dorsiflexion-eversion; (b) dorsiflexion; (c) dorsiflexion-inversion; (d) plantar flexion-eversion; (e) plantar flexion; and (f) plantar flexion-inversion.

8.3 Comparison of devices in passive mode

In this section, the passive behavior of the prototype is compared to that of two other devices: the Achilles Ankle Exoskeleton and the ankle module of the Symbitron+ WE2 exoskeleton. The behavior of the latter was already investigated in Section 6.2. For each of these devices, the version for the *right* foot is used. All are shown worn by one of the test subjects in Figure 8.3-1. For the comparison, the actuators in all three devices have been disconnected so that the exoskeletons are passive and fully back-drivable. The wearer only feels the mass and friction contributions of the device and the degrees-of-freedom and constraints provided by the device. The exoskeletons have been weighed (including the shoe) and the masses were found to be the following.

- Achilles Ankle Exoskeleton: 1.78 kg.
- Sybitron+ WE2 ankle module: 4.56 kg.
- The prototype: 3.58 kg.

Four test subjects were recruited for this experiment. Each subject executes the tasks that are listed in Section 8.3.1. They also answered the questions listed in Section 8.3.2. Two subjects

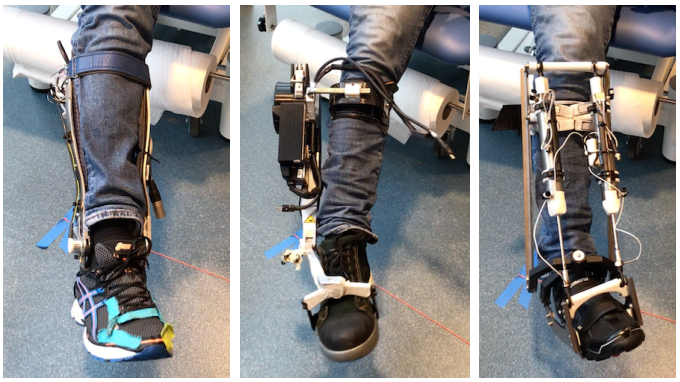

(a) (b) (c)

Figure 8.3-1
Comparison of three ankle exoskeletons: (a) the Achilles ankle exoskeleton [2]; (b) the ankle module of the Symbitron+ WE2 exoskeleton [1]; (c) the prototype developed in this research.

start the experiment with the Achilles, the other two start with the prototype. The WE2 is always tested as second. It is expected that the order influences the comments given by the test subjects, however, testing all permutations with a single subject requires 6 participants and testing all with two subjects requires 12.

The subjects are told what the mass of each of the devices is beforehand and they are requested to try not to consider the mass when answering the questions, but to purely focus on whether the device is comfortable and allows them to move naturally.

Note that all participants are colleagues from within the Department of Biomechanical Engineering. Their technical background allows for easy communication when answering the questions.

8.3.1 Tasks to be executed with each device

The subject executed the tasks listed below in the given order, for each of the three devices. A short break will be held before changing the device. Note that the questions listed in Section 8.3.2 will be asked *during* the tasks and that each of the tasks 2—5 is to be carried out at least twice. Movie frames of execution of some of the tasks with the prototype are shown in Figure 8.3-2. The tasks are based on the use cases that are described in Appendix B.

1. Donning The subject dons the device by himself.

2. Move freely The subject is sitting on a bench with their foot in the air and the lower leg under approximately 30° with respect to the ground. The subject is instructed to move their foot around in all possible directions. See Figure 8.3-2(a).

3. Walking Three cases:

- **3a. Straight line** The subject is instructed to walk along a straight line, drawn on the floor.
- **3b. CW Loop** The subject is instructed to walk in a clockwise (CW) loop with a diameter of 5 m. This requires the right foot to move in eversion.
- **3c. CCW Loop** The subject is instructed to walk in a counter-clockwise (CCW) loop with a diameter of 5 m. This requires the right foot to move in inversion.

4. Special tasks Three cases:

- **4a. Cross steps** The subject is instructed to walk along a line drawn on the floor, while making cross steps over this line. This forces the right foot in eversion. See Figure 8.3-2(b).
- **4b. Tilted path inversion** The subject walks on a path that is tilted in the frontal plane, so that the right foot makes an inversion motion. See Figure 8.3-2(c).
- **4c. Tilted path eversion** The subject walks on a path that is tilted in the frontal plane, so that the right foot makes an eversion motion. See Figure 8.3-2(d).

5. Stairs Two cases:

(a) (b) (c) (d) (e) (f)

Figure 8.3-2
Movie frames from execution of a selection of tasks by a subject using the prototype: (a) moving freely in the air; (b) cross steps over a line; (c) tilted path inversion; (d) tilted path eversion; (e) stair ascent; (f) stair descent.

5a. Stair ascent The subject is instructed to ascend a flight of stairs. The subject is required to descend backwards before repeating the task. See Figure 8.3-2(e).

5b. Stair descent The subject is instructed to descend a flight of stairs. The subject is required to ascend backwards before repeating the task. See Figure 8.3-2(f).

6. Doffing The subject is instructed to doff the device by himself.

8.3.2 Questions during and after the tasks

The following questions are asked while executing the task, so that the subject can repeat the task as necessary to formulate a good answer. Two types of questions are asked. The first questions for each task are statements and the subject is required to tell whether they agree or disagree on a 5-point Likert scale:

- Strongly agree
- Agree
- Neither agree nor disagree
- Disagree
- Strongly disagree

The final question after each task is an open question, in which the subject is asked to explain their previous answers and share any thoughts.

For tasks 1 and 6 (donning and doffing), the statements and question are the following.

S1 I find it easy to don/doff the device.

S2 Statement: The time required to don/doff the device is reasonable.

Q Do you have any comments on the behavior of the device during this task? Do you have recommendations on how to improve the device?

For tasks 2 to 5, the statements and question are the following.

S1 I feel that the degrees-of-freedom of the device allow me to execute the task.

S2 The device feels comfortable during execution of the task.

S3 The device hinders the natural movement of my foot during this task.

S4 I experience discomfort due to the device while executing the task.

Q Do you have any comments on the behavior of the device during this task? Do you have recommendations on how to improve the device?

Note that statements 1 and 3, and 2 and 4 are opposing each other. It is expected that the subject also gives opposing answers on the Likert scale.

After doing the tasks and answering the questions for each of the three devices, the following final questions are asked.

Q1 Do you have any remarks or comments on what you have just experienced, in particular when comparing the three devices?

Q2 Do you think that adding the additional degree-of-freedom, as is done in the prototype, is useful? Or is a single degree-of-freedom as in the Achilles sufficient?

8.3.3 Execution of the experiments

Four test subjects were interviewed. They each used the three devices, they executed the 11 tasks with each of the devices, and they answered the 5 questions for each of these tasks. All collected data has been included in tables in Appendix H.

Note that for the donning and doffing process there are only two statements. For the other nine tasks, there are four statements. The intention was that S1 and S3, and S2 and S4 would be interpreted as opposing statements, so that the test subject would also give opposing answers.

However, this turned out not (exactly) to happen, as the subjects had the tendency to interpret the statements differently.

For example, a participant might answer 'Agree' (A) to statement S1, while also answering 'Agree' (A) to statement S3. The train of thought being: "Yes, I can execute the task using this device; however, I do feel that my gait is altered". Another example is a participant answering 'Disagree' to S2 and 'Agree' to S4, with an argument like: "I can freely move my foot during the task and my ankle does not feel constrained; yet, my big toe hurts because the shoe size is not right".

Participants also tended to compare the device they were currently using to the previous device. Things were said like: "Donning this device is way easier than the previous. Then I answered Agree, so now it must be Strongly Agree". This confirms the expectation that the order in which the devices are tested influences the answers.

Finally, different participants interpreted the statements differently. For example, statement S1 was interpreted by some as "I can execute this task (albeit uneasily).", whereas others interpreted it more like "The degrees-of-freedom of the device match those of my ankle exactly."

In the end, the comments given by the participants are most useful. The statements have more of steering function and are, due to the various interpretations, only marginally insightful. However, an attempt will be made to present the answers, before discussing the comments and other answers that were given by the participants.

8.3.4 Visualization and interpretation of agreement with statements

A large data set was collected and visually presenting it is not straightforward. Figure 8.3-3 shows the final visualization, but the reader is advised to first read the following explanation before studying the figures.

Explanation of the diagrams

For this visualization, the data is presented per device. Four participants executed a total of 11 tasks with each device. The answers given to the statements are grouped per task.

A color-scale is used to indicate the answers on the Likert scale:

Dark-Green	Strongly agree (SA)
Light-Green	Agree (A)
Light-Gray	Neither agree nor disagree (N)
Light-Red	Disagree (D)
Dark-Red	Strongly disagree (SD)

For each of the tasks and for each of the statements, the answers given by all four subjects are shown as colored squares. The order of the subjects is:

S1	S2
S3	S4

Note that an empty (white) square means that the statement does not exist: there are no S3 and S4 for the donning and doffing tasks.

Finally, statements S1 and S2 are *positive* assessments, whereas statements S3 and S4 are *negative*. We wish to obtain a visual representation in which the overall color of the figure is an indication of the performance of the device. Therefore, in the visualization, the answers given to S3 and S4 are 'inverted' on the likert scale. That is, the following answers (end thereby the colors) are swapped for S3 and S4:

'Strongly Disagree' $\Leftrightarrow$ 'Strongly Agree', and

'Disagree' $\Leftrightarrow$ 'Agree'.

The overall color of the diagram of a device is an indication for the assessment by all four participants: green denotes a positive and red a negative assessment. The numeric responses can be found in the tables in Appendix H, as can the additional comments given by the participants.

Achilles

In comparison to the other two devices, the diagram of the Achilles shows quite a number of red squares. Generally, the participants were able to execute the tasks. However, as the device

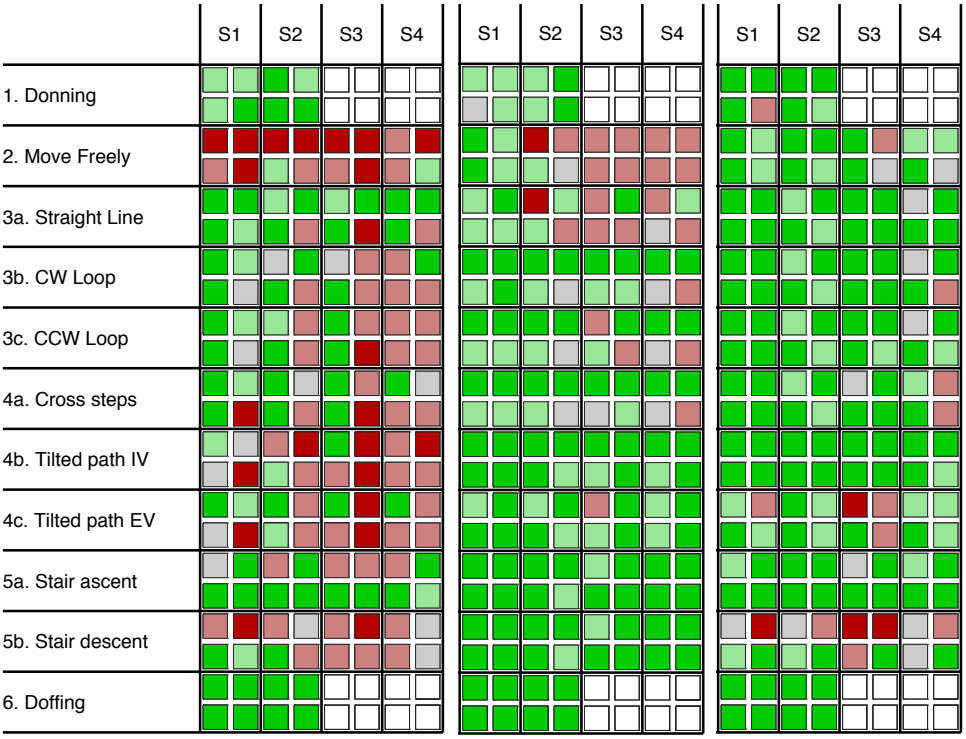

Figure 8.3-3

Color-grid showing to what extent the four test subjects agreed with statements S1 and S2, and the *opposite* of S3 and S4. Shown for each of the activities and for each device: (a) Achilles; (b) WE2; and (c) the prototype. Within the grid there are always four colored squares: top left denotes subject 1, top right denotes subject 2, bottom left denotes 3, and bottom right 4.

only has a single DoF and does not accommodate inversion–eversion, participants felt hindered by the device and wearing it during tasks that require inversion are eversion was considered uncomfortable. The participants preferred both the WE2 and the prototype over the Achilles.

Symbitron+ WE2 ankle module

The WE2 shows an overall green diagram. However, quite some red squares are shown for tasks 2, moving the ankle freely, and 3a, walking in a straight line.

The reason given by all participants is the behavior that is also described in Section 6.2. When the foot moves in inversion–eversion, the device rotates around the lower leg. The mass of the device is placed asymmetrically, with almost 3.5 kg hanging on the external side of the leg. During task 1, this mass needs to be lifted when the foot moves in inversion and it drops when the foot moves in eversion. This behavior is shown in Figure 6.2-3 on page 43.

While walking in a straight line, the mass of the device forces the foot in inversion at toe-off and in eversion at heel-strike. Some participants also reported this behavior during other tasks.

Overall, the device receives a rather positive assessment, as it is less constraining than the Achilles and allows for more natural movement of the ankle and foot—despite the rotation of the relatively large mass around the lower leg.

The prototype

The prototype receives a rather negative assessment when it comes to task 5b, the stair descent. The reason is that the dorsiflexion range-of-motion of the device turned out to be too limited. This part of the RoM was decreased in the design process to create more space for the mechanism at the ankle—this is described in Section 7.4.3.

During stair descent, when the left foot is about to be placed on the next (lower) step, a large dorsiflexion angle is required in the right ankle. The RoM of the prototype turned out to be too

small, so subjects 1, 2, and 3 hit the end stop. However, subject 4 reported no such problems and perceived stair descent as easy and comfortable.

A similar effect of the limited dorsiflexion RoM was also seen during task 4c, walking on a tilted path, which requires eversion. The eversion angle already pushes in the cylinder on the external side of the leg, so when this is combined with dorsiflexion, the range-of-motion is found too small.

On all other tasks, the prototype scores very well. Participants were very positive about the freedom of movement it provides to the ankle, in particular when compared to the Achilles. They did report some discomfort, but this was due to the shoe and lower leg interface.

8.3.5 Comments from the test subjects

We will continue with discussing some of the points that were mentioned by the participants. Note that all answers are included in Appendix H.

Donning and doffing

Donning and doffing were found to be easy and quick for all devices. Participants indicated that it is preferable for the back of the shoe to be free, so that one can pull on the shoe during donning, as one would do with a regular shoe.

Comfort of interfaces at the foot and lower leg

It is interesting to see that all participants pointed out different locations in the interfaces to the body that were perceived uncomfortable. The same lower-leg interface may be completely comfortable for the one test subject, whereas the other complains about it being to tight or causing a pressure point. This confirms that it indeed is difficult to make an interface that comfortably fits to a wide range of people.

There were complaints about all three devices; some participant mentioned something wrong with the shoe, the other with the lower leg brace, and again another noticed the Achilles being too narrow at the ankle. Unfortunately, no definite conclusions can be drawn from these complaints, since for every complaint there was another test subject saying that the device fitted perfectly.

However, one important conclusion *can* be drawn from the study: it is *really* important that the device does fit comfortably. The more tasks a participant executed with a device, the more he or she started to get annoyed by something that was said to be only a minor inconvenience during the first couple of tasks.

Note that the devices were turned off during these experiments; it would be interesting to investigate what happens when they are actually delivering torques.

Achilles

The most important results were already discussed in Section 8.3.4. Participants furthermore indicated that the range-of-motion, in both the plantar flexion and dorsiflexion direction is a bit too small. Stair descent is problematic, as the leaf spring at the back catches on the previous step. The leaf spring can be seen in Figure 1.1-2 on page 4.

Participants furthermore noticed the whole structure deform when they tried to make an inversion–eversion motion. The combined compliance of the body and the device, together with movement of the foot inside the shoe, still allows for some inversion–eversion.

Some participants complained about loss of balance during tasks which require inversion–eversion, such as the tilted path, because they ended up standing on the edge of the shoe sole.

Symbitron+ WE2 ankle module

Section 8.3.4 already discusses the most important comments on the WE2 ankle module. The foot can move in inversion–eversion, but it is coupled to a rotation of the device around the lower leg, as is also discussed in Section 6.2. The participants found this rotation annoying and complained about the placement of the mass of the device, which is asymmetrical about the leg, with the actuator hanging on the external side.

The prototype

The feedback on the prototype is of main interest for this report. For completeness, important comments are collected in the following list. Points marked with '⊖' should be improved, points marked with '⊕' are positive.

- Regarding comfort of the shoe and lower-leg interface:
  - ⊕ It is nice that the back of the shoe is free, so that one can don it like a normal shoe.
  - ⊖ The Velcro strap of the shoe at the toes is hard to reach due to the axle that is mounted above it.
  - ⊖ The brace of the distal cuff should be a bit wider, as some participants felt a pressure point.
  - ⊖ The shoe used in the prototype is a cycling shoe with a rigid sole. Participants did not really like this, as one cannot roll-off the foot in a natural way. During stair descent the foot is forced flat on the steps.
  - ⊖ One participant mentioned that the prototype is a bit too narrow at their toes.
- Regarding the degrees-of-freedom and range-of-motion:
  - ⊕ Participants felt that they can move their foot completely freely, although some mentioned that the range-of-motion of the device is slightly smaller than that of their ankle.
  - ⊕ They noticed almost no difference in behavior of the device during the different tasks; walking in circles or on a tilted path is just as easy as walking in a straight line.
  - ⊖ The dorsiflexion RoM is a bit too small, certainly when dorsiflexion is combined with inversion or eversion.
- Other comments:
  - ⊖ The overall size should be decreased. The actuators are a bit too high; they collide with the back of the other leg during cross steps. Participants expect the prototype to be too wide (on the internal side) for wearing one on either foot.

8.3.6 Answers to the final questions

Two final questions—see Section 8.3.2—were asked to all participants after execution of all tasks with the three devices. The answers (summarized and translated to English) relevant to the prototype or the project are listed below. The S1, S2, ..., indicates that the comment was made by subject 1, subject 2, et cetera.

Question 1, regarding the comparison of the three devices

S1 *RoM is really important. Hitting the end stop forces you to alter your gait and that is annoying.*
S1 *Comfort of shoes and cuffs seems difficult. A minor inconvenience quickly becomes disturbing. You feel all the small things.*

S2 *It would be ideal if the prototype had the same weight as the Achilles.*
S2 *Seems that all devices have a risk of hooking against something; either themselves or the environment. Seems difficult to solve. A challenge.*
S2 *Advantage of prototype is that it has a low actuator impedance; the other actuators were disconnected. They didn't cause noise and were very small. You barely feel them.*
S2 *The prototype is easier to don, because the heel is free. But there is a larger risk of hooking onto the other foot due to the structure on the internal side of the leg.*

S3 *The prototype feels best for freedom of motion for the ankle. Think least tiring to walk with this device.*
S3 *Maybe move actuators in prototype to the back for better mass distribution.*
S3 *Maybe make the prototype less wide on the internal side.*
S3 *Increase dorsiflexion RoM of prototype.*

Question 2, regarding the added value of providing an inversion–eversion DoF

S1 *Yes. All 1-DoF devices have some compliance in the interface so that you can still move in inversion–eversion. But you cannot control this. If you'd build a device that really constrains inversion–eversion, this would become extremely annoying. You can better build the additional DoF in your device: then you're in control.*

S2 *Feel like the additional DoFs of the WE2 and prototype are necessary for ADL[2] tasks; cannot ignore them.*
S2 *Don't feel that inversion–eversion has to be actuated.*

S3 *I feel that I could wear the prototype all day, without getting tired in my muscles and joints. Whereas I think the other two devices will start to bother me.*

S4 *Definitely necessary for balance.*
S4 *Think that keeping balance during the complex tasks with an Achilles on either leg would be very hard.*

8.3.7 Conclusions

The participants are, overall, very positive about the functional behavior of the prototype. They all see the value of adding inversion–eversion to ankle exoskeletons, in particular for experiments with more complex tasks.

However, the dorsiflexion range-of-motion of the prototype should be increased and comfort of the interfaces to the foot and lower leg should be improved.

8.4 Fulfillment of requirements

Section 3.5.3 defines the set of system requirements for the prototype. Table 8.4-1 lists the requirements and it shows whether they are fulfilled. We will continue with a discussion of each of the requirements.

Table 8.4-1
System requirements for the prototype (copied from Table 3.5-1): a '✓' indicates that the requirement is met and a '✗' indicates that it is not.

ID		Name
RQ01-DROM	✗*†	The maximum dorsiflexion angle shall be at least 30°.
RQ02-PROM	✗*†	The maximum plantar flexion angle shall be at least 50°.
RQ03-IROM	✓†	The maximum inversion angle shall be at least 15°.
RQ04-EROM	✓†	The maximum eversion angle shall be at least 15°.
RQ06-FREE	✓	The wearer shall be able to naturally move their ankle, only limited by the specified ends of the RoM.
RQ08-CTRL	✓	The plantar flexion–dorsiflexion torque of the device shall be controlled on-line.
RQ09-DTRQ	✓	The device shall be able to generate dorsiflexion torques of at least 35 Nm.
RQ10-PTRQ	✓	The device shall be able to generate plantar flexion torques of at least 35 Nm.
RQ12-LACT	✓	The device shall use linear actuators.
RQ14-WECR	✗	It shall be impossible for the wearer to crush or catch their fingers in the system.
RQ15-WRCR	✗	It shall be impossible for the researcher to crush or catch their fingers in the system.
RQ16-SHRP	✓	The system shall have no sharp edges.
RQ18-SHOE	✓	The prototype shoe size shall be EU 43.
RQ19-BDYL	✓	The prototype shall fit people with body lengths in the range of $[170, 190]$ cm.

* The *original* requirements are not met, but the revised requirements (Section 7.4.3) *are*.
† The maximum angles for either DoF are decreased when a 2-DoF motion is made.

[2] ADL denotes 'Activities of Daily Living'.

8.4.1 Requirements on the degrees-of-freedom and range-of-motion

A dorsiflexion range-of-motion of $\vartheta_{df} \in [-50, 30]°$ (RQ02-PROM and RQ01-DROM) and an inversion range-of-motion of $\vartheta_{iv} \in [-15, 15]°$ (RQ04-EROM and RQ03-IROM) are required.

Section 7.4.2 explains why rectangular steel tubes are used for the ring mechanism at the ankle. Subsequently, it is explained in Section 7.4.3 that the plantar flexion–dorsiflexion range-of-motion needed to be adjusted to make space for the larger mechanism. The dorsiflexion RoM is decreased to $\vartheta_{df} \in [-45, 20]°$, so the requirement on the dorsiflexion RoM that was initially set is *not* met.

Figure 7.3-4 on page 58 shows a 'reachability' grid for the intended RoM; Section 7.3.4 explains how the figure should be interpreted. Figure 8.4-1 shows the same figure, but for the actual prototype.

It can be seen that indeed a RoM $\vartheta_{df} \in [-45, 20]°$ is achieved when there is no inversion–eversion motion. An inversion–eversion RoM significantly larger than ±15° is achieved (note that the workspace is larger than the figure). However, the range-of-motion is limited when there is also plantar flexion–dorsiflexion. Specifically, limits occur for combined dorsiflexion–eversion and combined plantar flexion–inversion. The reason for this particular workspace 'shape' can be derived from the orientation of the inversion–eversion axis (shown in Section 2.3.2): the axis is tilted to the internal side of the leg.

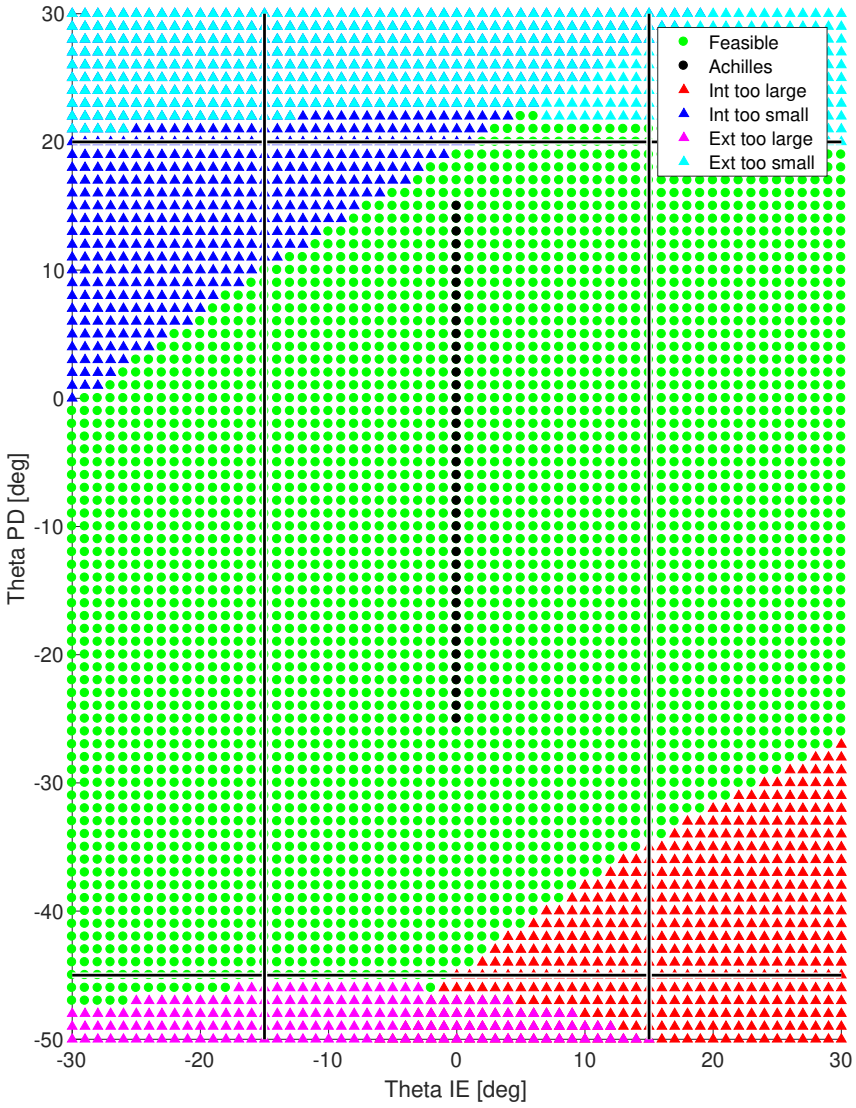

Figure 8.4-1

Discrete evaluation of workspace reachability with the actuator configuration of the prototype for combinations of dorsiflexion and inversion $(\vartheta_{df}, \vartheta_{iv})$. The (adjusted) required RoM is indicated by the black lines: $\vartheta_{df} \in [-45, 20]°$ and $\vartheta_{iv} \in [-15, 15]°$.

Section 8.3 discussed the evaluation of the prototype. Firstly, it was found that the dorsiflexion RoM is too small when descending stairs. Furthermore, test subjects indeed reported hitting the end stops of the actuator modules when tasks required the previously mentioned combined motion. This happens for example during walking on a tilted path.

Finally, it is required that the wearer (SH06-SUBJ) can freely and naturally move their ankle, within the available range-of-motion (RQ06-FREE). The evaluation and comparison in Section 8.3 shows that this is indeed achieved.

8.4.2 Torque and control requirements

It is required that the device is torque-controlled (RQ08-CTRL). This requirement is indeed met, as the cylinder forces are actively controlled. Based on the orthosis state, the moment arm for each actuator is known, so the desired force can be computed accordingly. Linear actuators are used, so RQ12-LACT is also satisfied.

As was explained, a minimum plantar flexion–dorsiflexion torque requirement was set to demonstrate the working principles. A minimum torque of 35 Nm in both directions is required (RQ09-DTRQ and RQ10-PTRQ). This requirement is indeed easily met, as is explained in Section 7.4.3 and verified in Section 8.1: the maximum plantar flexion torque that can be generated is 74 Nm.

8.4.3 Safety requirements

Three explicit safety requirements are defined. The first two are: it shall neither be possible for the wearer (SH06-SUBJ, RQ14-WECR) nor for the researcher (SH05-RESR, RQ15-WRCR) to crush or catch their fingers in the mechanical components of the system. The third requirement is that the device should have no sharp edges (RQ16-SHRP).

The first two requirements are *not* met, as no safety precautions are taken in the prototype design. The risk of hurting ones fingers is minimal during walking-related tasks, as the hands and fingers are far away from the device. However, there is a risk of finger injury when the device is powered while being donned, doffed, or adjusted, or when the device is touched while it is in use.

Covers should be designed that shield fingers—and other body parts—from moving parts in the orthosis mechanism. It is important that this small yet essential design update is carried out prior to further testing.

The prototype has no sharp edges, but it does use laser-cut sheet metal components. It is important that sharp edges are removed during assembly. Uncovered sheet metal edges should be avoided in future design updates.

8.4.4 Anthropometric requirements

Only two requirements were set regarding anthropometrics: the prototype should have a shoe size 43 (RQ18-SHOE) and it should accommodate body lengths in the range of $[170, 190]$ cm. They are met as the device is not too high and a cycling shoe of size 43 is built into the device.

8.5 Conclusions

Chapter 9 presents conclusions and recommendations based on the evaluation of the prototype. Chapter 10 then reflects on the design process and it considers the societal impact and relevance of this project.

CHAPTER 9

Conclusions and Recommendations

This chapter presents the conclusions drawn from the design and evaluation of the prototype. Recommendations are given regarding further development and evaluation of the hardware. The focus is on the design itself and not on the design *process*.

We reflect on the project in Chapter 10. Our design methodology is considered in Section 10.1 and the societal impact and relevance of the project are considered in 10.2.

9.1 Project summary and goal—*Can* we build a 2-DoF ankle exoskeleton?

The goal of the project is to develop an actuated ankle orthosis that does not constrain the natural movement of the ankle, while still being able to deliver significant plantar flexion–dorsiflexion torques.

First, we followed the iMS approach to create an orthosis without rigid links or hinges (see Chapter 5). The rationale behind the approach is that the ankle is left completely free and that no alignment between the human ankle joint and the orthosis joints is necessary—simply because the orthosis does not have any joints.

The iMS approach was found infeasible for the development of an ankle orthosis, so we reverted to rigid links and mechanical hinges, which is described in Chapter 6. First, an existing design (that of the Symbiton+ WE2 ankle module) was considered as a design solution. However, evaluation in Section 6.2 showed that the chosen concept has several limitations that need to be addressed.

As a result, a new mechanism—based on a model of the behavior of the human ankle joint—was developed (Section 6.3). After multiple design iterations and practical evaluations with human test subjects, an actuated prototype was developed (Chapter 7).

Evaluation of the prototype shows that it allows its wearer to freely move their ankle in both plantar flexion–dorsiflexion and inversion–eversion, only limited by the end-stops that define the range-of-motion (see Section 8.3). The structure of the prototype is designed to withstand the large forces created by the actuators. A stress test described in Section 8.1 confirmed that the design indeed is strong enough and safe to use. The device can deliver a maximum plantar flexion torque of 74 Nm.

Not all system requirements are satisfied (see Section 8.4). However, the project goal *is* achieved: the prototype allows the ankle to move naturally and it can deliver the required plantar flexion–dorsiflexion torques. The use of two independently controlled actuator modules may even allow for the control of inversion–eversion torques, which is very interesting for research into balance control.

9.2 Value of the second DoF—*Should* we build a 2-DoF ankle exoskeleton?

The prototype is developed with the intention that it can be used for human movement research. Yet, the main research question is: '*can* we build a 2-DoF ankle exoskeleton?' and not 'is it *useful* to do so?'.

In Section 9.1, we explain that the first question can be answered by 'yes', as a working prototype is delivered. Based on the feedback given by the test participants in Section 8.3, we can also comment on the second question.

The four participants executed a large number of tasks, while wearing three different devices: the prototype, the ankle module of the WE2 exoskeleton, and the Achilles. All participants agreed that the addition of an inversion–eversion degree-of-freedom is not just 'a nice feature', but that it really is valuable.

The human ankle makes inversion–eversion motion not only during complex tasks like taking cross-steps or walking on tilted paths, but even while simply walking in a straight line—this is shown in Section 2.2. Providing only a single exoskeleton axis perpendicular to the sagittal plane (as in the Achilles ankle exoskeleton) significantly constrains the human ankle; the test subjects found this annoying and uncomfortable.

Another interesting observation, made by one of the test subjects, is that the ankle *will* move in inversion–eversion during a wide variety of common tasks. When the exoskeleton does not explicitly provide this degree-of-freedom, it will somehow still be found in the compliance of the whole assembly. The exoskeleton frame will bend, the foot will move within the shoe, or the soft tissue of the human body will deform. This compliant behavior is very much present, but it is neither considered by the researcher using the device for experiments, nor is it measured or in any way controlled. Implementing an inversion–eversion DoF in an ankle exoskeleton, regardless of whether it is passive or actively controlled, not only benefits the wearer by providing comfort, it also benefits the accuracy of the research conducted with the device. We go from a simplified 2D gait analysis to studying real-world human movement in 3D.

In conclusion, yes we *can* and yes we *should* build a 2-DoF ankle exoskeleton.

9.3 Other applications of the prototype

The ankle joint mechanism is designed for use in a stand-alone ankle exoskeleton, but there are other possible applications.

9.3.1 Lower-body exoskeletons

It might be possible to integrate the 2-DoF ankle exoskeleton in a full lower-body exoskeleton, such as the modular Symbitron+ WE2 exoskeleton.

However, this will make the design more challenging, as the mass of the full exoskeleton—and possibly even the mass of its wearer—will be resting on the ankle joint mechanism. This would call for a complete redesign of the mechanism.

9.3.2 Prosthetic ankle joints

An interesting possible application of the joint mechanism is the design of lower-leg prosthetics. Currently, passive flexible ankle joints are often used and it might be possible to add an inversion–eversion degree-of-freedom to these joints.

The initial design process of the prototype started in Section 6.3.1 with the design of a mechanism that has the same degrees-of-freedom as the human ankle joint. The joint, which uses simple hinges, is shown in Figure 6.3-2 on page 45.

Figure 9.3-1 shows a proof-of-principle for a flexure-based mechanical implementation of the theoretical ankle joint model. The mechanism uses low-stiffness and large-RoM flexures for the main plantar flexion–dorsiflexion direction and stiffer internal flexures to provide a smaller inversion–eversion RoM. The design is based on a butterfly flexure hinge.

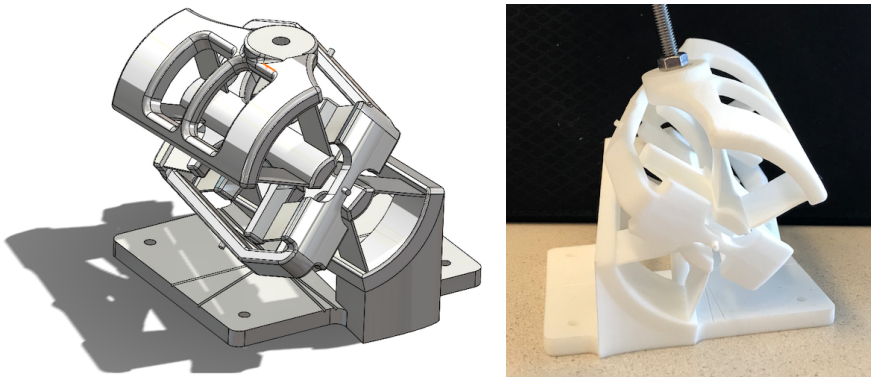

(a) (b)

Figure 9.3-1
Mechanical implementation of the theoretical ankle model for the right foot in a flexure-based joint: (a) CAD model in a view on the back and right side; (b) photograph of the 3D-printed mechanism.

9.4 Recommendations for further evaluation of the prototype

The next phase for the project is to test the device during real human movement experiments. This section provides some suggestions for further testing.

9.4.1 Inversion–eversion torques and balance

The independent control of both actuators not only allows for the generation of plantar flexion–dorsiflexion, but also for inversion–eversion torques. At the moment it is unknown whether independent control is beneficial, so this should be investigated.

The device may be an interesting platform to study human balance, or to develop balance control algorithms.

9.4.2 Metabolic cost of walking

The reduction of the metabolic cost of walking (per the use of an exoskeleton) is a popular research goal. Test subjects reported (Section 8.3) that the 1-DoF ankle exoskeleton is uncomfortable and alters their gait. It might be that the added comfort and freedom of ankle movement given by the prototype yields better results with the same assistance strategy.

To test this hypothesis, a second device should be manufactured for the left foot. Due to the high mass of the current proof-of-principle prototype, it is advisable to first further develop the design. Some recommendations are given in Section 9.5.

9.4.3 Other experiments

Appendix B lists a variety of exoskeleton use cases; the prototype should be suitable to provide assistance during any of the presented scenarios. Testing the device in these use cases does require the development of assistance strategies.

9.5 Recommendations for further development of the prototype

The prototype is only a proof-of-principle: it demonstrates the feasibility and usefulness of a 2-DoF ankle exoskeleton. However, it is still far from a consumer product and further development is needed.

9.5.1 Comfort, fit, and mass

Both the foot and lower-leg interface of the prototype are designed only to demonstrate the working principle of the device. Comfort should be improved, as test subjects reported various issues[1] (Section 8.3).

Unfortunately, no single solution can be designed that properly and comfortably fits 'everyone'. Different test subjects reported different problems. This means that probably a range of leg interfaces should be developed (for instance sized 'small', 'medium', 'large' for the lower leg and various shoe sizes for the foot). All participants agreed that the rigid sole of the cycling shoe is uncomfortable, as it does not allow natural roll-off at the ball of the foot, so the shoe should be replaced by a shoe that has a more flexible sole.

Preferably, the height of the ankle joint mechanism should be adjustable. There is a large variation in ankle height between individuals and problems with the particular joint height of the Achilles were reported. Misalignment causes motion of the device with respect to the leg; this is not only uncomfortable, but it also results in power losses and errors in the (computed) joint torque.

Steel plates are used in the prototype, which makes the device unnecessarily heavy. Revision of the interfaces to the foot and lower leg will automatically result in a reduction of mass, as steel is not the logical material for such components. The mass reduction will also yield an improvement in the perceived user comfort.

During the redesign, also EMG sensor placements and motion-tracking marker locations should be considered.

The design of interfaces to the body is a specialized skill and an orthotist *must* be involved.

9.5.2 Range-of-motion

The required dorsiflexion range-of-motion of $\vartheta_{\mathrm{df}} \in [-50, 30]^\circ$ is not achieved (requirements `RQ02-PROM` and `RQ01-DROM` are not met). The RoM had to be decreased due to the combination of the large ring mechanism and the relatively short-stroke actuators. During evaluation, it was found that the new RoM, in particular the maximum dorsiflexion angle, is a bit too small. The original requirements should be met in a design update.

9.5.3 Safety

It is explained in Section 8.4 that there currently is a (small) risk of injury to fingers when caught in the mechanism. Hence, requirements `RQ14-WECR` and `RQ15-WRCR` are not satisfied. A protective cover should be designed to solve this.

9.5.4 Actuation, sensing, and control

There are various ways to improve the performance and usefulness of the device.

Improvement of performance of the current device

The frictionless cylinders and their force control algorithm perform well enough for further experiments with the device. However, proper calibration of the sensors and further controller tuning (preferably after a system-identification of the parameters of the various pneumatic components) will yield better results. This does require additional measurement equipment that currently is not available.

[1] Not only with the prototype, but also with the WE2 ankle module and the Achilles.

The pressure sensors that are used in the prototype are low-budget devices. They are not properly calibrated and show high signal noise. This renders them unsuitable for use as force measurement in the force control feedback loop. Replacing them by more accurate sensors will directly improve the performance of the control algorithm. The force sensors may be removed if the new pressure sensors are sufficiently accurate and noise-free: the chamber pressures are a good representation of the actuator force. Removing the force sensors results in a decreased complexity of the mechanical, electrical, and software components of the device.

Additional sensors

Absolute angular encoders should be added to the joint axes[2] of the half ring mechanism to enable monitoring the state of the exoskeleton. This is both useful for control, human movement experiments, and further evaluation of the device—the sensor readings can for instance be used to optimize the RoM of the exoskeleton. Mounting the sensors should not be a problem, but properly routing the additional wiring will be challenging.

Depending on the intended use of the device, it may furthermore be valuable to add the following sensors: pressure insoles in the shoes; inertial measurement units (IMUs) on both the foot and lower leg interface; toe-off and heel-strike detection (the IMUs can be used for this); or integrated EMG sensors.

Control

Although the force control algorithm performs well, it may be interesting to consider more advanced force control and interaction control algorithms.

Redesign of actuator modules

The current pneumatic actuator modules are suboptimal. They are very long, as they are composed of a series of stock components interconnected by aluminum adapters, yet the maximum cylinder extension is not that large.

The minimum length of the actuator module is 331 mm and, with a stroke of $s = 125$ mm, the maximum length is 456 mm. This means that the modules only elongate by 38%. Significant improvements can be achieved by using custom components.

A better elongation ratio can be used in either of two ways: either the range-of-motion of the exoskeleton is enlarged, or the hight of the actuator anchors on the leg interface is decreased. This latter option reduces the overall size and volume of the exoskeleton. One can read in Section 8.3 that the current device is too high to comfortably make cross-steps, as the top of the actuators collides with the back of the other leg.

Replacement of actuator modules

Better than further development of the pneumatic actuator modules would be the replacement by another type of actuator. Within the HeRoS Project, an electro-hydraulic actuation system is under development. The intention is to use these high-power cylinders to replace the pneumatic ones.

9.5.5 Joint mechanism

The size and mass of the half rings of the prototype can be reduced by using more advanced materials and manufacturing methods. One can think of electrical discharge machining (EDM) or milling of optimized structures from aluminium, steel, or titanium; or the use of carbon reinforced polymers.

However, although mass and size reduction of the rings is useful, the focus should be on first implementing the other recommendations (which will also reduce the overall size and mass of the exoskeleton).

[2] Technically it is not necessary to measure all joint angles, as the actuator lengths are also measured. However, a more accurate state estimation may be obtained by fusing sensor signals.

CHAPTER 10

Reflection

This chapter is a reflection, both on the design process and on the societal relevance of the project. First, we look back at the design methodology in Section 10.1. Then, the societal impact of the project is considered in Section 10.2.

10.1 Design methodology

Section 1.2 described the HeRoS Project and the design methodology that was used. We explained that the iMS approach had to be used for the design of the ankle exoskeleton and that it was decided to use a 'hands-on' approach, by starting with the quick development of hardware. It is for this reason that the analysis in Chapter 5 is carried out *after* the evaluation of early prototypes. model

10.1.1 The Vee process model

Figure 10.1-1 shows the *Vee* process model; it is a well-known design process model and it is often used as an example of how a design project should be carried out[1]. The model provides a reasonable description of our project design process, as will be explained by discussing each of the steps in the model

[1] It is assumed that the reader is familiar with the Vee model; details can be found in [26].

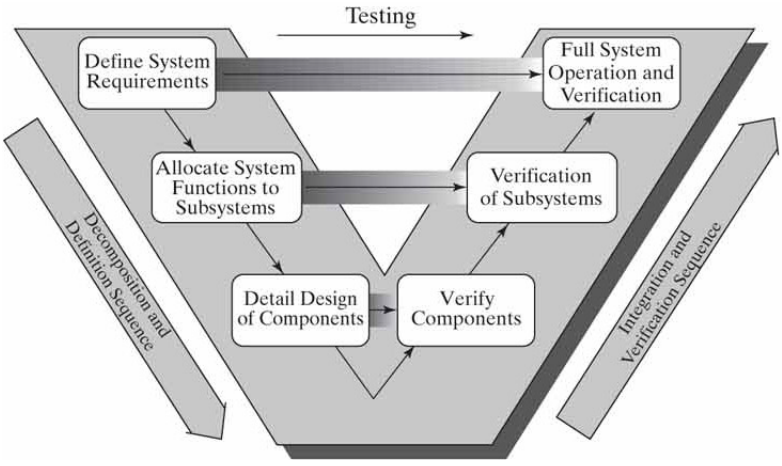

Figure 10.1-1
Vee model description of a design process. (Source: [26])

Define system requirements

The first step in the Vee model is to define the system requirements. This is described in Chapter 3 and the most fundamental requirement was (initially) that the iMS approach should be used for the prototype design.

Allocate system functions to subsystems

The next step in the Vee model is to allocate functions to the subsystems of the device that is being designed. Yet, this report does not contain a function analysis.

However, the iMS approach is a *complete* design description which defines both the subsystems and their functions. Examples of subsystems and their functions are: linear actuators that exert pushing forces; cables that are loaded with tension forces, and a shell that is loaded with a normal force. Although no explicit function analysis was carried out, the allocation of functions to the subsystem was implicitly defined by the iMS approach.

Detail design of components

The final prototype can be seen as consisting of the following components:

- the lower leg interface,
- the foot interface,
- the actuator modules, and
- the joint mechanism.

The development of the interfaces to the leg and foot are described in Chapter 5 and they are redesigned in Chapter 6 and again in Chapter 7.

The detail design of the actuator modules is described in Chapter 7 and the design of the control electronics and software is described in Appendix F.

The initial goal, according to the iMS approach, was to not have a rigid joint at the ankle. The function of the joint mechanism was to be fulfilled by a network of flexible materials, the design of which is described in Chapter 5. When the concept was found to be infeasible, a mechanism concept which used rigid joint was developed in Chapter 6 and its final design was described in Chapter 7.

Verify components

The following step according to the Vee model is the verification of system components. The force sensors, actuators, valves, straps, and other components have been tested separately whenever possible. However, the components were mostly tested together with the other components that make op the subsystems of the exoskeleton.

Verification of subsystems

This report describes the verification of the various subsystems. The evaluation of the lower leg interface is described in Sections 5.2.2 and 5.2.3 and evaluation of a variety of joint mechanisms is described in Chapter 6. The test platform built for evaluating these mechanisms is described in Section 6.1.

Full system operation and verification

Chapter 8 is dedicated to the evaluation of the complete ankle exoskeleton. Here all subsystems are tested together and the performance of the system as a whole is assessed.

10.1.2 Modified Vee process model

Hence, the design process followed the Vee model, although the function analysis was only implicitly defined by the prescribed iMS approach.

However, the model does not accurately represent the *many* design iterations of all subsystems in the ankle exoskeleton. For example, the joint mechanism required at least five significant iterations and for the lower leg interface, at least four iterations were made (without counting all the different shell shapes that were tried).

There are other process models, like the 'Spiral' that is shown in Figure 10.1-2, that represent the iterative nature of design projects better. The spiral is a series of subsequent Vee processes and includes the iterations of the project as a whole, describing development from a first prototype to an operational system. Yet, the iterations that are made for components and subsystems are not modeled.

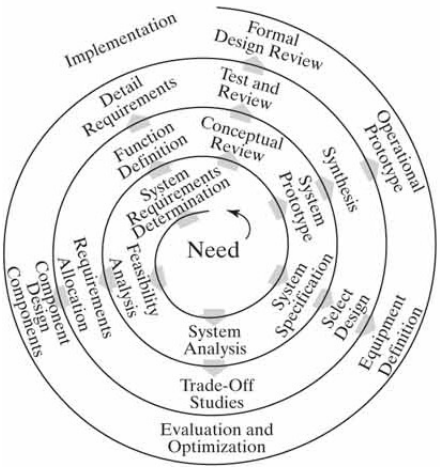

Figure 10.1-2
Spiral model description of a design process. (Source: [26])

Figure 10.1-3 shows a modified version of the Vee model that more accurately describes the PDEng process. The arrows no longer indicate a 'one-way' testing process, but are bidirectional representing the design iterations. The most important addition is the arrow from the subsystem verification to the system requirements. This shows that, after thorough investigation of the iMS approach, it was decided that it was infeasible to build a 2-DoF ankle exoskeleton using only flexible materials; the requirements had to be changed based on the evaluation of the prototypes.

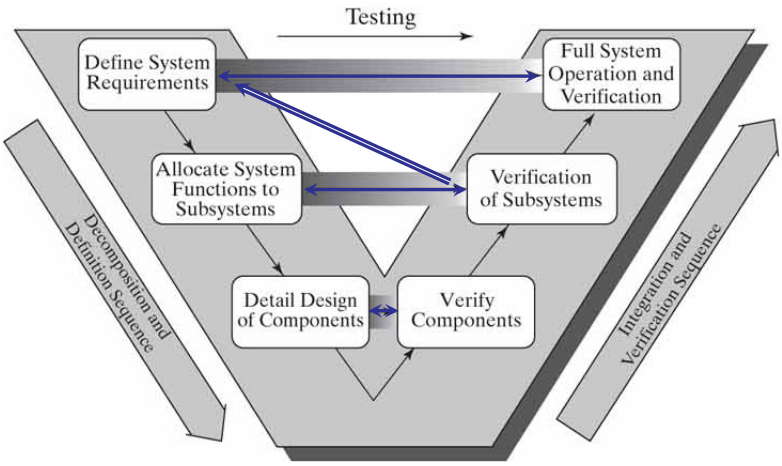

Figure 10.1-3
Modified Vee model description of the PDEng process. (Source: [26])

10.2 Societal impact and relevance

The prototype was developed for the Department of Biomechanical Engineering at the University of Twente and is intended to serve as a *research platform*. The device can be used to apply torques at the ankle of its wearer and various examples of (research) applications were given in Section 3.4. One of these examples is to use the device to provide assistance to patients with a motion impairment.

The prototype is a proof-of-principle to demonstrate the working principles; only a single device was made and it was used for experiments at the university. One could argue that there is no significant *socio-technological* context and that there is no intention to impact business and society yet. However, it is interesting to look at the project from a broader perspective and that is what will happen in this section. The *multi-level perspective on socio-technological systems* from [27] will be used as a framework.

10.2.1 The socio-technical system and the stable regime

The ankle exoskeleton can be seen as a part of a larger 'movement of innovations': the development of *wearable robotics* and *robot-assisted rehabilitation*. An example of a *lower-body exoskeleton* is shown in Figure 1.1-1 on page 3 and Figure 10.2-1 shows an example of a *robotic gait trainer*. These devices are intended to provide training and assistance to stroke survivors, patients with a (partial) spinal cord injury (SCI), the elderly, and others with a motion impairment.

Figure 10.2-1
LOPES gait trainer. (Source: [23])

If we look at the *current* socio-technical system that fulfills these function, then we are talking about, for instance, very simple plastic ankle braces as shown in Figure 10.2-2, or basic wheelchairs. It is not unlikely that a transition from wheelchairs to exoskeletons will occur, although it might take a considerable number of years.

We are considering a very broad spectrum of assistive devices, ranging from ankle braces to wheelchairs, but we can state that the socio-technological system that fulfills the function of providing assistance is *the current set of orthopedic tools*. The current state is stable and it is kept this way by a number of groups.

Health insurance Health insurance companies have a limited budget that needs to be divided over many patients; for this reason they often only reimburse the least expensive solutions. This means that it is unlikely that an expensive robotic ankle exoskeleton will be reimbursed when a simple plastic brace provides sufficient support.

Health care professionals Health care professionals and technicians are used to the currently available toolset and adoption of new technology by professionals tends to be slow. They

Figure 10.2-2
Passive ankle brace. (Source: [28])

are often skeptical towards innovations, and although the step from a rigid ankle brace to a robotic ankle orthosis is big, the step from a wheelchair to a full set of robotic legs is even bigger.

Patients Generally, patients are very critical and it is found to be very hard to have them adopt complex systems. The Sint Maartenskliniek in Nijmegen does studies where patients—after extensive training—get to take a full lower body exoskeleton home, but often they never touch the device. This is also because the technology is not yet fully developed; it is simply still easier to ride around in a wheelchair, than to go through the hassle of strapping oneself in a pair of robotic legs with limited capabilities and action radius. Another challenge is that patients don't want others to see that 'something is wrong': they would rather wear an inconspicuous plastic brace under their pants, than a robotic brace over it, even when the robotic version performs much better.

Rules, regulations, and ethics Until recently, robots were only used within confined and secured spaces in industry. Now we see that robots also start to make it into peoples homes. However, rules and (safety) regulations do not yet exist for assistive robotic devices and so-called 'co-bots' that interact with people. Only now are researchers starting to think about these topics and the ethical questions concerning them.

Government Government policies greatly influence what is reimbursed by insurance companies and what rules and regulations are being set. The government has a task in steering society and enabling research into the mentioned topics—for example by funding the research in this report.

10.2.2 Technological niche

In [27], it is explained how in the multi-level perspective transitions take place in multiple phases. For exoskeleton technology, the state-of-the-art is still within the first phase: novel hardware and ideas are developed within technological niches, at research institutes and universities.

For this PDEng project this is certainly the case, as is also clear by the funding of the project. It is funded by an NWO *Innovational Research Incentives Scheme*, which enables the investigation of novel ideas. The goal of the project is not to develop a product, but to investigate the applicability and feasibility of new technologies.

It is interesting to see that devices like those shown in Figures 1.1-1 and 10.2-1, are making it into the second phase of the transition. We see that institutions, such as the Roessingh and the Sint Maartenskliniek, are starting to use exoskeletons for training with patients. This is still at a very small scale and mainly intended as a feasibility study, but it is great to see that the hardware is getting adopted.

One of the patients that took part in an exoskeleton training pilot at the Sint Maartenskliniek was so excited about the device that he started a crowd-funding action to be able to buy one for himself [29]. This is an indication that the transition is going towards its next phase.

10.2.3 What is blocking further transition?

At this moment, there are no (negative) stakeholders that are actively preventing further transition. It is likely that health care insurances are not willing to pay for expensive robotic assistive devices, but this is not the reason that the technology is not being adopted: the reason is simply that the hardware is not yet functioning well enough compared to simpler alternatives—such as wheelchairs or passive rigid orthoses.

It is found to be *very* hard to design and build wearable robotics that stay in place, have enough power, and are comfortable. Furthermore, it is also found to be very difficult to properly *control* the hardware. The physical interaction between robots and people is extremely difficult. Robots are stiff and rigid, whereas people are soft and compliant. It is also challenging to detect the intention of the wearer: for instance, how does the robot know when its wearer wants to make a step?

We are still at the very early stages of development. More research needs to be done in designing both the hardware and the software, but also in the way healthy people move and behave. The PDEng assignment precisely fits within this research: we investigated whether it is possible to build a 2-DoF ankle exoskeleton. Now that we have built a working prototype, others will use the device to further investigate how to control it in such a way that it actually benefits its wearer.

10.2.4 Strategies and conclusion

The introduction of this section suggested that there might be no socio-technical context for the project, but we have seen that there are actually many things to consider regarding the adoption of the technology. We can, and *should*, already think about how parties such as health care insurance companies and therapists are going to react to the availability of new hardware. It is certain that current devices are too expensive to make it into peoples homes, but it is not yet time to try and minimize production costs: we first need to develop hardware that actually works.

Although it is not the direct goal of this PDEng project to realize embedment in society or business—as the main goal remains the exploration of technological possibilities—it is still important to keep society involved. For this reason we involved therapists and patients in the HeRoS Project while testing and evaluating hardware; it is crucial to get their feedback and keep them involved with the developments.

Furthermore, a ‘User Committee’ has been established for the HeRoS Project, in which a variety of companies and institutes take seat. We share our findings with the committee members and enable them to give feedback and commercialize (product) ideas resulting from the project. So far, the committee members only find the work interesting from a technological viewpoint, but not from a commercial one—both the hardware and the market simply are not yet ready.

In conclusion, this PDEng project took place in a small niche and significantly more development is needed before an actual transition to wearable robotics can be made. Yet, it is certainly interesting to consider what is needed for such a transition. In the future, great things may happen... see Figure 10.2-3.

Figure 10.2-3
Iron Man, art by Salvador Larroca.

PART IV

Appendices

APPENDIX A

Literature Review

This appendix contains background information that was collected during the literature review. Appendix A.1 describes the anatomy of the ankle, lower leg and foot. Appendix A.2 provides a state of the art of ankle exoskeletons.

A.1 Anatomy

Ankle exoskeletons are devices that are worn on the lower leg and foot of a person. They should fit well and support the biological bones, joints, and muscles of the wearer. It therefore is important to get a basic idea of the anatomy of the limbs on which the device is to be worn.

Section A.1.1 gives an overview of the bones and joints in the lower leg and foot and and Section A.1.2 shows the muscles that establish the motions of the ankle and foot.

The motions that the ankle and foot can make are shown in Figure A.1-1. They are: plantar flexion–dorsiflexion of the ankle; inversion–eversion of the foot; and flexion–extension of the toes.

Grant's Atlas of Anatomy [5] was used as the source for all material presented in this section.

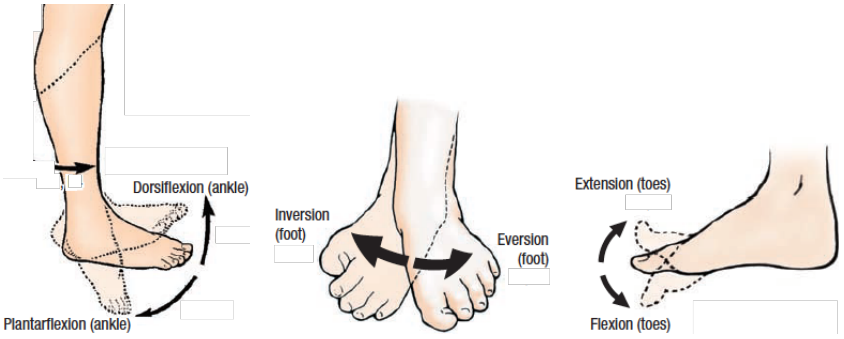

(a) (Source: [5]) (b) (Source: [5]) (c) (Source: [5])

Figure A.1-1

Motion of the ankle and foot. Figure (a) shows ankle plantar flexion–dorsiflexion; (b) shows how the foot moves in inversion–eversion; and (c) shows flexion–extension of the toes.

A.1.1 Bones and joints of the lower leg and foot

The bones of the lower leg and foot are shown in both an anterior and a posterior view in Figure A.1-2. The most important bones of the ankle are the *tibia* and *fibula* in the lower leg, and the *talus* in the foot. The tibia lies anterior to the fibia and it is larger and stronger.

Figures A.1-2 and A.1-3 also show important bones in the foot. They are the *calcaneus* (heel bone) which lies below the talus; the *navicular*, which lies anterior to the talus; and the *cuboid*, which lies anterior to the calcaneus and below the navicular.

Ankle plantar flexion–dorsiflexion, as shown in Figure A.1-1(a), is made possible by the three joints of the ankle:

- the *talocrural joint*;
- the *subtalar* joint; and
- the *inferior tibiofibular joint*.

The first joint is formed by the interface between the tibia and fibula on one side and the talus on the other. The second joint is formed by the interface between the talus and calcaneus. The third and final joint is formed by the interface between the tibia and fibula at their distal ends.

Furthermore, the interfaces between the talus, calcaneus, navicular, and cuboid make up joints in the foot that enable inversion–eversion, as is shown in Figure A.1-1(b). These joints are shown in Figure A.1-4 and their names are:

- the subtalar joint;
- the *talocalcaneonavicular joint*; and
- the *transverse tarsal joint*, which consists of
  - the *calcaneocuboid joint* and
  - the *talonavicular joint*.

Finally, Figure A.1-1(b) shows flexion–extension of the toes. This motion is made possible by the *metatarsophalangeal* and *interphalangeal* joints in the foot that are shown in Figure A.1-4.

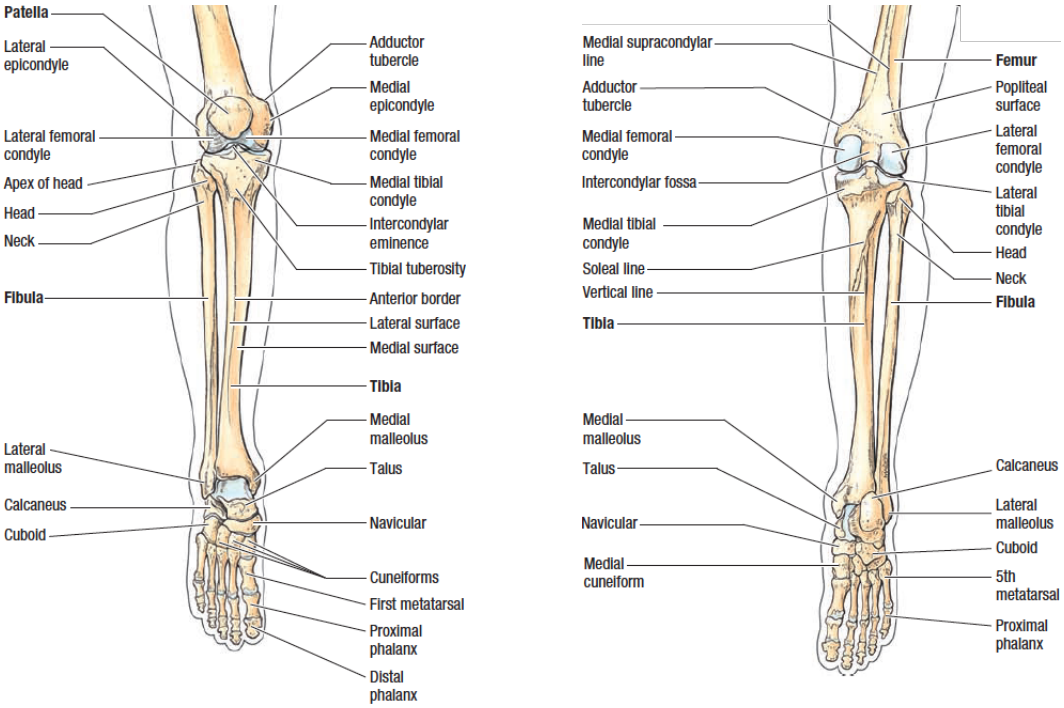

(a) (Source: [5])

(b) (Source: [5])

Figure A.1-2

Bones of the lower leg and foot, with the foot at full plantar flexion. Figure (a) shows the anterior and (b) the posterior view.

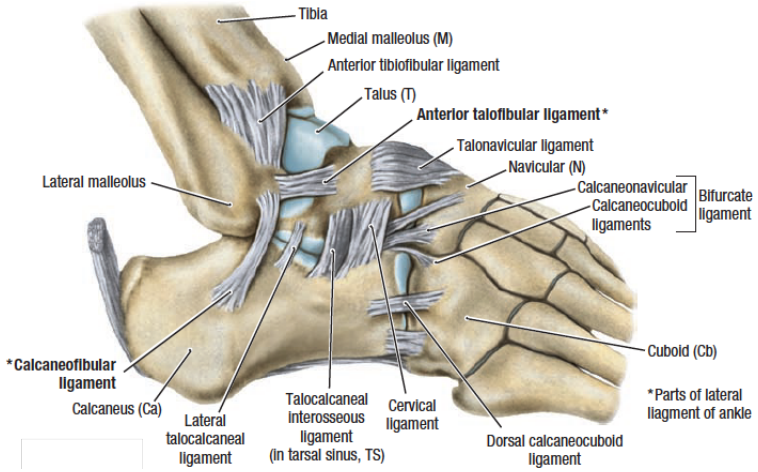

Figure A.1-3

Bones and ligaments of the ankle region, lateral view. (Source: [5])

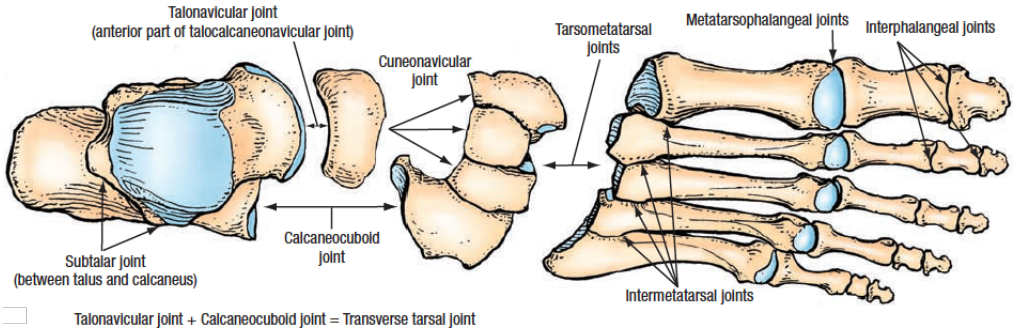

Figure A.1-4

Joints of the foot in a superior view. (Source: [5])

A.1.2 Muscles generating plantar flexion–dorsiflexion and inversion–eversion

Table A.1-1 lists the muscles of the lower leg and describes how they move both the ankle and the foot. The muscles are shown in Figure A.1-5. Multiple muscles contribute to both plantar flexion–dorsiflexion and inversion–eversion. Note that there are more muscles present in the foot for actuation of the digits and great toe.

Table A.1-1

Muscles in the lower leg and their functions. The muscles are shown in Figure A.1-5 in various views. The 'View' column of the table denotes in which view the muscles can be seen: A = anterior, AL = anterolateral and P = posterior.

Muscle	View	Function
Anterior muscles		
Tibialis anterior	(A, AL)	Ankle dorsiflexion; Foot inversion
Extensor hallucis longus	(A, AL)	Ankle dorsiflexion; Extension of the great toe
Extensor digitorum longus	(A, AL)	Ankle dorsiflexion; Extension of the four digits
Fibularis (peroneus) tertius		Ankle dorsiflexion; Aiding tertius in foot eversion
Lateral muscles		
Fibularis (peroneus) longus	(A, AL)	Weak ankle plantar flexion; Foot eversion
Fibularis (peroneus) brevis	(A, AL)	Weak ankle plantar flexion; Foot eversion
Posterior muscles—superficial		
Gastrocnemius	(AL, P)	Ankle plantar flexion (when knee is extended); Raising heel during gait; Knee flexion
Soleus	(AL, P)	Ankle plantar flexion; Steadying leg on foot
Plantaris	(P)	Weak ankle plantar flexion; Knee flexion
Posterior muscles—deep		
Popliteus	(P)	Unlocking extended knee; Weak knee flexion
Flexor hallucis longus	(P)	Ankle plantar flexion; Great toe flexion
Flexor digitorum longus	(P)	Ankle plantar flexion; Digit flexion
Tibialis posterior	(P)	Ankle plantar flexion; Foot inversion

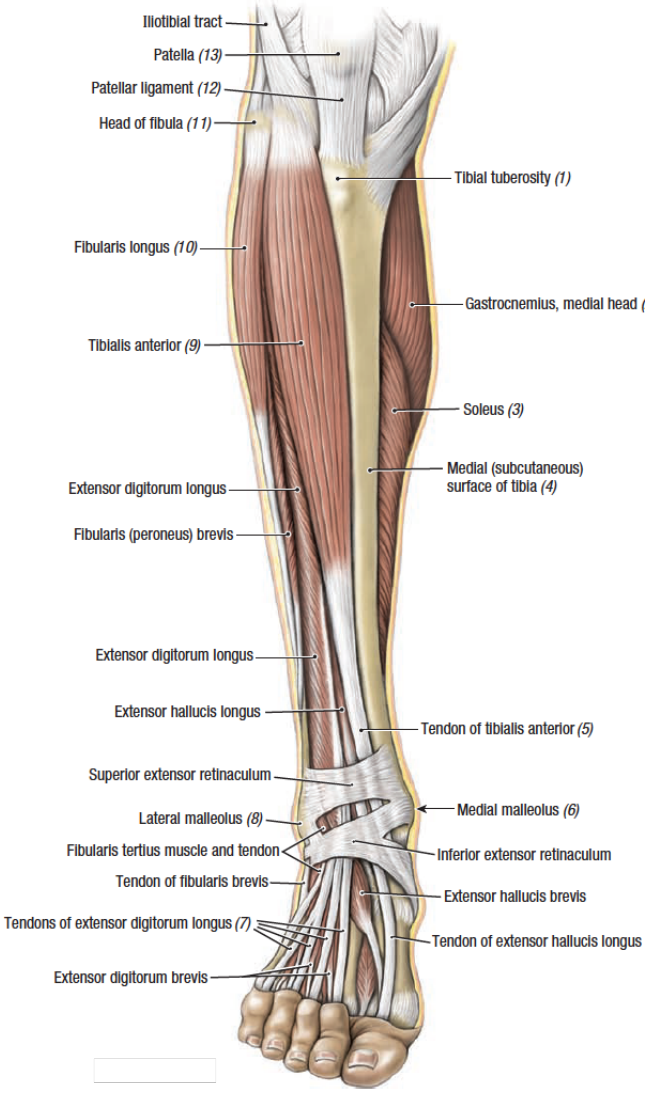

(a) (Source: [5])

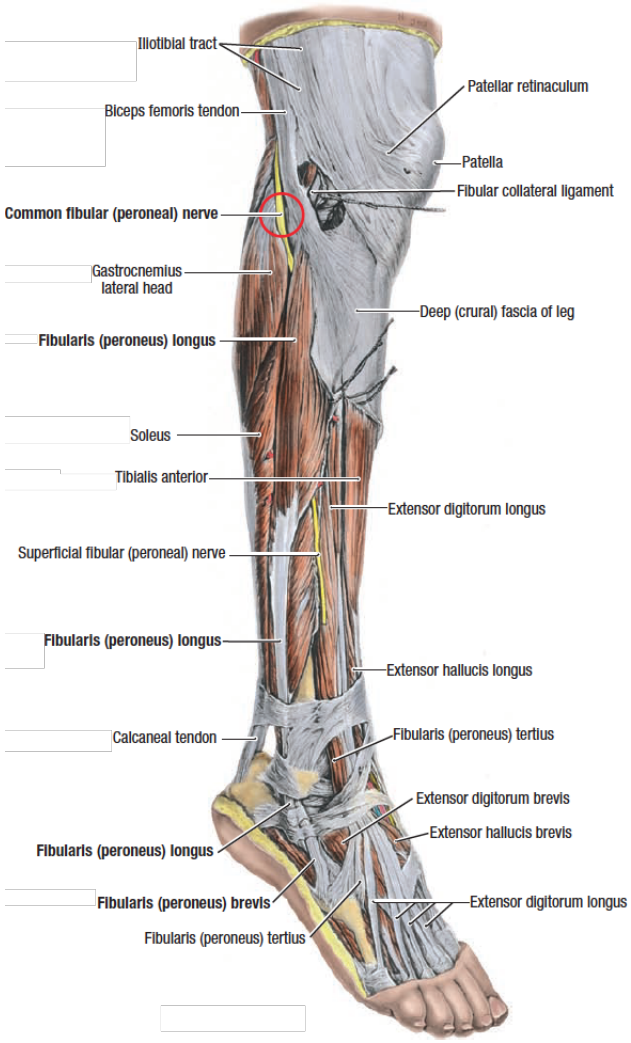

(b) (Source: [5])

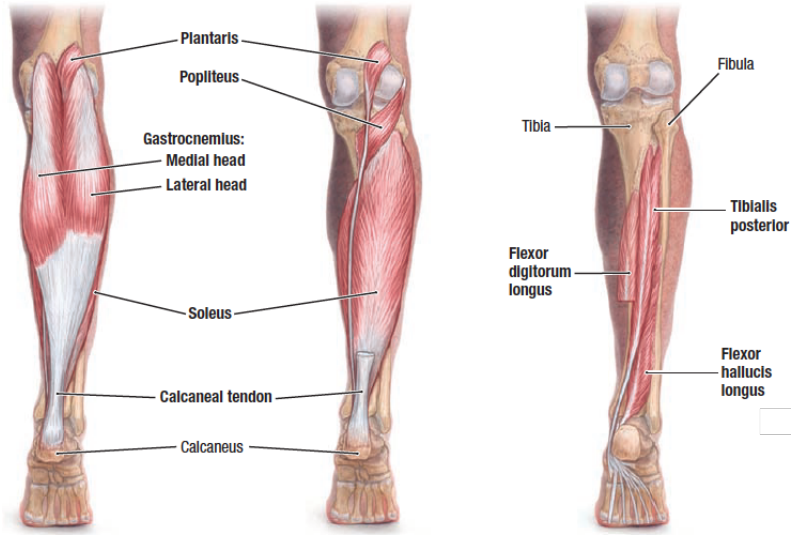

(c) (Source: [5])

Figure A.1-5

Muscles in the lower leg. Figure (a) shows an anterior, (b) an anterolateral and (c) a posterior view.

A.2 Ankle exoskeletons—State of the art and applications

This section discusses a wide variety of ankle exoskeletons and the applications for which they were developed. The devices are grouped by actuation principle:

- Section A.2.1: Pneumatically actuated ankle exoskeletons;
- Section A.2.2: Ankle exoskeletons with series elastic linear actuation;
- Section A.2.3: Tethered ankle exoskeletons;
- Section A.2.4: Unpowered ankle exoskeletons;
- Section A.2.5: Soft actuated ankle orthoses and exosuits;
- Section A.2.6: Multi-DoF ankle exoskeletons.

A.2.1 Pneumatically actuated ankle exoskeletons

Figure A.2-1 shows a number of pneumatically actuated ankle exoskeletons. These devices often use an external pressure supply and pneumatic muscles (McKibben actuators) which contract when they are pressurized [11, 30, 31, 32]. However, devices using rotary pneumatic actuators and portable bottles with compressed gas also exist [33].

Pneumatically actuated ankle exoskeletons have been used for a wide range of research applications, such as gait assistance for stroke survivors [11]; gait rehabilitation for patients with a spinal cord injury [31]; and to study locomotor adaptation after training with healthy subjects [30].

Recently it was shown that it is possible to reduce the metabolic cost of walking by up to 12% by using a pneumatic ankle exoskeleton that generates well-timed plantar flexion torques [34].

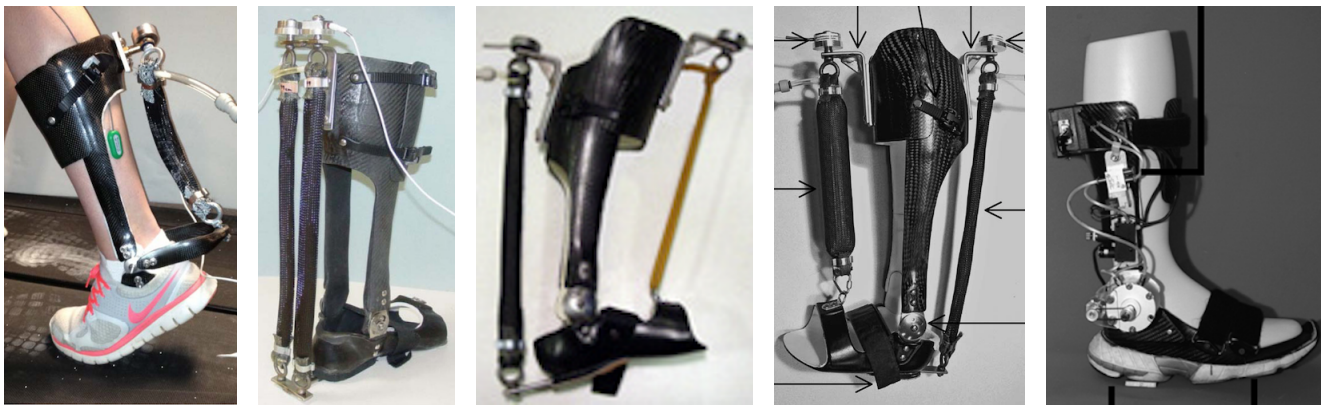

(a) (Source: [11]) (b) (Source: [30]) (c) (Source: [31]) (d) (Source: [32]) (e) (Source: [33])

Figure A.2-1
Various 1-DoF ankle exoskeletons that are pneumatically actuated. The devices in the first four figures use pneumatic muscles that can only generate tension forces. Figure (a) and (b) show devices that can only apply plantar flexion torques. The device in Figure (c) uses elastic bands to generate a dorsiflexion torque to counteract the pneumatic muscle. The device in Figure (d) uses bi-articulate pneumatic muscles, so that both plantar flexion and dorsiflexion torques can actively be generated. The device in Figure (e) uses a bidirectional rotary pneumatic actuator.

A.2.2 Ankle exoskeletons with series elastic linear actuation

It can be advantageous to place an elastic element in between an actuator and its load. This is called series-elastic actuation (SEA) and the advantages are, among others, that more accurate and stable force control can be implemented, that the actuator is protected from shock loads, and that energy can be stored in the elastic element [35].

Figure A.2-2 shows a number of ankle exoskeletons in which SEA is implemented. All devices use a linear actuator in series with an elastic element.

SEA is particularly suited for exoskeleton technology, as shock loads occur when the wearer hits objects (or the ground at foot contact). Series elastic actuation shows stable behavior during contact with both hard and soft environments [12]. The presence of the spring increases user comfort, as it compensates for small actuator and human errors and works as a safety mechanism [36].

Ankle exoskeletons with SEA have been used for a wide variety of research purposes. Among others are: compensation for drop-foot during walking [12]; push-off assistance during gait in both stroke survivors [37] and healthy individuals [38]; and studying the efficacy of balance controllers during perturbed standing [39]

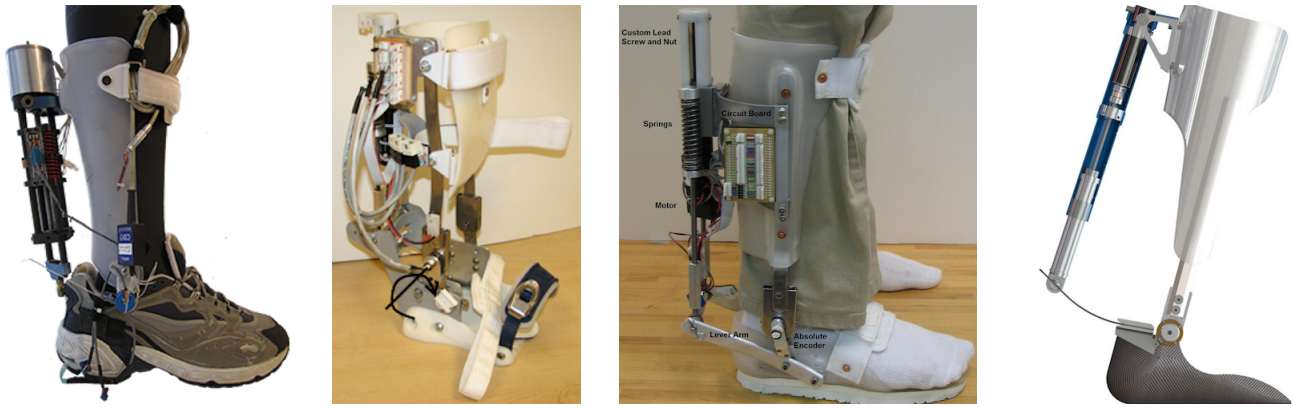

(a) (Source: [12]) (b) (Source: [36]) (c) (Source: [40]) (d) (Source: [2])

Figure A.2-2

1-DoF Ankle exoskeletons with series elastic actuation (SEA). All devices use a spindle drive in series with a spring. The first three devices use a coil spring, whereas the fourth uses a leaf spring as an elastic element.

A.2.3 Tethered ankle exoskeletons

Figure A.2-3 shows a 1-DoF ankle exoskeleton that is driven by a remote actuator [41]. A Bowden-cable is used to transmit the power to the exoskeleton.

An advantage of such a setup is that the an actuator with high torque and bandwidth can be used without adding weight to the orthosis. (In this case the mass that is being worn is less than 0.88 kg and torques up to 120 Nm can be generated [41].) This means that a variety of control strategies can be tested [13] and that it is also easy to update or change the orthosis design.

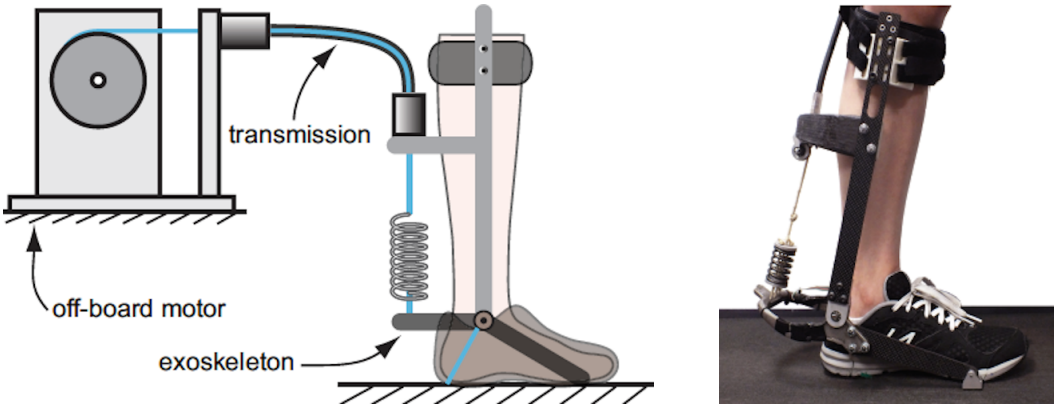

(a) (Source: [13]) (b) (Source: [13])

Figure A.2-3

A Bowden cable-driven ankle exoskeleton [41]. Figure (a) explains how an off-board motor is used to actuate the exoskeleton via a Bowden cable transmission. Figure (b) shows the design of the exoskeleton.

A.2.4 Unpowered ankle exoskeletons

The first three photos in Figure A.2-4 show devices that use a clutching element to engage and disengage a spring that delivers a plantar flexion torque. It was found to be possible to reduce the metabolic cost of walking by using the unpowered exoskeleton shown in Figure A.2-4(b) [42].

The device in Figure A.2-4(d) is intended as an assistive device that prevents foot-drop in patients with a gait impairment [14]. It uses a bellows pump in the sole of the shoe, which is compressed during stance and pressurizes a pneumatic mechanism that locks the ankle during swing to create foot clearance.

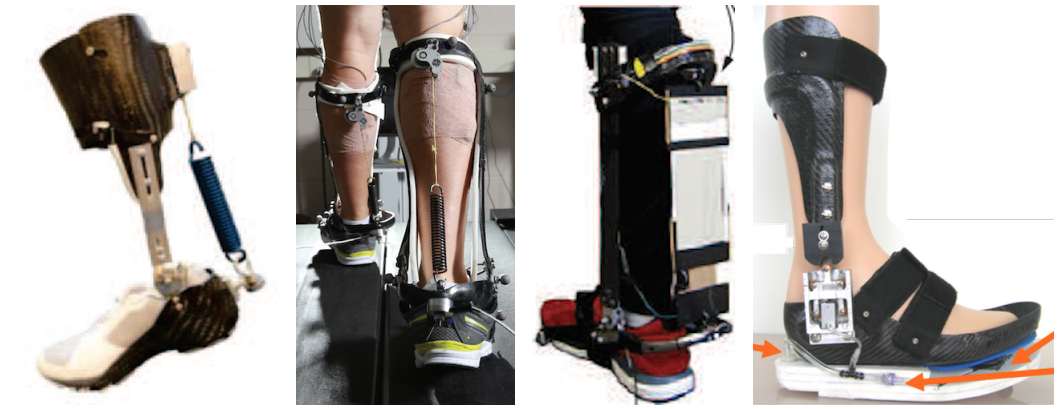

(a) (Source: [43]) (b) (Source: [42]) (c) (Source: [44]) (d) (Source: [14])

Figure A.2-4

Passive 1-DoF ankle exoskeletons that store and release energy during gait. The devices in Figure (a) and (b) use a mechanical clutch to engage and disengage a spring; the one in Figure (c) uses a low-power electro-adhesive clutch for this purpose. The device in figure (d) uses a pump in the shoe sole to pressurize an actuator that locks the ankle joint during swing.

A.2.5 Soft actuated ankle orthoses and exosuits

The devices that were discussed so far are all real “robots”, comprising rigid shells, mechanical hinges, and electric motors. Recently, researcher have also started to follow a more *biomimetic* design approach: using biology as a source of inspiration.

A first example are the pneumatically actuated orthoses described in Section A.2.1, which use McKibben actuators as artificial muscles. However, they still make use of a rigid orthosis structure with a single-axis mechanical hinge.

Figure A.2-5(a) shows a completely soft orthosis, without mechanical hinges, that uses pneumatic artificial muscles to support the three corresponding biological muscles at the anterior side of the distal leg segment (peroneus tertius, extensor digitorum longus and tibialis anterior).

Another implementation of such a biomimetic design approach is shown in the Figures A.2-5(b) and (c). The orthosis comprises no rigid frames or mechanical hinges, yet a Bowden-cable is used to act as an artifical muscle or tendon. An off-board actuation mechanism, like the one shown in Figure A.2-3(a), is used to drive the Bowden cables.

The term ‘Exosuit’ was proposed for these light-weight biomimetic suits that provide assistive joint torques to their wearer without using rigid frames [45]. They have been used for research into various topics, such as the reduction of the metabolic cost of walking [46, 47] and providing assistance to stroke survivors [48, 49]. Various portable solutions for the actuation module have also been proposed, so that the devices can become fully autonomous [50].

(a) (Source: [51]) (b) (Source: [48]) (c) (Source: [48])

Figure A.2-5

Soft active ankle orthoses. The device in Figure (a) uses artificial muscles to assist the corresponding human muscles. The devices in Figures (b) and (c) use a Bowden cable to act as an artificial muscle to assist dorsiflexion and plantar flexion respectively.

A.2.6 Multi-DoF ankle exoskeletons

All of the previously presented ankle exoskeletons provide only assistance in the plantar flexion–dorsiflexion degree-of-freedom. Except for the soft 'exosuits' discussed in Section A.2.5, they all constrain the other degrees-of-freedom of the human ankle joint.

The device shown in Figure A.2-6(a) uses three linear actuators while providing two degrees-of-freedom, plantar flexion–dorsiflexion and inversion–eversion—it is an *underactuated* mechanism. The total mass of the device is 4.9 kg (3.3 kg of which comes from the linear SEAs) [52], so it is significantly heavier than any of the devices discussed so far and far bulkier.

An update to this design, using three series elastic actuators that are driven by Bowden cables, is shown in Figure A.2-6(b). Each of these actuators has a mass of 1 kg and the ankle exoskeleton weighs almost 4.25 kg, while still being bulky. A similar device is shown in Figure A.2-6(c).

Figure A.2-6(d) shows the MIT Anklebot, which uses two linear actuators. It allows ankle movement in three degrees-of-freedom (plantar flexion–dorsiflexion, inversion–eversion, and endorotation–exorotation) and is said to be backdrivable and to have a low mechanical impedance [53]. However, it also includes a knee brace with a mechanical hinge and the mass of the device is 3.6 kg [54]. The photo shows that the device is rather bulky.

Multi-DoF devices were proposed for use in gait rehabilitation [52, 54, 55, 56] and as a tool to identify human ankle stiffness [53].

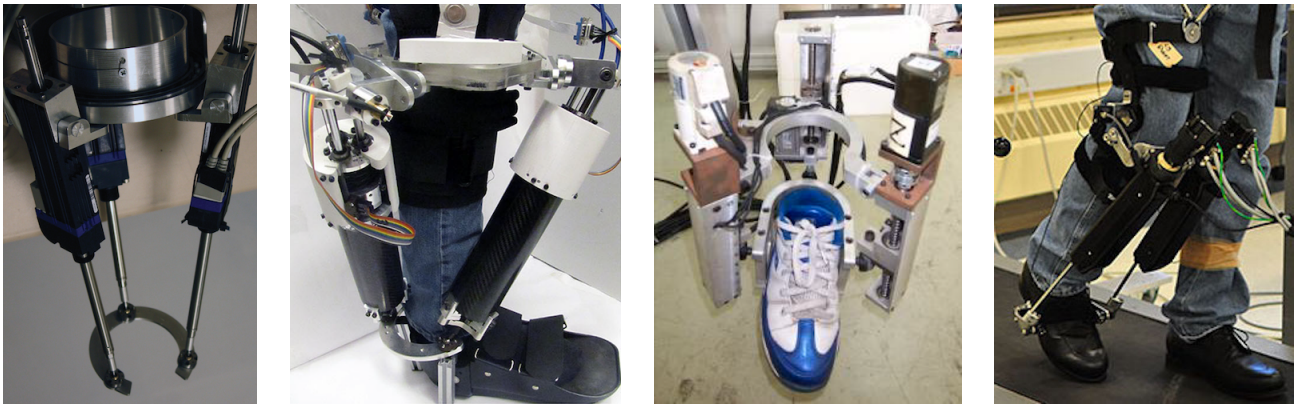

b

(a) (Source: [52]) (b) (Source: [55]) (c) (Source: [56]) (d) (Source: [53])

Figure A.2-6

Multi-DoF ankle exoskeletons. The underactuated devices in Figures (a), (b), and (c) use three linear actuators, while the device in Figure (d) uses two.

APPENDIX B

Use Cases

This appendix presents a series of use cases for a full lower-body exoskeleton. They are also relevant for the ankle module of such a device and for a stand-alone active ankle orthosis. The cases are used to define the requirements and technical specifications of the active ankle orthosis.

A significant number of the use cases are based on the challenges of the CYBATHLON 2020 exoskeleton race that are described in Section B.1. The use cases are listed in Section B.2 and a detailed description of each case is given in Section B.3

B.1 The CYBATHLON

"The CYBATHLON is a unique championship in which people with physical disabilities compete against each other to complete everyday tasks using state-of-the-art technical assistance systems" [16].

One of the disciplines is an exoskeleton race. The six obstacles and corresponding challenges that form the exoskeleton race track for the year 2020 are realistic representations of activities of daily living and they are the following.

- `CT01-SIST`: *Sit & Stand*
- `CT02-SLLM`: *Slalom*
- `CT03-RAMP`: *Ramp & Door*
- `CT04-TERR`: *Rough Terrain*
- `CT05-TILT`: *Tilted Path*
- `CT06-STAR`: *Stairs*

Figure B.1-1 shows each of the obstacles and Table B.1-1 lists the rules for each challenge. Note that the figures and rules are directly copied from [57] (© 2017 ETH Zürich / CYBATHLON).

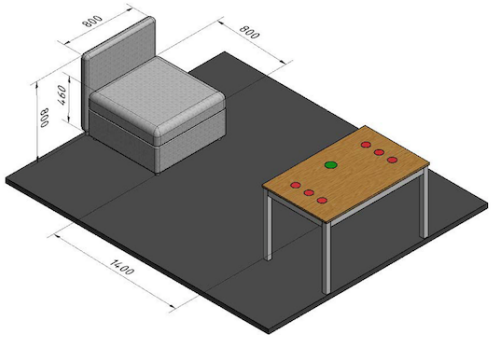

(a) CT01-SIST: Sit & Stand.

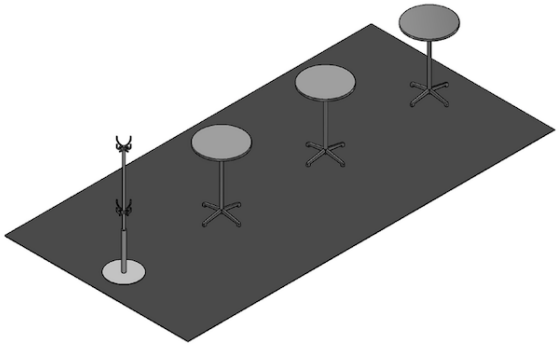

(b) CT02-SLLM: Slalom.

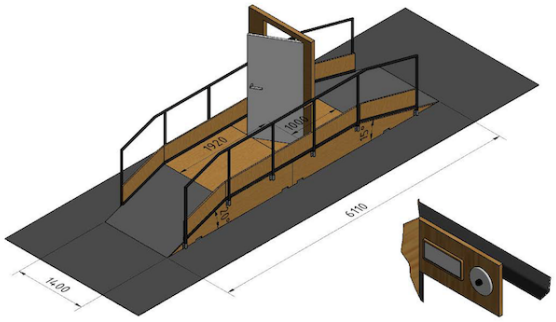

(c) CT03-RAMP: Ramp & Door.

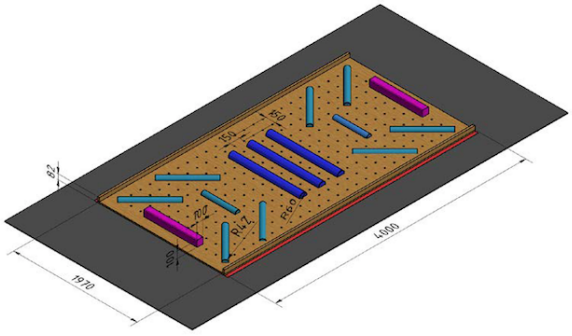

(d) CT04-TERR: Rough terrain.

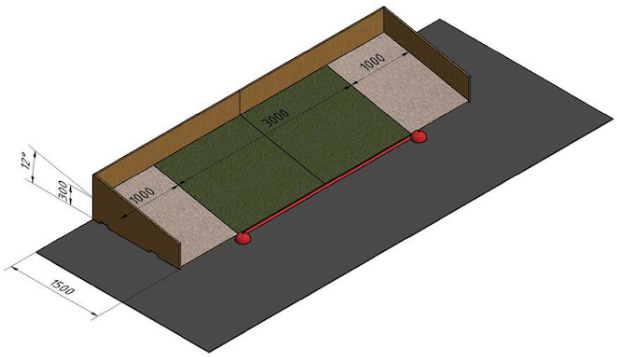

(e) CT05-TILT: Tilted path.

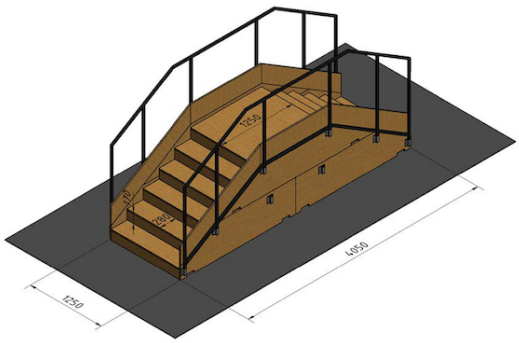

(f) CT06-STAR: Stairs.

Figure B.1-1
CYBATHLON 2020 obstacles. Taken fom [57] (© 2017 ETH Zürich / CYBATHLON).

Table B.1-1
CYBATHLON 2020 tasks and rules. Taken fom [57] (© 2017 ETH Zürich / CYBATHLON).

CT01-SIST	**Sit & Stand**
R-01	Pilots must sit down and stand up once.
R-02	Pilots must sit down completely, i.e. with their full body weight. The knees and the hip are flexed accordingly and the crutches must be lift off the ground once while sitting. Pilots are not asked to touch the backrest with their backs.
R-03	Pilots must stack six cups on the table. They are free to conduct the stacking task either with one hand or with both.
R-04	Use of hands, arms and crutches is allowed to stack the cups. If the stacked cups collapse when the pilot crosses the start line to the next task, the task is failed.
CT02-SLLM	**Slalom**
R-01	It is not allowed to touch the furniture.
R-02	Two consecutive pieces of furniture are considered a pair. To start the task, the first two pieces (i.e. pair) of furniture are entered from the left or from the right-hand side. All three pairs must be passed through once.
CT03-RAMP	**Ramp & Door**
R-01	The ramp must be ascended on the more inclined slope (20°) and descended on the less inclined slope (15°).
R-02	The doorbell must be rang.
R-03	The door must be opened, passed through and closed.
CT04-TERR	**Rough terrain**
R-01	The pilot is free to choose their or her path across the rough terrain.
R-02	Crossing the boundary on the sides is not allowed (i.e. the pilot can only exit at the start and finish). Touching the wooden rails placed on each side or the terrain is allowed, but it is not allowed to step on these rails.
R-03	The crutches may be placed anywhere on the obstacle (also outside the red lines).
CT05-TILT	**Tilted path**
R-01	It is only allowed to enter and exit the obstacle between the wooden rail and the red pole base.
CT06-STAR	**Stairs**
R-01	Pilots must ascend and descend the stairs once in the direction of the race track (once up, once down).
R-02	Pilots are allowed to place two feet on one step.
R-03	Pilots are not allowed to omit single steps or jump over steps. Thus, each step must be stepped on with at least one foot.

B.2 Use case definitions

Table B.2-1 gives an overview of the defined use cases; each use case has a unique identifier (ID). Detailed descriptions of the use cases are given in Section B.3.

The use cases 1–4, 7, and 10 are essential for an exoskeleton to be useful. The use cases 8, and 12–18 are based on the CYBATHLON 2020 track and the use cases 6, 9, 11, and 19 are wishes from therapists or patients.

A detailed description of the use cases is given in Section B.3.

Table B.2-1
List of use case IDs and names.

Case ID	Name
UC01-TRAN	Transport
UC02-DONN	Donning
UC03-DOFF	Doffing
UC04-SIST	Sit-to-stand
UC05-STSI	Stand-to-sit
UC06-SITW	Sitting with exoskeleton
UC07-STND	Standing
UC08-MANP	Standing—Object manipulation
UC09-BEND	Standing—Bending
UC10-WALK	Walking
UC11-NARR	Walking—Narrow space
UC12-SLLM	Walking—Slalom
UC13-SLPU	Walking—Walking up slope
UC14-SLPD	Walking—Walking down slope
UC15-TERR	Walking—Walking rough terrain
UC16-TILT	Walking—Walking tilted ground
UC17-STRA	Walking—Stair ascent
UC18-STRD	Walking—Stair descent
UC19-CRRY	Walking—Carrying object

B.3 Use case descriptions

For each use case an initial condition ('Init'), intermediate activities ('Inter') and a final condition ('Final') are described. A priority key, as defined in Table B.3-1, is assigned to each of the intermediate activities.

Table B.3-1
Priority keys assigned to use cases and requirements.

Key	Meaning	Explanation
M	Mandatory	This feature is absolutely necessary to have, either because the device would not function otherwise, or because project management requires it.
D	Desired	We aim for this feature to be in the design, but it should not hinder achieving the mandatory features.
O	Optional	This feature would be nice to have, but no great effort will be put in to achieve it.

`UC01-TRAN`: ***Transport***
This use case is essential for independent use of the exoskeleton.

Stage	Description	Pr.
Init	The user is sitting in their wheelchair.	
Inter	The user moves the individual exoskeleton components (for example to their car) by placing them on their lap and using their wheelchair.	M
Final	The user is sitting in their wheelchair.	

`UC02-DONN`: ***Donning***
This use case is essential for independent use of the exoskeleton.

Stage	Description	Pr.
Init	The user is sitting in a (wheel)chair with the exoskeleton components within reach.	
Inter	The user dons the exoskeleton components and couples them.	M
	The user turns the exoskeleton power on.	M
Final	The user is sitting in a (wheel)chair, wearing the exoskeleton.	

`UC03-DOFF`: ***Doffing***
This use case is essential for independent use of the exoskeleton.

Stage	Description	Pr.
Init	The user is sitting in a (wheel)chair, wearing the exoskeleton.	
Inter	The user turns the exoskeleton power off.	M
	The user uncouples the exoskeleton components and doffs them.	M
Final	The user is sitting in a (wheel)chair with the exoskeleton components within reach.	

`UC04-SIST`: ***Sit-to-stand***
This use case is essential for independent use of the exoskeleton. It is also relevant for CYBATHLON 2020 task `CT01-SIST` (Sit & Stand).

Stage	Description	Pr.
Init	The user is sitting in a (wheel)chair, wearing the exoskeleton.	
Inter	The user holds on to a support while the exoskeleton lets him stand up.	M
	The user exchanges the support for crutches. (If another type of support was used.)	M
Final	The user is standing upright, while maintaining balance using crutches.	

`UC05-STSI`: ***Stand-to-sit***
This use case is essential for independent use of the exoskeleton. It is also relevant for CYBATHLON 2020 task `CT01-SIST` (Sit & Stand).

Stage	Description	Pr.
Init	The user is standing upright, while maintaining balance using crutches.	
Inter	The user exchanges the crutches for another type of support if needed.	M
	The user holds on to a support while the exoskeleton lets him sit down.	M
Final	The user is sitting in a (wheel)chair, wearing the exoskeleton.	

`UC06-SITW`: ***Sitting with exoskeleton***
This use case was recommended by physio and occupational therapist attendees of the Wearable Robotics Workshop session of the NVDG congres 'Back to the future, dwarslaesierevalidatie in 2030,' April 21, 2018.

Stage	Description	Pr.
Init	The user is sitting in a (wheel)chair, wearing the exoskeleton.	
Inter	The user turns the exoskeleton *power off*.	M
	(The user adjusts the exoskeleton.)	M
	The user is able sit in their (wheel)chair for an extended period of time, without using the exoskeleton and without experiencing discomfort from the device.	M
Final	The user is sitting in a (wheel)chair, wearing the exoskeleton.	

`UC07-STND`: ***Standing***
This use case is essential for independent use of the exoskeleton. It is also relevant for all CYBATHLON 2020 tasks, but specifically for `CT01-SIST` (Sit & Stand) and `CT03-RAMP` (Ramp & Door).

Stage	Description	Pr.
Init	The user is standing upright, while maintaining balance using crutches.	
Inter	N/A.	–
Final	The user is standing upright, while maintaining balance using crutches.	

`UC08-MANP`: ***Standing—Object manipulation***
This use case is based on CYBATHLON 2020 tasks `CT01-SIST` (Sit & Stand) and `CT03-RAMP` (Ramp & Door).

Stage	Description	Pr.
Init	The user is standing upright, while maintaining balance using crutches.	
Inter	The user manipulates objects on a counter with at least one hand.	M
	The user manipulates objects on a regular desk or dinner table.	M
Final	The user is standing upright, while maintaining balance using crutches.	

`UC09-BEND`: ***Standing—Bending***
This use case was recommended by physio and occupational therapist attendees of the Wearable Robotics Workshop session of the NVDG congres 'Back to the future, dwarslaesierevalidatie in 2030,' April 21, 2018.

Stage	Description	Pr.
Init	The user is standing upright, while maintaining balance using crutches.	
Inter	The user bends bends to pick up objects from a coffee table.	M
	The user bends bends to pick up objects from the floor.	D
Final	The user is standing upright, while maintaining balance using crutches.	

`UC10-WALK`: ***Walking***
This use case is essential for independent use of the exoskeleton. It is also relevant for all CYBATHLON 2020 tasks.

Stage	Description	Pr.
Init	The user is standing upright, while maintaining balance using crutches.	
Inter	The user initiates walking.	M
	The user walks in a straight line on level ground.	M
	The user maintains balance during walking by using crutches.	M
	The user withstands small disturbances while walking.	D
	The user changes direction by using crutches to turn during a single-support gait phase.	M
	The user adjusts the walking speed while walking.	D
	The user walks at various speeds.	D
	The user terminates walking.	M
Final	The user is standing upright, while maintaining balance using crutches.	

`UC11-NARR`: ***Walking—Narrow space***
This use case was recommended by physio and occupational therapist attendees of the Wearable Robotics Workshop session of the NVDG congres 'Back to the future, dwarslaesierevalidatie in 2030,' April 21, 2018.

Stage	Description	Pr.
Init	The user is walking on level ground.	
Inter	The user walks through a narrow space, such as a narrow hallway.	M
	The user is able to make a turn in the narrow space.	D
Final	The user is walking on level ground.	

`UC12-SLLM`: ***Walking—Slalom***
This use case is based on CYBATHLON 2020 task `CT02-SLLM` (Slalom).

Stage	Description	Pr.
Init	The user is walking on level ground.	
Inter	The user executes a slalom whilst avoiding collision with the objects.	M
Final	The user is walking on level ground.	

`UC13-SLPU`: ***Walking—Walking up slope***
This use case is based on CYBATHLON 2020 task `CT03-RAMP` (Ramp & Door).

Stage	Description	Pr.
Init	The user is walking on level ground.	
Inter	The user walks up a slope.	M
Final	The user is walking on level ground.	

`UC14-SLPD`: ***Walking—Walking down slope***
This use case is based on CYBATHLON 2020 task `CT03-RAMP` (Ramp & Door).

Stage	Description	Pr.
Init	The user is walking on level ground.	
Inter	The user walks down a slope.	M
Final	The user is walking on level ground.	

`UC15-TERR`: ***Walking—Walking rough terrain***
This use case is based on CYBATHLON 2020 task `CT04-TERR` (Rough terrain).

Stage	Description	Pr.
Init	The user is walking on level ground.	
Inter	The user walks on rough terrain.	M
Final	The user is walking on level ground.	

`UC16-TILT`: ***Walking—Walking tilted ground***
This use case is based on CYBATHLON 2020 task `CT03-RAMP` (Tilted path).

Stage	Description	Pr.
Init	The user is walking on level ground.	
Inter	The user walks along a tilted path.	M
Final	The user is walking on level ground.	

`UC17-STRA`: ***Walking—Stair ascent***
This use case is based on CYBATHLON 2020 task `CT06-STAR` (Stairs).

Stage	Description	Pr.
Init	The user is walking on level ground.	
Inter	The user ascends a flight of stairs.	M
Final	The user is walking on level ground.	

`UC18-STRD`: ***Walking—Stair descent***
This use case is based on CYBATHLON 2020 task `CT06-STAR` (Stairs).

Stage	Description	Pr.
Init	The user is walking on level ground.	
Inter	The user descends a flight of stairs.	M
Final	The user is walking on level ground.	

`UC19-CRRY`: ***Walking—Carrying object***
This use case is a wish expressed by two paraplegics during a Cybathlon meeting at the University of Twente on May 9, 2018.

Stage	Description	Pr.
Init	The user is walking on level ground.	
Inter	The user is walking while carrying an object with one hand.	M
Inter	The user is walking while carrying either one object with both hands or one object in each hand.	D
Final	The user is walking on level ground.	

APPENDIX C

Specification of Technical Requirements

Section C.1 list collected data from a literature review. The derived HeRoS requirements are listed in Section C.2. See Section 3.5 for the relevance for this PDEng report.

C.1 Literature review

This appendix summarizes additional data collected in the compilation of the technical actuation and anthropometric data requirements. Regarding actuation requirements, a summary is given in Sections C.1.1–C.1.4 of all the average extremum data points (and standard deviations where available) used to define the requirements in Table C.2-1 as based on a number of data sources: internal biomechanics and Symbitron project actuation specifications, level ground gait (scaled to 0.8 m/s for calculation of velocities and powers), sit-to-stand, stair ascent, and stair descent data. Standard deviation (SD) of the data is listed where available.

In Section C.1.5 the data in Table C.2-2 is given for small-sized females (Table C.1-6) and large-sized males (Table C.1-7) where possible. There is also some additional foot size data given (Table C.1-8).

C.1.1 Joint angle data for various use cases

Table C.1-1

Minimum and maximum values of the joint angles from various sources with the chosen minimum and maximum requirements.

Source	Hip average(SD) [°]		Knee average(SD) [°]		Ankle average(SD) [°]	
	Min (extension)	Max (flexion)	Min (extension)	Max (flexion)	Min (plantar flexion)	Max (dorsiflexion)
Wearable actuation biomechanics specifications [58][§]	−20(−) [59, 60, 61, 62]	100(−) [63]	0(−) [64]	90(−) [63]	−15(−) [59, 60, 61, 62]	10(−) [63]
Symbitron WE1 [4]	–	–	−4.0(−)	111.2(−) [65]	−42.9(−)[†]	35.5(−)[†]
Symbitron WE2 [66]	−22.5(−)	107.7(−)	–	–	–	–
Gait - Winter [62]	−10.9(8.7)	21.8(4.8)	0.63(3.3)	64.7(5.5)	−19.7(5.8)	9.4(5.0)
Gait - Bovi [67]	−8.3(7.9)	33.7(8.3)	3.8(4.8)	63.4(4.8)	−39.9(7.8)	−7.6(3.0)
Gait - van den Bogert [68]	−17.4(5.3)	19.9(4.2)	4.3(2.8)	68.8(3.4)	−27.8(5.7)	3.2(2.9)
Sit-to-stand - Mak [63]	−18.3(−)	101.6(−)	0(−)	86.1(−)	8.9(−)	20.9(−)
Sit-to-stand - Pai [69]	−6.4(−)	90.1(−)	7.9(−)	98.5(−)	10.6(−)	25.9(−)
Sit-to-stand - Roebroeck [70]	−3.9(3.8)	91.6(10.5)	12.4(3.4)	100.6(3.4)	11.5(3.8)	28.4(8.1)
Stair ascent - Riener [71]	16.9(−)	75.0(−)	9.3(−)	101.8(−)	−22.9(−)	15.0(−)
Stair descent - Riener [71]	23.9(−)	50.0(−)	15.5(−)	101.2(−)	−28.1(−)	16.7(−)
Stair ascent - Protopapadaki [72]	6.3(7.6)	63.9(7.6)	1.2(5)	92.8(10)	−24.0(10.5)	16.9(10.1)
Stair descent - Protopapadaki [72]	9.5(7.5)	35.2(8.4)	1.2(5.8)	88.2(9.8)	−34.4(10.0)	25.6(10.8)
Stair ascent - McFadyen [73]	10.9(3)	58.8(1)	11.6(2)	101.4(2)	−8.0(3.7)	23.7(2.2)
Stair descent - McFadyen [73]	8.3(3)	35(1.5)	19.6(1.4)	104.9(2.8)	−26.6(2)	27.7(2)
Chosen requirement [°]	−30 [62]	115 [70]	0* [64]	115 [72]	−50* [64, 74]	30* [64, 74]

[§]Internal document based on external references
[†]Data average minus two standard deviations, or data average plus two standard deviations
*Limited to biological kinematic RoM limits

C.1.2 Joint torque data for various use cases

Table C.1-2

Minimum and maximum values of the joint torques from various sources with the chosen minimum and maximum requirements as based on the weight of a 80 kg user.

Source	Hip average(SD) [Nm/kg]		Knee average(SD) [Nm/kg]		Ankle average(SD) [Nm/kg]	
	Min (extension)	Max (flexion)	Min (extension)	Max (flexion)	Min (plantar flexion)	Max (dorsiflexion)
Wearable actuation biomechanics specifications [58][§]	−1.44(−) [63]	0.8(−) [59, 60, 61, 62]	−1.86(−) [63]	0.34(−) [59, 60, 61, 62]	−1.47(−) [59, 60, 61, 62]	0.59(−) [63]
Symbitron WE1 [4]	–	–	−1.86(−)[†] [75]	–	−2.38(−)[†] [75]	–
Symbitron WE2 [66]	−1.86(−)[†] [75]	–	–	–	–	–
Gait - Winter [62]	−0.59(0.32)	0.4(0.41)	−0.61(0.43)	0.27(0.34)	−1.62(0.26)	0.053(0.13)
Gait - Bovi [67]	−0.35(0.15)	0.74(0.22)	−0.42(0.19)	0.14(0.035)	−1.32(0.12)	0.051(0.039)
Gait - van den Bogert [68]	−0.39(0.092)	0.33(0.17)	−0.46(0.19)	0.26(0.13)	−1.76(0.14)	0.063(0.064)
Sit-to-stand - Mak [63]	−1.62(−)	0.4(−)	−1.72(−)	0.5(−)	−1.15(−)	0.41(−)
Sit-to-stand - Pai [69]	−1.19(−)	0.9(−)	−2.24(−)	−0.064(−)	−1.074(−)	0.81(−)
Sit-to-stand - Roebroeck [70]	−0.62(0.14)	0.28(0.081)	−0.82(0.18)	0.052(0.024)	−0.53(0.19)	−0.011(0.039)
Stair ascent - Riener [71]	−0.64(−)	0.18(−)	−1.15(−)	0.25(−)	−1.27(−)	0.0025(−)
Stair descent - Riener [71]	0.0079(−)	0.45(−)	−1.46(−)	0.1(−)	−1.15(−)	0.012(−)
Stair ascent - Protopapadaki [72]	−0.69(0.12)	0.18(0.23)	−0.45(0.28)	0.55(0.22)	−1.35(0.25)	0.021(0.022)
Stair descent - Protopapadaki [72]	−0.37(0.078)	0.1(0.37)	−0.36(0.24)	0.4(0.2)	−1.26(0.31)	0.024(0.031)
Stair ascent - McFadyen [73]	−0.95(0.36)	0.2(0.2)	−1.37(0.12)	0.35(0.071)	−1.52(0.19)	0(0)
Stair descent - McFadyen [73]	−0.25(0.07)	0.39(0.07)	−1.58(0.2)	0.28(0.04)	−1.37(0.28)	−0.0071(0)
Chosen requirement [Nm]	−150 [66, 75]	100 [62]	−180 [69]	80 [72]	−190 [4, 75]	65 [69]

[§]Internal document based on external references

[†]Data average minus two standard deviations, or data average plus two standard deviations

C.1.3 Joint velocity data for various use cases

Table C.1-3

Minimum and maximum values of the joint velocities from various sources with the chosen minimum and maximum requirements.

Source	Hip average(SD) [°/s]		Knee average(SD) [°/s]		Ankle average(SD) [°/s]	
	Min (extension)	Max (flexion)	Min (extension)	Max (flexion)	Min (plantar flexion)	Max (dorsiflexion)
Wearable actuation biomechanics specifications [58][§] [59, 60, 61, 62]	−154(−)	80(−)	−246(−)	246(−)	−178(−)	105(−)
Symbitron WE1 [4]	–	–	−195(−)	195(−)	−132(−)	–
Symbitron WE2 [66]	–	132(−)	–	–	–	–
Gait - Winter [62]	−52(−)	100(−)	−232(−)	196(−)	−140(−)	93(−)
Gait - Bovi [67]	−75(−)	120(−)	−244(−)	201(−)	−187(−)	113(−)
Gait - van den Bogert [68]	−71(−)	137(−)	−287(−)	238(−)	−189(−)	97(−)
Sit-to-stand - Mak [63]	−157(−)	73(−)	−112(−)	2.9(−)	−18(−)	26(−)
Sit-to-stand - Pai [69]	−202(−)	84(−)	−173(−)	49(−)	−39(−)	20(−)
Sit-to-stand - Roebroeck [70]	−101(23)	44(26)	−84(18)	−2(4.3)	−26(23)	22(16)
Stair ascent - Riener [71]	−125(−)	181(−)	−163(−)	414(−)	−202(−)	157(−)
Stair descent - Riener [71]	−96(−)	88(−)	−315(−)	219(−)	−142(−)	271(−)
Stair ascent - Protopapadaki [72]	−108(−)	186(−)	−275(−)	468(−)	−163(−)	182(−)
Stair descent - Protopapadaki [72]	−66(−)	111(−)	−398(−)	360(−)	−190(−)	255(−)
Stair ascent - McFadyen [73]	−88(−)	133(−)	−140(−)	393(−)	−140(−)	150(−)
Stair descent - McFadyen [73]	−120(−)	120(−)	−368(−)	206(−)	−216(−)	332(−)
Chosen requirement [°/s]	−200 [69]	185 [72]	−400 [72]	470 [72]	−215 [73]	330 [73]

[§]Internal document based on external references

C.1.4 Joint power data for various use cases

Table C.1-4

Minimum and maximum values of the joint powers from various sources with the chosen minimum and maximum requirements as based on the weight of a 80 kg user. Note all values are averages unless otherwise indicated.

Source	Hip [W/kg]		Knee [W/kg]		Ankle [W/kg]	
	Min (extension)	Max (flexion)	Min (extension)	Max (flexion)	Min (plantar flexion)	Max (dorsiflexion)
Wearable actuation biomechanics specifications [58][§] [59, 60, 61, 62]	–	0.62	−1.03	–	–	2.05
Symbitron WE1 [4, 76]	–	–	–	2.79 [†]	–	3.57 [†]
Symbitron WE2 [66, 76]	–	1.97 [†]	–	–	–	–
Gait - Winter [62]	−0.15	0.43	−0.67	0.36	−0.33	2.17
Gait - Bovi [67]	−0.47	0.49	−0.52	0.19	−0.38	2.22
Gait - van den Bogert [68]	−0.07	0.5	−0.43	0.46	−0.54	4.54
Sit-to-stand - Mak [63]	−0.8	2.09	−0.22	2.36	−0.057	0.22
Sit-to-stand - Pai [69]	−0.28	3.04	−0.5	4.09	−0.16	0.52
Sit-to-stand - Roebroeck [70]	−0.042	0.81	−0.013	0.9	−0.12	0.19
Stair ascent - Riener [71]	−0.11	1.27	−0.3	3.07	−0.28	3.27
Stair descent - Riener [71]	−0.15	0.4	−5.14	0.019	−3.39	1.19
Stair ascent - Protopapadaki [72]	−0.11	1.25	−0.42	0.94	−0.27	2.77
Stair descent - Protopapadaki [72]	−0.32	0.18	−1.64	0.56	−4.36	2.35
Stair ascent - McFadyen [73]	−0.2	1.33	−0.7	2.46	−0.52	3.43
Stair descent - McFadyen [73]	−0.23	0.53	−5.15	0.84	−4.9	0.96
Chosen requirement [W]	−65 [63]	245 [69]	−410 [73]	330 [69]	−390 [73]	365 [68]

[§]Internal document based on external references

[†]Data average minus two standard deviations, or data average plus two standard deviations

Table C.1-5

Torque operating points corresponding to the powers in Table C.1-4 as based on the weight of a 80 kg user. Note all values are averages.

Source	Hip [Nm/kg]		Knee [Nm/kg]		Ankle [Nm/kg]	
	Min (extension)	Max (flexion)	Min (extension)	Max (flexion)	Min (plantar flexion)	Max (dorsiflexion)
Wearable actuation biomechanics specifications [58][§] [59, 60, 61, 62]	–	−0.27	−0.27	–	–	−1.2
Symbitron WE1 [4]	–	–	–	–	–	–
Symbitron WE2 [66]	–	–	–	–	–	–
Gait - Winter [62]	0.36	0.29	0.21	0.25	−0.47	−1.07
Gait - Bovi [67]	0.56	0.31	−0.18	−0.4	−0.98	−0.85
Gait - van den Bogert [68]	0.19	0.28	0.11	0.24	−1.29	−1.5
Sit-to-stand - Mak [63]	−1.04	−1.16	0.25	−1.6	−1.12	−0.91
Sit-to-stand - Pai [69]	−0.4	−0.93	−0.58	−1.65	−0.92	−0.8
Sit-to-stand - Roebroeck [70]	0.067	−0.57	0.039	−0.78	−0.38	−0.42
Stair ascent - Riener [71]	0.18	−0.62	0.16	−1.14	−0.52	−0.93
Stair descent - Riener [71]	0.18	0.37	−1.44	−0.024	−0.97	−0.75
Stair ascent - Protopapadaki [72]	0.18	−0.69	0.099	−0.44	−0.4	−1.12
Stair descent - Protopapadaki [72]	−0.29	−0.31	−0.36	0.4	−1.08	−0.85
Stair ascent - McFadyen [73]	−0.18	−0.95	0.32	−1.21	−0.53	−1.44
Stair descent - McFadyen [73]	0.22	0.37	−1.47	−1.04	−1.15	−0.61
Torque at chosen power requirement [Nm]	−85 [63]	−75 [69]	−120 [73]	−130 [69]	−90 [73]	−120 [68]

[§]Internal document based on external references

C.1.5 Anthropometric data

Table C.1-6

Ranges of anthropometric properties from Schneider *et al.* [77], derived where possible from a small-sized female adult sample. The minimum and maximum values are the average value less and plus one standard deviation respectively.

Property	Minimum value	Average value	Maximum value
Body mass (kg)	44.5	46.9	49.3
Hip width (m)	0.338	0.356	0.374
Femur joint center-center length (m)	0.363	0.381	0.399
Tibia length (m)	0.328	0.346	0.364
Waist circumference (m)	0.655	0.708	0.761
Max abdominal circumference (m)	0.704	0.754	0.804
Upper thigh circumference (m)	0.475	0.501	0.527
Mid thigh circumference (m)	0.403	0.427	0.451
Knee circumference (m)	0.323	0.339	0.355
Calf circumference (m)	0.301	0.315	0.329
Ankle circumference (m)	0.200	0.214	0.229

Table C.1-7

Ranges of anthropometric properties from Schneider *et al.* [77], derived where possible from a large-sized male adult sample. The minimum and maximum values are the average value less and plus one standard deviation respectively.

Property	Minimum value	Average value	Maximum value
Body mass (kg)	97.6	102.6	107.6
Hip width (m)	0.417	0.439	0.461
Femur joint center-center length (m)	0.446	0.466	0.486
Tibia length (m)	0.442	0.452	0.462
Waist circumference (m)	1.007	1.075	1.143
Max abdominal circumference (m)	1.018	1.082	1.146
Upper thigh circumference (m)	0.606	0.639	0.672
Mid thigh circumference (m)	0.524	0.559	0.594
Knee circumference (m)	0.421	0.434	0.447
Calf circumference (m)	0.387	0.406	0.425
Ankle circumference (m)	0.229	0.247	0.265

Table C.1-8

Ranges of anthropometric foot properties for adult male and female samples [78]. The minimum and maximum values are the average value less and plus one standard deviation respectively.

Gender	Property	Minimum value	Average value	Maximum value
Male	Foot length (m)	0.247	0.26	0.273
	Foot width (m)	0.084	0.094	0.104
	Shoe length (m)	0.274	0.287	0.301
	Shoe width (m)	0.095	0.106	0.116
Female	Foot length (m)	0.222	0.233	0.243
	Foot width (m)	0.081	0.082	0.084
	Shoe length (m)	0.237	0.250	0.263
	Shoe width (m)	0.081	0.092	0.103

C.2 HeRoS Project robotic suit requirements

The actuated degrees-of-freedom for the HeRoS flexible robotic suit are

- Ankle plantar flexion–dorsiflexion;
- Knee flexion–extension;
- Hip flexion–extension.

C.2.1 Angles, torques, velocities, and powers

Table C.2-1 lists the minimum and maximum values of the angles, torques, velocities, and powers for each of the actuated joints. These are based on the extremums of average data (or average +/- two standard deviations as indicated) for level ground gait (0.8 m/s), sit-to-stand, stair ascent, and stair descent of an 80 kg user (see maximum weight in Table C.2-2). The data extremums from the data sets from which they were extracted are detailed in Appendix B.1. The requirements are assumed to be sufficient for the use cases described in Section 3.4.

C.2.2 Effect of spasticity

The spasticity score of the exoskeleton user should be three or less on the Modified Ashworth Scale (MAS) [79, 80]. This will enable the exoskeleton to support normal walking at a speed of at least 0.1–0.2 m/s. Depending on the severity of spasticity the exoskeleton will be able to support other use cases such as sit-to-stand, stair ascent or descent, or slope ascent or descent, but this can only be assessed on a user-by-user basis. If, in these latter use cases, large torques are generated due to spasticity, the exoskeleton will be able to absorb these torques, but may need to slow down or stop, depending on the resistance caused by the spasticity.

These conclusions are drawn based on the research carried out in the Symbitron project [80] on the spasticity of complete and incomplete SCI patients with a maximum MAS of three. There it was found that torques and powers required to support 0.1–0.2 m/s gait were 1.0 Nm/kg and 0.4 W/kg at the hip and 0.65 Nm/kg and 0.65 Nm/kg at the knee (ankle data was not collected). These requirements are less than those in Table C.2-1 and hence at the very minimum, the exoskeleton can support slow gait (gait torque and power requirements increase with gait speed [81]).

Table C.2-1
Minimum and maximum values of the joint angles, torques, velocities, and powers.

Joint	Direction	Angle [°]	Torque [Nm]	Velocity [°/s]	Power [W]	Torque at power [Nm]
Ankle	Minimum (plantar flexion)	−50 [64, 74]	−190 [4, 75]†	−215 [73]	−390 [73]	−90 [73]
	Maximum (dorsiflexion)	30 [64, 74]	65 [69]	330 [73]	365 [68]	−120 [68]
Knee	Minimum (extension)	0 [64]	−180 [69]	−400 [72]	−410 [73]	−120 [73]
	Maximum (flexion)	115 [72]†	80 [72]†	470 [72]	330 [69]	−130 [69]
Hip	Minimum (extension)	−30 [62]†	−150 [66, 75]†	−200 [69]	−65 [63]	−85 [63]
	Maximum (flexion)	115 [70]†	100 [62]†	185 [72]	245 [69]	−75 [69]

†Data average minus two standard deviations, or data average plus two standard deviations

C.2.3 Anthropometrics

Table C.2-2 lists the ranges for the anthropometric properties of the intended users (minimum and maximum values are the average minus and plus one standard deviation).

Table C.2-2
Ranges of anthropometric properties, derived where possible from a mid-sized male adult sample. The minimum and maximum values are the average value less and plus one standard deviation respectively.

Property	Minimum value	Average value	Maximum value	Reference
Body mass (kg)	73.2	76.7	80.2	[77]
Pelvis height (m)	0.204	0.218	0.232	[82][§]
Pelvis width (m)	0.266	0.287	0.308	[82][§]
Hip width (m)	0.367	0.385	0.403	[77]
Femur joint center-center length (m)	0.429	0.447	0.465	[77]
Tibia length (m)	0.382	0.402	0.422	[77]
Waist circumference (m)	0.853	0.904	0.955	[77]
Max abdominal circumference (m)	0.860	0.913	0.966	[77]
Upper thigh circumference (m)	0.548	0.579	0.610	[77]
Mid thigh circumference (m)	0.474	0.504	0.534	[77]
Knee circumference (m)	0.378	0.392	0.406	[77]
Calf circumference (m)	0.357	0.373	0.389	[77]
Ankle circumference (m)	0.212	0.229	0.247	[77]
Foot length (m)	0.247	0.26	0.273	[78][†]
Foot width (m)	0.084	0.094	0.104	[78][†]

[§]Mixed adult male and female data (not specifically of a mid-sized sample)
[†]Adult male data (not specifically of a mid-sized sample)

APPENDIX D

The inverted Muscle Skeleton Approach

This chapter is based on the paper that was presented at the BioRob 2018 IEEE RAS/EMBS International Conference on Biomedical Robotics and Biomechatronics. It is published as:

[3] M. E. Grootens, E.E.G. Hekman, and H. V. D. Kooij, "The inverted Muscle Skeleton approach: moving beyond rigid exoskeletons," in *2018 7th IEEE International Conference on Biomedical Robotics and Biomechatronics (Biorob)*, 2018, pp. 659–664.

Abstract

Exoskeleton technology has improved significantly over the past decades, yet devices are still not user-friendly. Recently, so-called *exosuits*—soft wearable suits that assist walking—have been proposed, but their torques are limited.

In this paper we propose the *inverted Muscle Skeleton* (iMS) *approach*; this method allows for the design of wearable robotics that are less rigid and more lightweight than exoskeletons, but more powerful than exosuits.

We have applied our approach to the design of a low-power knee orthosis that assists knee extension. Evaluation of the prototype during one-legged squats shows that the device can successfully generate knee extension torques that reduce muscle activity in the knee extensor muscles.

The approach is promising and we believe that higher joint torques can be generated with more powerful actuators. Future work includes testing the device during walking and applying the method to the design of orthoses for other joints.

D.1 Introduction

Exoskeleton technology has advanced considerably over the past decades. Robotic gait trainers, such as the *Lokomat* [83] and *LOPES* [84], are increasingly being used in rehabilitation clinics and a number of lower extremity exoskeletons, such as the *ReWalk* [85], *Ekso GT* [86], and Indego Personal [87], is becoming available for home use.

However, despite the improvements that have been made, exoskeletons remain bulky and heavy—although it is known that adding mass to the legs increases the metabolic cost of walking [15]. Exoskeletons require considerable donning times and the alignment of their joints with those of their wearer is critical, since misalignment may cause discomfort or injury [20]. In brief, exoskeletons are not yet user-friendly.

Some exoskeletons, such as the BLEEX [88], serve to relieve their wearer from loads. Most exoskeletons however, are used to apply joint torques. For this type, the provision of an external *skeleton* is not a goal per se. Considering the shortcomings of current exoskeletons and the fact

that it is not *required* to use an exoskeleton to deliver joint torques, it is sensible to focus on more flexible solutions.

Over the past decade, various soft actuated orthoses have been developed for applications ranging from shoulder rehabilitation [89] to the treatment of gait pathologies [51], and more recently, so-called *exosuits* have been proposed: flexible robotic suits that are meant to assist human walking [45, 90]. These designs are created by following a *biomimetic* approach, in which artificial muscles act in parallel to the human muscles.

Current exosuits mainly focus on delivering assisting torques to the ankle and hip joints. Applications include assisting gait in healthy individuals [90, 91], improving gait in stroke survivors [49], and reducing the metabolic cost of walking [47]. However, exosuits cannot yet replace rigid exoskeletons, since the torques they generate are generally not larger than 40% of the torques required for human gait.

The joint torques delivered by exosuits are limited by their biomimetic design. Biological muscles exert large shear forces on the bones to which they are attached. Similar shear forces occur in exosuits, due to the artificial muscles. These shear forces act directly on the skin and underlying tissue of the wearer of the suit, which means that the maximum joint torques are limited by the maximum shear force that the wearer of an exosuit can support [19].

In this paper, we investigate a new approach: we show that by not mimicking, but *inverting* biology, we can avoid loading the human body with excessive shear forces. Therefore, our *inverted Muscle Skeleton* (iMS) *approach* has the potential to deliver joint torques as high as those delivered by exoskeletons. We believe that our design approach can help to find an alternative to rigid exoskeletons.

D.2 The inverted Muscle Skeleton approach

D.2.1 The iMS approach

In the human body, muscles generate tension forces between the bones of body segments in order to generate joint torques. Figure D.2-1(a) shows how the quadriceps muscles generate a knee extension torque and how the calf muscles generate an ankle plantar flexion torque. The muscle forces are almost collinear with the bones on which they pull and their moment arms are small. The required muscle forces are therefore very high and a large shear component (along the axes of the bones) loads the bones with high compression forces.

Exosuits based on a *biomimetic* design approach, such as those presented in [90] and [91], use muscle-like actuators that exert tension forces on the limbs of their wearer. Figure D.2-1(b) shows how a knee extension torque is generated by tensioning a cable between the proximal and distal leg segments and how an ankle plantar flexion torque is generated using a cable between the distal leg segment and the heel. Again, moment arms are small and the cables are almost collinear with the axes of the limbs. The cable forces need to be high in order to generate a significant joint torque, but this also means that the resulting shear forces will be high. Unfortunately, these high shear forces are acting on the body of the wearer and, although they can be routed to locations such as the hips, they will cause discomfort. Furthermore, the high compliance of human tissue makes it difficult to keep the orthosis in place, which causes power losses and a reduction in control bandwidth [19].

We propose the *iMS approach*. By using actuators that provide *compression*—rather than tension—forces, the direction of the shear forces is inverted. Figure D.2-1(c) shows how linear actuators provide a knee extension and an ankle plantar flexion torque. Fundamental to the approach is the use of a network of cables to interconnect both actuator anchor points. These cables are loaded with the undesired shear forces and must cross through the joint axis when they go from one body segment to the other. The shear forces carried by the cables can either cancel each other, for example at the knee joint, or they can be transformed to compression forces on other body parts, such as the hips or sole of the foot.

Note that the key difference between the iMS approach and a ‘pushing orthosis’, such as the RoboKnee [92], is that the shear forces are carried by straps, rather than by a rigid frame. This allows for higher torques compared to exosuits, and a smaller size and mass compared to exoskeletons.

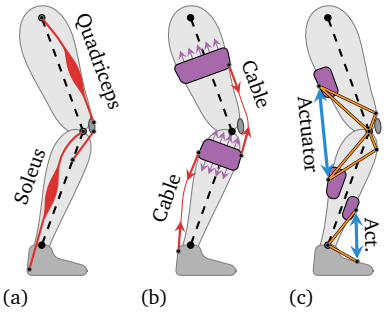

Figure D.2-1
Knee extension and ankle plantar flexion using (a) the human musculoskeletal system, (b) a biomimetic exosuit, and (c) the iMS approach.

D.2.2 Knee extension using the iMS approach

We consider the knee orthosis that is shown in Figure D.2-1(c). The concept comprises a linear actuator, hinged to shells, interconnected by a network of straps. The network is symmetrical about the sagittal plane; it crosses over the leg, just above and below the patella. The actuator delivers a pushing force, so the orthosis generates an extension torque.

The parameters h [m], d [m] and h_a [m] that define the dimensions of the orthosis are shown in Figure D.2-2(a). We assume the configuration to be symmetrical about the bisector of $\angle HKA$. This means that the orthosis only exerts compression forces on the leg segments, since the shear components are carried by the cables and cancelled at the knee joint.

The actuator force F_a [N], as shown in Figure D.2-2(c), needed for a knee torque $T \leq 0$ Nm at knee angle ϑ [°] (full knee extension corresponds with $\vartheta = 0°$ and the flexion direction is taken positive) is computed as

$$F_a(\vartheta, T) = -\frac{T}{d\cos(\vartheta/2) + h\sin(\vartheta/2)}.$$

Figure D.2-2(c) shows the compression forces f_c [m] that act on the leg both posteriorly (at the shells) and anteriorly (above and below the patella). They are equal and can be found as

$$f_c(T) = -\frac{T}{h - h_a}.$$

Pain Pressure Threshold (PPT) data (e.g. [22]) can be used to determine the surface area required to distribute the forces.

Note Due to a difference in thickness of the proximal and distal leg segments and due to deformation of the soft tissue underlying the shells and anterior pads, it is not realistic to assume

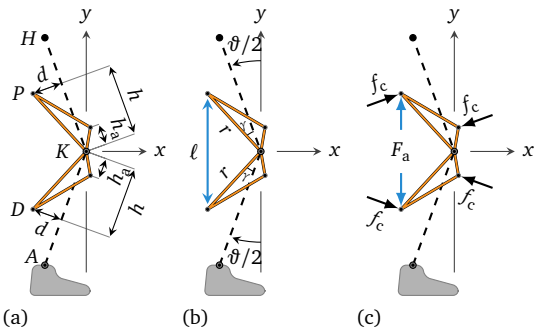

Figure D.2-2
Conceptual configuration for the knee orthosis: (a) anchor positions, (b) derived dimensions, (c) actuator and compression forces F_a and f_c.

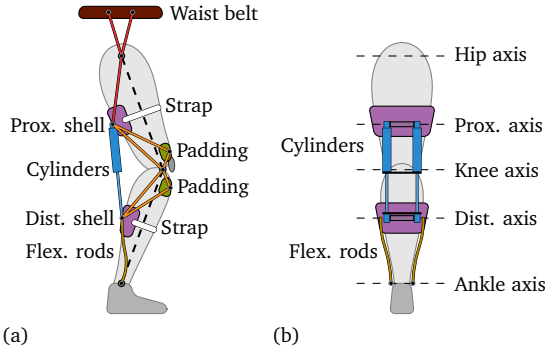

Figure D.3-1
Prototype schematic overview: (a) lateral view, (b) posterior view.

that all shear forces fully cancel. However, it is reasonable to assume that the major parts of the shear forces cancel out, so that only residual shear forces need to be transferred to the body. This can be done by connecting the proximal actuator hinge via a cable to a waist belt and the distal hinge via a cable to the shoe.

D.3 Prototype design

A low-power prototype, based on the concept from Section D.2.2, was constructed. It uses pneumatic cylinders, 3D-printed shells, and a network of straps. This section describes the mechanical design, actuation, and control.

All stock components, such as cylinders, valves, and sensors, are listed in Table D.3-1.

D.3.1 Mechanical design

A detailed design is shown in Figure D.3-1. Two parallel pneumatic cylinders are used in order to increase the total actuator force and to avoid bending moments in the cylinder rods. Some components have been added, in order to keep the device in place and aid donning. Firstly, straps around the leg segments are added to keep the shells in contact with the leg. Secondly, a waist belt is added, from which the mass of the upper part of the prototype is suspended. Finally, thin flexible rods with heim joints at their ends, are hinged to both sides of the shoe. The axes of the hinges are aligned with the ankle joint and the rods support the mass of the lower part of the prototype. The flexibility of the rods and the heim joints allow for unconstrained ankle movement.

Table D.3-1
Pneumatic, sensor, and control components.

Description	Type
Festo	
Cylinders 20/150 mm (2×)	DSNU-20-150-P-A-S11
Prop. dir. 5/3-way valve	MPYE-5-1/8-LF-010-B
Solenoid valve	VUVS-L20-M32C-MD-G18-F7-1C1
Plastic tubing	PUN-8X1,25-SW
Push-in fittings	QS-G1/4-8, QSL-G1/8-8, and similar
Linear Hall sensor	SDAT-MHS-M160-1L-SA-E-0.3-M8
Pressure sensors (3×)	SPTE-P10R-S6-B-2.5K
Other	
Load cells (2×)	Strain Measurement Devices S402
DAQ card	National Instruments PCI-6229
Real-time DAQ/control	MATLAB/Simulink Real-Time

Two cylinders with a 20 mm piston diameter, 8 mm rod diameter and 150 mm stroke are used. Each cylinder can generate a compression force of up to 235 N at the available absolute supply pressure of 8.5 bar. The choice for pneumatic cylinders was made based on their ease of use and off-the-shelf availability. Although their need for a pressurized air supply makes them less suitable for untethered applications, they are suitable to demonstrate the principle.

The shells that are used to distribute the actuator force at the back of the leg are made from Polyamide using an SLS 3D-printing machine. Hardened steel axles pass through the shells, just behind the leg, and make up the rotation axes for the cylinders. The flexible part of the orthosis comprises 20 mm nylon straps, Velcro strips, elastic bands and padding. Boa dials and laces are used to adjust and tighten the orthosis. All strap lengths can be adjusted using dials placed at the back of the shells and on the anterior padding.

Figure D.3-2 shows the final prototype, which has a mass of 1.5 kg (excluding shoes and external pneumatic components). The cylinders are spaced 120 mm apart and their hinges are placed at $h = 0.215$ m above and below the knee and at approximately $d = 0.090$ m behind the axes of the leg segments. The cylinders have a moment arm of 90 mm about the knee joint when the knee is stretched; an extension torque of up to -42 Nm can then be delivered. The prototype allows for knee flexion up to 62°, which is sufficient for walking.

D.3.2 Actuation

Figure D.3-3 shows an overview of the pneumatic system.

A 50 L tank is used as pressure supply for the cylinders; a compressor maintains the pressure between 8.5 and 10 bar. A solenoid 3/2-way valve is used to connect and disconnect the prototype to and from the air supply; the prototype is disconnected from the pressure supply and exhausted to the atmosphere when any of the emergency buttons is pressed.

A proportional directional 5/3-way control valve is used to control the air flow to and from the cylinder. It controls both the flow *rate* and the *direction*: it either connects the extension chamber to the supply and the retraction chamber to the atmosphere, or the other way around.

All pneumatic tubing has an inner diameter of 5.7 mm and push-in fittings are used to interconnect all components.

D.3.3 Sensing

Two load cells, positioned inline with the pneumatic cylinders, are used to measure the total actuator force $F_a = f_1 + f_2$ [N]. A linear Hall sensor is used to measure the piston position ε [m] at one of the cylinders. Two pressure sensors measure the pressure in the cylinder chambers and a third sensor measures the available supply pressure just before the control valve. All sensors are shown in Figure D.3-3.

The piston position ε is taken as zero when the piston is fully retracted and extension is considered positive. The knee angle ϑ can be estimated based on ε and the dimensions of the prototype (

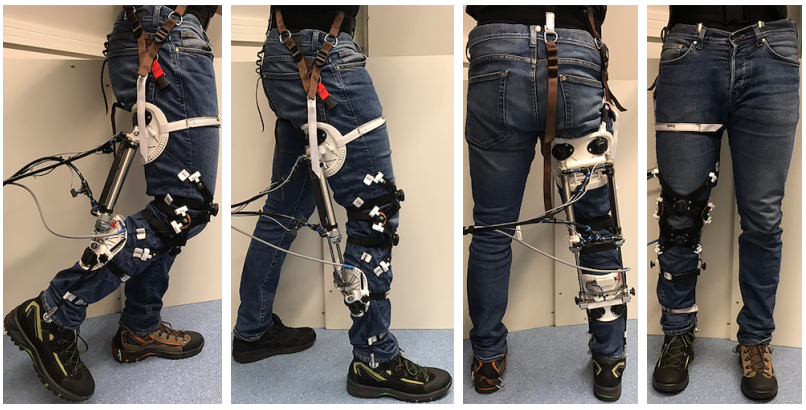

Figure D.3-2
Prototype realization.

denotes the estimate of •):

$$\hat{\vartheta}(\varepsilon) = 180° - 2\gamma - 2\arcsin((\ell_0 + \varepsilon)/(2r)),$$

where $\gamma := \arctan(d/h)$ [°] and $r := \sqrt{d^2 + h^2}$ [m], as shown in Figure D.2-2(b). Finally $\ell_0 := 2h - \varepsilon_{\max}$ [m] is the minimum distance between the proximal and distal actuator hinges; $\varepsilon_{\max} = 0.150$ m is the cylinder stroke.
The actuator moment arm R [m] about the knee joint can be estimated by

$$\hat{R}(\varepsilon) = \sqrt{r^2 - 1/4(\ell_0 + \varepsilon)^2}$$

and the delivered joint torque T [Nm] can be estimated by

$$\hat{T}(\varepsilon, F_a) = -\hat{R}(\varepsilon)F_a.$$

Note that a *positive* actuator force results in a *negative* knee torque—an extension torque.

D.3.4 Control

The compressibility of air and the highly nonlinear behavior of air flow through pneumatic systems make position and force control of pneumatic cylinders difficult [93]. The nonlinear behavior of cylinders actuated by proportional control valves is modeled in [93] and a sliding mode force control strategy for such systems is presented in [94]. This strategy is adopted and uses all sensor data to control the cylinder force. The closed-loop system has both a reference force F_r [N] and a reference force rate of change $\dot{F}_r$ [N/s] as inputs. The friction of the cylinders is overcome by using the force measurements from the load cells instead of an estimate based on the chamber pressures.

Section D.3.3 presented estimates of the knee angle and actuator moment arm based on the cylinder position. The desired actuator force can be computed based on a desired knee torque and these estimates.

Data acquisition and control are implemented using Matlab/Simulink R2016B. A target PC running Simulink Real-Time is equipped with two National Instruments 6229 PCI data acquisition cards to interface with the hardware.

D.4 Prototype evaluation

Testing the device during walking, for which it is intended, would require a gait assistance strategy, the effectiveness of which would greatly influence the results. We therefore decided to use one-legged squats as a *device test*, as we expected to see a reduction in extensor muscle activity if the device is effective in providing an assistive extension torque.

D.4.1 Method

Two healthy subjects performed multiple series of one-legged squats with the device worn on their right leg. A 0.5 Hz metronome was used to regulate the timing of the squats.

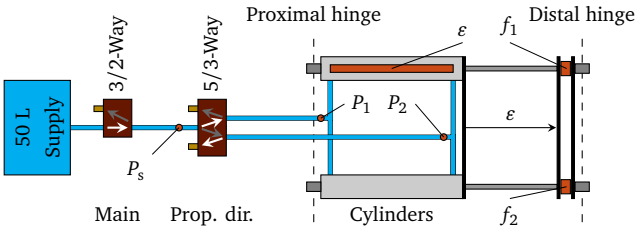

Figure D.3-3
Schematic overview of the pneumatic system with sensors (orange), valves (maroon), cylinders (grey), tubing (cyan), and exhausts (yellow).

The subjects were instructed to keep their knee behind their toes; to move as smoothly as possible; to reverse the direction of motion at the beat of the metronome; and to use the hand rails only for balance. They were given a couple of minutes to practice and were asked to perform the squats over the full range-of-motion of the device.

A virtual prestressed compression spring was implemented on the prototype. The reference force and reference force rate of change that were given as inputs to the controlled orthosis are computed as follows:

$$F_{\mathrm{r}}(\varepsilon) = f_{\mathrm{pre}} + \varphi k_{\mathrm{s}}(\varepsilon_{\max} - \varepsilon),$$
$$\dot{F}_{\mathrm{r}}(\dot{\varepsilon}) = -\varphi k_{\mathrm{s}}\dot{\varepsilon},$$

where f_{pre} [N] is the prestress of the virtual spring. (This prestress was set to 10 N, so that the cylinders always provide a small force to compensate for the mass of the upper part of the prototype.) The virtual spring stiffness k_{s} [N/m] is subject specific and based on the body mass of the subject: $k_{\mathrm{s}} = \xi m_{\mathrm{subject}}$. A value of $\xi = 32$ N/m/kg was chosen to ensure that we never require more force from the actuator than can be delivered (considering the minimum available supply pressure and maximum expected body mass). Finally, the gain φ determines the amount of assistance being given.

The subjects performed squats at three levels of assistance—in randomized order and with a two-minute rest interval. The levels are: minimal impedance ($\varphi = 0$); 50% assistance ($\varphi = 0.5$); and 100% assistance ($\varphi = 1$). The subjects performed approximately 20 squats at each level.

A Delsys Trigno wireless EMG system was used to measure the muscle activity of the three knee extensor muscles of the right leg: the Rectus Femoris, Vastus Medialis, and Vastus Lateralis. All data was captured at 1000 Hz.

Ethical approval was granted by the institutional review board and the participants gave written informed consent.

D.4.2 Data processing

The EMG data was processed using the following three steps: (1) 2nd order Butterworth high-pass filter with a cut-off frequency at 10 Hz; (2) absolute value; (3) 2nd order Butterworth low-pass filter with a cut-off frequency at 1 Hz.

Figure D.4-1 shows the cylinder position and both the reference force F_{r} and actual force F_{a} for subject 1 performing squats at assistance level $\varphi = 1$. (Note that $\varepsilon = 0$ m corresponds to $\vartheta \approx 62°$ and $\varepsilon = 0.150$ m to $\vartheta = 0°$. The scaling is almost linear.) We clearly see that the first couple of squats are not deep enough, because the subject is still getting used to the high level of assistance. There is also quite some variation in the motion profiles of the individual squats.

We can furthermore see that the actuator force F_{a} nicely tracked the reference force F_{r}, but that the subject hit the cylinder end stop at $\varepsilon = 0$ m and 'sat' on it, thereby causing the peaks in F_{a}. The subject never fully stretched their leg.

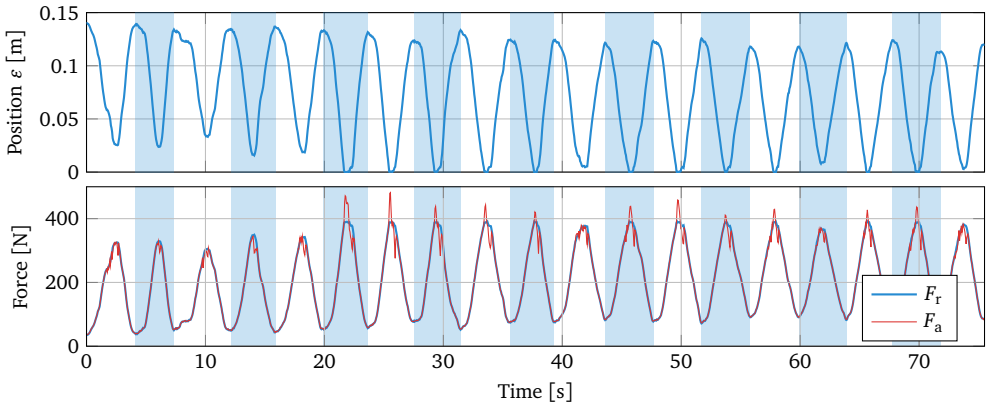

Figure D.4-1

Motion for subject 1 at the maximum assistance level of $\varphi = 1$: the top graph shows the cylinder position ε; the bottom graph shows the reference force F_{r} and actuator force F_{a}. The peaks in F_{a} show that the subject was 'sitting' on the end stop at $\varepsilon = 0$ m.

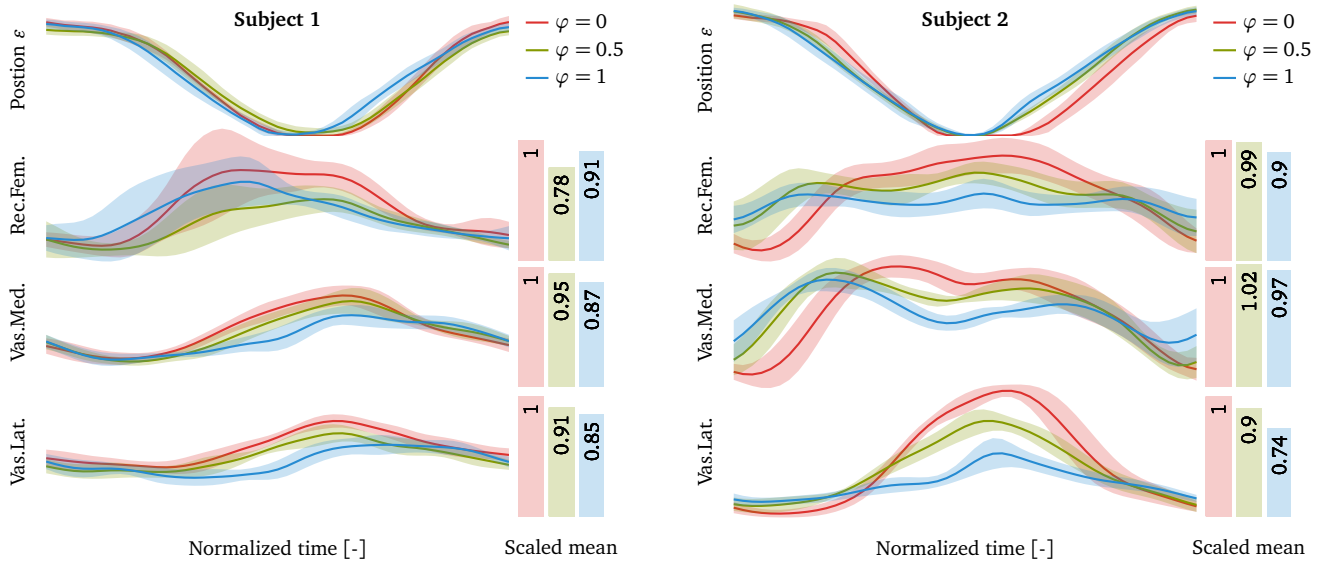

Figure D.4-2

Average data for 10 squats at $\varphi = 0, 0.5, 1$ for both subjects. The top graph for each subject shows the cylinder motion and the following graphs show the extensor muscle activity. The thick lines denote the mean value and the shaded areas indicate the standard deviation. The bar graphs on the right show the mean value of the signals, scaled with the mean value of the $\varphi = 0$ condition.

All the time series data was cut into separate blocks for each squat motion (identified by the tops in the time series of ε and indicated in Figure D.4-1 by the shaded areas) and then resampled to a dimensionless time $t \in [0, 1]$, to compensate for small differences in the timing of the squats.

For each assistance level, a combination of the 10 most similar (that is the combination with the lowest standard deviation) squat motions were selected from the squats that were recorded. In this way, the squats during which the subject was still getting used to the level of assistance, or lost balance, were discarded.

D.4.3 Results

Figure D.4-2 shows the mean and standard deviation of the cylinder motion and EMG activity of both subjects, based on 10 squats at each assistance level.

We can clearly see, in particular for subject 2, that the motion profile for $\varphi = 0$ (no assistance) differs from the other two conditions. The subject is really 'sitting' on the end stop at $\varepsilon = 0$ m and the motion upwards is slightly delayed. This sitting on the end stop means that the subject is temporarily *relieving* their extensor muscles, so that the measured EMG activity is probably lower than it would have been without the device—this has no positive influence on our results.

The figures furthermore show that all three extensor muscles are relieved by the assistance given by the device. The EMG activity at half the normalized time, the moment at which the extensor muscles must deliver the highest force, is lower at $\varphi = 0.5$ and even lower at $\varphi = 1$.

The figure also shows bar graphs for the mean value of the muscle activity (that is the mean value of the mean muscle activity over 10 squats). The values are normalized with the mean value of the $\varphi = 0$ (no assistance) condition, so that the relative muscle activity can be inspected.

We see that giving assistance induces a decrease in muscle activity. The exception being the Vastus Medialis of subject 2, which shows 2% more activity at $\varphi = 0.5$ than at $\varphi = 0$. In general we also see that the muscle activity decreases with increasing assistive torque. The exception is the Rectus Femoris for subject 1, which shows more activity at $\varphi = 1$ than at $\varphi = 0.5$. The exceptions may be due to the subject still getting used to the assistance or due to the one-legged squats being a rather difficult task (w.r.t. balance and effort).

D.5 Discussion

We have used our iMS approach for the design of an actuated knee orthosis and have shown that the prototype can successfully apply assistive torques. We believe that it is possible to generate higher torques with stronger actuators.

D.5.1 EMG reduction

We implemented a virtual spring on the prototype to provide an assistive torque. The reduction in muscle activity due to the given assistance is evident and shows that the device can successfully deliver a knee extension torque. However, the assistance strategy is very simple and a more intelligent strategy, for instance based on inverse dynamics or EMG measurements, is likely to be more effective.

D.5.2 Challenges of the iMS approach

The prototype stays in place during squats, though keeping it in place during walking is not straightforward. Hip adduction-abduction and endorotation–exorotation vary the tension in the straps to the hip belt, so that the prototype slightly rotates about, and slides down along, the leg. It needs to be regularly adjusted and further design improvements are needed to keep the device in place.

D.5.3 Application of the iMS approach to other joints

Application of the iMS approach to the design of an orthosis for ankle plantar flexion, as is shown schematically in Figure D.2-1(c), is a logical next application of the approach. The design of an orthosis for ankle dorsiflexion also seems feasible, for example by using an actuator between a shell behind the lower leg and the shoe, just behind the heel.

The approach may also be applied to joints of the upper extremities; one can think of elbow extension, or finger extension in an orthosis for rehabilitation of patients with finger contractures.

D.5.4 Limitations of the iMS approach

However, the iMS approach cannot be applied to all joints. For instance, it is not possible to generate knee flexion torques, as it is not feasible to place linear actuators anterior to the leg and keep them in place using only straps.

Furthermore, application to the hip joint seems infeasible due to the large range of flexion–extension motion and the soft tissue around the stomach onto which compression forces cannot comfortably be exerted.

D.5.5 Hybrid designs

Combining designs based on the iMS principle and biomimetic designs may be an interesting solution to overcome some of the limitations of the iMS approach. Considering the knee for instance, the addition of a hip belt and connections to the ankle (as already present in the prototype) allows for the actuators to also deliver a *tension* force. This means that the same device can also generate a knee flexion torque, which could be used to provide assistance during the swing phase of gait.

D.5.6 Comparison to exoskeletons and exosuits

If we compare designs based on the iMS approach to those based on exoskeleton technology, then the former can become less bulky, more lightweight, less constraining and less conspicuous than the latter. However, exoskeletons still can be more powerful than designs based on the iMS approach, because their torques are not necessarily dependent on user comfort and because they can transfer loads directly to the ground.

Compared to exosuits, designs based on the iMS approach do contain some rigid components (actuators and shells), but in turn exert no shear forces on their wearer. The iMS approach thus allows for the design of actuated orthoses that can provide higher joint torques than exosuits, yet are less rigid and constraining than exoskeletons.

D.6 Conclusions and future work

We have proposed the new iMS approach; it may be taken during the design of flexible wearable robotics that can deliver higher joint torques than biomimetic alternatives.

We have successfully applied the principle to the design of an actuated knee orthosis and evaluation during one-legged squats shows that the prototype can deliver assistive knee extension torques that induce a reduction of knee extensor muscle activity in the wearer of the device.

Future updates to the design include increasing the range-of-motion and joint torque that can be delivered. Furthermore, user comfort and ease-of-use can be improved and size and weight can be optimized. Future experiments include testing the device during walking and characterization of the forces that act on the wearer of the device.

APPENDIX E

Modeling and Analysis

This appendix contains various models and analyses. Section 5.3.1 presents a 2-DoF model of the behavior of the human ankle joint. Four actuator configurations for the iMS prototypes are discussed in Section E.2 and they are analyzed in Section E.3.

E.1 Modeling 2-DoF motion of the ankle

The biomechanics of the ankle are discussed in Section 2.3 and the orientation of the the plantar flexion–dorsiflexion and inversion–eversion axis are shown again in Figure E.1-1 (originally shown in Figures 2.3-1 and 2.3-2). Note that these orientations are mean values obtained from 46 cadavers and that they are measured for a straight ankle. A large variation between individuals was found, as is indicated by the shaded areas.

For analysis purposes, we need to model the movement of the ankle. However, it is unknown what happens with the orientation of both axes while the ankle moves. Doing measurements is beyond the scope of this project and the variation between individuals would result in subject-specific models.

Therefore, a simple model is proposed, in which the orientation of the foot with respect to the lower leg is a function of two angles: ϑ_{df} and ϑ_{iv}, which denote a plantar flexion–dorsiflexion and an inversion–eversion angle respectively. Note that the 'zero configuration' (with $\vartheta_{\text{df}} = \vartheta_{\text{iv}} = 0$) is a straight ankle and that dorsiflexion and inversion are the positive directions. We consider the right foot.

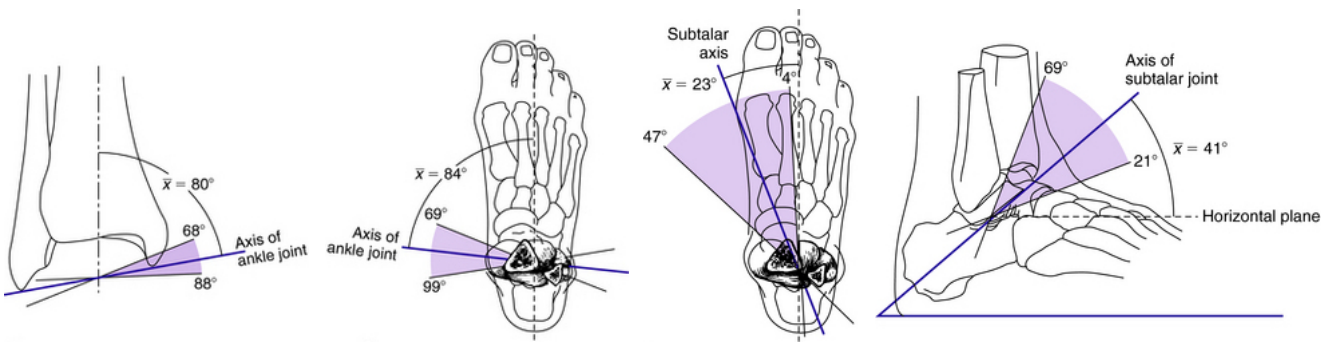

(a) (Source: [7]) (b) (Source: [7]) (c) (Source: [7]) (d) (Source: [7])

Figure E.1-1
Orientation of the axes of the ankle: (a) and (b) plantar flexion–dorsiflexion axis; and (c) and (d) inversion–eversion axis.

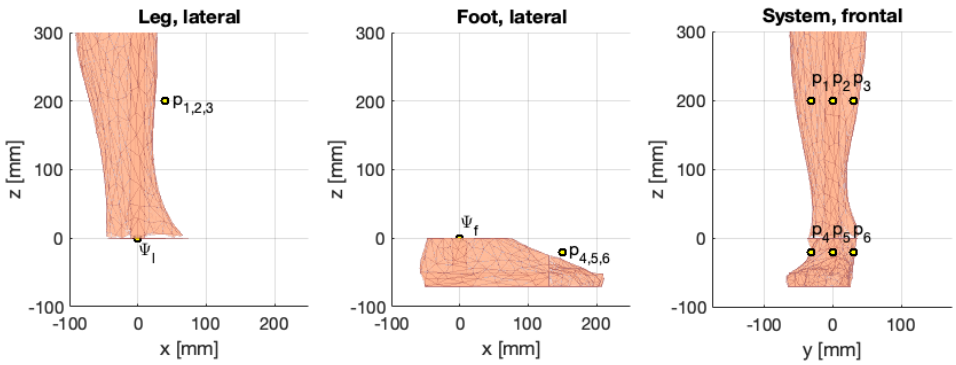

Figure E.1-2
Definition of coordinate systems and points at the leg and foot. The left and middle figure provide a lateral view on the leg and foot respectively and the right figure shows a frontal view on both body parts in the reference configuration.

E.1.1 Coordinate systems and anchor points

See Figure E.1-2. We define three coordinate systems: a reference frame Ψ_0 which is indicated by the figure axes; a frame Ψ_l at the leg; and a frame Ψ_f at the foot. The geometry of the body parts is obtained from a 3D scan of the leg of one of the team members of the HeRoS Project. The coordinate frames are chosen so that in the reference configuration all three frames share the same origin and have the same orientation.

Furthermore, we define three points, p_1, p_2, and p_3, rigidly attached to the leg segment. To the foot we also attach three points: p_4, p_5, and p_6. The rigid attachment ensures that points 1, 2 and 3 are constant in Ψ_l and the points 4, 5 and 6 are constant in Ψ_f, that is: $\dot{p}_i^\mathrm{l} = 0$ for $i = 1, 2, 3$ and $\dot{p}_i^\mathrm{f} = 0$ for $i = 4, 5, 6$.

We need to model motion of the ankle and we can either look at the orientation of the foot with respect to the leg, or the other way around. We choose this first option, which means that we assume that Ψ_l remains fixed in Ψ_0; the homogeneous transformation matrix from Ψ_l to Ψ_0 then is:

$$H_\mathrm{l}^0 = \begin{bmatrix} I_3 & 0 \\ 0 & 1 \end{bmatrix} = I_4.$$

Furthermore, we assume that the origin of Ψ_f remains fixed in the origin of $\Psi_0 = \Psi$, but we allow the *orientation* of the foot to change. We have thus created a hinge:

$$H_\mathrm{f}^0 = \begin{bmatrix} R_\mathrm{f}^0 & 0 \\ 0 & 1 \end{bmatrix}$$

Note that the rotation matrix R_f^0 describes the behavior of the ankle as a joint and that it is yet to be determined. Furthermore, looking at both H_l^0 and H_f^0, we can conclude that the only variable that is of interest, is the rotation matrix R_f^0.

E.1.2 Axes and angles

We wish to define behavior of the ankle based on the biological plantar flexion–dorsiflexion and inversion–eversion axes. We therefore need to define the vectors that indicate the orientation of the axes; this can easily be done based on Figure E.1-1:

$$\omega'_\mathrm{df} := \begin{bmatrix} -\tan 6^\circ \\ -1 \\ \tan 10^\circ \end{bmatrix} \quad \text{and} \quad \omega'_\mathrm{iv} := \begin{bmatrix} 1 \\ \tan 23^\circ \\ \tan 41^\circ \end{bmatrix}.$$

The first vector ω'_df indicates the direction of the plantar flexion–dorsiflexion axis, so that dorsiflexion is the positive direction. The second vector ω'_iv indicates the direction of the inversion–eversion axis, so that inversion is the positive direction. We use ϑ_df to denote a dorsiflexion rotation about ω_df and ϑ_iv to denote an inversion rotation about ω_iv.

Note that both vectors have arbitrary length and need to be normalized for use in the remainder of the analysis. We define the following unit vectors:

$$\omega_{\text{df}} := \frac{\omega'_{\text{df}}}{\left\|\omega'_{\text{df}}\right\|}, \qquad \omega_{\text{iv}} := \frac{\omega'_{\text{iv}}}{\left\|\omega'_{\text{iv}}\right\|}, \quad \text{and} \quad \omega_{\text{l}} := \begin{bmatrix} 0 \\ 0 \\ 1 \end{bmatrix}.$$

The vector ω_{l} is the unit vector pointing upwards through the axis of the leg segment. As the lower leg interface was found to rotate around the leg, this ω_{l} must also indicate an axis of rotation—albeit an undesirable one.

E.1.3 Rotation about an axis

For a unit vector ω, $\|\omega\| = 1$, the rotation matrix for rotation by an angle ϑ about this vector can be found using Rodriques' formula:

$$R(\omega, \vartheta) = I + \tilde{\omega} \sin\vartheta + \tilde{\omega}^2(1 - \cos\vartheta). \tag{E.1-1}$$

Here $\tilde{\omega}$ is the skew symmetric matrix of the vector ω. The tilde operator is defined as

$$\tilde{v} = \begin{bmatrix} 0 & -v_3 & v_2 \\ v_3 & 0 & -v_1 \\ -v_2 & v_1 & 0 \end{bmatrix} \quad \text{so that} \quad v = -v^\top \quad \text{and} \quad v \wedge w = \tilde{v}w,$$

where $\wedge$ denotes the vector cross product.

E.1.4 Ankle model—Description

The most important degree-of-freedom of the ankle, with the largest range-of-motion, is plantar flexion–dorsiflexion. The range-of-motion for inversion–eversion is rather small in comparison and it is unknown what happens to the orientation of the inversion–eversion axis when the ankle makes a plantar flexion–dorsiflexion motion. However, it is unlikely that it is constant for large angles, so we make an assumption regarding its motion.

The simple model, which describes the orientation of the foot with respect to the leg for a given set of angles $(\vartheta_{\text{df}}, \vartheta_{\text{iv}})$, is defined as follows.

1. We assume that the foot first makes a rotation ϑ_{df} around ω_{df}.
2. We assume that the orientation of ω_{iv} is not constant, but that it is rotated about ω_{df} over *half* the dorsiflexion angle, that is $\vartheta_{\text{df}}/2$. A new and *rotated* inversion–eversion axis $\hat{\omega}_{\text{iv}}$ is obtained.
3. Finally, the foot rotates by an angle ϑ_{iv} about $\hat{\omega}_{\text{iv}}$.

The new orientation of the foot thus is a combination of two subsequent rotations: first about ω_{df} and then about $\hat{\omega}_{\text{iv}}$, where the orientation of $\hat{\omega}_{\text{iv}}$ depends on ϑ_{df}.

E.1.5 Ankle model—Mathematically

Ultimately, we need to capture the described ankle behavior in a single rotation matrix $R_{\text{f}}^0(\vartheta_{\text{df}}, \vartheta_{\text{iv}})$. First, we define the rotation matrix for the dorsiflexion rotation:

$$R_{\text{df}}(\vartheta_{\text{df}}) := R(\omega_{\text{df}}, \vartheta_{\text{df}}),$$

where $R(\omega, \vartheta)$ is given by Equation (E.1-1). We can use this rotation matrix to find the orientation of $\hat{\omega}_{\text{iv}}$:

$$\hat{\omega}_{\text{iv}}(\vartheta_{\text{df}}) := R_{\text{df}}(\vartheta_{\text{df}}/2)\omega_{\text{iv}}.$$

The matrix for an iv rotation about this new axis is defined as

$$R_{\text{iv}}(\vartheta_{\text{df}}, \vartheta_{\text{iv}}) := R(\hat{\omega}_{\text{iv}}(\vartheta_{\text{df}}), \vartheta_{\text{iv}}).$$

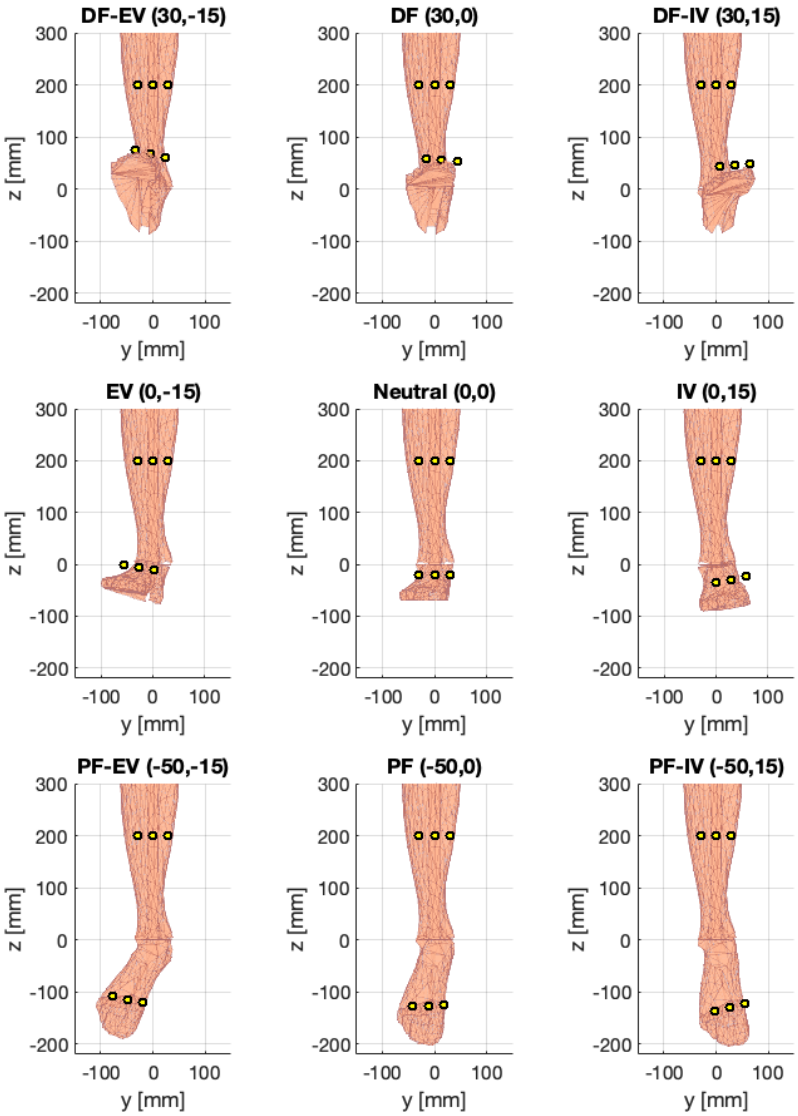

Figure E.1-3

Motion of the foot in the ankle model. The zero configuration is shown in the center. From left to right: eversion to inversion. Bottom to top: plantar flexion to dorsiflexion. The following abbreviations are used in the titles. DF: dorsiflexion; PF: plantar flexion; IV: inversion; EV: eversion.

Finally, the rotation matrix that describes the motion of the ankle can be found using the chain rule:

$$R_{\mathrm{f}}^{0}(\vartheta_{\mathrm{df}},\vartheta_{\mathrm{iv}}) := R_{\mathrm{iv}}(\vartheta_{\mathrm{df}},\vartheta_{\mathrm{iv}})R_{\mathrm{df}}(\vartheta_{\mathrm{df}}).$$

Points that are fixed to the foot and defined in Ψ_{f}, can be transformed to Ψ_0 using this rotation matrix R_{f}^{0}:

$$p^0 = R_{\mathrm{f}}^{0}(\vartheta_{\mathrm{df}},\vartheta_{\mathrm{iv}})p^{\mathrm{f}}.$$

This holds for the points p_i with $i = 4,5,6$, but also for the coordinates that define the 3D geometry of the leg.

A realistic range-of-motion for ϑ_{iv} is $[-50,30]^\circ$ and for ϑ_{iv} it is $[-15,15]^\circ$. We evaluate the orientation of the foot (and the points p_i) for all possible combinations of $\vartheta_{\mathrm{df}} \in \{-50,0,40\}^\circ$ and $\vartheta_{\mathrm{iv}} \in \{-15,0,15\}^\circ$, so that a grid of nine configurations is obtained. This grid is shown in Figure E.1-3 and these nine configurations will be used in the further analysis.

E.2 iMS actuator configuration concepts

Section 5.2.5 describes how the lower leg interfaces of the prototypes rotate around the lower leg—that is about axis ω_{l}—as soon as the cylinders are pressurized. The phenomenon needs to be investigated and a solution needs to be found to prevent this.

All prototypes that were tested use two parallel pneumatic cylinders (see Figure 5.2-2). However, it might be that choosing a different actuator configuration is a solution to the issue. Therefore, the four different actuator concepts shown in Figure E.2-1 are investigated. They are: Single (S), Double (D), V-shape (V) and A-shape (A).

The actuator concepts make use of the anchor points p_i with $i = 1,\ldots,6$ that we previously connected to the leg and foot. A connection matrix is used to define the actuator layout of an actuator concept with n actuators:

$$C = \begin{bmatrix} i_1 & j_1 \\ \vdots & \vdots \\ i_n & j_n \end{bmatrix} \quad \text{with} \quad i_k \in \{1,2,3\} \quad \text{and} \quad j_k \in \{4,5,6\}.$$

The four connection matrices defining the concepts are:

$$C_{\mathrm{S}} := \begin{bmatrix} 2 & 5 \end{bmatrix}, \quad C_{\mathrm{df}} := \begin{bmatrix} 1 & 4 \\ 3 & 6 \end{bmatrix}, \quad C_{\mathrm{V}} := \begin{bmatrix} 1 & 5 \\ 3 & 5 \end{bmatrix}, \quad \text{and} \quad C_{\mathrm{A}} := \begin{bmatrix} 2 & 4 \\ 2 & 6 \end{bmatrix}.$$

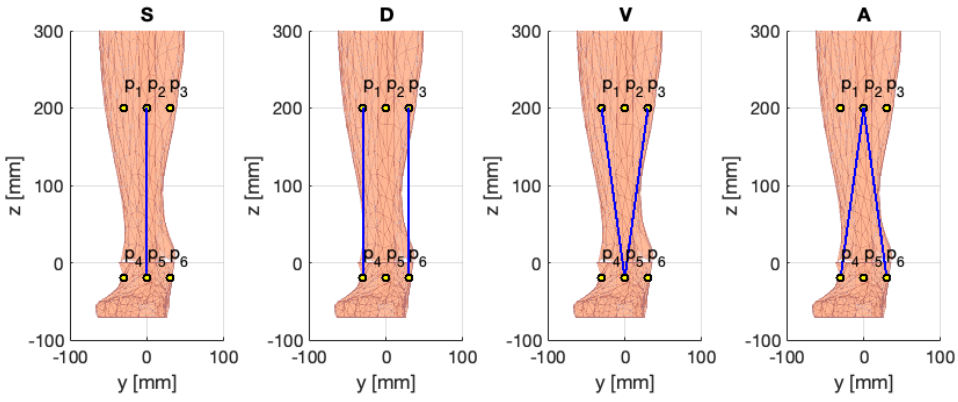

Figure E.2-1
Frontal view of four actuator concepts; the position of the linear actuators are indicated by the blue lines. From left to right: Single actuator (S); Double actuator (D); V-shape (V); and A-shape (A).

To allow for easy numerical evaluation, the following realistic locations (all units are [mm]) were chosen for the actuator anchor points:

$$p_1^{\mathrm{l}} = \begin{bmatrix} 40 \\ -30 \\ 200 \end{bmatrix} \quad p_2^{\mathrm{l}} = \begin{bmatrix} 40 \\ 0 \\ 200 \end{bmatrix} \quad p_3^{\mathrm{l}} = \begin{bmatrix} 40 \\ 30 \\ 200 \end{bmatrix} \quad p_4^{\mathrm{f}} = \begin{bmatrix} 150 \\ -30 \\ -20 \end{bmatrix} \quad p_5^{\mathrm{f}} = \begin{bmatrix} 150 \\ 0 \\ -20 \end{bmatrix} \quad p_6^{\mathrm{f}} = \begin{bmatrix} 150 \\ 30 \\ -20 \end{bmatrix}.$$

Optimization is required to determine the best locations for a new prototype.

E.3 Analysis of the rotation of iMS prototypes

We have defined a simple 2-DoF model for the motion of the foot with respect to the lower leg as a function of a dorsiflexion and an inversion angle ϑ_{df} and ϑ_{iv} respectively. We have also defined four actuator configurations, (S), (D), (V), and (A). We need to understand why the lower leg interface rotates around the leg and whether it can be prevented.

The hypothesis is that the rotation phenomenon can be explained by the actuators generating a net torsion moment on the lower leg interface, acting around the axis of the lower leg, ω_{l}. The interface then rotates, as there is no counteracting moment.

Nine leg configurations for combinations of ϑ_{df} and ϑ_{iv} were shown in Figure E.1-3. For each of the four actuator concepts, the actuator orientation can be found for the nine ankle configurations. Figure E.3-1 shows a frontal view for each actuator concept in all nine configurations; this shows how the actuators move when the ankle goes through its range-of-motion.

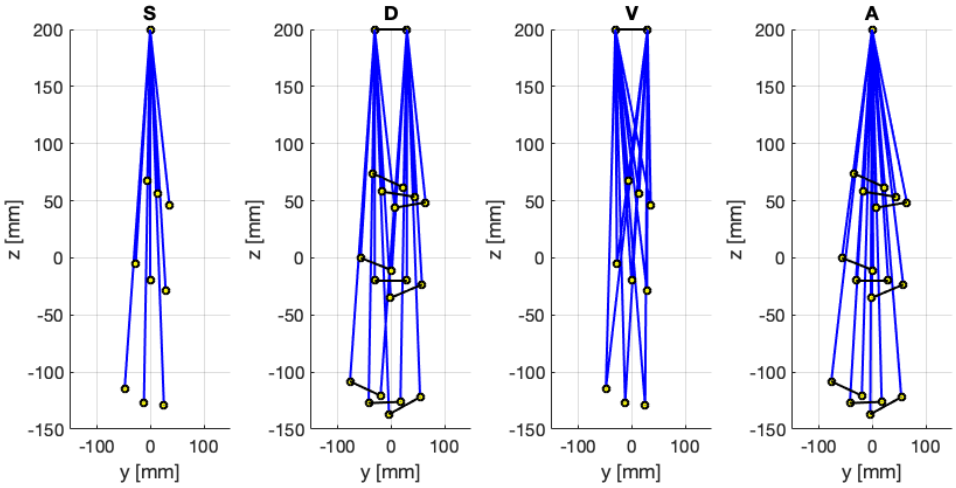

Figure E.3-1
Orientation of the actuators in nine ankle configurations, for each the four actuator concepts. From left to right: Single actuator (S); Double actuator (D); V-shape (V); A-shape (A).

More interesting is Figure E.3-2. It shows a top view on the leg and the actuators of concept (D). The force action lines of the actuators are shown and so is the location of the leg axis ω_{l}, pointing upwards out of the figure. We assume that both actuators deliver equal force. One can see that for the zero configuration in the center plot, the moments about ω_{l} due to both actuators cancel. However, one can see that there are net moments about the leg axis for the other configurations.

E.3.1 Torques generated by the actuators

Suppose that a linear actuator k generates a compression force between a point on the leg p_i with $i = 1, 2, 3$, and a point on the foot p_j with $j = 4, 5, 6$. (The values of i and j are defined by the connection matrix of the actuator concept.)

The *unit force vector* acting on the point p_i on the leg, as seen in the reference frame Ψ_0, can be

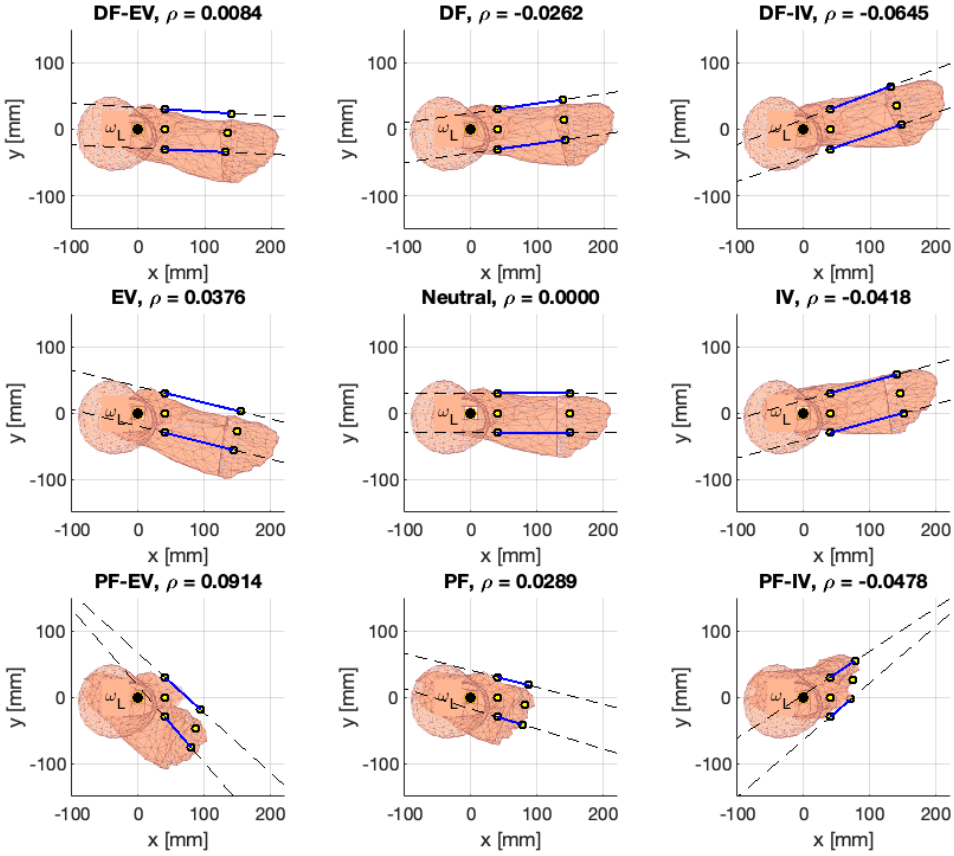

Figure E.3-2
Top views showing the force action lines for the double actuator concept (D).

computed as

$$\hat{f}_i^0 := \frac{p_i^0 - p_j^0}{\left\| p_i^0 - p_j^0 \right\|}.$$

Note that the rotation matrix R_f^0 was used to compute $p_j^0 = R_\mathrm{f}^0(\vartheta_\mathrm{df}, \vartheta_\mathrm{iv}) p_j^\mathrm{f}$ for $j = 4, 5, 6$. The unit force vector of actuator k causes a torque, which can be computed as

$$\tau_k := p_i^0 \wedge \hat{f}_i^0.$$

We omit the superscript "0" for the remainder of the analysis.

This actuator torque τ_k acts in an arbitrary direction, but it has a *useful* contribution about the plantar flexion–dorsiflexion axis ω_df and an *undesired* contribution about the axis of the lower leg ω_l. These contributions can easily be computed by taking the inner product with the corresponding unit vector of the axis:

$$\begin{aligned} \tau_{k,\mathrm{df}} &:= \langle \tau_k, \omega_\mathrm{df} \rangle \\ \tau_{k,\mathrm{l}} &:= \langle \tau_k, \omega_\mathrm{l} \rangle, \end{aligned}$$

where $\langle v, w \rangle$ denotes the inner product of vectors v and w. Note that τ_k is a vector, while $\tau_{k,\mathrm{df}}$ and $\tau_{k,\mathrm{l}}$ are scalars.

Finally, to compute the *total* torque about both ω_df and ω_l, we need to sum the scalar torque contributions of all actuators in the concept:

$$\begin{aligned} T_\mathrm{df} &:= \sum_{k=1}^{N_\mathrm{act}} \tau_{k,\mathrm{df}} \\ T_\mathrm{l} &:= \sum_{k=1}^{N_\mathrm{act}} \tau_{k,\mathrm{l}}. \end{aligned}$$

Here N_{act} is the number of actuators that is present in the concept (that is the number of rows in the connection matrix). The torques T_{df} and T_l represent the total torque that is generated about the dorsiflexion axis ω_{df} and about the leg axis ω_l, when *all* actuators generate a *unit* force.

We can use this relation to compute the actuator force that is needed to generate a *desired* torque M_{df} about the plantar flexion–dorsiflexion axis ω_{df}:

$$f_{act} = \frac{1}{N_{act}} \frac{M_{df}}{T_{df}}.$$

In this equation, we have taken into account both the number of actuators and their direction.

E.3.2 Ratios of torques

A nonzero torque T_l causes a problem, as this is the *parasitic torque* about the leg axis ω_l and it causes the leg interface to twist around the leg. We wish to compare the various actuator concepts, but simply comparing T_l is not fair, as different concepts use a different number of actuators and each concept generates a different dorsiflexion torque when all actuators produce a unit force.

The final step in the analysis is the definition of the following ratio:

$$\rho = \frac{T_l}{T_{df}}.$$

This ratio defines the parasitic torque as a fraction of the generated useful dorsiflexion torque. Suppose a dorsiflexion torque M_{df} is to be generated, then the resulting parasitic torque about the leg axis is

$$M_l = \rho M_{df}.$$

We can compute the value of ρ for each actuator concept and in each of the nine leg configurations. The grid that is obtained is shown in Figure E.3-3. The values of ρ for the (D) concept are also shown in the titles of the subplots in Figure E.3-2.

We observe the following. All four concepts show similar values of ρ for the parasitic torque about the lower leg. The only configuration for which no parasitic moments occur ($\rho = 0$), is the zero configuration. The *direction* (sign) of the parasitic moment depends on the ankle configuration; eversion corresponds with the interface rotating inwards and inversion with it rotating outwards.

The reason that parasitic torques also occur for pure plantar flexion–dorsiflexion, is that ω_{df} is not perpendicular to the xz plane. Were this the case, then ρ would be zero when $\vartheta_{iv} = 0$.

Note that although the values of the ratios are relatively small (all within $[-0.06, 0.1]$), and are smaller for smaller angles $(\vartheta_{df}, \vartheta_{iv})$, the intended plantar flexion–dorsiflexion torques for the orthosis are very high, so the resulting moments around the leg are very much significant—as was already found in practice.

E.3.3 Cable tension

The configurations in Figure E.1-3 are also used to investigate the changes in distance between the actuator anchor points and the connection points on either side of the ankle. These distances are not constant, so the problems with (loss of) cable tension that was described in Section 5.2.6 is indeed confirmed by the model—the problem cannot be solved by choosing a different actuator concept.

E.3.4 Final remarks

This section draws conclusions based on the numerical evaluation of various actuator concepts with specific dimensions. We furthermore used a simple model of the human ankle and evaluated the configurations at specific angles. Indeed, different numerical results would be obtained were we to pick other values. However, the general behavior that is seen will not change.

An important feature of the model, is that it does *not* assume rotation about a dorsiflexion axis perpendicular to the sagittal (xz) plane. Although we are not sure about the exact motion of the

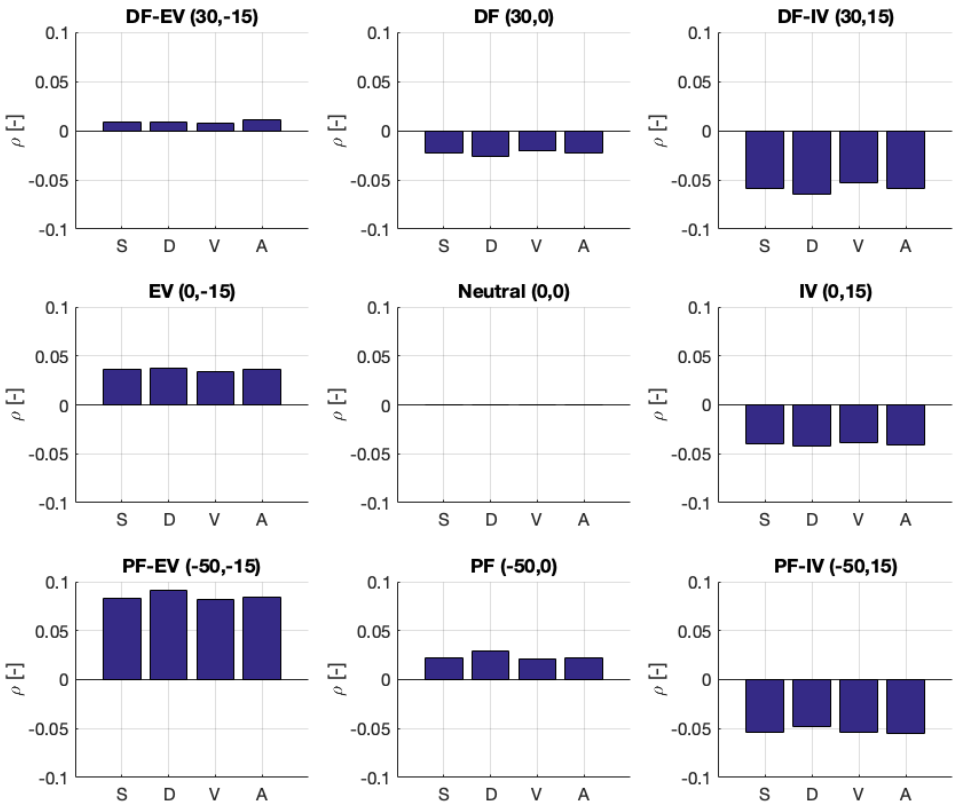

Figure E.3-3

Grid of bar plots for the ratio ρ. The grid corresponds to the leg configurations that are shown in Figure E.1-3. Each bar graph shows the value of ρ for each of the actuator concepts in the specific leg configuration; Single actuator (S); Double actuator (D); V-shape (V); A-shape (A)

ankle, we *are* sure that it will never be exactly in the sagittal plane. The slightly tilted dorsiflexion axis explains why even when a test subject moves only in plantar flexion–dorsiflexion, the lower leg interface still rotates.

Finally, we can conclude that the iMS approach result in inherently unstable systems, as the flexible materials cannot be used to generate a moment to counteract T_1. We assumed all actuators in a given concept to deliver equal force. It might be possible to control the actuators independently in such a way that their contributions to the dorsiflexion torque add up to the desired torque, while their individual contributions to the parasitic torque T_1 cancel each other. However, this would introduce such (control) complexity that this is undesired.

APPENDIX F

Nonlinear Force Control for Pneumatic Cylinders

Accurate and high-bandwidth force control is not easily achieved using pneumatic cylinders. This is due the high compressibility of air and the time delays in, and nonlinear behavior of, pneumatic systems. This chapter describes the force control strategy that is used to drive the pneumatic cylinders in the prototype.

The control strategy is based on the work of Richer *et al.* They have presented a nonlinear model of a pneumatic system [93] and a nonlinear 'sliding mode' force control strategy for this system [94]. Some modifications to their model and controller were made, to adapt it to our system.

For completeness of this report, all the equations that are used in the control law are presented in this chapter. The goal is to describe how the theoretic approach from [93, 94] is used in a practical control approach. However, for a thorough understanding of the matter, the reader is advised to read both papers.

F.1 Description of the pneumatic setup and its components

The pneumatic components (excluding computer hardware) that are used in the prototypes are shown in Figure F.1-1. A short description of the components is given below; the exact product ID's are listed in Table F.1-1.

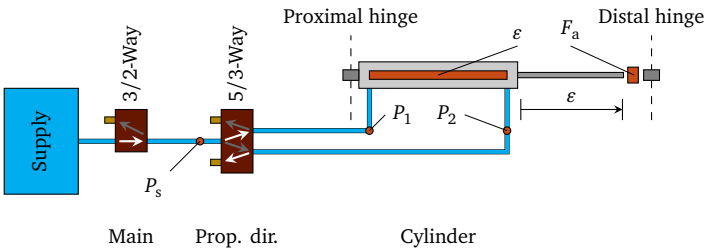

Figure F.1-1
Schematic overview of the pneumatic system with sensors (orange), valves (maroon), cylinders (grey), tubing (cyan), and exhausts (yellow).

Supply The pressurized air in the workshops at the University of Twente is used as the pressure supply for the system. The available pressure is not constant, but varies between 7 and 8

Table F.1-1
Pneumatic, sensor, and control components that are used in the system that is shown in Figure F.1-1.

Description	Type
Cylinder	Airpel M24D125UM; 24 mm diameter, 125 mm stroke, magnet on piston
Control valve	Festo MPYE-5-1/8-LF-010-B; 5/3-way
Main valve	Festo VUVS-L20-M32C-MD-G18-F7-1C1: 3/2-way
Plastic tubing	Festo PUN-8X1,25-SW
Push-in fittings	Festo QS-G1/4-8, QSL-G1/8-8, and similar
Position sensor	Festo SDAT-MHS-M160-1L-SA-E-0.3-M8; linear Hall encoder
Pressure sensors (3×)	Festo SPTE-P10R-S6-B-2.5K
Load cell	Strain Measurement Devices S402 Load Cell
DAQ card	National Instruments PCI-6229
Real-time DAQ/control	MATLAB/SIMULINK Real-Time R2016B

bar.

Main 3/2-Way valve A 3/2-Way valve is used to connect the system either to the pressure supply, or to the air. The connection to the pressure supply is closed when one of the emergency buttons is pressed.

Proportional directional 5/3-Way valve This is the control valve that regulates the flow from and to the cylinder. It either lets pressurized air flow from the supply into the extension chamber and from the retraction chamber into the air, or vice versa. It is a bi-directional proportional valve: it regulates the direction of the flow, but also the size of the valve openings.

Cylinder A special 'anti-stiction' pneumatic cylinder is used. It uses a glass liner, a precision-fit graphite piston, and no lubrication. A magnet is mounted on the piston; its position can be measured using a linear HAL encoder. Figure F.3-1 shows a schematic drawing of the components of the cylinder.

Pressure sensors For control purposes, pressure measurements are needed. One pressure sensor is used to measure the supply pressure P_{sup}—as it is not constant—and two sensors are used to measure respectively the pressure P_1 in the left and P_2 in the right cylinder chamber.

Position sensing A linear HAL encoder is mounted on the cylinder to measure the extension ε of the piston. (The position of the magnet on the piston is measured.)

Force sensor As the cylinder is frictionless, pressure measurements suffice to compute the force F_{p} that is exerted *by* the cylinder. However, we also need to measure the force exerted *onto* the cylinder; forces can be exerted onto the end-stops while this is not seen in the pressure measurement. A force sensor is connected to the cylinder rod to measure the real interaction force F_{a}.

DAQ and Software Finally, all control and sensor components are attached to a digital I/O card in a SIMULINK Real-Time target PC; MATLAB/SIMULINK is used for data acquisition and control.

F.2 Force control reference signal

Suppose we want the cylinder to generate a desired output force F_{d}. We assume this desired force to be a function of time, and, as it is specified by the user, we also assume its time derivative $\dot{F}_{\text{d}}$ to be known. That is, the following reference signals are assumed available:

$$(F_{\text{d}}, \dot{F}_{\text{d}}).$$

The goal of the controller is to realize

$$(F_{\text{p}}, \dot{F}_{\text{p}}) = (F_{\text{d}}, \dot{F}_{\text{d}}).$$

The controller consists of two components: a model-based part that is described in Section F.3 and a disturbance-rejection part that is described in Section F.4.

F.3 Force control—Part 1: Nonlinear model-based control

This section describes step-by-step how the model-based part of the controller is constructed. Note that friction and other disturbances are neglected in this part. Key for the control strategy, is that the control signal, which is the area A_v of the valve orifice, scales linearly with the control variable, which is the cylinder force F_p.

A number of (gas) constants is used in the equations. Their numerical values are listed in Table F.3-1.

Table F.3-1
List of constants used in the equations. Note that some constants are only defined at the end of this chapter.

Constant	Value	Description
T_{room}	293.15 K	Room temperature
P_{atm}	101325 Pa	Atmospheric pressure
R	287.058 J/kg/K.	Specific gas constant for dry air
k	1.40	Heat capacity ratio for air
c	343 m/s	Speed of sound in dry air at T_{room}
μ	$1.85 \cdot 10^{-5}$ Pas	Dynamic viscosity of air at T_{room}
C_1	0.040418 J/K	Gas-specific constant for air; see Equation (F.3-6)
C_2	0.156174 J/K	Gas-specific constant for air; see Equation (F.3-6)
P_{cr}	0.528	Critical pressure ratio; see Equation (F.3-6)
α	1.2	Coefficient in Equation (F.3-2)
α_{in}	k	Coefficient in Equation (F.3-7)
α_{ex}	1	Coefficient in Equation (F.3-7)

F.3.1 Cylinder force

We consider the Airpel cylinder that is shown in Figure F.3-1. It has an internal diameter of $D_{cyl} = 0.024$ m and the diameter of the piston rod is $D_{rod} = 0.006$ m. The area of the cylinder rod then is

$$A_{rod} = \frac{1}{4}\pi D_{rod}^2.$$

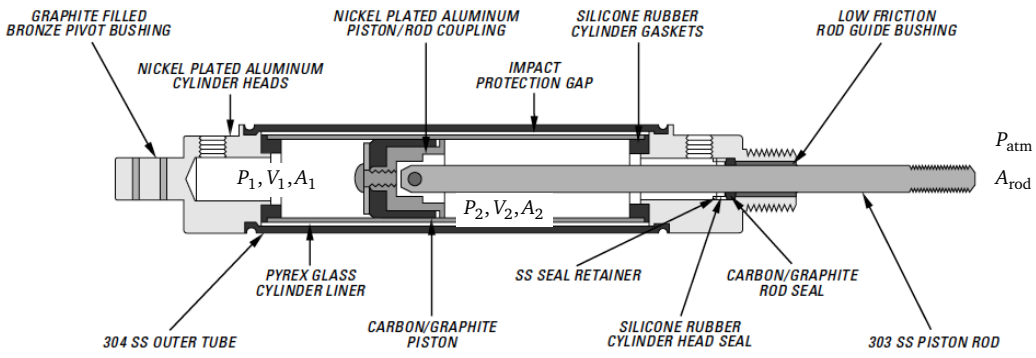

Figure F.3-1
Airpot's Airpel: "The Anti-Stiction Air Cylinder". Schematic overview of components. (Source: [95]) Shown are: Chamber 1 with pressure P_1, volume V_1, and piston area A_1; Chamber 2 with pressure P_2, volume V_2, and piston area A_2; Cylinder rod area A_{rod}; and atmospheric pressure P_{atm}.

We denote the left chamber with the subscript '1' and the right chamber with subscript '2'. The respective piston surface areas for both chambers are

$$A_1 = \frac{1}{4}\pi D_{\text{cyl}}^2,$$
$$A_2 = \frac{1}{4}\pi D_{\text{cyl}}^2 - A_{\text{rod}} = \frac{1}{4}\pi\left(D_{\text{cyl}}^2 - D_{\text{rod}}^2\right).$$

We can easily compute the volumes of both chambers as

$$V_1 = V_{01} + A_1\varepsilon,$$
$$V_2 = V_{02} + A_2(L - \varepsilon),$$

where $L = 0.125$ m is the maximum stroke of the cylinder and ε is the measured piston position. Note that $\varepsilon = 0$ corresponds to the rod being fully retracted. Furthermore, V_{01} and V_{02} are 'dead volumes' on either side of the cylinder. These dead volumes can be seen in Figure F.3-1 on either side of the cylinder, but they also include the volumes of the tubing from the valve up to the cylinder. It is important to take these volumes into account, as they influence the dynamic behavior.

If the pressures P_1 and P_2 in both cylinders are known (i.e. measured with the sensors), then the 'pneumatic force' F_{p} can be computed:

$$F_{\text{p}} = P_1A_1 - P_2A_2 - P_{\text{atm}}A_{\text{rod}}, \tag{F.3-1}$$

Note that this is the *theoretical* actuator force, under the assumption that there is no friction and ignoring the possibility that external forces act upon the end-stops of the cylinder. The *real* actuator interaction force F_{a} is measured using a force sensor at the cylinder rod; see Figure F.1-1. If no friction is present—which should be the case for the 'anti-stiction' cylinder—and if the piston is not in contact with either of the end-stops, then $F_{\text{a}} = F_{\text{p}}$.

F.3.2 Force rate of change due to piston motion

Richer *et al.* propose the following equation for the rate of change of the pressure P for a changing volume V:

$$\dot{P}_{\dot{V}} = -\alpha\frac{P}{V}\dot{V}. \tag{F.3-2}$$

The coefficient α depends on the heat transfer characteristics and a value of $\alpha = 1.2$ is recommended. The equation shows that the pressure decreases as the volume increases.

The piston is moving and therefore the volume of the cylinder chambers is changing. The volume rate of change for both chambers is easily found as a function of the piston velocity $\dot{\varepsilon}$:

$$\dot{V}_1 = A_1\dot{\varepsilon},$$
$$\dot{V}_2 = -A_2\dot{\varepsilon}.$$

The rate of change of the chamber pressures is

$$\dot{P}_{1,\dot{\varepsilon}} = -\alpha\frac{P_1}{V_1}A_1\dot{\varepsilon},$$
$$\dot{P}_{2,\dot{\varepsilon}} = \alpha\frac{P_2}{V_2}A_2\dot{\varepsilon}.$$

Finally, based on Equation F.3-1, we can compute the rate of change of the pneumatic force due to the piston velocity:

$$\dot{F}_{\text{p},\dot{\varepsilon}} = -\alpha\left[\frac{P_1A_1}{V_1} + \alpha\frac{P_2A_2}{V_2}\right]\dot{\varepsilon}, \tag{F.3-3}$$

where V_1 and V_2 depend on the piston position ε. The values of P_1, P_2, and ε are measured in real-time and $\dot{\varepsilon}$ must be estimated—this is done by numerical differentiation and a low-pass filter.

Note that the force rate of change $\dot{F}_{\text{p},\dot{\varepsilon}}$ is *only* due to the piston being in motion and *not* due to mass flowing into or out from the cylinder chambers. The equation shows the spring-like behavior of the cylinder: if $\dot{\varepsilon} > 0$ then $\dot{F}_{\text{p}} < 0$.

F.3.3 Controlling the force rate of change

When we neglect friction and higher order dynamics, the actuator force rate of change is the sum of two contributions:

$$\dot{F}_{\mathrm{p}} = \dot{F}_{\mathrm{p},\dot{\varepsilon}} + \dot{F}_{\mathrm{p},\dot{m}}.$$

The first term, $\dot{F}_{\mathrm{p},\dot{\varepsilon}}$, is given by Equation (F.3-3) and it is a state variable which depends on the current piston motion. The second term, $\dot{F}_{\mathrm{p},\dot{m}}$, is due to the mass flows into and from the cylinder chambers and it is realized by the control valve.

In Section F.2, we specified the *desired* force rate of change $\dot{F}_{\mathrm{d}}$. We want that $\dot{F}_{\mathrm{p}} = \dot{F}_{\mathrm{d}}$, which means that we can easily compute the required force rate of change that should be realized by the control valve:

$$\dot{F}_{\mathrm{p},\dot{m}} = \dot{F}_{\mathrm{d}} - \dot{F}_{\mathrm{p},\dot{\varepsilon}}. \tag{F.3-4}$$

We need to control the valve in such a way that this specific $\dot{F}_{\mathrm{p},\dot{m}}$ is obtained, because then

$$\dot{F}_{\mathrm{p}} = \dot{F}_{\mathrm{p},\dot{\varepsilon}} + \dot{F}_{\mathrm{p},\dot{m}} = \dot{F}_{\mathrm{p},\dot{\varepsilon}} + (\dot{F}_{\mathrm{d}} - \dot{F}_{\mathrm{p},\dot{\varepsilon}}) = \dot{F}_{\mathrm{d}}.$$

F.3.4 Behavior of the control valve

The control valve that is used is shown in Figure F.3-2(a). The pneumatic diagram in Figure F.3-2(b) explains the possible *internal* port connections in the valve. The external port connections of the valve are also shown: Port 1 is connected to the supply; Ports 3 and 5 are exhausts to the air; Port 4 is connected to chamber 1; Port 2 to chamber 2.

The valve can make the following internal connections.

Case 1 Port 1 to 4 *and* 2 to 3: that is chamber 1 to the supply and chamber 2 to the exhaust.

Case 2 Port 1 to 2 *and* 4 to 5: that is chamber 2 to the supply and chamber 1 to the exhaust.

This means that there are always *two* internal connections. The *size* of the opening of both internal connections are equal, but they are variable (it is a *proportional* bi-directional valve). The area of the internal valve opening is denoted by A_{v} and it is controlled by providing a voltage set point to the valve.

F.3.5 Mass flow through a valve opening

Suppose air is flowing through a valve opening with area A_{v}. The upstream pressure is P_{u} and the downstream pressure is P_{d}. The mass flow $\dot{m}$ through the valve can be computed as

$$\dot{m}(P_{\mathrm{u}}, P_{\mathrm{d}}) = \begin{cases} C_{\mathrm{f}} A_{\mathrm{v}} C_1 \frac{P_{\mathrm{u}}}{\sqrt{T}} & \text{if } \frac{P_{\mathrm{d}}}{P_{\mathrm{u}}} \le P_{\mathrm{cr}}, \\ C_{\mathrm{f}} A_{\mathrm{v}} C_2 \frac{P_{\mathrm{u}}}{\sqrt{T}} \left(\frac{P_{\mathrm{d}}}{P_{\mathrm{u}}}\right)^{1/k} \sqrt{1 - \left(\frac{P_{\mathrm{d}}}{P_{\mathrm{u}}}\right)^{(k-1)/k}} & \text{if } \frac{P_{\mathrm{d}}}{P_{\mathrm{u}}} > P_{\mathrm{cr}}. \end{cases} \tag{F.3-5}$$

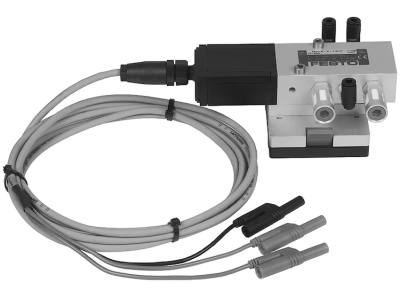

(a)

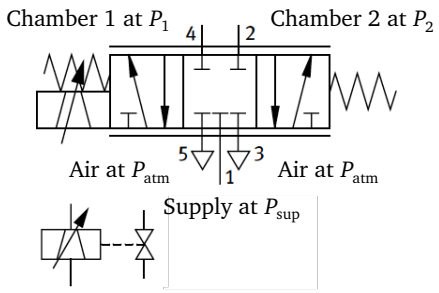

(b)

Figure F.3-2
Festo MPYE 5/3-way proportional valve: (a) photo and (b) pneumatic diagram. (Source: Festo)

Here C_f is a *discharge coefficient* that is to be determined experimentally. The constants C_1 and C_2 are gas-specific and P_{cr} is a critical pressure ratio. The values are computed as follows:

$$C_1 = \sqrt{\frac{k}{R}\left(\frac{2}{k+1}\right)^{(k+1)/(k-1)}}, \qquad C_2 = \sqrt{\frac{2k}{R(k-1)}}, \qquad P_{cr} = \left(\frac{2}{k+1}\right)^{k/(k-1)}. \tag{F.3-6}$$

The numerical values can be found in Table F.3-1.

Note that *by definition* $P_u > P_d$, so that the gas flows from high to low pressure. Both in modeling of the system components and control of the actual system, it is important to *explicitly* check which side of the valve must be considered 'upstream' and which 'downstream'.

For instance, it might seem reasonable to assume that the pressure supply *always* is 'upstream' and that the atmosphere *always* is 'downstream'. However, as the cylinder is loaded with (unpredictable) external forces, it could happen that the cylinder is compressed so much that air is pushed back into the supply. Or it could happen that the cylinder is extended so much, that air from the atmosphere is sucked back in, due to a vacuum being created.

F.3.6 Pressure rate of change due to mass flow

Richer *et al.* propose the following equation for the rate of change of the pressure P for a volume V with a mass inflow $\dot{m}_{in}$ and an outflow $\dot{m}_{ex}$:

$$\dot{P}_{\dot{m}_{in},\dot{m}_{ex}} = \frac{RT}{V}\left(\alpha_{in}\dot{m}_{in} - \alpha_{ex}\dot{m}_{ex}\right). \tag{F.3-7}$$

In this equation, R is the specific gas constant and T is the temperature. The coefficients α_{in} and α_{ex} are charge and discharge coefficients that depend on the heat exchange characteristics. The recommended values are $\alpha_{in} \approx k$, and $\alpha_{ex} \approx 1$. This k is is the heat capacity ratio $k = C_P/C_V$, with C_P and C_V the heat capacity at constant pressure and at constant volume respectively. These constants are properties of the gas and their numerical values are listed in Table F.3-1. Note that for control purposes approximate values of α_{in}, α_{ex}, and α (in Equation (F.3-3)) suffice.

F.3.7 Mass flow rate attenuation due to tubes

The mass flow rate through a tube will be attenuated:

$$\dot{m}_{ex} = \varphi\dot{m}_{in}, \quad \text{with} \quad \varphi \in [0,1].$$

That is, the mass flow rate $\dot{m}_{ex}$ exiting the tube will be less than or equal to the mass flow rate $\dot{m}_{in}$ entering it.

Richer *et al.* propose the following attenuation component for flow through a tube of length L_t and diameter D_t:

$$\varphi(P) = e^{R_t RT/(2P)\tau}, \quad \text{with} \quad \tau = \frac{L_t}{c} \quad \text{and} \quad R_t = \frac{32\mu}{D_t^2}. \tag{F.3-8}$$

Here τ is a time constant based on the tube length and the speed of sound c; R_t is the tube resistance for fully developed laminar flow, based on the tube diameter D_t and the dynamic viscosity μ of the gas; and P is the pressure at the tube outlet.

F.3.8 Computing the required valve area

Equation (F.3-4) gives the force rate of change that should be realized by regulating the mass flow to and from the cylinder. Section F.3.4 describes how the internal connections in the control valve work and Equation (F.3-5) describes the mass flow through an orifice with area A_v, depending on the up- and downstream pressures. Finally, Section F.3.7 describes the flow attenuation due to the tubes. We need to combine these results to compute the valve area that is needed in the control valve.

Looking at Equation (F.3-5), we see that the mass flow scales linearly with the valve area. We can thus define the mass flow through a *unit* valve area:

$$\dot{m}'(P_u, P_d) := \begin{cases} C_f C_1 \frac{P_u}{\sqrt{T}} & \text{if } \frac{P_d}{P_u} \le P_{cr}, \\ C_f C_2 \frac{P_u}{\sqrt{T}} \left(\frac{P_d}{P_u}\right)^{1/k} \sqrt{1 - \left(\frac{P_d}{P_u}\right)^{(k-1)/k}} & \text{if } \frac{P_d}{P_u} > P_{cr}, \end{cases} \tag{F.3-9}$$

so that

$$\dot{m}(P_u, P_d) = A_v \dot{m}'(P_u, P_d).$$

It was explained in Section F.3.5 that by definition $P_u > P_d$. Suppose a container at arbitrary pressure P_i is connected to a valve with unit opening area and that the valve output is connected to a tube of length L_t and diameter D_t. This tube is then connected to a cylinder chamber at arbitrary pressure P_j. This is shown in Figure F.1-1. We assume tubes of equal length and diameter connecting each cylinder chamber to the valve. The mass flow into the chamber can then be computed as follows:

$$\dot{\mu}(P_i, P_j) := \text{sign}(P_i - P_j) \cdot \varphi(P_j) \cdot \dot{m}'(P_u, P_d), \quad \text{where} \quad \begin{cases} P_u = \max(P_i, P_j), \\ P_u = \min(P_i, P_j). \end{cases} \tag{F.3-10}$$

Note that we also included the attenuation component φ given by Equation (F.3-8). Mass flow from i to j is considered positive; if it happens to be that the pressure P_j is higher than P_i, the result is a negative mass flow.

Equation (F.3-7) describes the pressure rate of change as a function of both mass inflow and outflow. However, due to the construction of the valve, we have *either* inflow *or* outflow to each cylinder chamber. If we let a positive mass flow denote inflow and a negative mass flow denote outflow, then the equation becomes

$$\dot{P}_{\dot{m}}(\dot{m}, V) := \frac{RT}{V} \alpha_{\dot{m}} \dot{m}, \quad \text{with} \quad \alpha_{\dot{m}} = \begin{cases} \alpha_{\text{in}} \text{ if } \dot{m} \geq 0, \\ \alpha_{\text{ex}} \text{ if } \dot{m} < 0. \end{cases} \tag{F.3-11}$$

As was described in Section F.3.4, we can choose which ports are connected, as was denoted by 'Case 1' and 'Case 2'. Note that *both* internal connections in the valve have the same area A_v.

Case 1: Chamber 1 to supply, chamber 2 to exhaust

In Case 1, chamber 1 is connected to the supply and chamber 2 is connected to the exhaust. The mass flow through a unit valve area and then through the tube into chamber 1 then is

$$\dot{\mu}_1 = \dot{\mu}(P_{\text{sup}}, P_1)$$

and the air flow into chamber 2 is

$$\dot{\mu}_2 = \dot{\mu}(P_{\text{atm}}, P_2).$$

Generally, $\dot{\mu}_1$ will be positive and $\dot{\mu}_2$ will be negative. However, this need not always be the case as was described in Section F.3.5.

The pressure rate of change in both chambers due to the mass flows can be computed using Equation (F.3-11):

$$\dot{P}_{1,\dot{\mu}} = \dot{P}_{\dot{m}}(\dot{\mu}_1, V_1),$$
$$\dot{P}_{2,\dot{\mu}} = \dot{P}_{\dot{m}}(\dot{\mu}_2, V_2).$$

The force rate of change that is established by these changes in pressure is:

$$\dot{f}_{p,\dot{\mu}}^{\text{Case 1}} = A_1 \dot{P}_{1,\dot{\mu}} - A_2 \dot{P}_{2,\dot{\mu}}.$$

Substitution of the previous equations yields

$$\dot{f}_{p,\dot{\mu}}^{\text{Case 1}} = A_1 \dot{P}_{\dot{m}}\left(\dot{\mu}(P_{\text{sup}}, P_1), V_1\right) - A_2 \dot{P}_{\dot{m}}\left(\dot{\mu}(P_{\text{atm}}, P_2), V_2\right). \tag{F.3-12}$$

This is the force rate of change that would occur due to the mass flows for a unit valve area in Case 1, when chamber 1 is connected to the supply and chamber 2 to the exhaust.

Case 2: Chamber 2 to supply, chamber 1 to exhaust

In Case 2, the connections are swapped, that is: chamber 2 is connected to the supply and chamber 1 to the exhaust. Following the same reasoning we obtain

$$\dot{f}_{p,\dot{\mu}}^{\text{Case 2}} = A_1 \dot{P}_{\dot{m}}\left(\dot{\mu}(P_{\text{atm}}, P_1), V_1\right) - A_2 \dot{P}_{\dot{m}}\left(\dot{\mu}(P_{\text{sup}}, P_2), V_2\right). \tag{F.3-13}$$

Computing the control valve direction and opening area

Equation (F.3-4) gives the force rate of change $\dot{F}_{\mathrm{p},\dot{m}}$ that should be realized by regulating the mass flows with the valve. Furthermore, we have computed the force rate of change that would occur through a unit valve area for Case 1 in Equation (F.3-12) and for Case 2 in Equation (F.3-13). We choose the correct connection case based on the *sign* of $\dot{F}_{\mathrm{p},\dot{m}}$:

$$\text{Case } i \text{ so that } \operatorname{sign} \dot{F}_{\mathrm{p},\dot{m}} = \operatorname{sign} \dot{f}_{\mathrm{p},\dot{\mu}}^{\text{Case } i} \quad \text{where } i \text{ can be either 1 or 2.}$$

The actual force rate of change $\dot{F}_{\mathrm{p},\dot{m}}$ due to a valve area A_{v} (which is not 1) simply is

$$\dot{F}_{\mathrm{p},\dot{m}}^{\text{Case } i} = A_{\mathrm{v}} \dot{f}_{\mathrm{p},\dot{\mu}}^{\text{Case } i}.$$

Finally, the required valve area is

$$A_{\mathrm{v}} = \frac{\dot{F}_{\mathrm{p},\dot{m}}}{\dot{f}_{\mathrm{p},\dot{\mu}}^{\text{Case } i}},$$

where i was chosen as described and $\dot{F}_{\mathrm{p},\dot{m}}$ is given by Equation (F.3-4).

F.3.9 Summary and remarks

The *desired* force rate of change $\dot{F}_{\mathrm{d}}$ is specified by the user. The *actual* force rate of change of the cylinder $\dot{F}_{\mathrm{p}}$ is the sum of two components: (1) a contribution $\dot{F}_{\mathrm{p},\dot{s}}$ due to the piston motion and (2) a contribution $\dot{F}_{\mathrm{p},\dot{m}}$ due to the mass flows through the control valve. We computed the value of $\dot{F}_{\mathrm{p},\dot{m}}$ that is needed to achieve $\dot{F}_{\mathrm{d}}$, given the contribution $\dot{F}_{\mathrm{p},\dot{s}}$.

Based on the required value of $\dot{F}_{\mathrm{p},\dot{m}}$, we decided in which (binary) direction the valve should be opened. Finally, the valve area A_{v} was determined so that the desired value of $\dot{F}_{\mathrm{p},\dot{m}}$ is obtained. Theoretically, this means that $\dot{F}_{\mathrm{p}} = \dot{F}_{\mathrm{d}}$, as desired. If the initial conditions for the desired and actual force agree, that is if $F_{\mathrm{p}}\big|_{t=0} = F_{\mathrm{d}}|_{t=0}$, then we have also realized perfect tracking of the desired force F_{d}, because

$$\begin{aligned} F_{\mathrm{p}}(t) &= F_{\mathrm{p}}\big|_{t=0} + \operatorname{int}_0^t \dot{F}_{\mathrm{p}}(\tau)\mathrm{d}\tau, \\ &= F_{\mathrm{d}}|_{t=0} + \operatorname{int}_0^t \dot{F}_{\mathrm{d}}(\tau)\mathrm{d}\tau, \\ &= F_{\mathrm{d}}(t). \end{aligned}$$

However, this won't be the case in reality, as the model is simplified significantly. We ignored friction and omitted higher-order dynamics. Furthermore, there is parameter uncertainty and there is significant leakage in the valve. Moreover, it could be that the required valve area A_{v} is larger than the maximum area of the valve. Therefore, an additional contribution to the controller is needed, in the form of a disturbance rejector. This is described in Section F.4.

F.4 Force control—Part 2: Disturbance rejection

A very simple proportional feedback controller is added to reduce the error between the desired force F_{d} and actual force F_{a}. Note that here the force measurement from the sensor is used, instead of the pneumatic force F_{p}.

The force error is

$$F_{\mathrm{e}} = F_{\mathrm{a}} - F_{\mathrm{d}}.$$

The proportional control law requires both a binary valve direction and a proportional valve area. The valve direction is found as

$$\text{Case } i, \quad \text{where} \quad i = \begin{cases} 1 & \text{if} \quad \operatorname{sign} F_{\mathrm{e}} = -1, \\ 2 & \text{if} \quad \operatorname{sign} F_{\mathrm{e}} = 1. \end{cases}$$

The valve area proportional to the error is computed as

$$A_v = \begin{cases} \bar{A}_{fb} \text{ if } |F_e/F_{adm}| \geq 1, \\ \bar{A}_{fb}\,|F_e/F_{adm}| \text{ if } |F_e/F_{adm}| < 1, \end{cases}$$

Here $\bar{A}_{fb}$ is the maximum valve area that we allow the proportional part of the controller to demand; and F_{adm} is a maximum admissible force error. Both parameters are controller settings that need to be tuned.

F.5 Force control—Final control law

Both parts of the controller return a direction 'Case' and an area for the valve orifice. We need to combine them, to come to a final control signal for the valve.
We define

$$u(A_v, i) := \begin{cases} A_v \text{ for Case } i = 1, \\ -A_v \text{ for Case } i = 2. \end{cases}$$

Let A_v^{mb} and i^{mb} denote the valve area and direction case for the model-based controller and A_v^{fb} and i^{fb} the valve area and direction case for the feedback controller. We then compute

$$U := u(A_v^{mb}, i^{mb}) + u(A_v^{fb}, i^{fb}).$$

Finally, the direction that is sent to the valve is

$$\text{Case } i, \quad \text{where} \quad i = \begin{cases} 1 \text{ for sign } U = 1, \\ 2 \text{ for sign } U = -1, \end{cases}$$

and the valve area that we require is

$$A = |U|\,.$$

We have effectively combined the control signals from both controller parts.

F.6 Conclusions and remarks

We have constructed a control law that ensures tracking of the desired actuator force F_d. The controller consists of a model-based part and a part that rejects disturbances and model uncertainties. Key in the model-based part is that the control signal, which is the control valve orifice area A_v, scales linearly with the time derivative of the control variable, which is the output force F_p.
Note that the control valve, which is a commercial off-the-shelf device from Festo, uses an internal control-loop. It regulates the direction and valve opening area based on a voltage set point. Unfortunately, no information regarding the properties of the device are provided; the relation between the voltage set point U and valve area A_v are unknown. The manufacturer told us that no data is available and that variation between valves is to be expected.
There is also a number of system parameters in the model-based part of the controller that is unknown, such as the various (dis)charge coefficients α, α_{in}, and α_{ex}; or the size of the dead volumes V_{01} and V_{02}.
Ideally, the valve characteristics and other parameters would be determined by doing a system identification. However, various devices such as flow rate sensors would be required. Unfortunately, this equipment is not available. Moreover, a proper system identification would require a significant amount of time, which is not available within this project. Finally, the pneumatic cylinders are only a temporary solution, while the electro-hydraulic actuators are under development; the pneumatics are only used as a proof-of-principle. Therefore, all unknown system parameters and both proportional control gains were estimated and tuned on the actual setup.

APPENDIX G

Design of a Leg Test Bench

Within the HeRoS Project, many prototypes will be built to test various working principles. It is of course not possible to test al these principles on people, so we need a setup that can be used as a *mannequin* and as a *test bench*.

G.1 Description of the test bench

The test setup will be used for tests of actuation of the knee and ankle. It consists of an upper and lower leg, a foot and toes, all with realistic dimensions. The setup is shown in Figure G.1-1 on the next page.

The foot, ankle, knee and hip joints all have one degree-of-freedom and are equipped with a rotary position sensor. The hip joint is connected to a cart on a linear guidance, so that the system has two degrees-of-freedom when the toes are fixed on the frame. The leg moves in a 2D plane.

The 'skeleton' of the leg is made from Bosch Rexroth 20 × 20 mm aluminium strut profiles. The custom joints are made from aluminium. They use hardened steel axles and bushes and thrust washers with a bronze backing and teflon coating. Each joint is equipped with an AMS AS5048A 14-bit absolute rotary position sensor. The sensors have an SPI interface and are connected serially via cables that pass through the leg. The body parts are CNC milled from NECURON 651, a hard foam that has properties similar to those of wood. The CAD drawings of the leg were obtained from 3D photographs that were made at Orthin, in Drachten.

The setup can be used in three configurations:

Knee actuation We obtain a test setup with *one* degree-of-freedom when we mount the ankle joint to the frame. The cart can move along the linear guidance as the knee is actuated.

Ankle actuation The cart can be fixed to the guidance and the toe joint can be mounted to the frame. (Or the cart could be left free, the toe joint fixed and the knee joint locked.) We then obtain a system with *one* degree-of-freedom which can be used to test ankle actuation principles.

Knee-Ankle actuation By fixing the toe joint to the frame, a system with *two* degrees-of-freedom is obtained. The cart can move along the guidance and there is an internal degree-of-freedom. This can be used to test combined actuation of knee and ankle.

(a)

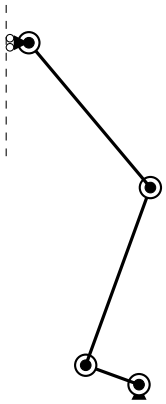

(b)

(c)

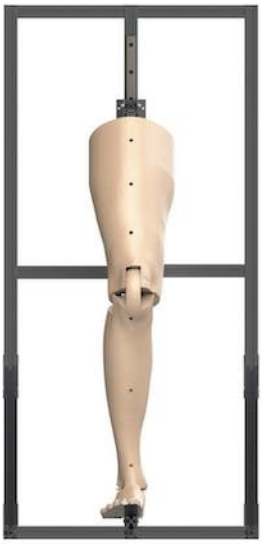

(d)

(e)

Figure G.1-1

2-DoF test setup that represents a human leg: (b) photograph; (a) kinematic chain; (c) CAD drawing lateral view; (d) CAD drawing frontal view; (d) CAD drawing dimetric view.

APPENDIX H

Interviews with Test Subjects

Section 8.3 describes how three devices have been compared in passive mode, with the actuators detached. The test subjects executed a number of tasks, described in Section 8.3.1, with each of the prototypes. The order in which they used the devices differs per participant. Questions were asked both during execution of the tasks, as well as after completing all tasks with all three prototypes. The questions are described in Section 8.3.2.

H.1 Tabulated data

This appendix presents the tables with the answers given by the test subjects. The answers are summarized and translated from Dutch to English. Note that the corresponding questions are listed in Section 8.3.2. Answers given on a five-point Likert scale are abbreviated as follows:

- Strongly agree (SA)
- Agree (A)
- Neither agree nor disagree (N)
- Disagree (D)
- Strongly disagree (SD)

Table H.1-1 gives an overview of the tables with answers. Note that the order in which the devices were tested are shown in the caption of the tables.

Table H.1-1
Overview of tables.

Subject ID	Page	Achilles	WE2	prototype	Final questions
Subject 1	Page 158	Table H.1-2	Table H.1-3	Table H.1-4	Table H.1-5
Subject 2	Page 159	Table H.1-6	Table H.1-7	Table H.1-8	Table H.1-9
Subject 3	Page 160	Table H.1-10	Table H.1-11	Table H.1-12	Table H.1-13
Subject 4	Page 161	Table H.1-14	Table H.1-15	Table H.1-16	Table H.1-17

Table H.1-2
Subject 1: Achilles (tested 1st).

Task	S1	S2	S3	S4	Comments
1. Donning	A	SA			You cannot don it like a shoe; you cannot pull at the back, as the actuator is in the way.
2. Move Freely	SD	SD	SA	A	PF/DF motion is OK. Until you hit the end-stops. PF end stop is too soon. DF is better, but still too limiting. IV/EV is not enabled by the device, but your foot can move within the shoe, so you can still move. There is a pressure point on the internal side at the distal shell.
3a. Straight Line	SA	A	D	SD	I sometimes hit the PF end stop. But this happens less than half the steps.
3b. CW Loop	SA	N	N	A	EV is constrained. But foot can move in shoe. The combined compliance of human-shoe-device still allows for some EV motion. But not comfortable.
3c. CCW Loop	SA	A	SD	A	Pressure point at internal side of distal cuff. Foot is moving within shoe. Can still do the task.
4a. Cross steps	SA	SA	SD	SD	Small steps over the line are OK because you're standing on your toes.
4b. Tilted path IV	A	D	SD	A	IV really uncomfortable due to pressure point at cuff. Really feel that IV is not a DoF of the device. It feels weird, but you can still do the task due to the combined compliance foot-shoe-device.
4c. Tilted path EV	SA	SA	SD	SD	Feel that you can do the task due to compliance. You're not constrained. Pressure point on leg. Moving within the exo. Pressure points change during task. Not uncomfortable.
5a. Stair ascent	N	D	A	A	Top of actuator hits back of upper leg. DF end stop at each step. Sometimes PF end stop at push-off.
5b. Stair descent	D	D	A	A	Cannot descend normally, since the leaf spring hits the steps. Can descend by making adjusted steps, but you hit the DF end stop with every step. Walking down on your heel.
6. Doffing	SA	SA			–

Table H.1-3
Subject 1: WE2 ankle module (tested 2nd).

Task	S1	S2	S3	S4	Comments
1. Donning	A	A			Takes a bit longer than Achilles, due to the double strap.
2. Move Freely	SA	SD	A	A	Uncomfortable: same pressure point as Achilles; internal distal shell. Mass hanging on external side; causes a torque about the leg. Mass rotates around the leg during IV/EV; you feel the inertia.
3a. Straight Line	A	SD	A	A	Pressure point. Gait is being altered; the mass on the external side forces the foot into IV. You also feel a torque in the hip which you need to counteract.
3b. CW Loop	SA	SA	SD	SD	Mass is hanging on the inner side of the loop. Feels comfortable and easy; as if the device is built for CW loops. The 'EV axis' is touching the end stop and foot is moving within shoe.
3c. CCW Loop	SA	SA	A	SD	Same as with straight walking: you feel a torque in the hip due to the mass on the external side. Not uncomfortable as it is rotating with you, but you feel that you're gait is altered.
4a. Cross steps	SA	SA	SD	SD	Works perfectly: the mass now is between your legs when they are crossed. Gives additional balance.
4b. Tilted path IV	SA	SA	SD	SD	Unfair not to take into account the device mass. It is the location of the mass that is bothering. The mass forces the foot into iv and that is helping for this particular task.
4c. Tilted path EV	A	A	A	D	You feel that the end-stop of the 'EV axis' is reached. Not always, but sometimes. Not bothering; compliance shoe-foot-device still allows you to move.
5a. Stair ascent	SA	SA	D	SD	Same as straight walking. External mass forces the foot into IV and you feel a torque at the hip.
5b. Stair descent	SA	SA	D	SD	Same.
6. Doffing	SA	SA			It is easier than Achilles, because you can reach the back of the shoe.

Table H.1-4
Subject 1: prototype (tested 3rd).

Task	S1	S2	S3	S4	Comments
1. Donning	SA	SA			Comparable with the other devices. Strap near toes is under the axle; hard to reach. Nice that the back of the shoe is accessible: can really don it like a shoe.
2. Move Freely	SA	SA	SD	D	It feels like the distal cuff is rotated about an axis perpendicular to the frontal plane.
3a. Straight Line	SA	A	SD	N	Brace of distal cuff touches leg at calf muscle. Should be wider; feel it at toe-off, when muscle contracts. Movement of ankle completely comfortable. Cycling shoe with rigid plate not great.
3b. CW Loop	SA	A	SD	N	Exactly the same as walking in a straight line: no difference.
3c. CCW Loop	SA	A	SD	N	Same.
4a. Cross steps	SA	A	N	D	Stiff plate under the shoe is annoying. Cannot roll-off naturally. Feeling at cuff now less bothering.
4b. Tilted path IV	SA	SA	SD	SD	–
4c. Tilted path EV	A	SA	SA	D	External cylinder hits the DF end stop at toe-off. Hit end stop quite soon with combined DF and EV.
5a. Stair ascent	A	SA	N	D	Hit DF end stop during swing. Stiff sole of cyclin shoe makes that the foot is forced flat on the step.
5b. Stair descent	N	N	SA	N	Hitting DF end stop on internal side. DF RoM too small. Gets worse with increased IV/EV angle.
6. Doffing	SA	SA			Very easy. But again hard to reach the strap near the toes.

Table H.1-5
Subject 1: answers to questions after trying all three devices.

Question 1
The asymmetry of the WE2 is bothersome. Mass really makes a big difference. RoM is really important. Hitting the end stop forces you to alter your gait and that is annoying. Comfort of shoes and cuffs seems difficult. A minor inconvenience quickly becomes disturbing. You feel all the small things.
Question 2
Yes. All 1-DoF devices have some compliance in the interface, s.t. you can still move in IV/EV. But you cannot control this. If you'd build a device that really constrains IV/EV, this would become extremely annoying. You can better build the additional DoF in your device: then you're in control.

Table H.1-6
Subject 2: Achilles (tested 3rd).

Task	S1	S2	S3	S4	Comments
1. Donning	A	A			Laces are less easy than Velcro. Metal structure close to rear of heel gets in the way when donning.
2. Move Freely	SD	SD	SA	SA	Not much DF. When making IV the metal spring clamp on the external side collides with foot. Really hurts. Cannot make EV, except within compliance of shoe.
3a. Straight Line	SA	SA	SD	SD	Strange spring in my step. Maybe due to the carbon foot plate or how it fits in the shoe.
3b. CW Loop	A	SA	A	SD	Feel that device has no IV/EV DoF when making corners. Acting against compliance of device. Doesn't hurt.
3c. CCW Loop	A	D	A	A	The top of the distal shell is pushing on the internal side of the leg. Further same is CW.
4a. Cross steps	A	N	A	N	You can complete the task fine. Comfort is borderline; pressure point not as bad as with CCW Loop. No IV/EV so foot is rolling on the ball of the foot on the floor. Decreased stability. Feel like falling.
4b. Tilted path IV	N	SD	SA	SA	Same pressure point again; causing lot of pain. It also causes you to veer off your path; no longer walking straight. Causes loss of stability.
4c. Tilted path EV	A	D	SA	A	No EV in device, so moving within the structure. Feel pressure point on the top of the distal shell on external side and at the ankle on the internal side. Latter hurts.
5a. Stair ascent	SA	SA	A	SD	Can complete the task, but slight limitation in DF just before heel strike of right foot.
5b. Stair descent	SD	N	SA	N	Limitation in DF. Carbon spring is a stumble hazard when catching on edges of steps.
6. Doffing	SA	SA			–

Table H.1-7
Subject 2: WE2 ankle module (tested 2nd).

Task	S1	S2	S3	S4	Comments
1. Donning	A	SA			There is something in the shoe that is in the way of my toes. It's a bit more difficult than donning the cycling shoe. Cannot stretch the back of the shoe like normally, due to the metal components.
2. Move Freely	A	D	A	A	When trying to move in IV/EV, whole device twists around leg. Makes it a lot harder to move.
3a. Straight Line	SA	A	SD	D	Back of the shoe is chafing, due to wrong shoe size. Tthe exo shoe is bit higher than own shoe. Pressure point on internal side at distal bracket; discomfort increased by mass on external side.
3b. CW Loop	SA	SA	SD	SD	–
3c. CCW Loop	SA	SA	SD	SD	The pressure point becomes worse.
4a. Cross steps	SA	SA	SD	SD	The secondary axis sometimes touches the end stop in maximum eversion. But it does not hinder.
4b. Tilted path IV	SA	SA	SD	SD	–
4c. Tilted path EV	SA	SA	SD	SD	–
5a. Stair ascent	SA	SA	SD	SD	–
5b. Stair descent	SA	SA	SD	SD	There is a small risk of stumbling due to the back of the device catching on the edge of the step.
6. Doffing	SA	SA			–

Table H.1-8
Subject 2: prototype (tested 1st).

Task	S1	S2	S3	S4	Comments
1. Donning	SA	SA			Inconvenient that straps of shoe are hard to reach.
2. Move Freely	A	SA	A	D	Not uncomfortable to move, but limits extrema of RoM. Limits are very big: in some directions, RoM of foot larger than of device, in others RoM of device larger than of foot.
3a. Straight Line	SA	SA	SD	SD	No comments on behavior. But can imagine that wearing two might cause collisions.
3b. CW Loop	SA	SA	SD	SD	Can move foot really quickly and it feels good.
3c. CCW Loop	SA	SA	SD	SD	The same.
4a. Cross steps	SA	SA	SD	A	Feel pressure point at top of anterior band at shin. Start to notice now after multiple tasks.
4b. Tilted path IV	SA	SA	SD	SD	–
4c. Tilted path EV	D	A	A	D	Hitting the end stop of the external cylinder. Combination of EV and DF at toe-off.
5a. Stair ascent	SA	SA	SD	SD	–
5b. Stair descent	SD	D	SA	A	Limited RoM in DF direction. It is not hurting, but it is hindering. It Is annoying.
6. Doffing	SA	SA			–

Table H.1-9
Subject 2: answers to questions after trying all three devices.

Question 1
It would be ideal if the 2-DoF had the same weight as the Achilles. After wearing two heavy devices, Achilles feels like a normal shoe. Seems that all devices have a risk of hooking against something; either themselves or the environment. Seems difficult to solve. A challenge. Advantage of 2-DoF is that it has a low actuator impedance; the other actuators were disconnected. They didn't cause noise and were very small. You barely feel them. WE2 seems to have a larger RoM in PF/DF, but the twisting around the leg is unacceptable. The 2-DoF is easier to don, because the heel is free. But there is a larger risk of hooking onto the other foot due to the structure on the internal side of the leg.
Question 2
Feel like the additional DoFs of the WE2 and 2-DoF are necessary for ADL tasks; cannot ignore them. Don't feel that IV/EV has to be actuated.

Table H.1-10

Subject 3: Achilles (tested 1st).

Task	S1	S2	S3	S4	Comments
1. Donning	A	SA			Maybe cut-off the front half if the inlay-sole
2. Move Freely	D	A	A	A	Maybe add a padding layer on the inside at the bottom of the device. Internal side collides with ankle.
3a. Straight Line	SA	SA	SD	SD	Hitting the PF end stop at toe-off, but not disturbing
3b. CW Loop	SA	SA	SD	A	Pressure point at the ankle on the internal side of the leg.
3c. CCW Loop	SA	SA	SD	A	Same as CW loop.
4a. Cross steps	SA	SA	SD	A	Same.
4b. Tilted path IV	N	A	A	A	No IV in the device. You lose balance due to the stiffness; falling to the right (external side, down-hill).
4c. Tilted path EV	N	A	A	A	No EV in the device. Lose balance due to stiffness; falling to the left (internal side; down-hill). Pressure point at internal side ankle gets worse.
5a. Stair ascent	SA	SA	SD	SD	Perfectly.
5b. Stair descent	SA	SA	A	A	The carbon leaf spring hits the steps. Uncomfortable. Need to alter gait and walk on heel.
6. Doffing	SA	SA			Very easy.

Table H.1-11

Subject 3: WE2 ankle module (tested 2nd).

Task	S1	S2	S3	S4	Comments
1. Donning	N	A			Bit harder to reach the laces.
2. Move Freely	SA	A	A	A	Center of gravity of device does not fall on the center line of leg. You have to lift the weight of the actuator during IV and mass pulls foot in EV.
3a. Straight Line	A	A	A	N	At toe-off, the foot is rotated in IV due to the external mass of the actuator module. Shoe is more comfortable than Achilles.
3b. CW Loop	A	A	D	N	Exactly the same experience as walking in a straight line.
3c. CCW Loop	A	A	D	N	Exactly the same experience as walking in a straight line.
4a. Cross steps	A	A	N	N	The frontal bar at the distal cuff collides with the upper back of the left lower leg, at the calf muscle.
4b. Tilted path IV	SA	SA	D	D	The asymmetrical load (mass on external side) remains a point of attention. But you get used to it.
4c. Tilted path EV	SA	SA	D	D	Same as tilted path IV.
5a. Stair ascent	SA	SA	SD	SD	The forced IV at toe-off due to the external mass is less of a problem during stair ascent when compared to normal walking.
5b. Stair descent	SA	SA	SD	SD	Same as ascent.
6. Doffing	SA	SA			Easy.

Table H.1-12

Subject 3: prototype (tested 3rd).

Task	S1	S2	S3	S4	Comments
1. Donning	SA	SA			
2. Move Freely	SA	SA	SD	SD	Very large RoM. Can hit the PF/DF end stops, but almost at my own RoM.
3a. Straight Line	SA	SA	SD	SD	Complete freedom for the ankle. Completely comfortable. No pressure points.
3b. CW Loop	SA	SA	SD	SD	Feels really good.
3c. CCW Loop	SA	SA	SD	SD	Same as CW Loop.
4a. Cross steps	SA	SA	SD	SD	Top of the actuator at distal shell collides with upper back of left leg at the calf. Keeping balance goes really well. Better than with both other devices.
4b. Tilted path IV	SA	SA	SD	SD	You almost don't feel that you're wearing it: you have full RoM. But maybe a bit too wide on the internal side of the foot. Collision with right foot.
4c. Tilted path EV	SA	SA	SD	SD	Same as IV. Device perfectly follows your ankle motion.
5a. Stair ascent	SA	SA	SD	SD	Do not hit end stops.
5b. Stair descent	A	A	A	N	At left foot heel-strike, hit DF end stop. RoM too small. But no problem for balance, as you lean into the cuff at the shin.
6. Doffing	SA	SA			–

Table H.1-13

Subject 3: answers to questions after trying all three devices.

Question 1
2-DoF feels best for freedom of motion for the ankle. Think least tiring to walk with this device. Maybe move actuators in 2-DoF to the back for better mass distribution. Maybe make the 2-DoF less wide on the internal side. Increase DF RoM of 2-DoF.
Question 2
I feel that I could wear the 2-DoF all day, without getting tired in my muscles and joints. Whereas I think the other two devices will start to bother me.

Table H.1-14

Subject 4: Achilles (tested 3rd).

Task	S1	S2	S3	S4	Comments
1. Donning	SA	SA			–
2. Move Freely	SD	D	SA	D	Not uncomfortable, but constrained. RoM too small for task.
3a. Straight Line	A	D	SA	A	Pressure point at back on heel. Always hit PF end stop and sometimes DF end stop.
3b. CW Loop	N	D	A	A	Again pressure point at heel. Feel like the whole structure is being bent to make EV motion.
3c. CCW Loop	N	D	SA	A	Feel a sideways shearing force in the knee. During CW loop the structure bent, but I now feel it in my knee. Structure feels a bit more stiff; foot is forced flat on the floor without allowing IV.
4a. Cross steps	SD	D	SA	A	Feel the structure deforming. Cannot really move in IV/EV. Losing balance.
4b. Tilted path IV	SD	D	SA	A	Same as with CCW loop; cannot make IV , so feel shear in my knee.
4c. Tilted path EV	SD	D	SA	A	Feel that the device deforms. Knee is pushed inwards due to the tilted path and the fact that the device wants to be perpendicular to the floor, not allowing IV/EV.
5a. Stair ascent	SA	SA	SD	D	–
5b. Stair descent	A	D	A	N	Leaf spring collides with edge of steps. Hit DF end stop at left foot heel-strike.
6. Doffing	SA	SA			–

Table H.1-15

Subject 4: WE2 ankle module (tested 2nd).

Task	S1	S2	S3	S4	Comments
1. Donning	A	SA			Straps around lower leg a bit too short.
2. Move Freely	A	N	A	A	Device rotates around calf and shin. Uncomfortable. Hinders a bit.
3a. Straight Line	A	D	A	A	The device forces the foot into IV at toe-off, due to actuator mass at external side of leg.
3b. CW Loop	SA	N	D	A	The device rotates around the shin and calf, due to the mass of the actuators, which is annoying. I don't feel like I can walk like this for a whole day.
3c. CCW Loop	A	N	A	A	Foot is being forced into IV, so that foot is dragging over the floor. Annoying. Do not hit end stops.
4a. Cross steps	A	N	D	A	I feel my knee due to the device rotating around the lower leg.
4b. Tilted path IV	SA	A	SD	SD	–
4c. Tilted path EV	SA	A	SD	SD	The same as tilted IV.
5a. Stair ascent	SA	A	SD	SD	–
5b. Stair descent	SA	A	SD	SD	Same as ascent. But still forcing your foot in IV; happens with all tasks.
6. Doffing	SA	SA			–

Table H.1-16

Subject 4: prototype (tested 1st).

Task	S1	S2	S3	S4	Comments
1. Donning	D	A			Hard to reach the straps of the shoe, at toes under axle and under rings. Foot hits the rings when donning the shoe. Could be faster with a shoe horn.
2. Move Freely	A	A	N	N	Can hit PF end stop. The RoM is only slightly smaller than the RoM of the foot. So not really limiting. Light pressure of the distal bracket on internal side of leg.
3a. Straight Line	SA	A	SD	SD	Shoe fit is not optimal, bit too small and narrow.
3b. CW Loop	SA	A	SD	A	Device not wide enough at toes; internal side of foot presses against the side of the device at big toe.
3c. CCW Loop	SA	A	D	D	No longer pressure at toe. Feels slightly different than CW loop. Feel slight spring-like behavior in IV direction.
4a. Cross steps	SA	A	SD	A	Collision of the upper part of the actuators with the back of the left leg at the calf muscle.
4b. Tilted path IV	SA	SA	SD	D	–
4c. Tilted path EV	A	A	A	D	Hit the DF end-stop of the external cylinder at toe-off with combined EV.
5a. Stair ascent	SA	SA	SD	SD	–
5b. Stair descent	SA	SA	SD	SD	–
6. Doffing	SA	SA			–

Table H.1-17

Subject 4: answers to questions after trying all three devices.

Question 1
Rotating asymmetrical mass of WE2 is annoying; better to have it symmetrical like the other two. Mass itself not really an issue. Actuators of WE2 and Achilles were disconnected. Might make a difference when they are connected.
Question 2
Definitely necessary for balance. Think that keeping balance during the complex tasks with an Achilles on either leg would be very hard.

Bibliography

[1] Symbitron+, "Symbitron—Symbiotic man-machine interactions in wearable exoskeletons to enhance mobility for paraplegics." [Online]. Available: http://www.symbitron.eu/

[2] C. Meijneke, W. van Dijk, and H. van der Kooij, "Achilles: An autonomous lightweight ankle exoskeleton to provide push-off power," *5th IEEE RAS/EMBS International Conference on Biomedical Robotics and Biomechatronics*, pp. 918–923, 2014. [Online]. Available: http://ieeexplore.ieee.org/lpdocs/epic03/wrapper.htm?arnumber=6913898

[3] M. E. Grootens, E. E. Hekman, and H. V. D. Kooij, "The inverted Muscle Skeleton approach: Moving beyond rigid exoskeletons," in *2018 7th IEEE International Conference on Biomedical Robotics and Biomechatronics (Biorob)*, 2018, pp. 659–664.

[4] S. Wang, V. Sluiter, C. Meijneke, H. Muijzer-witteveen, E. van Asseldonk, A. Wu, F. Dzeladini, A. Arami, and G. van Oort, "D5.3—System Requirements Document for WE1 personalised prototypes," Symbitron, Tech. Rep. March, 2016.

[5] A. M. Agur and A. F. Dalley, *Grant's Atlas of Anatomy (Thirteenth Edition)*. Wolters Kluwer, 2013.

[6] D. J. Magee, *Orthopedic Physical Assessment*, 6th ed. Elsevier, 2014.

[7] A. Haskell and R. A. Mann, "Biomechanics of the foot," in *AAOS Atlas of Orthoses and Assistive Devices*, 4th ed., J. D. Hsu, J. Michael, and J. Fisk, Eds., 2008.

[8] R. Donatelli, "Normal biomechanics of the foot and ankle," *the Journal of Orthopaed˜C and Sports Physical Therapy*, pp. 91–96, 1985. [Online]. Available: www.jospt.org

[9] R. Isman and V. T. Inman, "Anthropometric studies of the human foot and ankle," *Bull Prosthet Res*, vol. 11, pp. 97–129, 1969. [Online]. Available: http://www.rehab.research.va.gov/jour/69/6/1/97.pdf

[10] A. Haskell and R. A. Mann, "Biomechanics of the foot and ankle," in *Mann's Surgery of the Foot and Ankle*, 9th ed., M. J. Coughlin, C. L. Saltzman, and R. B. Anderson, Eds. Elsevier, 2014, pp. 3–31.

[11] K. Z. Takahashi, M. D. Lewek, and G. S. Sawicki, "A neuromechanics-based powered ankle exoskeleton to assist walking post-stroke: A feasibility study," *Journal of NeuroEngineering and Rehabilitation*, vol. 12, no. 1, pp. 1–13, 2015.

[12] J. Blaya and H. Herr, "Adaptive control of a variable-impedance ankle-foot orthosis to assist drop foot gait," *Neural Systems and Rehabilitation Engineering, IEEE Transactions on*, vol. 12, no. 1, pp. 24–31, 2004. [Online]. Available: 10.1109/TNSRE.2003.823266

[13] J. Zhang, C. C. Cheah, and S. H. Collins, "Experimental comparison of torque control methods on an ankle exoskeleton during human walking," *Proceedings - IEEE International Conference on Robotics and Automation*, vol. 2015-June, no. June, pp. 5584–5589, 2015.

[14] R. Chin, E. T. Hsiao-Wecksler, E. Loth, G. Kogler, S. D. Manwaring, S. N. Tyson, K. A. Shorter, and J. N. Gilmer, "A pneumatic power harvesting ankle-foot orthosis to prevent foot-drop," *Journal of NeuroEngineering and Rehabilitation*, vol. 6, no. 1, pp. 1–11, 2009.

[15] R. C. Browning, J. R. Modica, R. Kram, and A. Goswami, "The effects of adding mass to the legs on the energetics and biomechanics of walking," *Medicine and Science in Sports and Exercise*, vol. 39, no. 3, pp. 515–525, 2007.

[16] ETH Zürich, "CYBATHLON," January 15, 2019. [Online]. Available: http://www.cybathlon.ethz.ch

[17] International Council on Systems Engineering (INCOSE), *Guide for Writing Requirements (Version 2)*, 2015.

[18] K. Staman, A. J. Veale, and H. van der Kooij, "The PREHydrA: A passive return, high force density, electro-hydrostatic actuator concept for wearable robotics," *IEEE Robotics and Automation Letters*, vol. 3, no. 4, pp. 3569–3574, 2018. [Online]. Available: https://ieeexplore.ieee.org/document/8408751/

[19] A. T. Asbeck, S. M. De Rossi, K. G. Holt, and C. J. Walsh, "A biologically inspired soft exosuit for walking assistance," *The International Journal of Robotics Research*, vol. 34, no. 6, pp. 744–762, 2015.

[20] A. Schiele, "Ergonomics of exoskeletons: Subjective performance metrics," *2009 IEEE/RSJ International Conference on Intelligent Robots and Systems, IROS 2009*, pp. 480–485, 2009.

[21] A. M. Baroja, "User-Centered Design of a Flexible Robotic Ankle Orthosis (BSc. Thesis)," 2018.

[22] J. C. Moreno, F. J. Brunetti, J. L. Pons, J. M. Baydal, and R. Barberà, "Rationale for multiple compensation of muscle weakness walking with a wearable robotic orthosis," *Proceedings - IEEE International Conference on Robotics and Automation*, vol. 2005, no. April, pp. 1914–1919, 2005.

[23] J. Meuleman, "Design of a Robot-Assisted Gait Trainer: LOPES II," Ph.D. dissertation, University of Twente, 2015.

[24] K. Langlois, M. Moltedo, T. Bacek, C. Rodriguez-Guerrero, B. Vanderborght, and D. Lefeber, "Design and development of customized physical interfaces to reduce relative motion between the user and a powered ankle foot exoskeleton," *IEEE RAS/EMBS International Conference on Biomedical Robotics and Biomechatronics*, p. [submitted], 2018.

[25] "The SPACAR software package for the dynamic modelling and control of flexible multibody systems," 2019. [Online]. Available: www.spacar.nl

[26] B. S. Blanchard and Wolter J. Fabrycky, *Systems Engineering and Analysis—5th Edition*, 2010.

[27] R. K. Mitchell, B. R. Agle, and D. J. Wood, "Toward a theory of stakeholder identification and salience: defining the principle of who and what really counts," *Management*, vol. 22, no. 4, pp. 853–886, 1997.

[28] Ottobock, "Ottobock," August 27, 2019. [Online]. Available: https://www.ottobock.com/

[29] O. Gelderland, "Dwarslaesiepatient nijmegen wil robotpak niet teruggeven en zamelt geld in," December 16, 2015. [Online]. Available: www.omroepgelderland.nl/nieuws/2102935/Dwarslaesiepatient-Nijmegen-wil-robotpak-niet-teruggeven-en-zamelt-geld-in

[30] P. C. Kao, C. L. Lewis, and D. P. Ferris, "Short-term locomotor adaptation to a robotic ankle exoskeleton does not alter soleus Hoffmann reflex amplitude," *Journal of NeuroEngineering and Rehabilitation*, vol. 7, no. 1, pp. 1–8, 2010.

[31] G. S. Sawicki, A. Domingo, and D. P. Ferris, "The effects of powered ankle-foot orthoses on joint kinematics and muscle activation during walking in individuals with incomplete spinal cord injury," *Journal of NeuroEngineering and Rehabilitation*, vol. 3, 2006.

[32] D. P. Ferris, K. E. Gordon, G. S. Sawicki, and A. Peethambaran, "An improved powered ankle-foot orthosis using proportional myoelectric control," *Gait and Posture*, vol. 23, no. 4, pp. 425–428, 2005.

[33] K. A. Shorter, G. F. Kogler, E. Loth, W. K. Durfee, and E. T. Hsiao-Wecksler, "A portable powered ankle-foot orthosis for rehabilitation," *The Journal of Rehabilitation Research and Development*, vol. 48, no. 4, p. 459, 2011. [Online]. Available: http://www.rehab.research.va.gov/jour/11/484/pdf/shorter484.pdf

[34] S. Galle, P. Malcolm, S. H. Collins, and D. De Clercq, "Reducing the metabolic cost of walking with an ankle exoskeleton: interaction between actuation timing and power," *Journal of NeuroEngineering and Rehabilitation*, vol. 14, no. 1, pp. 1–16, 2017.

[35] G. A. Pratt and M. M. Williamson, "Series Elastic Actuators," in *1995 IEEE/RSJ International Conference on Intelligent Robots and Systems. Human Robot Interaction and Cooperative Robots, Pittsburgh, PA, USA, 1995*, 1995, pp. 399–406 vol.1.

[36] A. W. Boehler, K. W. Hollander, T. G. Sugar, and D. Shin, "Design, implementation and test results of a robust control method for a powered ankle foot orthosis (AFO)," *Proceedings - IEEE International Conference on Robotics and Automation*, pp. 2025–2030, 2008.

[37] A. Mehmet Oymagil, J. K. Hitt, T. Sugar, and J. Fleeger, "Control of a regenerative braking powered ankle foot orthosis," *2007 IEEE 10th International Conference on Rehabilitation Robotics, ICORR'07*, vol. 00, no. c, pp. 28–34, 2007.

[38] W. Van Dijk, C. Meijneke, and H. Van Der Kooij, "Evaluation of the achilles ankle exoskeleton," *IEEE Transactions on Neural Systems and Rehabilitation Engineering*, vol. 25, no. 2, pp. 151–160, 2017.

[39] A. R. Emmens, E. H. Van Asseldonk, and H. Van Der Kooij, "Effects of a powered ankle-foot orthosis on perturbed standing balance," *Journal of NeuroEngineering and Rehabilitation*, vol. 15, no. 1, pp. 1–13, 2018.

[40] J. Ward, T. Sugar, J. Standeven, and J. R. Engsberg, "Stroke survivor gait adaptation and performance after training on a powered ankle foot orthosis," *Proceedings - IEEE International Conference on Robotics and Automation*, pp. 211–216, 2010.

[41] K. A. Witte, J. Zhang, R. W. Jackson, and S. H. Collins, "Design of two lightweight, high-bandwidth torque-controlled ankle exoskeletons," *Proceedings - IEEE International Conference on Robotics and Automation*, vol. 2015-June, no. June, pp. 1223–1228, 2015.

[42] S. H. Collins, M. Bruce Wiggin, and G. S. Sawicki, "Reducing the energy cost of human walking using an unpowered exoskeleton," *Nature*, vol. 522, no. 7555, pp. 212–215, 2015.

[43] B. Wiggin, S. H. Collins, and G. S. Sawicki, "An exoskeleton using controlled energy storage and release to aid ankle propulsion," *American Society of Biomechanics*, 2010.

[44] S. Diller, C. Majidi, and S. H. Collins, "A lightweight, low-power electroadhesive clutch and spring for exoskeleton actuation," *Proceedings - IEEE International Conference on Robotics and Automation*, vol. 2016-June, pp. 682–689, 2016.

[45] M. Wehner, B. Quinlivan, P. M. Aubin, E. Martinez-villalpando, M. Bauman, K. Holt, R. Wood, and C. Walsh, "A lightweight soft exosuit for gait assistance," *2013 IEEE International Conference on Robotics and Automation (ICRA)*, pp. 3347–3354, 2013.

[46] S. Lee, S. Crea, P. Malcolm, I. Galiana, A. Asbeck, and C. Walsh, "Controlling negative and positive power at the ankle with a soft exosuit," *Proceedings - IEEE International Conference on Robotics and Automation*, vol. 2016-June, no. c, pp. 3509–3515, 2016.

[47] B. T. Quinlivan, S. Lee, P. Malcolm, D. M. Rossi, M. Grimmer, C. Siviy, N. Karavas, D. Wagner, A. Asbeck, I. Galiana, and C. J. Walsh, "Assistance magnitude versus metabolic cost reductions for a tethered multiarticular soft exosuit," *Science Robotics*, vol. 2, no. 2, p. eaah4416, 2017.

[48] J. Bae, S. M. M. De Rossi, K. O'Donnell, K. L. Hendron, L. N. Awad, T. R. Teles Dos Santos, V. L. De Araujo, Y. Ding, K. G. Holt, T. D. Ellis, and C. J. Walsh, "A soft exosuit for patients with stroke: Feasibility study with a mobile off-board actuation unit," *IEEE International Conference on Rehabilitation Robotics*, vol. 2015-Septe, no. August, pp. 131–138, 2015.

[49] L. N. Awad, J. Bae, K. O'Donnell, S. M. M. De Rossi, K. Hendron, L. H. Sloot, P. Kudzia, S. Allen, K. G. Holt, T. D. Ellis, and C. J. Walsh, "A soft robotic exosuit improves walking in patients after stroke," *Science Translational Medicine*, vol. 9, no. 400, p. eaai9084, 2017.

[50] N. Karavas, J. Kim, I. Galiana, Y. Ding, A. Couture, D. Wagner, A. Eckert-erdheim, and C. Walsh, "Autonomous soft exosuit for hip extension assistance," vol. 16, pp. 3–7, 2017. [Online]. Available: http://link.springer.com/10.1007/978-3-319-46532-6

[51] Y. L. Park, B. R. Chen, D. Young, L. Stirling, R. J. Wood, E. Goldfield, and R. Nagpal, "Bio-inspired active soft orthotic device for ankle foot pathologies," *IEEE International Conference on Intelligent Robots and Systems*, pp. 4488–4495, 2011.

[52] a. Erdogan, A. Satici, and V. Patoglu, "Design of a reconfigurable force feedback ankle exoskeleton for physical therapy," *2009 ASME/IFToMM International Conference on Reconfigurable Mechanisms and Robots*, pp. 400–408, 2009.

[53] A. Roy, H. I. Krebs, S. L. Patterson, T. N. Judkins, I. Khanna, L. W. Forrester, R. M. Macko, and N. Hogan, "Measurement of human ankle stiffness using the Anklebot," *2007 IEEE 10th International Conference on Rehabilitation Robotics, ICORR'07*, vol. 00, no. c, pp. 356–363, 2007.

[54] A. Roy, S. Member, C. Chornay, L. W. Forrester, C. E. Hafer, and R. F. Macko, "Quantifying human autonomy recovery during ankle robot-assisted reversal of foot drop after stroke," in *2018 7th IEEE International Conference on Biomedical Robotics and Biomechatronics (Biorob)*, 2018, pp. 523–530.

[55] A. Erdogan, B. Celebi, A. C. Satici, and V. Patoglu, "AssistOn-Ankle: A reconfigurable ankle exoskeleton with series-elastic actuation," *Autonomous Robots*, vol. 41, no. 3, pp. 743–758, 2017.

[56] Y. Fan and Y. Yin, "Mechanism design and motion control of a parallel ankle joint for rehabilitation robotic exoskeleton," *2009 IEEE International Conference on Robotics and Biomimetics, ROBIO 2009*, pp. 2527–2532, 2009.

[57] ETH Zürich, "Race task description CYBATHLON 2020 (Preliminary, V_2017-12)," Tech. Rep., 2017.

[58] A. J. Veale, "Biomechanics specifications for actuation of the body's joints," Tech. Rep., 2017.

[59] A. B. Zoss, "Actuation design and implementation for lower extremity human exoskeletons," Ph.D. dissertation, University of California, Berkeley, CA, 2006.

[60] C. Kirtley, "CGA Normative Gait Database," http://www.clinicalgaitanalysis.com/data/, 2013.

[61] J. Linskell, "CGA Normative Gait Database," http://www.clinicalgaitanalysis.com/data/, 2013.

[62] D. A. Winter, *Biomechanics and Motor Control of Human Movement (2nd Edition)*. University of Waterloo, 1990. [Online]. Available: http://onlinelibrary.wiley.com/book/10.1002/9780470549148{%}5Cnhttp://doi.wiley.com/10.1002/9780470549148

[63] M. K. Y. Mak, O. Levin, J. Mizrahi, and C. W. Y. Hui-Chan, "Joint torques during sit-to-stand in healthy subjects and people with parkinson's disease," *Clin. Biomech.*, vol. 18, no. 3, pp. 197–206, 2003.

[64] M. Rybski, *Kinesiology for occupational therapy*, 2nd ed. Thorofare, NJ: Slack Incorporated, 2004.

[65] S. R. Chang, R. Kobetic, and R. J. Triolo, "Understanding stand-to-sit maneuver: Implications for motor system neuroprostheses after paralysis," *J. Rehabil. Res. Dev.*, vol. 51, no. 9, p. 1339, 2014.

[66] S. Wang, V. Sluiter, C. Meijneke, H. Muijzer-witteveen, E. van Asseldonk, A. Wu, F. Dzeladini, A. Arami, and G. van Oort, "D5.5—System Requirements Document for WE2 personalised prototypes," Symbitron, Tech. Rep. April, 2016.

[67] G. Bovi, M. Rabuffetti, P. Mazzoleni, and M. Ferrarin, "A multiple-task gait analysis approach: Kinematic, kinetic and EMG reference data for healthy young and adult subjects," *Gait & Posture*, vol. 33, no. 1, pp. 6–13, 2011. [Online]. Available: http://linkinghub.elsevier.com/retrieve/pii/S0966636210002468

[68] A. J. Van Den Bogert, T. Geijtenbeek, O. Even-Zohar, F. Steenbrink, and E. C. Hardin, "A real-time system for biomechanical analysis of human movement and muscle function," *Medical and Biological Engineering and Computing*, vol. 51, no. 10, pp. 1069–1077, 2013.

[69] Y.-C. Pai and M. W. Rogers, "Speed variation and resultant joint torques during sit-to-stand," *Arch. Phys. Med. Rehabil.*, vol. 72, no. 11, pp. 881–5, 1991.

[70] M. E. Roebroeck, C. A. M. Doorenbosch, J. Harlaar, R. Jacobs, and G. J. Lankhorst, "Biomechanics and muscular activity during sit-to-stand transfer," *Clin. Biomech.*, vol. 9, no. 4, pp. 235–44, 1994.

[71] R. Riener, M. Rabuffetti, and C. Frigo, "Stair ascent and descent at different," *Gait and Posture 15*, vol. 15, pp. 32–44, 2002.

[72] A. Protopapadaki, W. I. Drechsler, M. C. Cramp, F. J. Coutts, and O. M. Scott, "Hip, knee, ankle kinematics and kinetics during stair ascent and descent in healthy young individuals," *Clinical Biomech.*, vol. 22, no. 2, pp. 203–10, 2007.

[73] B. J. McFadyen and D. A. Winter, "An integrated biomechanical analysis of normal stair ascent and descent," *J. Biomech.*, vol. 21, no. 9, pp. 733–44, 1988.

[74] S. Siegler, J. Chen, and C. D. Schneck, "The three-dimensional kinematics and flexibility characteristics of the human ankle and subtalar joints–Part I: Kinematics," *J. Biomech. Eng.*, vol. 110, no. 4, pp. 364–73, 1988.

[75] A. N. Lay, C. J. Hass, and R. J. Gregor, "The effects of sloped surfaces on locomotion: A kinematic and kinetic analysis," *J. Biomech.*, vol. 39, no. 9, pp. 1621–8, 2006.

[76] S. Nadeau, B. J. McFadyen, and F. Malouin, "Frontal and sagittal plane analyses of the stair climbing task in healthy adults aged over 40 years: What are the challenges compared to level walking?" *Clin. Biomech.*, vol. 18, no. 10, pp. 950–9, 2003.

[77] L. Schneider, D. Robbins, M. Pflüg, and R. Snyder, "Development of anthropometrically based design specifications for an advanced adult anthropomorphic dummy family, volume 1," p. 426, 1983.

[78] H. Ozden, Y. Balci, C. Demirüstü, A. Turgut, and M. Ertugrul, "Stature and sex estimate using foot and shoe dimensions," *Forensic Science International*, vol. 147, no. 2-3 SPEC.ISS., pp. 181–184, 2005.

[79] *Introduction to Indego®: Technical Data*, http://www.parker.com/parkerimages/Indego/en/Indego%20English%20Data%20Sheet__Rev%20B.pdf, Parker Hannifin Corporation, Macedonia, OH, 2015.

[80] A. Arami, N. L. Tagliamonte, F. Tamburella, G. V. Oort, and E. van Asseldonk, "D2.4—Report on spasticity and impedance modulation during human walking," Tech. Rep., 2016.

[81] J. L. Lelas, G. J. Merriman, P. O. Riley, and D. C. Kerrigan, "Predicting peak kinematic and kinetic parameters from gait speed," *Gait Posture*, vol. 17, no. 2, pp. 106–12, 2003.

[82] C. F. Schroeder, S. Z. Schmidtke, and M. W. Bidez, "Measuring the human pelvis: A comparison of direct and radiographic techniques using a modern United States–based sample," *Am. J. Phys. Anthropol.*, vol. 103, no. 4, pp. 471–9, 1997.

[83] Hocoma, "Lokomat," February 8, 2018. [Online]. Available: https://www.hocoma.com/solutions/lokomat/

[84] J. Meuleman, E. Van Asseldonk, G. Van Oort, H. Rietman, and H. Van Der Kooij, "LOPES II—Design and evaluation of an admittance controlled gait training robot with shadow-leg approach," *IEEE Transactions on Neural Systems and Rehabilitation Engineering*, vol. 24, no. 3, pp. 352–363, 2016.

[85] Rewalk Robotics, "ReWalk Personal 6.0," February 8, 2018. [Online]. Available: http://rewalk.com/rewalk-personal-3/

[86] Ekso Bionics, "Ekso GT," March 7, 2018. [Online]. Available: https://eksobionics.com/eksohealth/products/

[87] Indego, "Indego Personal," March 7, 2018. [Online]. Available: http://www.indego.com/indego/en/Indego-Personal

[88] A. B. Zoss, H. Kazerooni, and A. Chu, "Biomechanical design of the Berkeley Lower Extremity Exoskeleton (BLEEX)," *IEEE/ASME Transactions on Mechatronics*, vol. 11, no. 2, pp. 128–138, 2006.

[89] S. B. Kesner, L. Jentoft, F. L. Hammond, R. D. Howe, and M. Popovic, "Design considerations for an active soft orthotic system for shoulder rehabilitation," *Proceedings of the Annual International Conference of the IEEE Engineering in Medicine and Biology Society, EMBS*, pp. 8130–8134, 2011.

[90] A. T. Asbeck, R. J. Dyer, A. F. Larusson, and C. J. Walsh, "Biologically-inspired soft exosuit," *IEEE International Conference on Rehabilitation Robotics*, no. June, pp. 1–8, 2013.

[91] A. T. Asbeck, K. Schmidt, I. Galiana, D. Wagner, and C. J. Walsh, "Multi-joint soft exosuit for gait assistance," *IEEE International Conference on Robotics and Automation*, no. June, pp. 6197–6204, 2015.

[92] J. Pratt, B. Krupp, C. Morse, and S. Collins, "The RoboKnee: An exoskeleton for enhancing strength and endurance during walking," *IEEE International Conference on Robotics and Automation, 2004. Proceedings. ICRA '04. 2004*, no. April, pp. 2430–2435 Vol.3, 2004.

[93] E. Richer and Y. Hurmuzlu, "A high performance pneumatic force actuator system: Part I—Nonlinear mathematical model," *Journal of Dynamic Systems, Measurement, and Control*, vol. 122, no. 3, p. 416, 2000.

[94] ——, "A high performance pneumatic force actuator system: Part II—Nonlinear controller design," *Journal of Dynamic Systems, Measurement, and Control*, vol. 122, no. 3, p. 426, 2000.

[95] Airpot, "Airpel—The Anti-Stiction Air Cylinders," Tech. Rep., 2006.